

The phenomenon of vehicle park brake rollaway

By

Andrew James McKinlay

Submitted in accordance with the requirements for the degree of
Doctor of Philosophy (PhD)

The University of Leeds
School of Mechanical Engineering

August, 2007

The candidate confirms that the work submitted is his/her own and that appropriate credit has been given where reference has been made to the work of others.

This copy has been supplied on the understanding that it is copyright material and that no quotation from the thesis may be published without proper acknowledgement.

Acknowledgements

This work is dedicated to my parents. I would like to thank them for their continued support and encouragement throughout my time studying and without whom none of this would be possible. I would also like to thank all of my friends and family for keeping me going throughout my period of further study and keeping a smile on my face.

I would like to express my sincere gratitude to my two supervisors Dr. Peter Brooks and Professor David Barton for their invaluable support and advise. I would also like to thank all of the members of staff from the School of Mechanical Engineering for their assistance over the years. A special thank you goes to Tony Wiese and Dave Readman for their help and enthusiasm during all of the dynamometer work.

I wish to thank all the members of staff at Federal Mogul for their assistance, financial support and collective knowledge, especially Alastair Bissett and David Pindar.

Last but not least, I would like to thank Louise for her patience, understanding and encouragement. Thank you.

Abstract

When a vehicle is parked on a slope with hot brakes, what appears to be a sufficient parking brake action can sometimes become insufficient. When the brakes cool down, the braking force reduces due to relaxation of the entire parking brake system, and the vehicle may start to move, leading to obvious catastrophic consequences. This phenomenon is known as vehicle rollaway. This thesis describes the problem in detail and postulates a mechanism that accounts for the occurrence of the rollaway event on vehicles using integrated rear callipers.

Different testing methods are presented that are used to investigate the propensity of a vehicle's parking brake system to rollaway. These include on-vehicle evaluations and laboratory based measurements. A description is given of a novel dynamometer facility that was developed for this research that is capable of testing vehicle parking brake systems for rollaway.

Two mathematical modelling techniques are presented that demonstrate how the parking brake system parameters influence the likelihood of rollaway occurring. A finite element model was used to simulate the change in contact pressure at the frictional interface during a rollaway event. A numerical model was also used to predict the change in torque developed by a parking brake system cooling from an initial elevated temperature. The change in clamp load at the frictional interface was modelled using an essentially 1-D quasi-static system that showed how the stiffness and the thermal properties of the system qualitatively affect the phenomenon.

The research found that rollaway does not always start with a uniform motion, but with a stick/slip motion. The likelihood of rollaway occurring was found to be directly linked to the temperature of the brake when the vehicle is parked. Rollaway can be reduced by lowering the initial temperature of the brake prior to parking. Rollaway can also be reduced by increasing the input load to the system when applying the parking brake. The research identifies the key design parameters of the brake system components whose values require close control within the real system if rollaway is to be avoided.

Contents

Acknowledgements	ii
Abstract	iii
Contents	iv
Figures	ix
Tables	xiv
Nomenclature	xvi
Chapter 1 Introduction	1
1.1. The rollaway problem	1
1.2. Aim and objectives.....	3
1.2.1. Aim.....	3
1.2.2. Objectives.....	3
1.2.3. Structure of thesis.....	4
Chapter 2 Brake system fundamentals	6
2.1. Brake system overview	6
2.2. Park brake overview.....	7
2.3. Parking brake levers	11
2.4. Cables.....	12
2.5. Callipers.....	14
2.6. Pads	18
2.6.1. Friction materials.....	20
2.7. Discs	21
Chapter 3 Literature Review	22
3.1. Introduction	22
3.2. Parking brake mechanisms.....	22
3.3. Friction pair performance	24
3.3.1. Friction material	24
3.3.1.1. Binders.....	25
3.3.1.2. Fibres.....	26
3.3.1.3. Abrasives.....	27

3.3.1.4. Lubrication	28
3.3.1.5. Fillers.....	28
3.3.2. Friction level.....	29
3.3.3. Disc.....	31
3.3.4. Transfer films (third body layers)	31
3.3.5. Thermal effects.....	32
3.4. Experimental techniques and testing methods	33
3.4.2. Legislation and industrial testing	35
3.5. System modelling and simulation methods.....	36
3.5.1. Finite element modelling.....	36
3.5.2. Friction pair modelling.....	37
3.6. Summary	38
Chapter 4 On-Vehicle tests	40
4.1. Introduction	40
4.2. Vehicles and Components.....	40
4.2.1. Vehicles.....	40
4.2.2. Pads	44
4.2.3. Callipers.....	45
4.3. Methods.....	45
4.4. Results	48
4.4.1. Performance of the OE parking brake system.....	52
4.4.2. Rollaway propensity as a function of friction pair.....	54
4.4.3. Rollaway propensity as a function of calliper design.....	56
4.5. Summary	57
Chapter 5 Development of a Rollaway Dynamometer Experimental Facility	60
5.1. Introduction	60
5.2. Description of the original dynamometer.....	60
5.2.1. Drive rig	61
5.2.2. Apply rig.....	62
5.2.3. Operation.....	64
5.3. Dynamometer requirements	69
5.4. Preliminary test programme	70
5.4.1. Heating the brakes to a specified temperature.....	70

5.4.2. Application of a specified constant torque.....	71
5.4.3. Actuating the parking brake	72
5.5. Control and data acquisition system design and development.....	74
5.5.1. Introduction	74
5.5.2. Hardware	75
5.5.3. Software.....	76
5.6. Modifications to dynamometer	81
5.6.1. Dead weight system.....	81
5.6.2. Parking brake apply system.....	85
5.6.3. Axle rotation measurement	86
5.7. Dynamometer operation.....	87
5.8. Commissioning tests.....	87
5.8.1. Heating the brakes to a specified temperature.....	88
5.8.2. Application of a constant torque	88
5.8.3. Actuating the parking brake and measurig the clamp load	89
5.8.4. Clamp force measurement as a function of temperature.....	92
5.8.5. Measuring the static coefficient of friction a s a function of temperature.....	92
5.9. Summary	93
Chapter 6 Experimental characterisation of rollaway	94
6.1. Introduction	94
6.2. Foundation brake components.....	94
6.2.1. On-vehicle pads.....	94
6.2.2. Pressure scorched pads.....	94
6.2.3. Modified formulation pads.....	98
6.2.4. Modified original equipment formulations	98
6.2.5. Disc.....	98
6.2.6. Calliper	99
6.3. Methods.....	99
6.3.1. Compression tests.....	100
6.3.2. Thermal Expansion tests	100
6.3.3. Dynamometer clamp load evaluations	102
6.3.4. Dynamometer static friction tests.....	102
6.3.5. Surface characterisation	102
6.3.6. Calliper tests.....	103

6.4. Original Equipment Performance results	105
6.4.1. Compression.....	105
6.4.2. Thermal expansion	107
6.4.3. Dynamometer clamp load	110
6.4.4. Varying test temperature	112
6.4.5. Varying pad thickness	113
6.4.6. Calliper tests.....	114
6.4.7. Dynamometer static friction.....	116
6.4.8. Surface characterisation	117
6.5. Stiffness results.....	121
6.6. Thermal expansion results.....	125
6.7. Dynamometer clamp load results	126
6.7.1. Investigating the effect of disc thickness	129
6.8. Calliper results.....	131
6.9. Dynamometer Static friction results.....	132
6.9.1. On-vehicle pads.....	132
6.9.2. Modified OE pad formulations.....	134
6.10. Summary	134
Chapter 7 Rollaway simulation using the finite element method	136
7.1. Introduction	136
7.2. Methodology	136
7.2.1. Define input parameters	139
7.2.2. Define model geometry	142
7.2.3. Thermal analysis.....	144
7.2.4. Structural analysis	144
7.3. Results	148
7.3.1. Thermal results.....	148
7.3.2. Clamp load	148
7.4. Summary	154
Chapter 8 Rollaway simulation using Matlab/Simulink.....	155
8.1. Introduction	155
8.2. Methodology	155
8.2.1. Input variables	156

8.2.2. Cooling model	158
8.2.3. Torque required to hold vehicle	160
8.2.4. Description of the clamp load model	162
8.2.5. Static coefficient of friction.....	167
8.2.6. Torque model	169
8.2.7. Rollaway model output	170
8.3. Simulation and Results.....	170
8.3.1. Cooling results.....	170
8.3.2. Dynamometer clamp load	171
8.3.3. Rollaway output model	179
8.3.4. Cable temperature variation	182
8.4. Summary	183
Chapter 9 Discussion.....	185
Chapter 10 Conclusions and recommendations for further work.....	193
10.1. Conclusions	193
10.2. Recommendations for further work	194
References	196
Appendices	201

Figures

Figure 1.1 Schematic of a manually operated parking brake system with integrated rear callipers	2
Figure 2.1 Drum brake assembly.....	7
Figure 2.2 Disc brake assembly.....	7
Figure 2.3 Parking brake lever mechanism	8
Figure 2.4 Parking brake pedal apply system.....	9
Figure 2.5 Parking brake pull rod apply system.....	9
Figure 2.6 An integrated rear floating calliper used on a Ford vehicle.....	10
Figure 2.7 Drum in hat parking brake assembly	11
Figure 2.8 Photograph of an independent park brake calliper.....	11
Figure 2.9 Manual parking brake lever	12
Figure 2.10 Cross sectional photograph of a Jaguar S-Type parking brake cable.....	13
Figure 2.11 Cable system and connecting link.....	14
Figure 2.12 Parking brake cable attachment point to the calliper	14
Figure 2.13 Schematic of a ball in ramp mechanism with parking brake not applied	16
Figure 2.14 Schematic of a ball in ramp mechanism with parking brake applied	16
Figure 2.15 Schematic of a Bosch BIR3 calliper design.....	17
Figure 2.16 Back plate with Nucap Retention System.....	19
Figure 2.17 Schematic of a brake pad	19
Figure 3.1 Location of the 'neck' on a brake disc	32
Figure 3.2 Schematic of an inboard vented disc brake.....	33
Figure 4.1 Jaguar S-Type used for the on-vehicle tests.....	41
Figure 4.2 Layout of the Jaguar S-Type parking brake system.....	42
Figure 4.3 Dimensions of the Jaguar S-Type OE pad	42
Figure 4.4 Dimensions of the Jaguar S-Type rear disc	43
Figure 4.5 Cross section of Jaguar S-Type rear disc	43
Figure 4.6 Jaguar S-Type rear brake	44
Figure 4.7 Jaguar S-Type wheel base dimensions.....	44
Figure 4.8 Position of the thermocouple on the disc	47
Figure 4.9 Diagram of parking brake applying bracket	47

Figure 4.10 Parking brake lever with load cell and displacement transducer attached.....	48
Figure 4.11 Microphone positioned inside the cabin	48
Figure 4.12 Test type 1 -No movement no rollaway. Taken from the on-vehicle result for Pad 3 bedded facing up the 8% gradient with the brake cooling down from 50°C	49
Figure 4.13 Test type 2 - Stick/slip, noise, no rollaway. Taken from the on-vehicle result for Pad 2 bedded facing down the 8% gradient with brake cooling down from 50°C	50
Figure 4.14 Test type 3 - Stick/slip, noise, followed by rollaway. Taken from the on-vehicle result for Pad 1 bedded facing up the 8% gradient with brake cooling down from 100°C	50
Figure 4.15 Test type 4 - Stick/slip, noise, followed by a period of movement, then stick/slip and noise continues, then rollaway. Taken from the on-vehicle result for Pad 1 bedded facing down the 8% gradient with brake cooling down from 100°C	51
Figure 5.1 Schematic of drive rig (top view)	61
Figure 5.2 End view of drive rig	62
Figure 5.3 Side view of drive rig.....	62
Figure 5.4 Cable connecting bracket.....	63
Figure 5.5 Layout of apply rig (side view).....	63
Figure 5.6 End view of apply rig.....	64
Figure 5.7 Schematic of hydraulic circuit	65
Figure 5.8 Schematic of the hydraulic actuator circuit.....	66
Figure 5.9 Jaguar S-Type handbrake mounted on the dynamometer	66
Figure 5.10 Position of the thermocouple on the disc	67
Figure 5.11 ABS wheel measurement	68
Figure 5.12 Photograph of proximity sensor on the ABS wheel	68
Figure 5.13 Schematic of load cell in line with parking brake cable	69
Figure 5.14 Load cell in line with parking brake cable.....	69
Figure 5.15 Temperature of brake during preliminary heating test.....	70
Figure 5.16 Torque produced by the hydraulic actuator system	72
Figure 5.17 Layout of clamp load cell mechanism	73
Figure 5.18 Cable load and clamp load for each click on the Jaguar S-Type handbrake mechanism	74
Figure 5.19 Schematic of dynamometer control and DAQ system hardware.....	76
Figure 5.20 Operation of rollaway program.....	79
Figure 5.21 Read, write, calibrate and plot DAQ data subsystem of rollaway program	80

Figure 5.22	Diagram of the dead weight apply system.....	81
Figure 5.23	Side view of the modified apply rig.....	82
Figure 5.24	Pulley bearing blocks.....	83
Figure 5.25	Cable attachment bracket.....	83
Figure 5.26	Diagram of the weight hanger arrangement.....	84
Figure 5.27	Diagram of the electrical parking brake actuation system.....	85
Figure 5.28	Electrical parking brake actuation system	86
Figure 5.29	Shaft encoder on drive axle of the dynamometer	87
Figure 5.30	Temperature of the brake during commissioning test.....	88
Figure 5.31	Torque on the dynamometer axle during commissioning test.....	89
Figure 5.32	Cable load and clamp load produced by Jaguar S-Type parking brake system with the location of the 11 ratchet positions.....	90
Figure 5.33	Cable load and clamp load produced by the Jaguar S-Type parking brake system with a load of 0.6kN applied and released	90
Figure 5.34	Clamp load measured on the dynamometer and the mathematical approximation.....	91
Figure 5.35	Measured cable load and derived clamp load as the brake cools from 250°C to 30°C	92
Figure 5.36	Coefficient of static friction as a function of temperature	93
Figure 6.1	Schematic of the pressure scorching machine	96
Figure 6.2	Photograph of the pressure scorching machine.....	97
Figure 6.3	Cross sectional photograph of the disc machined down to 9mm thickness	99
Figure 6.4	Position of the surface profile measurements on the pad.....	103
Figure 6.5	S-Type calliper with deflection measurement point 15mm from tip of calliper finger	104
Figure 6.6	Location of the measurement positions on the calliper finger	104
Figure 6.7	Compression of Pad 1 at varying pressures and constant temperatures	105
Figure 6.8	Compression of Pad 1 at varying temperatures and constant pressures	106
Figure 6.9	Thermal expansion of a sample from Pad 1 - test 1	107
Figure 6.10	Thermal expansion of a sample from Pad 1 - test 2.....	107
Figure 6.11	Thermal expansion of a sample from Pad 1 - test 3.....	108
Figure 6.12	Thermal expansion of a sample from a cast iron disc - test 1	108
Figure 6.13	Thermal expansion of a sample from a cast iron disc - test 2	109
Figure 6.14	Thermal expansion of a sample from a cast iron disc - test 3	109

Figure 6.15 Cable load and derived clamp load from the OE parking brake system.....	111
Figure 6.16 Percentage of lost cable load and derived clamp load produced by the Jaguar S-Type OE parking brake system cooling from various temperatures	112
Figure 6.17 Percentage of lost cable load and derived clamp load produced by the Jaguar S-Type OE parking brake system with pads of varying thickness	114
Figure 6.18 Deflections of the calliper finger for different niches on the parking brake ratchet mechanism at different constant temperatures	115
Figure 6.19 Deflections of the calliper finger with different applied pressures at different constant temperatures	115
Figure 6.20 Static friction level variation with temperature for the Jaguar S-Type OE parking brake system	117
Figure 6.21 Surface profile of the bedded pad at 20°C from position 1	118
Figure 6.22 Surface profile of the bedded pad at 100°C from position 1	118
Figure 6.23 Surface profile of the bedded pad at 200°C from position 1	119
Figure 6.24 Surface profile of the un-bedded pad at 20°C from position 1	119
Figure 6.25 Surface profile of the un-bedded pad at 100°C from position 1	119
Figure 6.26 Surface profile of the un-bedded pad at 200°C from position 1	120
Figure 6.27 Compression of pads 1 to 4 with varying temperature and an applied constant pressure of 160bar	122
Figure 6.28 Compression of pads 1 to 4 with varying temperature and an applied pressure of 40bar	123
Figure 6.29 Percentage of lost cable load and derived clamp load during the dynamometer clamp load evaluations	127
Figure 6.30 Wear on pad from piston side of calliper.....	129
Figure 6.31 Wear on pad from finger side of calliper	129
Figure 6.32 Percentage of lost cable load and derived clamp load produced by the Jaguar S-Type OE parking brake system with discs of varying thickness	130
Figure 6.33 Deflections of the aluminium BOSCH BIR3 calliper finger	131
Figure 6.34 Deflections of the cast iron BOSCH BIR3 calliper finger.....	131
Figure 6.35 Static friction level variation with temperature for pads 1 to 4	133
Figure 6.36 Static friction level variation with temperature for pads 1, 11, 12 and 13	134
Figure 7.1 Overview of the finite element model.....	138
Figure 7.2 Coefficient of static friction as a function of temperature for Pads 1 to 4 as measured on the dynamometer and approximated by the mathematical model polynomial	141

Figure 7.3 Simplified finite element model of the brake disc and pad with the pad comprising a back plate and friction material	143
Figure 7.4 Dimensions (mm) of the brake disc and pads used in the FE model...	143
Figure 7.5 Beam elements in the centre of the disc.....	146
Figure 7.6 Location of the apply springs on the back plate of the pads	147
Figure 7.7 Cooling of the brake disc predicted by the FE model and measured on the dynamometer.....	148
Figure 7.8 Pressure distribution of the contact pressure produced at the pad surface for the parking brake system with Pad 1 installed when cooling from 250°C to 30°C	150
Figure 7.9 Percentage of lost clamp load of Pads 1 to 10 as measured on the dynamometer and predicted by the FE model.....	151
Figure 7.10 Percentage of lost clamp load predicted by the FE model for Pads 1a to 1e.....	152
Figure 7.11 Simulated torque produced by the parking brake system with Pads 1 to 4 installed cooling from 250°C to 30°C	153
Figure 8.1 Overview of mathematical model	156
Figure 8.2 Diagram of vehicle parked on a gradient.....	160
Figure 8.3 Overview of the system modelled.....	163
Figure 8.4 Schematic of clamp load model	164
Figure 8.5 Coefficient of static friction as a function of temperature for Pads 1 to 4 as measured on the dynamometer and approximated by the mathematical model polynomial	168
Figure 8.6 Coefficient of static friction as a function of temperature for Pads 1, 11, 12 and 13 as measured on the dynamometer and approximated by the mathematical model polynomial	168
Figure 8.7 Temperature of the brake components as predicted by the mathematical model and the disc temperature measured on the dynamometer	171
Figure 8.8 Percentage of lost clamp load predicted by the model and lost cable load measured on the dynamometer	172
Figure 8.9 Varying the system parameters by $\pm 10\%$ for Pad 1 cooling from 250°C to 30°C	173
Figure 8.10 Percentage of clamp load that is lost as the brake cools from 250°C to 30°C for Pads 1 to 10 as predicted by the model and measured on the dynamometer	175
Figure 8.11 Percentage of lost clamp load produced by changing the stiffness of Pad 1 at 250°C and 30°C	177
Figure 8.12 Percentage of lost clamp load as the brake cools with Pad 1 installed with modified thermal expansion coefficients.....	179

Figure 8.13 Torque produced by the parking brake system with Pads 1 to 4 installed 180

Figure 8.14 Torque produced by Pad 1 with varying levels of fused alumina..... 181

Figure 8.15 Clamp load produced by Pad 1 with cable at varying initial temperatures 183

Figure 9.1 Frictional interface during stick slip event before cooling 186

Figure 9.2 Frictional interface during stick slip event after cooling 186

Tables

Table 4.1 Details of the callipers used in the research 45

Table 4.2 Description of the on-vehicle results 49

Table 4.3 Un-bedded results for Jaguar S-Type OE pad (Pad 1) 52

Table 4.4 Bedded results for Jaguar S-Type OE pad (Pad 1)..... 53

Table 4.5 Un-bedded results from Jaguar S-Type OE pad (Pad 1) 54

Table 4.6 Bedded results from Jaguar S-Type OE pad (Pad 1)..... 54

Table 4.7 Un-bedded results from Pad 2 54

Table 4.8 Bedded results from Pad 2..... 55

Table 4.9 Un-bedded results from Pad 3 55

Table 4.10 Bedded results from Pad 3..... 55

Table 4.11 Un-bedded results from Pad 4 55

Table 4.12 Bedded results from Pad 4..... 55

Table 4.13 Results using Calliper 2..... 57

Table 4.14 Results using Calliper 3..... 57

Table 5.1 Description of the software commands 77

Table 5.2 Command script to heat a brake to 250°C then allow it to cool to 30°C 77

Table 6.1 List of pad numbers and pressure scorch conditions..... 97

Table 6.2 Pad 1 compression at varying applied load and temperature 105

Table 6.3 Pad 1 Young’s modulus at varying applied pressure and temperature 106

Table 6.4 Thermal expansion coefficient values of the OE pad and disc..... 109

Table 6.5 Cable load and derived clamp load for the Jaguar S-Type OE parking brake system..... 111

Table 6.6 Roughness values from the bedded and un-bedded pads 118

Table 6.7	Pad 1 compression.....	121
Table 6.8	Pad 2 compression.....	121
Table 6.9	Pad 3 compression.....	122
Table 6.10	Pad 4 compression.....	122
Table 6.11	Compression at ambient temperature with 40bar applied	123
Table 6.12	Compression results at an elevated temperature of 300°C for Pads 1 to 4 and 400°C for Pads 5 to 10 with 40bar applied.....	124
Table 6.13	Stiffness and Young’s modulus of Pads 1 to 10 at a temperature of 30°C and 250°C	124
Table 6.14	Results from the DMA test.....	125
Table 6.15	Results from the Jurid testing machine.....	125
Table 7.1	Fixed values used in the FE model.....	139
Table 7.2	Properties of Pads 1 to 10 used in FE simulation.....	140
Table 7.3	Static coefficient of friction approximations as a function of temperature.....	140
Table 7.4	R^2 values from the polynomial approximations.....	141
Table 7.5	Properties of Pads 1a to 1e	152
Table 8.1	Values of the system parameters used in the model.....	157
Table 8.2	The stiffness of Pads 1 to 10 at 30°C and 250°C	158
Table 8.3	Static coefficient of friction approximations as a function of temperature.....	167
Table 8.4	R^2 values from the polynomial approximations.....	169
Table 8.5	Optimal temperature of the calliper when used with Pads 1 to 10.....	174
Table 8.6	Modified stiffness values of Pad 1 at 30°C and 250°C.....	176
Table 8.7	Different values of the thermal expansion coefficient of Pad 1 used in the simulation.....	178

NOMENCLATURE

ABS = Anti-lock braking system

BIR = Ball in ramp

NRS = Ncap retention system

NVH = Noise vibration and harshness

DTV = Disc thickness variation

EPB = Electronic parking brake

NAO = Non asbestos organic

SUV = Sports utility vehicle

OE = Original equipment

SPL = sound pressure level

DAQ = Data acquisition

NI = National Instruments

VI = Virtual instrument

DMA = Dynamic Mechanical Analyser

LVDT = Linear variable differential transformer

FEA = Finite element analysis

APDL = ANSYS parametric design language

F = frictional force (N)

N = Normal force (N)

μ = Friction coefficient

Ra = surface roughness

x = position along sample (m)

z = deviation from mean surface (m)

L = length of sample (m)

- F_i = Normal force at the frictional interface (N)
- F_a = Force in parking brake apply system (N)
- k_d = Stiffness of the disc (Nm^{-1})
- k_p = Stiffness of the pad (Nm^{-1})
- k_{p30} = Stiffness of the pad at 30°C (Nm^{-1})
- k_{p250} = Stiffness of the pad at 250°C (Nm^{-1})
- k_a = Stiffness of the parking brake apply system (Nm^{-1})
- l_{0p} = Original thickness of the pad (m)
- l_{0d} = Original thickness of half of the disc (m)
- l_{0cab1} = Original length of cable 1 (m)
- l_{0cal} = Original length of the calliper bridge (m)
- α_p = Thermal expansion coefficient of the pad (C^{-1})
- α_d = Thermal expansion coefficient of the disc (C^{-1})
- α_{cab1} = Thermal expansion coefficient of cable 1 (C^{-1})
- α_{cal} = Thermal expansion coefficient of the calliper (C^{-1})
- k_{cab1} = Stiffness of cable 1 (Nm^{-1})
- k_{cab2} = Stiffness of cable 2 (Nm^{-1})
- A_p = Cross-sectional area of pad (m^2)
- A_d = Cross-sectional area of disc (m^2)
- E_p = Young's modulus of the pad (Nm^{-2})
- E_d = Young's modulus of the disc (Nm^{-2})
- u_1 = Input displacement to parking brake system (m)
- u_2 = Input displacement to caliper (m)
- u_3 = Output displacement of caliper (m)
- u_4 = Displacement of frictional interface (m)
- ΔT = Change in temperature ($^{\circ}\text{C}$)
- T = Instantaneous temperature ($^{\circ}\text{C}$)
- T_0 = Temperature at start of test ($^{\circ}\text{C}$)
- T_{amb} = Ambient temperature ($^{\circ}\text{C}$)

h = Heat transfer coefficient ($\text{Wm}^{-2} \text{C}^{-1}$)

C_{pdisc} = Specific heat capacity of disc ($\text{J kg}^{-1} \text{C}^{-1}$)

C_{ppad} = Specific heat capacity of the pad ($\text{J kg}^{-1} \text{C}^{-1}$)

C_{pcal} = Specific heat capacity of the calliper ($\text{J kg}^{-1} \text{C}^{-1}$)

ρ_d = Density of disc (kg m^{-3})

ρ_p = Density of the pad (kg m^{-3})

ρ_{cal} = Density of the calliper (kg m^{-3})

ρ_{cabl} = Density of cable 1 (kg m^{-3})

V_d = Volume of disc (m^3)

V_p = Volume of the pad (m^3)

V_{cal} = Volume of the calliper (m^3)

V_{cabl} = Volume of cable 1 (m^3)

R_c = Calliper lever ratio

Δl = Change in length or thickness (m)

r_{brake} = mean rubbing radius of the pad (m)

r_{wheel} = rolling radius of the wheel (m)

T_r = Torque required to hold vehicle on gradient (Nm)

Chapter 1

Introduction

1.1. The rollaway problem

Rollaway is a generic name that has been coined to describe a particular type of brake system failure that is associated with the progressive decay of the actuation load within the parking brake system. In extreme cases, this loss of load has permitted the in-plane component of vehicle weight to overcome the net brake force with the result that the vehicle rolls down the slope on which it is parked. The phenomenon is most commonly encountered on vehicles fitted with a particular brake system as discussed below.

Automotive vehicles that use a rear disc brake installation with an integrated rear calliper usually have a common set of pads to apply the primary and secondary (parking) brakes. In each case the pads are pushed against the rear wheel discs in order to produce the frictional force that is used for braking. When using the foot brake, or primary circuit, the pads are actuated by increasing the pressure in the brake lines, which in turn forces a piston to push the pads against the disc. The parking brake (secondary circuit) is commonly operated by manually applying a force to the parking brake lever. This causes the lever to rotate and displace the parking brake cable that is connected to the two rear callipers via a connecting link which transmits the load and displacement in a roughly equal proportion between the two callipers. This cable displacement causes a shaft within each calliper to rotate. The rotation of the shaft is converted into a linear displacement that is used to actuate the piston, pushing the pads against the disc to produce the frictional force required to keep the vehicle stationary whilst it is parked. A schematic of such a parking brake system is shown in Figure 1.1.

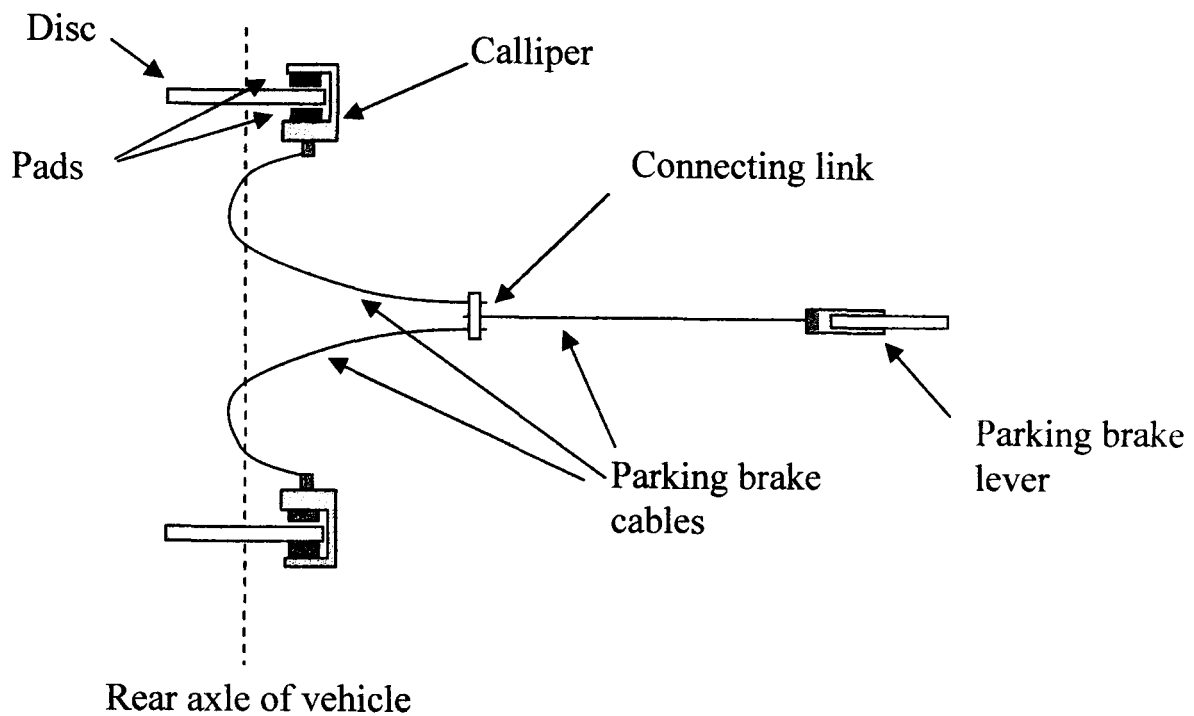


Figure 1.1 Schematic of a manually operated parking brake system with integrated rear callipers

During the course of vehicle operation, the primary brake may be applied numerous times, which generates heat at the pad/disc interface. Normal usage of the vehicle can permit the temperature at the rear pad/disc interface to reach 300°C [1]. This rise in temperature from ambient causes differential expansion of the complete foundation brake assembly. The parking brake can then be applied with the pads and discs at this elevated temperature and with the vehicle stationary on a known gradient. As the pads and disc begin to cool they start to contract back to their ambient dimensions. These shrinkage effects cause the pads and disc to effectively contract away from each other producing a reduction in the normal load at the friction pair interface. If the corresponding reduction in static braking force is great enough to cause this braking force to drop below that required to hold the vehicle on the gradient, the vehicle will begin to roll down the incline in an uncontrolled fashion. This phenomenon has been termed “rollaway”.

To date, the study of the rollaway phenomenon has received little reported attention in industry and in the world of academia. Vehicle manufacturers conduct tests specifically designed to check for rollaway, but there is currently no legislation that vehicles must satisfy. The rollaway phenomenon is believed to most commonly

occur on vehicles that use a disc brake with an integrated rear calliper in the parking brake system. Vehicle manufacturers are tending to favour rear disc over drum brakes in new car designs due to the performance advantage, and so the number of vehicles using integrated rear callipers is increasing along with the potential for rollaway. The increasing risk of rollaway suggests the need for a comprehensive understanding of the subject due to the obvious catastrophic consequences that can occur from a rollaway event. This therefore provides the motivation for the current research project.

The industrial collaborators associated with this project, Federal-Mogul, instigated a pilot study at the University of Leeds in 2002/03 as a fourth year MEng team project [2]. The project delivered a basic test rig and sufficient new knowledge to support the current program of research. The level four project was awarded 1st prize in the British Gear Association and IMechE transmission engineering prize.

1.2. Aim and objectives

1.2.1. Aim

The aim of the research is to characterise the rollaway phenomenon through on-vehicle and laboratory based experimental work and to produce a validated simulation model which can be used as a design tool by an automotive brake engineer. Use of the model will contribute to the elimination of the rollaway phenomenon at the design stage of a new vehicle. The model can also be applied to vehicles in service that have a parking brake system which exhibits rollaway in order to identify system modifications that can be implemented to eliminate rollaway.

1.2.2. Objectives

The specific objectives of the research are listed below:

- Conduct extensive on-vehicle rollaway evaluations using a vehicle that is believed to exhibit the rollaway phenomenon.
- Complete the design and commissioning of a comprehensive laboratory based rollaway dynamometer test facility.

- Characterise the performance of a parking brake system known to exhibit rollaway through extensive laboratory experiments involving dynamometer and material testing.
- Develop a detailed 3D finite element model that is capable of replicating the on-vehicle evaluations, and which is validated against the laboratory experimental data
- Develop a mathematical model of a rollaway event that can be used as a design tool by brake engineers.
- Determine through numerical trials the key system parameters that enable the brake system engineer to control and minimise the likelihood of rollaway.

1.2.3. Structure of thesis

The remainder of this thesis is comprised of nine other chapters that are summarised below.

Chapter 2: The brake system fundamentals for a typical automotive application are discussed. A detailed account of vehicle parking brake systems is given.

Chapter 3: A literature review of published material relevant to vehicle rollaway is given. A review is given of experimental and numerical methods used to evaluate brake systems.

Chapter 4: The on-vehicle evaluations that have been conducted for this research project are described. The vehicles were used to conduct rollaway tests to investigate the phenomenon of rollaway under ‘real world’ conditions.

Chapter 5: This chapter describes how the laboratory based dynamometer test facility and data acquisition system was developed and commissioned for this research. Commissioning tests are described that demonstrate the functionality of the test facility.

Chapter 6: This chapter describes the laboratory based tests that were used to characterise the material properties of the parking brake system components. The

dynamometer evaluations are also discussed that investigate the performance of the parking brake components.

Chapter 7: The finite element model of the parking brake system is described along with the results that have been generated.

Chapter 8: A description of the mathematical model that was developed to investigate rollaway is presented. The model is used to investigate the sensitivity of the likelihood of rollaway to changes in the parking brake system parameters.

Chapter 9: This chapter presents a discussion of the results and theories generated during the research project.

Chapter 10: The conclusions made from the overall findings of the research are discussed along with recommendations for areas of further research.

Chapter 2

Brake system fundamentals

2.1. Brake system overview

An automotive brake system is a device that is required to conduct three main functions: [3]

1. Decelerate a vehicle including stopping.
2. Maintain vehicle speed during downhill operation.
3. Hold a vehicle stationary on a gradient in either direction and when connected to a trailer.

A brake system typically consists of the primary foundation brake and a secondary parking brake. The foundation brake converts the driver's muscular energy into a braking force via a brake pedal. The pedal pushes a piston inside the master cylinder which forces hydraulic fluid into the brake circuit. The pedal force is usually assisted by a vacuum operated brake servo. It is important that no air is present in the brake hydraulic circuit as air is compressible, which causes the brake to feel "spongy" and severely reduces braking efficiency. The hydraulic fluid is usually split between the two front and two rear brakes by a proportioning valve which restricts the pressure delivered to the rear brakes to prevent rear wheel lock up. Most modern vehicles use an anti-lock braking system (ABS) to regulate the brake pressure at each wheel to improve the vehicles stability. The brakes can be one of two basic geometric forms, either a disc or a drum. Drum brakes use two brake shoes lined with an arc of friction material. The brake is actuated when the shoes are displaced in an outward radial motion to contact with the internal surface of the drum. The drum is attached to the wheel and hence produces a braking force when actuated.

A disc brake consists of two pads located on either side of a flat disc which is attached to the wheel stub axle. The pads are supported within a calliper assembly. The brake is actuated when hydraulic fluid is forced inside the calliper, which causes a piston to displace the pads in a normal direction to the disc. The contact surface between the pad and disc surface produces the frictional force. Figures 2.1 and 2.2 illustrate the basic layout of a drum and disc brake respectively.

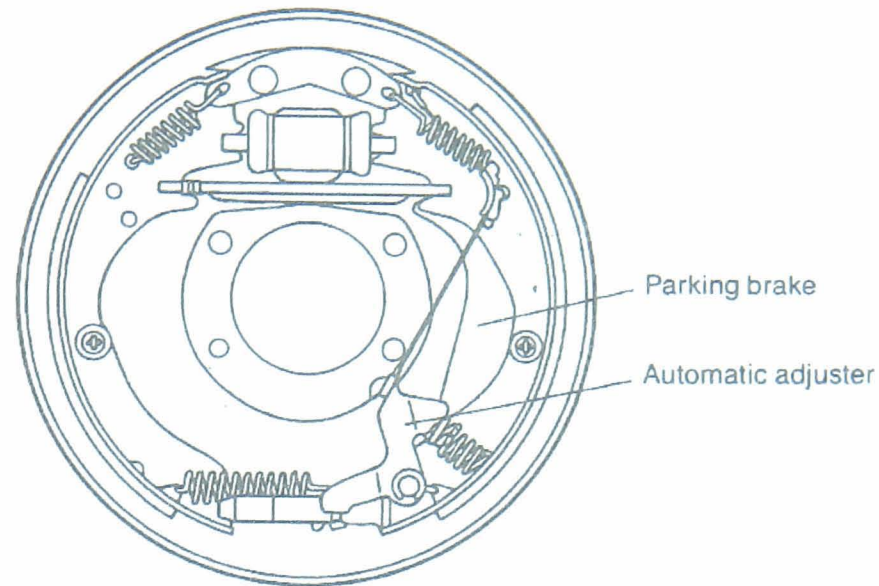


Figure 2.1 Drum brake assembly (Duo-servo) [3]

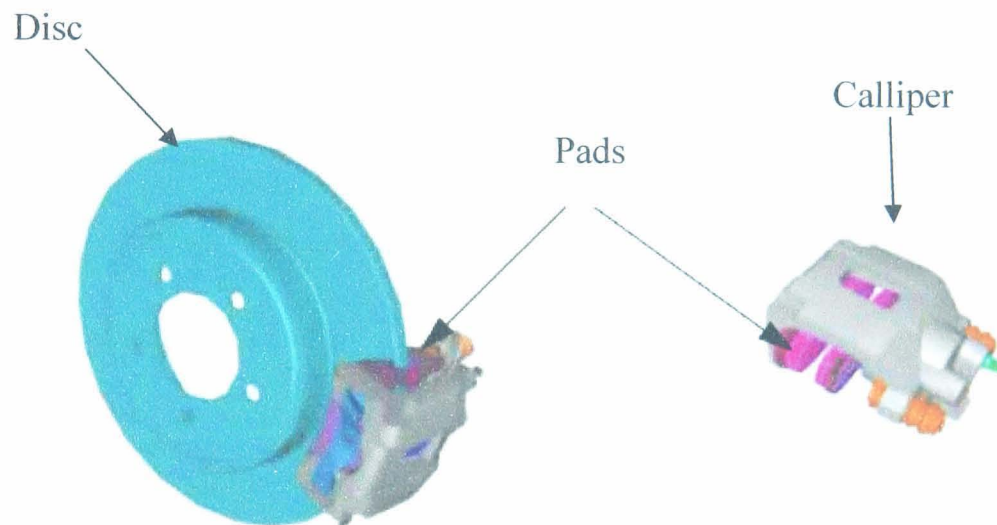


Figure 2.2 Disc brake assembly [4]

2.2. Parking brake overview

The primary use of the parking brake is to prevent the vehicle from moving while it is stationary. The parking brake can also be used as an emergency brake to bring a vehicle to rest if the primary brake fails, as it operates independently from the primary system's hydraulic circuit. The manual parking brake can be actuated by a lever, pedal or push rod located inside the cabin. An example of each of these

mechanisms is shown in Figures 2.3 to 2.5. Cables connect the lever, pedal or push rod to the brake which is generally located at the rear wheels of the vehicle. Some vehicle manufacturers mount the parking brake on the front wheels or on the propeller shaft. Electric parking brakes can also be used, which use an electrically controlled actuator or motor to apply the parking brake.

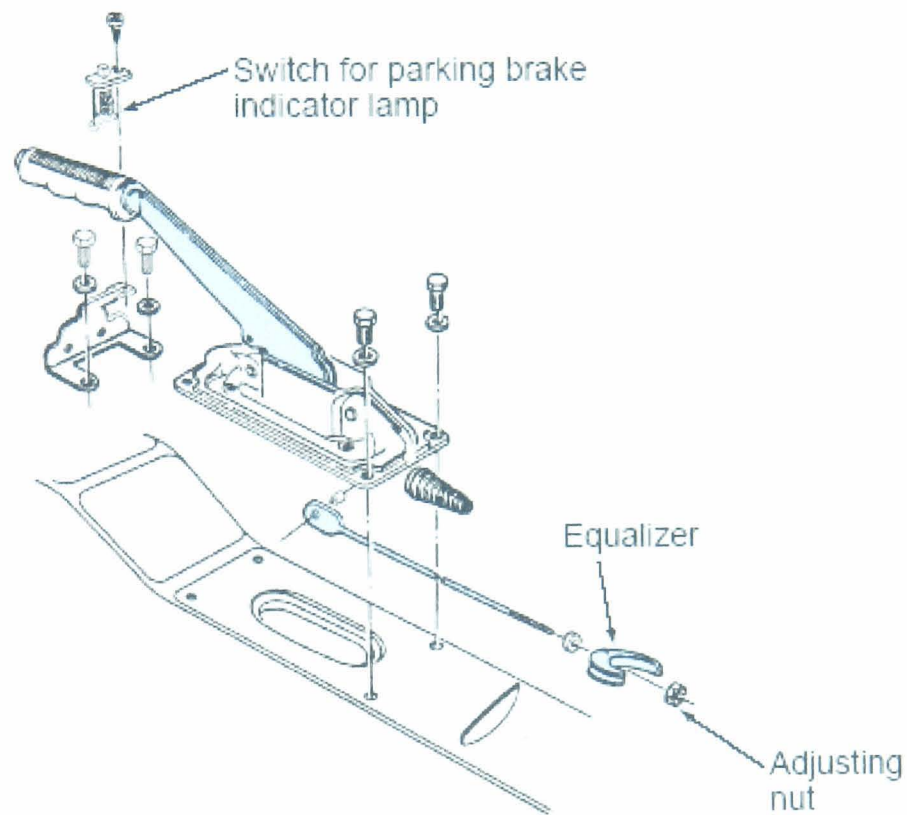


Figure 2.3 Parking brake lever mechanism [5]

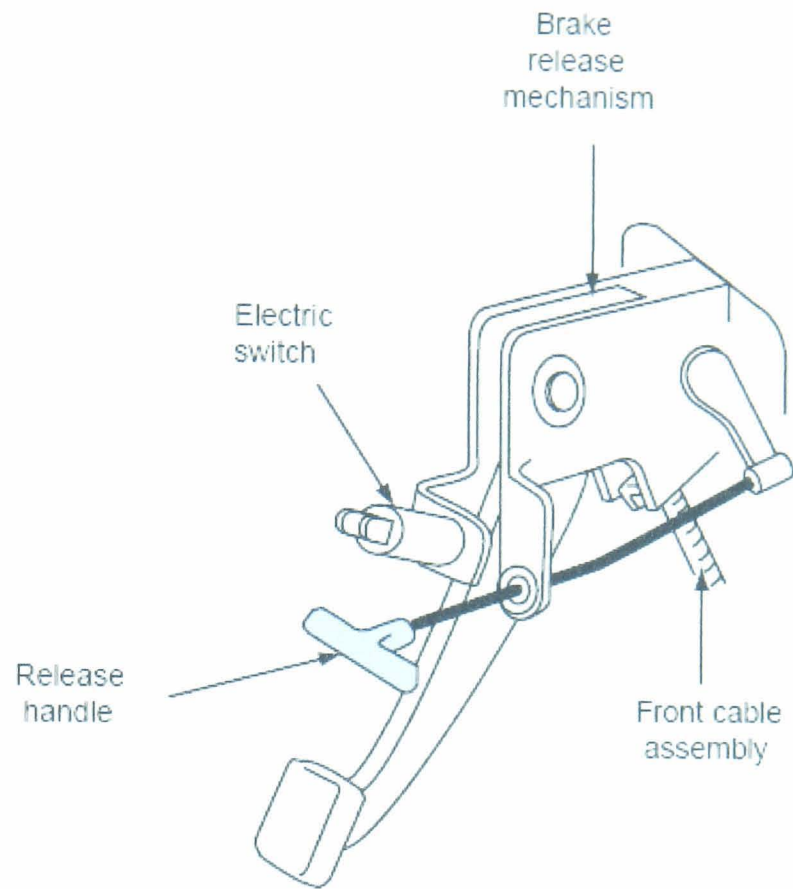


Figure 2.4 Parking brake pedal apply system [5]

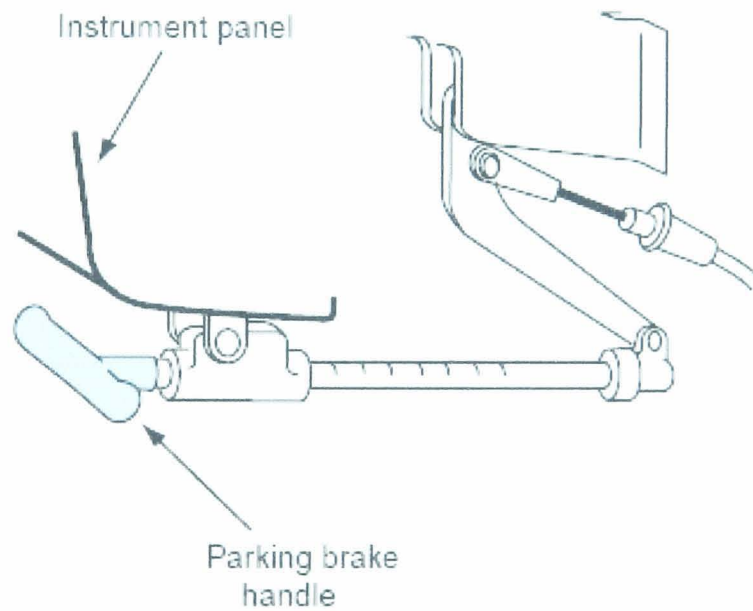


Figure 2.5 Parking brake pull rod apply system [5]

Vehicles using drum brakes at the rear wheels have the parking brake integrated into the drum brake assembly. The cable connects to a lever which when under load pushes the brake shoes against the drum to produce the frictional force. Passenger

car vehicles using discs at the rear brakes most commonly use three different methods of applying the parking brake:

- a) Integrated rear callipers have the parking brake actuation method integrated within the same calliper that is used to apply the hydraulic brake. This can be achieved by using an actuator screw or a push rod type mechanism on either a fixed or floating calliper design. An example of an integrated rear calliper is shown in Figure 2.6.
- b) Vehicles can use a ‘drum in hat’ mechanism on the rear brakes. This uses a calliper on the disc to apply the hydraulic brake, and a drum assembly inside the disc to apply the parking brake as shown in Figure 2.7.
- c) Vehicles can also use a separate calliper mounted on the disc to apply the parking brake which is independent from the hydraulic brake calliper as shown in Figure 2.8.

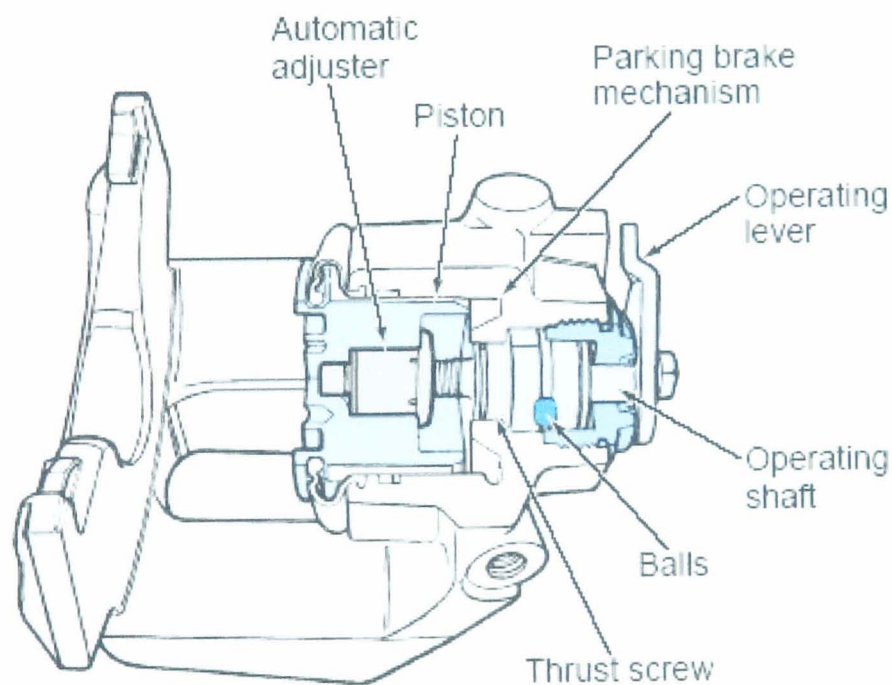


Figure 2.6 An integrated rear floating calliper used on a Ford vehicle [5]

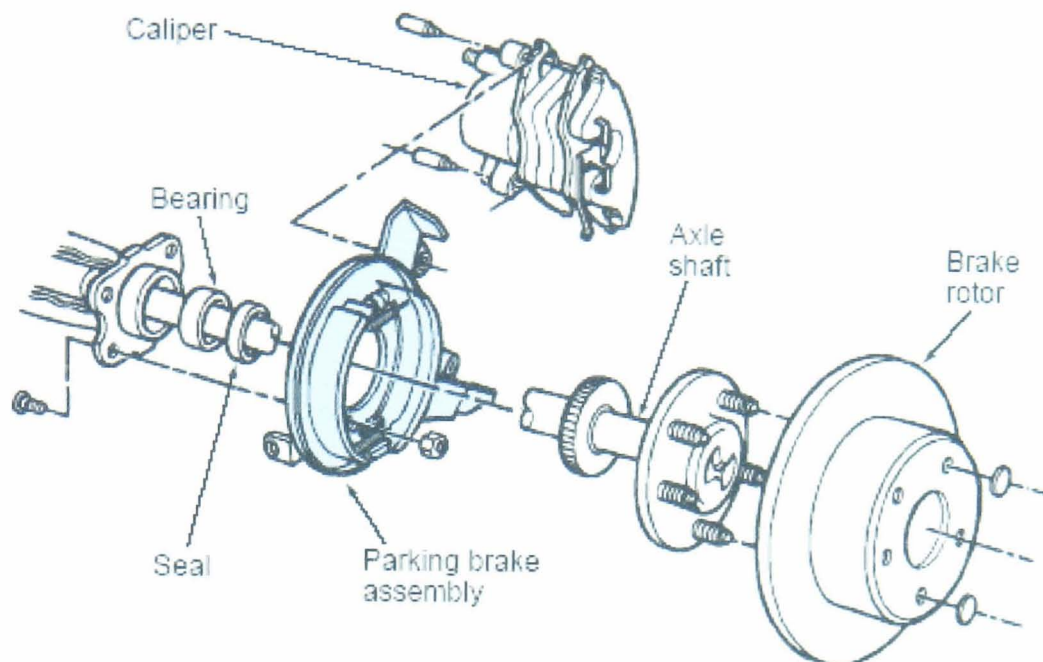


Figure 2.7 Drum in hat parking brake assembly [5]



Figure 2.8 Photograph of an independent park brake calliper

The focus of this research is on vehicles that use a manual parking brake lever with rear discs and an integrated floating calliper.

2.3. Parking brake levers

The manual parking brake lever is usually positioned in the centre of the cabin and is connected to the parking brake cables. It is operated when the driver applies a displacement to the lever, which results in a displacement being applied to the cable. The lever has an integrated ratchet mechanism that allows the displacement to be fixed at intervals specified by the vehicle manufacturer. The ratchet mechanism has a release button which allows the parking brake to be disengaged. An example of a

manual parking brake lever is shown in Figure 2.9. Pedal and pull rod parking brakes are attached to the cables using a similar lever mechanism that also employs a ratchet mechanism to fix the displacement.

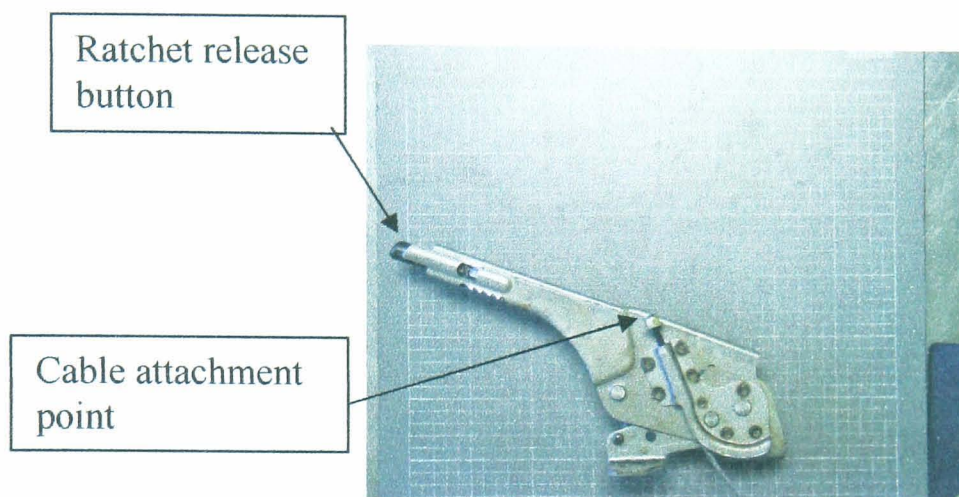


Figure 2.9 Manual parking brake lever

2.4. Cables

The cables used in parking brakes are generally manufactured from strands of steel wire laid concentrically around a central wire and woven together to form the cable. The cable can also include a coating to protect the wire from environmental effects. A cross sectional photograph of a sample of cable cut from a Jaguar S-Type's parking brake is shown in Figure 2.10. The sample was mounted in a black wax in order to obtain the image.

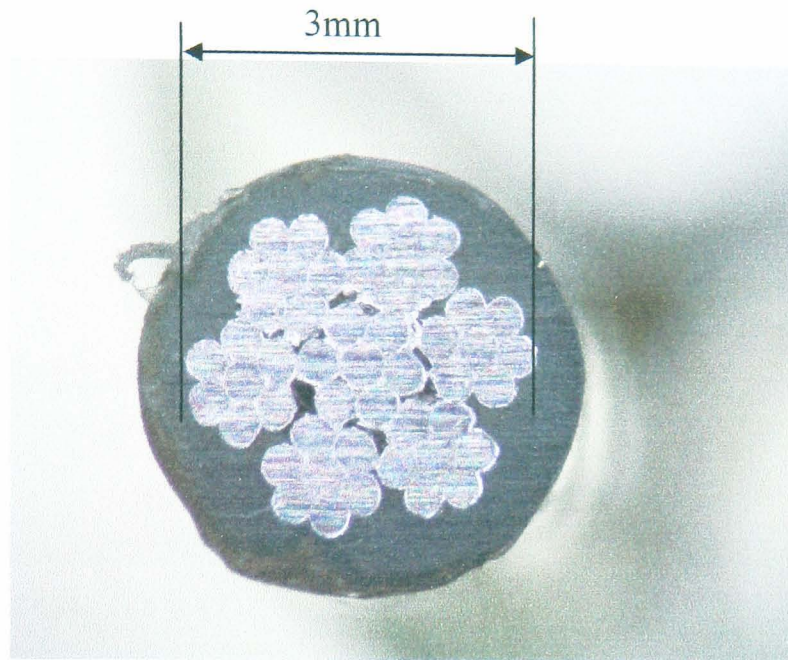


Figure 2.10 Cross sectional photograph of a Jaguar S-Type parking brake cable.

The cable routing is an important consideration when designing the parking brake system as it can affect the efficiency of the brake. It is desirable to have the cable system with a large radius of curvature so that the frictional forces are minimised and the load is transferred from the apply lever to the brake with a high efficiency. The cable is routed through a protective sheath that is fixed to the vehicle chassis. A lubricant is used inside the sheath to reduce friction and increase efficiency.

The cables are connected together using a connecting link, also known as a yolk, which transmits load and displacement from the apply lever to the callipers. A photograph of the cable system and connecting link from the Jaguar S-Type is shown in Figure 2.11. A photograph of the cable attachment point to the calliper is shown in Figure 2.12.



Figure 2.11 Cable system and connecting link



Figure 2.12 Parking brake cable attachment point to the calliper

The cables have end fittings that are crimped onto the cable and allow the cables to be connected to the calliper, connecting link or apply lever. The end fittings are an important part of the system and it is important that they remain attached to the cable under the operating loads.

2.5. Callipers

A brake calliper is a component that is used to press the brake pads onto the disc. There are two main types of calliper, fixed and floating. Fixed callipers use pistons at both sides of the disc and do not move relative to the disc. Floating callipers only

use pistons at one side of the disc. The hydraulic pressure in a floating calliper forces the piston and pad towards the disc and also forces the floating part of the calliper assembly in the opposite direction, which applies the opposite pad. Floating calliper designs offer advantages over fixed callipers because they can be smaller and easier to package inside the wheel. They have fewer leaking points and are easier to bleed than fixed callipers. Floating callipers tend to exhibit more degrees of freedom than fixed callipers and are therefore can be more prone to brake squeal.

A parking brake mechanism can be integrated into a floating calliper that is used to apply the hydraulic brake. This type of calliper is known as an integrated calliper and is generally used on the rear brakes. The parking brake uses a mechanical actuation system, which can be operated independently from the hydraulic circuit. The calliper has an external lever mechanism that is connected to the parking brake cable system. The external lever is connected to an internal piston actuation mechanism, which can be either an actuator screw or a push rod. When the parking brake cable is displaced the actuator screw is rotated and a helical thread on the screw attempts to turn the piston. The piston is constrained from rotation as it is engaged with a notch on the brake pad, which results in the piston being displaced in a normal direction to the disc pushing the pad into contact with the disc. A push rod system has an adjusting cam connected to the calliper lever, which when rotated displaces a connecting rod into the push rod component, which forces the piston to apply the pad. This mechanism is commonly used by calliper manufacturers and has evolved to a more efficient ball in ramp (BIR) design. The BIR mechanism uses three balls as connector rods and three ramps as the adjuster cams. When the lever is rotated the displacement forces the balls to move out of the ramps which actuates the piston as shown in Figures 2.13 and 2.14 A diagram of an integrated calliper assembly is shown in Figure 2.15.

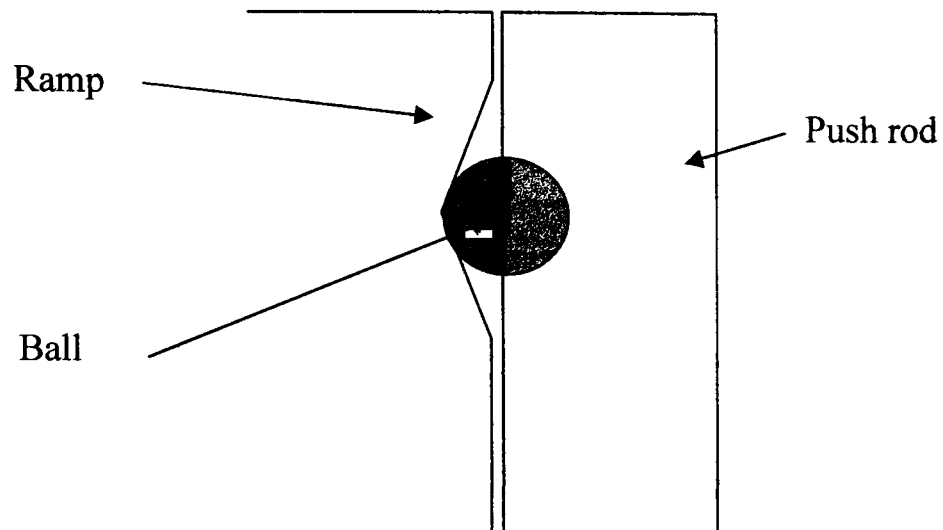


Figure 2.13 Schematic of a ball in ramp mechanism with parking brake not applied

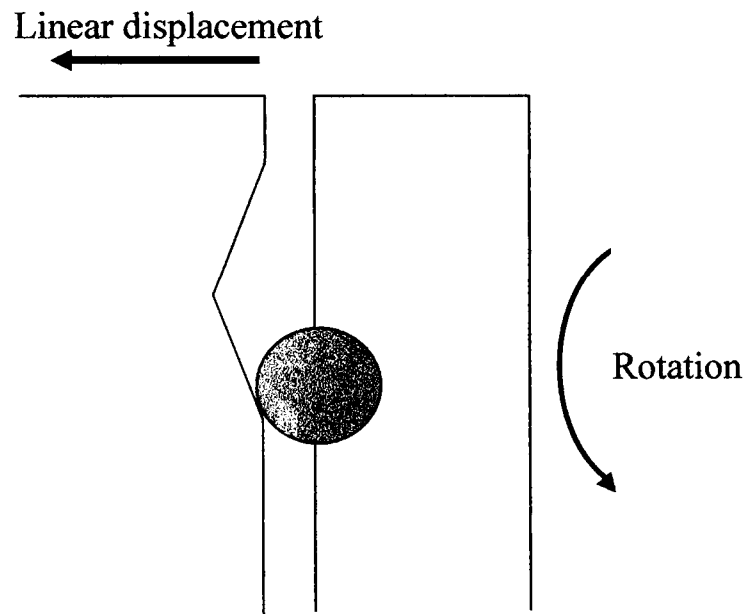
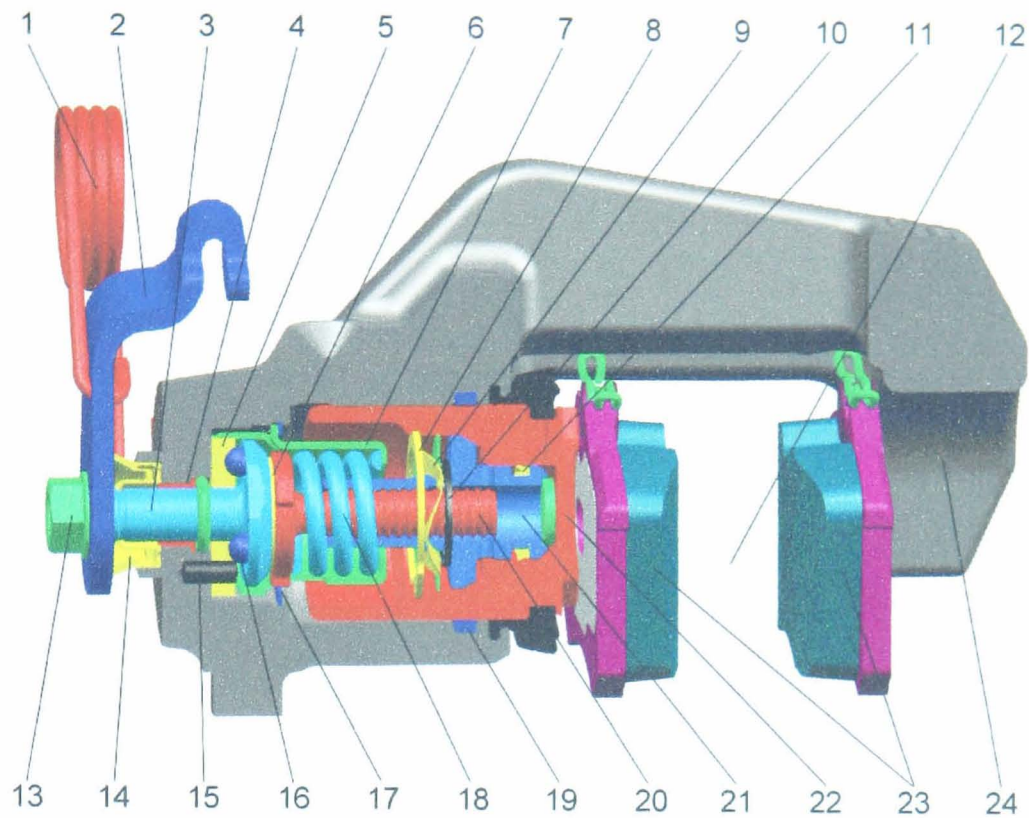


Figure 2.14 Schematic of a ball in ramp mechanism with parking brake applied



- | | |
|--------------------|------------------------|
| 1. Spring torsion | 13. Nut hexagon |
| 2. Lever | 14. Bush |
| 3. Operating shaft | 15. Pin |
| 4. Sleeve | 16. Ball |
| 5. Ramp | 17. Circlip |
| 6. Bearing, plain | 18. Spring compression |
| 7. Spring cage | 19. Seal |
| 8. Circlip | 20. Push rod |
| 9. Washer, spring | 21. Nut adjuster |
| 10. Ball bearing | 22. Piston |
| 11. O-ring | 23. Brake pads |
| 12. Disc | 24. Calliper body |

Figure 2.15 Schematic of a Bosch BIR 3 calliper design [6]

The calliper body material is generally spheroidal graphite (SG) cast iron but aluminium alloy can also be used. The size of the calliper is limited by the packaging volume available inside the wheel. It is desirable to have as much braking force available as possible and therefore the calliper is designed to house as large a pad as possible inside the wheel.

2.6. Pads

A brake pad is a key component found within a disc brake assembly. During a deceleration or drag braking event the friction pair formed by the disc and pad employ dynamic friction to generate in-plane force at the interface which in turn manifests as a brake force in the tyre-ground plane which either slows the vehicle or enables it to proceed at a constant velocity. The kinetic or potential energy, linked to the vehicle forward motion is converted into heat at the friction pair interface and is dissipated to the environment via the process of conduction, convection and radiation. When a vehicle with an integrated parking brake is parked, the same friction pair is required to hold the vehicle stationary through use of static friction present at the friction pair interface. This process does not generate any heat as no relative motion takes place between the pad and disc. However, the foundation brake components may be at an elevated temperature as a result of earlier dynamic braking events.

A typical commercial vehicle brake pad consists of a friction material mounted onto a steel back plate. The friction material is generally fixed to the back plate by heat resistant adhesive, but mechanical retention systems can also be used. Some back plates have a mesh welded to them, which aids adhesion and shear properties. Back plates can also use a Nucap Retention System (NRS), which uses a series of hooks that protrude from the surface of the back plate, as shown in Figure 2.16. The NRS aids the adhesion of the friction material to the back plate and reduces the need for adhesives within the friction material.

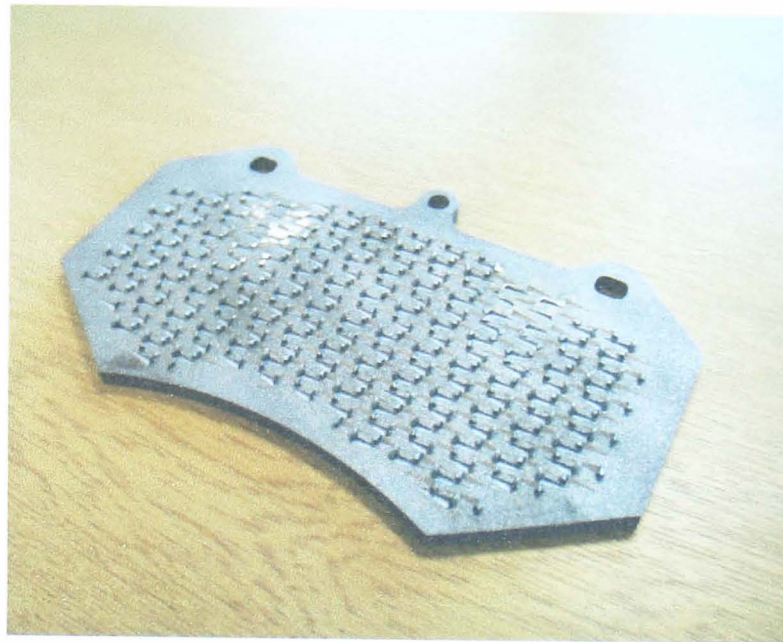


Figure 2.16 Back plate with Nucap Retention System

The pad may also include an under layer, spring, shim, and wear indicator as shown in Figure 2.17. The under layer acts as a thermal barrier between the friction material and back plate. The under layer is typically 2mm thick and can be used to increase the shear capacity of the pad and to absorb vibrations in order to reduced noise, vibration and harshness (NVH). The spring is used to locate the pad inside the calliper. A shim is a component made from different layers of plastic, rubber and metal. It is designed to absorb the vibrations produced by the brake system and reduce NVH. Shims are generally attached to the back plates by cold welding or by using an adhesive. The wear indicator is a sensor that is used to inform the driver when pads need replacing.

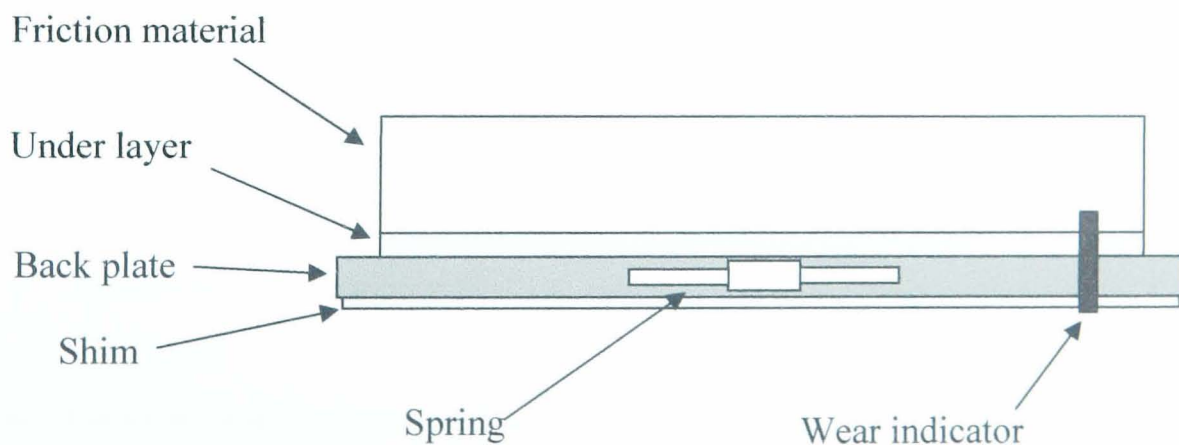


Figure 2.17 Schematic of a brake pad

2.6.1. Friction materials

Herbert Froad is credited with inventing the first brake lining materials in 1897. He used a water driven dynamometer in the hamlet of Combs near Chapel-en-le-frith, Derbyshire, to test his friction material formulations [7]. The demand for his early friction materials on horse drawn carriages led to the formation of the Ferodo company (now part of Federal Mogul), which still supplies friction materials today.

It is traditionally thought by many people, such as Smales [8], that the development of friction materials is a so-called ‘black art’, but this is not necessarily the case. Modern friction materials are developed using highly scientific processes that control performance and quality. The friction material industry has traditionally had a culture of keeping the make up and composition of automotive friction materials secret. Therefore it can be difficult to obtain information in this field. Friction materials are complex multi-component composites made from various constituent ingredients. More than 2000 different materials and their variants are now used in the development and production of commercial friction materials [1]. A typical friction material may contain between 10 and 15 different constituent materials. These constituents have different functions and properties, which when combined within the material matrix produce desirable effects for the friction material. There are many performance criteria that a friction material must satisfy, which include:

- **Low cost.** This is perhaps the main consideration in developing a friction material for the modern automotive market. This applies both to the raw materials and the manufacturing process.
- **High and stable coefficient of friction** for both the static and dynamic case in all possible driving conditions.
- **Low wear** to promote long life spans for the pads and minimize wear on the disc.
- **Adequate shear strength** to avoid the material being detached from the back plate.
- **Good corrosion resistance** to avoid the friction material deterioration due to water, road salt, mud, sand etc.
- **Low squeal or judder generating characteristics** to enhance customer satisfaction.

- **Good pedal feel and travel.** Pads require an optimum stiffness to prevent a spongy pedal feel, or a very stiff harsh pedal feel.
- **Conformance to the counter surface.** The pad requires a good conformance to the counter surface in order to obtain uniform heat generation and wear.
- **Dimensional stability** is required so that the pad maintains its dimensions as closely as possible before, during, and after a brake application.

2.7. Discs

A brake disc is a component that is attached to the wheel of a vehicle and used to apply a torque to the wheel during a braking application. The most common material for a disc brake is grey cast iron, although other materials such as carbon ceramic composites and aluminium-based alloys can also be used. The design of brake discs vary according to the vehicle manufacturer's specifications. Discs can be solid or include extra features such as ventilation, groves, and drilled holes. The ventilation in a disc enhances the dissipation of heat. The groves and drilled holes were originally designed to release the gas produced at the friction surface on racing cars. Modern friction materials are designed to release any gas through the pad and so modern discs are grooved and drilled mainly for cosmetic reasons; although the groves and holes can release trapped water when driving in wet conditions. They also increase the wear rate of the friction material.

It is important that the disc surfaces are parallel with a constant thickness in order to achieve a stable braking torque. Disc thickness variation (DTV) can result in the brake producing cyclic variations in torque output. Forces can be induced by the torque variations which can be felt by the driver in the form of a 'judder' on the steering wheel or inside the vehicle cabin.

Chapter 3

Literature Review

3.1. Introduction

Vehicle rollaway has received little reported attention in industry and in the world of academia. The competitive nature of the automotive industry along with the fact that manufacturers do not wish to highlight potential problems with their products has meant that the only published research on rollaway has been co-written by the author of this thesis [9] and [10]. The first paper [9] describes the development of a rollaway dynamometer facility along with a simple mathematical model of a rollaway event. The model predicted that by reducing the thermal expansion coefficients of the brake pads and disc, the vehicle would be less likely to roll away. The model had reasonable correlation with on-vehicle results but lacked the detail required to fully understand the mechanisms involved during a rollaway event. The mathematical model was improved and presented in [10]. The updated model focused on the parking brake clamp force and was developed using analytical finite element techniques. The model was validated against laboratory based dynamometer results. The paper also describes a stick/slip phenomenon, which occurred prior to the onset of rollaway. This indicates that an instability is present at the frictional interface before the vehicle rolls away.

Since no additional literature is available on the subject of vehicle rollaway, the remainder of this chapter will focus on topics related to rollaway such as parking brake mechanisms, friction pair performance, experimental techniques and system modelling.

3.2. Parking brake mechanisms

This section discusses published literature on parking brake mechanisms relevant to this research project. A detailed description of each of the parking brake mechanisms discussed is given in Chapter 2.

Harding et al [11] investigated instability in handbrake performance which could result in brake lock and in the shock loading of brake components. The research

focused on leading/trailing shoe drum brakes with a strut operated hand-brake. The experimental work was conducted on a vehicle and was complimented with analytical results. The authors found that, in some circumstances, a trailing shoe may operate as a leading shoe and actuate the opposite shoe via a reaction across the strut. This was possible at normal levels of lining friction and can result in brake lock and possible damage to components. The effect can be avoided by ensuring that there is no initial “heel and toe” contact on the trailing shoe, and by reducing the lining arc at the trailing end. The instability effects were found to be more likely in brakes with small diameters.

Elvenkemper [12] used Six Sigma tools to investigate the cause for high torque output variations in a duo-servo drum park brake system. Six Sigma is a system of practices used to systematically improve processes by eliminating defects. The brake system investigated often failed the quasi-static test procedure simulating the brake effectiveness of an un-bedded system under hill hold conditions. The torque output values that he measured ranged between 450Nm and 1400Nm. He tested three different friction material formulations on the parking brake system and found that they all exhibited similar variation in measured torque output. The mean torque output values for the three materials were different but the errors were so large that it was difficult to distinguish between the performances of the different pads. Elvenkemper found that by changing the manufacturing process he could change the measured torque output produced by the same friction material formulation. The manufacturing process used in the study was not described. The pad grinding process was changed and found to have no effect on the measured torque output. Elvenkemper found that a more bedded rotor produced higher torque outputs than an un-bedded rotor and that the grind radius of the linings had a significant effect on the measured torque output. A thinner lining was found to produce higher torque levels than a thicker lining of the same material. By virtue of their design the torque output from a duo servo drum brake is extremely sensitive to changes in the friction level between the lining and drum which could account for the reported variations.

Perkins [13] describes the operation of an electric parking brake (EPB) system. The system described replaces the lever inside the cabin with an electronic switch connected to an electromechanical actuator. The actuator is attached to the parking

brake cable system. The paper is lacking in technical detail and appears to be more of an advertisement for the company sponsoring the research than an academic reference piece. An alternative paper is put forward by Balnus [14] who gives a review of current EPB systems. The EPB can be either a cable puller as described by Perkins [13] or an integrated solution, which uses an electronic motor integrated within the calliper design to apply the parking brake. Balnus describes the features of the EPB and the customers' perceptions of such features. He explains that the clamp force produced by the EPB is controlled by the vehicle's ECU, which is supplied with information including brake temperature and road surface gradient. This suggests that the EPB can be programmed to take rollaway into consideration when parking and therefore eliminate the problem. Balnus explains that the EPB's will become more widespread in the future as they have numerous advantages over manually operated parking brakes. The advantages are that the EPB can generate higher clamp loads at the frictional interface without the need to apply a high input load to a parking brake lever. The EPB does not require the cabin space necessary for a parking brake lever, which can improve the interior styling of the vehicle and reduce the need for strengthening of the vehicle floor. The EPB can reduce or eliminate the need for packaging of cables within the vehicle.

3.3. Friction pair performance

The performance of the friction pair is the most important factor in the overall performance of the brake system. This section discusses the friction level at the frictional interface and the performance of the pads and disc. The friction material used in the brake pad and the constituent ingredients of the friction material are discussed as they have a significant influence on the performance of the brake. The build up of a boundary layer at the interface and the temperature of the components can also affect the brake performance and are discussed in this section.

3.3.1. Friction material

The constituents used in a friction material can be separated into five main groups, binders, fibres, abrasives, lubricants, and fillers. The role of each of these groups in the performance of the friction material is discussed in Sections 3.3.1.1 to 3.3.1.5.

3.3.1.1. Binders

The binder acts as a glue to hold the composite friction material together. Binders form the major organic portion of all modern non-asbestos organic (NAO) friction material formulations, usually representing anywhere between 25 – 40% of the component by volume, or around 5 – 15% by mass [15]. The binder is critical to the performance of NAO friction materials since, more than any other constituent, it dictates the mechanical properties of the pad and in particular, the thermal load capacity prior to failure. If insufficient binder is used, the material can be too weak however if too much binder is used, there can be a drop off in friction at high temperatures, known as fade.

Phenolic resins are typically used as the binding agent for automotive applications [16]. Phenol resin is a type of polymer formed by a condensation reaction between phenol and formaldehyde. This condensation reaction may be initiated by acidic or alkali catalysts, resulting in different classes of phenolic resins. For example, phenolic resins produced using an acid catalyst and reacted with insufficient formaldehyde are called novolac resins [17]. Novolac resins are often modified with rubber to soften them and improve damping properties. The rubber content, type and its dispersion within the matrix control the damping of the brake pad and consequently contribute to one aspect of a formulation's propensity to generate brake noise. Tribological effects of the resin components also have a strong influence on brake noise. The rubber is used as a resin modification, a latex co-binder or as a binder for a premix. Anti-oxidants need to be compounded in with most rubber-based systems. They can also be modified with other additives (Si, B, P, Ti etc) to improve temperature stability.

Phenolic resins require heat to effect the cure, with processing temperatures between 150°C and 250°C. Overall resin content is determined by the granularity of the other components in the formulation; the aim is to provide sufficient resin coverage for mechanical integrity but not enough to fill all the voids in the matrix. Permeability through the brake pad is important for controlling the oxidation at the friction interface during high speed fade conditions. Cured, re-ground resin, called "friction dust" is also used as a control on pad compressibility. Spurr [18] states that, "friction dust is generally based on a phenolic monomer which has a very long hydrocarbon

side chain and makes the polymer rubbery”. The friction dust assists in the manufacture of the material, and improves its friction and wear behaviour.

Phenolic resins carbonise at approximately 450°C [19], and decompose at temperatures above this by charring and evaporation. This decomposition produces fumes that are likely to contain constituents which are poisonous. According to the Occupational Health and Safety administration of the U.S. Department of Labour, formaldehyde is classified as a human carcinogen that can cause nasal and lung cancer, whilst phenol causes liver damage and blindness, amongst other effects that are described in [17].

3.3.1.2. Fibres

Fibres are included in a friction material to maintain mechanical integrity in extreme duty conditions. Jang et al [20] state that fibrous ingredients are primarily used to provide mechanical strength, but they also directly affect the friction performance because they contact the disc surface during braking. The mechanical influence of the fibre content (elastic modulus, compressibility, flexural, compressive and especially shear strength) is considered to be of greater significance than its tribometric properties [21]. In order to impart these physical properties, a minimum concentration of dispersed fibres is necessary such that fibre-overlapping is possible, after which the pad properties are influenced by the following characteristics: [22]

- Fibre volume fraction
- Fibre orientation
- Fibre aspect ratio – influences matrix-fibre load transfer
- Fibre / binder adhesion – influences matrix-fibre energy transfer
- Fibre strength
- Fibre morphology / size – to minimize stress concentrations

Different fibres are usually selected in a friction material formulation as they provide different properties. Carbon fibres provide high temperature stability of the friction coefficient, aramid fibres improve strength and wear resistance, and glass and ceramic fibres reduce the thermal conductivity [23]. Steel fibres, aramid (“Kevlar”) and various mineral fibres are common but Smales [8], states that.

“Kevlar is too expensive and can only be used in very low concentrations”. Glass fibre is uncommon in friction materials used in conjunction with disc brakes as it tends to melt on to the disc surface causing severe fade and NVH problems.

Friction material formulations used in conjunction with a disc can be classified into three groups depending on the nature of the fibrous reinforcement. Formulations without steel fibre, using instead both aramid and mineral fibres, such as potassium titanate, are known as non-asbestos organic (NAO) friction materials. These generally contain only small amounts of soft abrasives and produce typically very low pad and disc wear with moderate temperature stability and integrity. Formulations with up to 10% steel fibre are known as “Low Steel” formulations. These have higher abrasive contents and are typically used for European vehicle applications where high speeds and temperatures can be expected. Formulations with high steel fibre or iron powder contents are known as “Semi-Metallics”. These formulations are generally resin, steel and graphite component formulations with few other additives being used. Fade resistance, thermal conductivity and brake noise is poor but pad and disc life is good particularly at high temperatures. Typical applications are light trucks and Sport Utility Vehicles (SUV’s) for the North American market.

3.3.1.3. Abrasives

Bissett [23] explains that abrasive particulates are used within a friction material in order to increase the general level of dynamic friction. Coarse particle sizes of hard abrasives are generally not used due to the adverse effects on disc wear. Motor racing pads are however the exception to this rule of thumb because the disc wear is not of primary concern. The abrasive can be used to clean up the disc surface. “Polishing” grades of alumina are common for general purpose pads. Hard sands, such as zirconium silicate, are used in a range of sizes. Small amounts of hard abrasives, such as fused alumina or silicon carbide are used to give “bite” to the initial part of the brake application. Other common abrasives include chromia, silica magnesia, and magnetite. Optimised formulations generally contain mixed abrasive systems to get the best compromise between friction and wear.

Different abrasives have optimum effects in different temperature zones. As the temperature at the frictional interface increases, changes to the organic matrix result in a lowering of friction, or fade, as a result of decomposition, or merely softening, of the binder, [24]. Therefore friction material formulations typically contain several different abrasives, each being effective at a particular temperature. A suitable blend of abrasives will result in a continuous but approximately constant friction level throughout the required temperature range.

3.3.1.4. Lubrication

Lubrication content enables the engineer to maintain the balance between pad and disc wear at an acceptable level without causing adverse effects on the friction characteristics of the friction pair. Both natural flake and synthetic granular graphite are in common use [23]. Controlling the ratio of these two types of graphite is a useful strategy for controlling the compressibility of the pad. For lubrication at higher temperatures, metal sulphides are used with molybdenum disulphide or tin disulphide. Antimony disulphide has been used extensively in the past but is being replaced due to environmental concerns.

Solid lubricants aid the formation of the third-body layer at the frictional interface by breaking down alongside the softer matrix material. They provide frictional stability over the range of operating temperatures experienced by the brakes. At lower temperatures, materials such as graphite are most effective, while at higher temperatures materials such as copper can be beneficial [24]. The effect of the lubricant depends on the amount added and there is an optimum amount of lubricant for different requirements. For example, the lubricants used in racing pad formulations can be used to optimise the frictional stability at higher temperatures. Lubricants are typically added in small amounts as they reduce the load bearing capacity of the friction material.

3.3.1.5. Fillers

Fillers are generally low cost additives that are added in relatively high proportions as bulking agents. They can also be used to enhance the performance of the friction material. Since fillers can be added to relatively high inclusion levels, they can have a significant effect on the performance of a friction material [24].

Mineral powders are used as fillers mainly to reduce cost. However, they also have important tribological characteristics in that they reduce wear by forming in-organic glass. They influence the overall friction stability of the interface. The glass forming nature of barytes (barium sulphate) is thought by Bissett [23] to play a major role in the friction stability of NAO formulations. The addition of barites aids to reduce high temperature wear and increase the density. Granular inorganic fillers, for example mica or vermiculite, have strong synergistic effects with other formulation components to influence friction and wear. Petroleum coke is also a common filler often used in large amounts in brake pads. It has reasonable basic friction stability and its porous nature helps gas flow thorough the brake pad under fade conditions. It is available and used in a wide range of particle sizes. Hildred [25] states that, “some fillers can also be utilised to help condition the pH levels in order to prevent corrosive adhesion attack of the rotor”. This is a reasonable assumption to make but he does not present any evidence to quantify the reduced corrosion.

3.3.2. Friction level

Jang et al. [26] investigated the frictional characteristics of friction materials containing different amounts of antimony trisulfide (Sb_2S_3) and zirconium silicate ($ZrSiO_4$). Antimony trisulfide is generally classed as a lubricant and zirconium silicate is classed as a hard abrasive. They used a brake dynamometer with a single piston floating calliper to conduct drag (constant speed) and stop (decreasing speed) tests. They measured the change of the dynamic friction coefficient, torque variation and the level of wear. They found that the friction level generally increased to a temperature between 250°C and 350°C (depending on the formulation) and then decreased for further increases in temperature. By increasing the level of $ZrSiO_4$ they found that the friction level increased and its variation with temperature also increased. They found a formulation with lower $ZrSiO_4$ and increased levels of Sb_2S_3 had a lower friction coefficient which was stable with temperature. Jang et al. attributed this to the lubricant which enables a third body layer to be formed that increases the friction stability. The third body layer reduces the effect of the hard abrasives in the formulation which reduces the friction level.

Tarr et al. [27] investigated the friction characteristics of phenolic resin based friction materials against grey cast iron as a function of normal load and temperature. They used a single piston sliding calliper, a disc with a thermocouple located at the centre of the wear track, semi-metallic and organic friction materials. They calculated the friction coefficient by applying a constant hydraulic pressure in the calliper, then increased the torque on the disc until rotation occurred. All the tests were conducted after a “break-in” period, but no description of the break-in (bedding) procedure is given. They found that the static friction force, F , obeyed the following general equation:

$$F = \mu N^{\alpha^{(T)}} \quad (3.1)$$

Where: F = static friction force (N)
 μ = static coefficient of friction
 N = normal load (N)
 $\alpha^{(T)}$ = temperature dependant constant

With the value of a varying between 1.03 and 1.41 for the organic friction material and between 1.10 and 1.37 for the semi-metallic friction material.

Jang et al. [28] investigated the effect of metallic fibres upon friction and wear performance of various brake friction couples. They used a small-scale friction tester with a hydraulic press to apply the normal load. A Labview data acquisition system was used to record the test results. Samples of friction materials with dimensions of 2cm x 2cm x 1cm were tested. They measured the dynamic friction level as a function of temperature for friction materials containing copper fibres, low carbon steel fibres and aluminium fibres against a grey cast iron rotor. The friction materials containing copper fibres and steel fibres maintained a relatively constant dynamic friction level. The friction material containing aluminium fibres showed a large reduction of the friction level with increasing temperature. Jang et al. report that this is due to the softening of aluminium at temperatures above 200°C and that the temperature at the interface can be much higher than the measured temperature which can result in the aluminium fibres melting.

3.3.3. Disc

Cast iron is a common material used in the design of brake discs. Mace et al [29] explain that the graphite flake arrangement of grey cast iron microstructure provides the high thermal conductivity requirements of brake discs, discussed in Chapter 2. although with the brittle characteristics of cast iron. Therefore the design of cast iron brake discs is a compromise between a thermally efficient design to reduce the operating temperature and a design with a controlled tensile stress level to prevent crack failure with as little mass penalty as possible.

Metzler [30] explains that, “the brake rotor has been steadily developed since the first disc brakes were introduced in the late 50’s”. In his research he discusses the development of cast iron brake discs. He explains that grey cast iron is the material of choice for disc manufacturers due to its greater thermal conductivity, lower modulus of elasticity and that it is thermally stable above temperatures of 500°C. He found carbon and silicon carbide reinforced cast iron to be unsuitable due to the “unacceptably high costs”. He explains that the disc and pad manufacturers must work together to develop the best materials combination.

3.3.4. Transfer films (third body layers)

Mace et al. [29] studied the effects of bedding in on grey cast iron brake discs to identify causes of crack propagation and failure. They found that the disc undergoes a light heat treatment during the bedding procedure which toughens the disc and reduces the likelihood of cracking. They found the flake structure of carbon to be unaffected by the heat treatment but the pearlite matrix breaks down under the high interface temperatures. During the breakdown of pearlite, the carbon particles near graphite flakes agglomerate around the latter, leaving large areas as ductile ferrite around graphite/carbon couples which is thought to greatly increase the resistance to crack propagation.

Wirth et al [31] present evidence which relates friction characteristics of the brake pair to transfer film chemistry. They found that the friction characteristics of asbestos free composites rubbing against grey cast iron were influenced by the composition of the transfer layer and to a lesser extent by the transfer film coverage.

They found that, “the addition of black iron oxide to the friction material destroyed the transfer layer”.

Wirth et al [32] studied the influence of friction material composition on transfer film chemistry and film stability during rubbing of simple asbestos free friction materials against grey cast iron. They used analytical scanning electron microscopy, X-ray diffraction and X-ray photoelectron spectroscopy to study the characteristics of the transfer film. They found that the friction characteristics of the pad friction material against grey cast iron were influenced to a great extent by the composition of the transfer layer. The friction performance was found to be independent of the transfer film thickness and transfer film topography.

3.3.5. Thermal effects

Okamura et al [33] studied the thermal behaviour of reverse vented disc brakes with varying geometries and discs both with and without holes in the neck. The ‘neck’ of a disc brake is identified in Figure 3.1. They found that discs with larger holes in the neck cooled faster than discs with smaller holes. The discs with smaller holes heated up more quickly than those with larger holes and the discs with larger holes exhibited less coning than discs with smaller holes. They found that discs with larger offsets and thicker friction plates reduced coning.

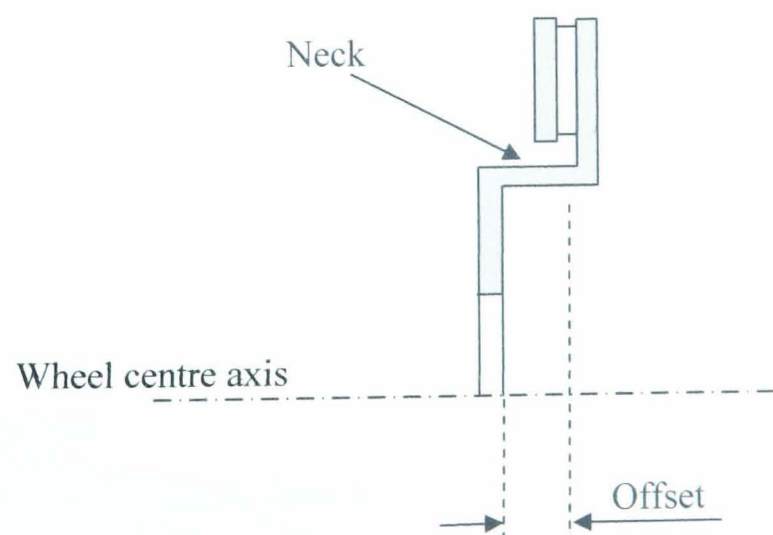


Figure 3.1 Location of the ‘neck’ on a reverse vented brake disc

Valvano et al [34] also looked at disc coning using an analytical method to predict the thermal distortion of brake discs. They modelled a disc with the cooling veins on the inboard side of the disc as opposed to the outer side of the disc, known as reverse vented discs, like the work conducted by Okamura et al [33]. Brake discs with the cooling veins on the inboard side of the disc are generally better at cooling the disc than reverse vented discs due to the way the air flows over the disc. Reverse vented discs are generally better for reducing disc coning and stress in the disc due to them having a longer top hat section. A diagram of an inboard vented disc brake is given in Figure 3.2. The Jaguar S-Type uses an inboard vented brake disc.

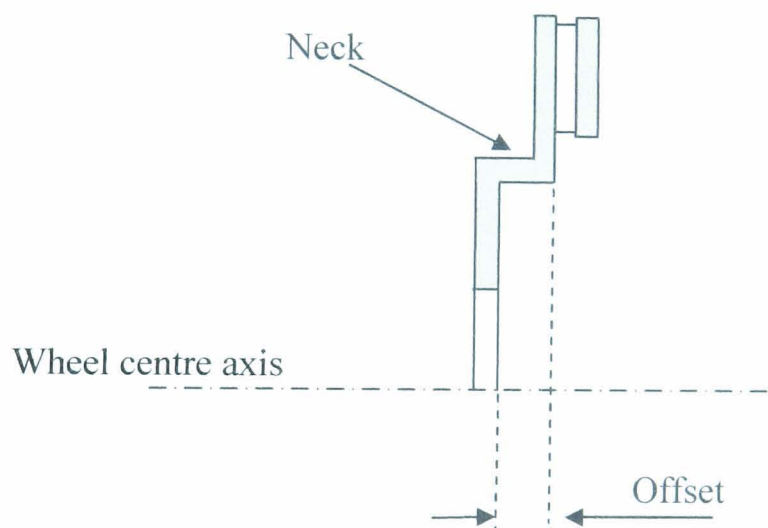


Figure 3.2 Schematic of an inboard vented disc brake

3.4. Experimental techniques and testing methods

Newcomb and Spurr [35] explain that, “testing is absolutely vital during the development of a new friction material”. They explain that the major difficulty in brake friction material testing is to decide what the test conditions should be. This is because vehicles are driven over many different roads and terrains with varying conditions. The drivers of the vehicles also have “varying skills and very different temperaments”.

Dubensky [36] presented two experimental techniques that were used to measure the brake rotor surface temperature and the pressure distribution on the rotor caused by flexibility in the rotor and calliper mounting system. An inframetric 510 scanner (thermal imaging camera) was used to obtain the temperature distribution in the rotor and the images were calibrated against measurements taken from thermocouples. He described the tests as requiring minimal preparation time. The pressure distribution between the rotor and pad was measured using prescale pressure sensitive paper. The prescale paper provided a record of the pressure distribution at the frictional interface for the static case. The results he obtained can be used as inputs and validation tools for finite element models.

Fieldhouse et al [37] measured the dynamic centre of pressure during a braking event to investigate how the centre of pressure affects noise generation. They achieved this by embedding a pressure sensitive film within the pad. The pressure sensitive film was bonded to a smooth pressure plate. A volume of friction material was removed from the pad and the pressure plate was fitted into the recessed volume. A volume of friction material was then used to fill the remaining recessed volume to maintain the original pad geometry. The assembly is only capable of recording the pressure distribution under one condition and therefore many repeat tests are required to generate the pressure distribution as a function of different brake parameters such as applied pressure and friction level. The authors found the results to be dynamic and as a result the centre of pressure moves constantly as the pad wears and pressure varies. Low brake pressures led to larger instabilities.

Harding et al [11] conducted handbrake instability tests and found their results to be of a fugitive nature and non-repeatable. They describe the dynamometer tests as, “not being a successful means of investigation”, and their preferred experimental method was on-vehicle tests. The main reason for the unsuccessful dynamometer tests appears to be that the hand brake was actuated using air pressure or a hydraulic system which produces different application characteristics to those produced by a cable and lever system. Their work suggests that the complete parking brake apply system is required for a successful dynamometer test program.

Yuhas et al [38] used an ultrasonic measurement process to measure the spatial variation of the ultrasonic velocity and attenuation of several brake pads. They correlated the ultrasonic results to results obtained by conventional compressibility tests to obtain the Young's modulus, shear modulus and Poisson's ratio of the pads as a function of load. The influence of the steel back plate was removed so that the results are only dependent on the friction material and under layer. In measuring the elastic properties they found variations of more than 10% for samples of the same friction material. They state that multiple measurements need to be taken to obtain the sample average due to the variations encountered. They found reasonable correlation between the results obtained through the ultrasonic measurement and conventional compression tests. The elastic modulus was found to be dependant on the applied normal load.

3.4.2. Legislation and industrial testing

The functionality of the parking brake system is required to satisfy current legislation and may also be required to meet additional standards specified by vehicle manufacturers. ECE regulation 13H [39] specifies that vehicles at gross weight must be capable of being held on a 20% hill with a maximum force of 400N applied at the hand lever or 500N applied to the pedal. They also state that parking brake must be capable of decelerating a vehicle from an initial speed of 30km/h at a rate of at least 1.5m/s^2 . These legislations ensure that the driver of the vehicle is capable of applying the required force to park the vehicle. The current ECE regulations do not include any parking brake tests that consider the phenomenon of rollaway.

Vehicle manufactures have developed tests to ensure that their vehicles satisfy the current ECE regulations [39]. Some vehicle manufacturers have also developed tests to ensure that their vehicles do not roll away. This shows that vehicle manufacturers are aware of the potential problem of rollaway. Ford has developed a parking brake test to ensure that their vehicles satisfy current ECE regulations. The test requires the vehicle to be parked on a 30% gradient by applying a load of 400N to the parking brake lever and it is deemed to pass the test if the vehicle remains stationary. The test does not take into account the temperature of the brake. Federal Mogul has

developed a test that does take the brake temperature into consideration called the Federal Mogul 20minute Hot Hill Hold test. The test requires the vehicle to be parked on gradients of 30%, 16% and 12% with the disc at an initial temperature of 50°C, 100°C, 200°C and 300°C. The test requires the driver to apply the parking brake until the vehicle is held on the gradient without the use of the foot brake. The parking brake is then applied further until the next available notch on the ratchet mechanism is engaged. The brake is then allowed to cool for 20 minutes. During this time the driver of the vehicle estimates the magnitude of any movement of the vehicle. If the vehicle moves more than 1m it is deemed to fail the test. The author considers that the Federal Mogul Hot Hill hold test is better than the Ford test because it considers the temperature of the brake; however it could be improved by replacing the displacement estimates made by the driver with a sensor to record displacement. The test could also be improved if the duration of the test was extended to allow the brake to cool to ambient temperature rather than just 20 minutes of cooling. A summary of the Ford and Federal Mogul 20minute Hot Hill Hold test procedures are given in Appendices A and B.

3.5. System modelling and simulation methods

3.5.1. Finite element modelling

Elvenkemper [12] produced a finite element model of a duo-servo parking brake system. His model included the rotor and the brake linings. He used his model to calculate the torque output produced by the parking brake system for varying parameters. The parameters that were varied were the Young's modulus of the friction material, the coefficient of static friction at the frictional interface and the thickness of the friction material on the brake linings. He found that the Young's modulus had a low influence on torque output. The friction material thickness had a large effect on torque output with thinner materials producing a reduced torque variation than thicker materials.

Liu et al [40] produced a finite element model of a brake pad in an attempt to reduce high frequency brake squeal. The properties of the pad used in the model were measured using ultrasound equipment. The results from the model were validated against dynamometer results and were found to have, "excellent correlation". The

FE model was simple and easy to build and modify with only the friction material information required.

3.5.2. Friction pair modelling

Aleksendric et al [41] employed a neural network technique to predict the cold performance of friction materials under prescribed testing conditions. The neural network model is an excellent approach to modelling friction material performance. In order for the model to function correctly a large amount of data is required to setup the neural networks. The model must also employ a suitable learning algorithm to simulate artificial intelligence. Aleksendric et al [41] investigated 15 different neural network architectures to establish which one would be best suited to their model. They found that a one-layered neural network trained by a Bayesian algorithm showed the best results. The model requires accurate data about the friction material properties and so many sets of measurements are required to characterise the materials to deliver a high level of statistical reliability which could be a significant constraint of the model.

Busso et al [42] attempted to use a neural network technique to predict the performance of friction materials. They encountered problems because some of the input variables are categorical and could not be processed within the framework. Instead they adopted a rules based ensemble learning approach which they demonstrated to be a powerful tool for the design of friction materials. They showed that their model was capable of predicting the performance of friction materials with an error of less than 5% which is the same order as the dynamometer tests' intrinsic deviation. The model allows the process of simplifying a mixture while maintaining performance to be speeded up by reducing the number of experimental trials required. This saves the friction material formulators both time and money. The model presented is only designed to investigate frictional properties but it could be extended to simulate properties such as wear and comfort.

A successful model of friction materials, such as the ones being developed by Aleksendric et al [41] and Busso et al [42], would be a significant development for

the friction material formulator. Although the model would not eliminate experimental testing it would significantly reduce the number of tests required saving both time and money.

Ostermeyer et al [43] developed a 3 dimensional surface topography model of a brake pad. They state that, “Coulomb’s friction law is good as a first approximation but not realistic for brake systems”. A theory was developed with the dynamic interaction of friction and wear at the boundary layer. The dynamic friction law was extended to a 3 dimensional cellular automation model to describe the surface topography. The model includes hard particles in a softer matrix which when at the surface of the pad change the local friction and the local temperature can reach over 1300C. The model takes into account growth and destruction of particles and when a hard particle reaches the surface the wear next to the particle in the direction of disc rotation is reduced due to the hard particle protecting the matrix. After a period of time the hard particle is destroyed leaving a hill of softer matrix which exhibits high wear until it is eventually smoothed.

3.6. Summary

The literature review conducted for this research has highlighted the need for work on vehicle rollaway to be undertaken as there is currently no research available in the open literature other than that previously presented by the author of this thesis. The research on brake testing has highlighted the fugitive nature of the results and that significant variations in the results can be common. The work conducted by Harding et al [11] suggests that the dynamometer for the present research should include the complete parking brake system to fully replicate the on-vehicle system configuration.

The investigation into friction material formulations has identified materials that may have an effect on the friction level developed by the brake. Jang et al [26] have found that the addition of hard abrasives can increase the dynamic friction level of the brake. This research can be used in this thesis to investigate if the addition of hard abrasives can also increase the static friction level of a brake as this can influence the likelihood of rollaway.

The third body layer developed at the frictional interface was found to influence the friction level. Therefore bedding should be conducted for the test work in order to generate a stable and consistent friction level in order to reduce variations in the results.

Chapter 4

On-Vehicle tests

4.1. Introduction

To fully understand the phenomenon of vehicle rollaway it is important to observe a rollaway event occurring on a vehicle parked on a gradient. The literature review in Chapter 3 has highlighted the need for tests to be conducted on a vehicle to evaluate the performance of a parking brake system under service operation conditions. This chapter discusses the on-vehicle tests that have been conducted for this research on two vehicles with parking brake systems believed to exhibit rollaway tendencies. The author of this thesis was responsible for designing the test procedure, which is described in Section 4.3. The test vehicles used for this research were driven by an experienced Federal Mogul test driver with the author of this thesis in the passenger seat overseeing the process and controlling the data logging equipment. The vehicles and brake system components investigated in this chapter are discussed in Section 4.2. The test procedures used are discussed in Section 4.3 and the results are presented in Section 4.4.

4.2. Vehicles and Components

This section describes the vehicles that have been used for this research along with the different brake system components that have been investigated.

4.2.1. Vehicles

Two vehicles have been used for this research project that have integrated rear callipers and are believed to exhibit rollaway. The main vehicle used throughout the project is a Jaguar S-Type, shown in Figure 4.1. A Jaguar X-Type has also been used to evaluate the performance of two different callipers that could not be installed on the Jaguar S-Type. The original equipment (OE) installed on the Jaguar S-Type has been used to characterise the performance of the parking brake system designed by Jaguar. The OE parking brake system consists of the parking brake lever, three parking brake cables, a cable connecting bracket, two integrated callipers, two sets of brake pads and two discs. A diagram of the parking brake system layout is shown in Figure 4.2. The parking brake lever has 11 notches on the ratchet mechanism to

fix the cable displacement and an auto adjustment mechanism to reduce slack in the cable. The parking brake cables are 3mm in diameter and are protected by a lubricated sheath. The length of the front (primary) cable is 1.04m and the two rear (secondary) cables are 1.35m long. The cable connecting bracket, also known as the yoke, connects the cable from the parking brake lever, Cable 1, to the two cables attached to the rear callipers, Cables 2 and 3, and transmits an equal load from Cable 1 to Cables 2 and 3. The rear callipers have an integrated parking brake mechanism which uses a ball in ramp mechanism to apply the piston. The piston has a diameter of 42.8mm and has a threshold pressure of 0.5bar. The OE pads are manufactured by Federal Mogul and are referred to as Pad 1 throughout this research. Pad 1 consists of a 5.6mm thick steel back plate, a 2mm thick under layer and a friction material of 9.4mm thickness giving the pad a total thickness of 17mm. The dimensions of the pad are given in Figure 4.3. Three additional pads are assessed in the on-vehicle tests and are described in Section 4.2.2. The disc is manufactured from cast iron and has internal cooling vents. The dimensions of the disc are given in Figure 4.4 and a cross sectional photograph of the disc is given in Figure 4.5. The rubbing radius of the centre of the pad on the disc is 125mm. A photograph of the Jaguar S-Type rear brake assembly is shown in Figure 4.6. The gross vehicle weight of the Jaguar S-Type is 1900kg. The rolling radius of the vehicle tyres is 317mm and the wheel base dimensions are given in Figure 4.7.



Fig 4.1 Jaguar S-Type used for the on-vehicle tests

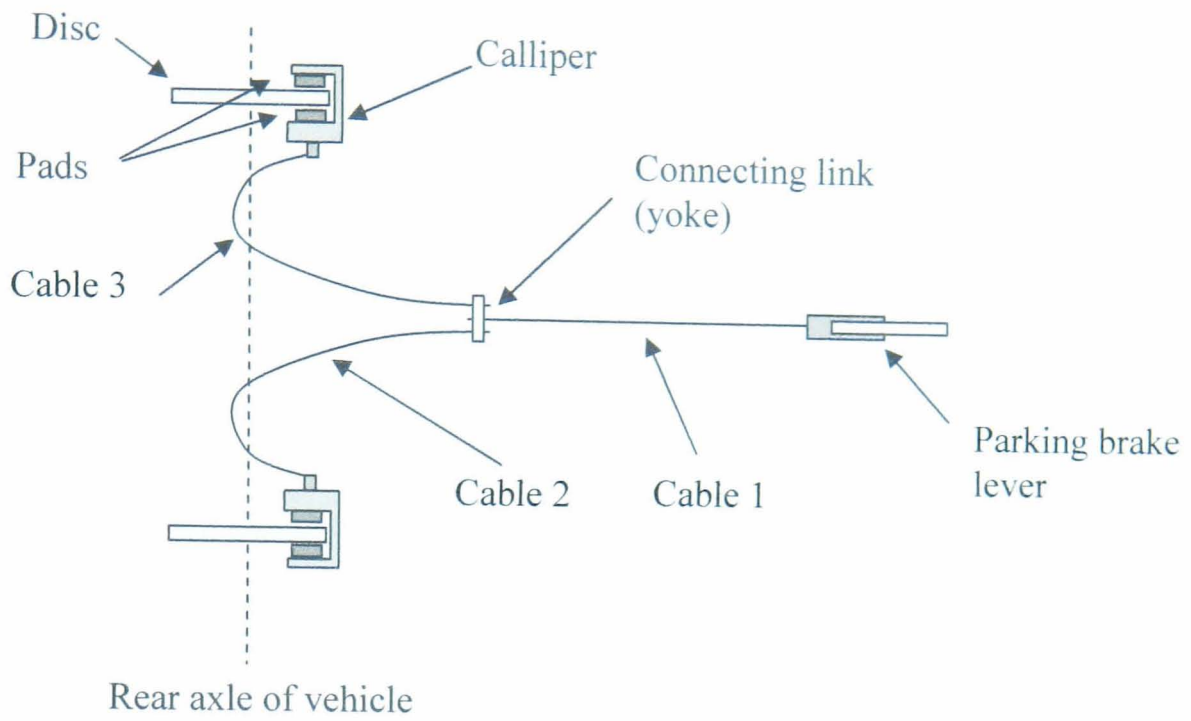


Figure 4.2 Layout of Jaguar S-Type parking brake system

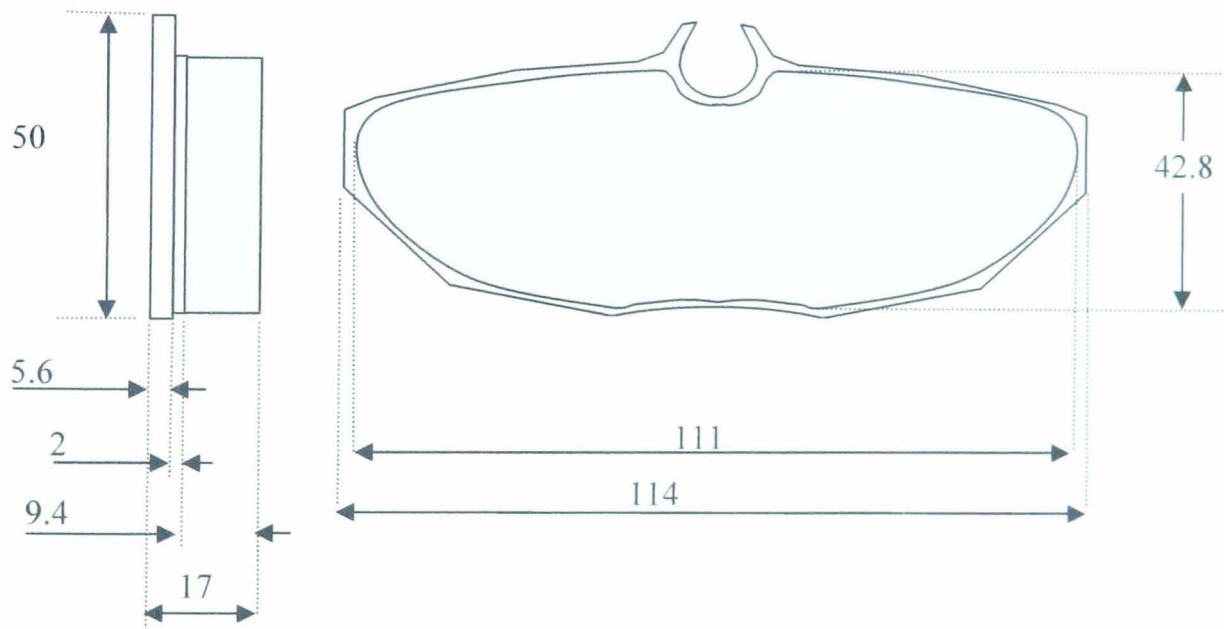


Figure 4.3 Dimensions of the Jaguar S-Type OE pad given in millimetres (not to scale)

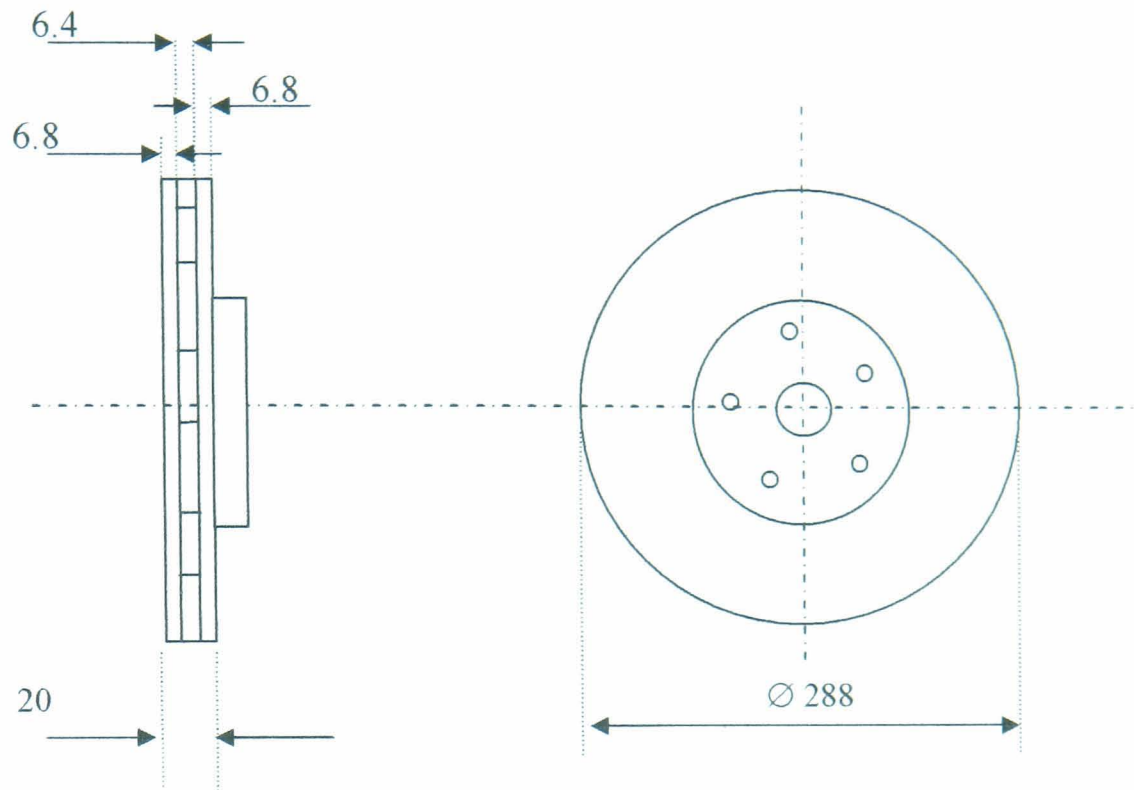


Figure 4.4 Dimensions of the Jaguar S-Type rear disc given in millimetres (not to scale)

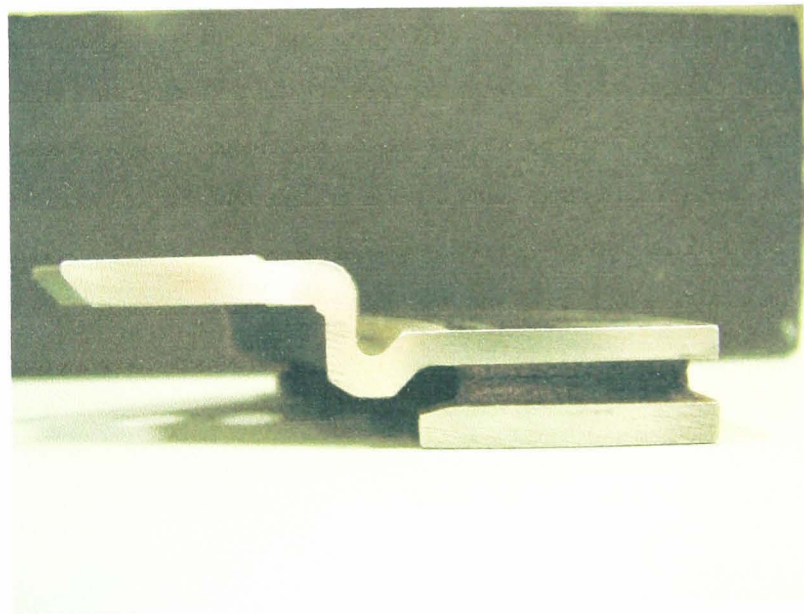


Figure 4.5 Cross section of Jaguar S-Type rear disc



Figure 4.6 Jaguar S-Type rear brake

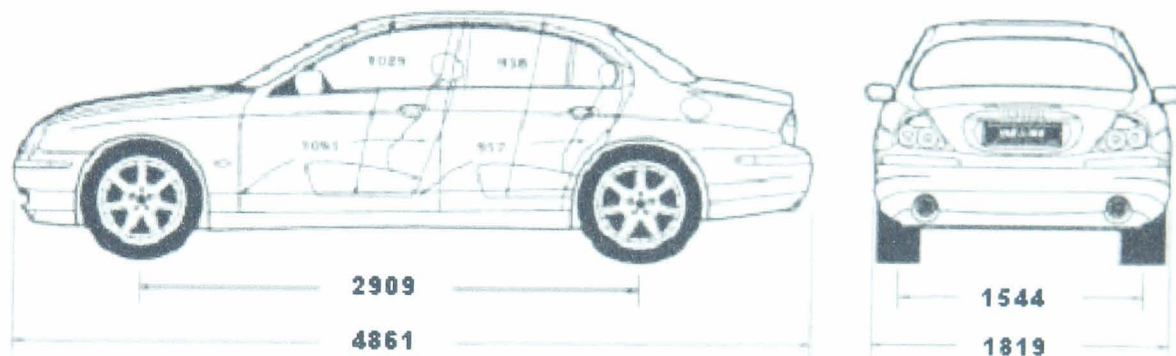


Figure 4.7 Jaguar S-Type wheel base dimensions [46]

4.2.2. Pads

Four different sets of brake pads have been investigated during the on-vehicle evaluations which include the Jaguar S-Type OE pad (Pad 1) and three additional brake pads, labelled Pads 2 to 4. Pads 2 to 4 were formulated and manufactured by Federal Mogul to assess the effect of pad composition on rollaway propensity. The friction materials used in Pads 2 to 4 were formulated from different constituent ingredients from those used in the formulation of Pad 1. This was done to vary the properties of the different pads to see if the performance of the vehicle was affected. The properties of pads that were varied for this research include the stiffness and thermal expansion coefficient. The dimensions of Pads 2 to 4 are identical to the dimensions of the OE pad shown in Figure 4.3.

4.2.3. Callipers

Three different sets of callipers have been used for the on-vehicle evaluations, labelled Callipers 1 to 3. Calliper 1 is the OE calliper used in the Jaguar S-Type parking brake system. Two additional callipers were selected, Callipers 2 and 3, to compare the performance of different calliper materials and designs. Details of the callipers used in this research are given in Table 4.1. The values given in the table have been obtained from the work conducted by Ioannidid [44].

Calliper bridge	1	2	3
Manufacturer and Model	TRW C48-20/10 BIR	Bosch BIR3	Bosch BIR3
Material	cast iron	cast iron	Aluminium
Material density (kgm^{-3})	7850	7850	2700
Material Young's modulus (GPa)	200	200	70
Material thermal expansion coefficient (K^{-1})	10.8×10^{-6}	10.8×10^{-6}	22.2×10^{-6}
Calliper mass (kg)	4.25	3.5	2.2

Table 4.1 Details of the callipers used in the research

It was originally thought that the two Bosch callipers would be identical in design but on inspection it was noticed that the designs were slightly different. The cast iron calliper has fingers of 13mm thickness and the aluminium calliper has fingers 25mm thick. The varying calliper finger thickness could be due to the calliper designer modifying the design to compensate for the varying material properties and ensure that both designs had an equal stiffness. The aluminium calliper would be preferable to vehicle manufacturers due to its reduced weight which will enhance vehicle performance and minimise the un-sprung mass.

4.3. Methods

The on-vehicle test procedure used for this research was adapted from the Ford parking brake and Federal Mogul 20 minute Hot Hill Hold test procedures that are discussed in Chapter 3 and Appendices A and B. The test consists of heating the rear brakes to a specified temperature by driving the vehicle on a test track and applying

the brakes. Once at the correct temperature, the vehicle is driven onto the test gradient and the parking brake lever applied to the point where the vehicle is held on the gradient without the use of the hydraulic foot brake. This is known as the ‘hold’ condition. The parking brake lever is then applied further until the next available notch on the ratchet mechanism is engaged, known as the ‘park’ condition. The brakes are allowed to cool to a temperature 10°C above ambient and any movement of the vehicle during this time is recorded. The vehicle is deemed to fail the test if it moves more than 1m down the gradient. The full test procedure used for the on-vehicle tests is given in Appendix C.

All of the on-vehicle tests were conducted at the Federal Mogul proving ground in Derbyshire which has straight roads and gradients of 8%, 16.6% and 25%. All of the surfaces were smooth tarmac and all tests were conducted in dry or slightly damp conditions. Tests were conducted with the pads in a bedded and un-bedded condition. The bedding procedure consisted of 200 brake stops with the vehicle decelerating from 60km/h to 0km/h with a constant brake pressure of 30bar applied. The speed of the vehicle was measured using the vehicle’s speedometer and the brake line pressure was measured with a pressure sensor installed in line with the hydraulic circuit. The temperature of the rear brakes was measured using two K-type rubbing thermocouples located at the mean rubbing radius of the pad on the disc as shown in Figure 4.8. The normal load applied to the parking brake lever was measured using a load cell mounted between the parking brake lever and a handle used to apply the load. The driver of the vehicle must pull the handle to apply the parking brake and the load perpendicular to the parking brake is measured by the load cell. A diagram of the parking brake lever, load cell and applying handle is shown in Figure 4.9. A displacement transducer was used to measure the angle of the parking brake lever. A photograph of the parking brake lever on the Jaguar S-Type is shown in Figure 4.10. Any movement of the vehicle during a rollaway test was measured using a shaft encoder connected to one of the rear wheels. A microphone was used to measure the sound pressure level (SPL) of any noise associated with the test and was located on the passenger seat as shown in Figure 4.11. The SPL was filtered to record noise between 70dB and 500dB because any noise below 70dB could not be distinguished from the background noise. All of the

recorded data was logged using a Federal Mogul data acquisition system installed in the vehicle.

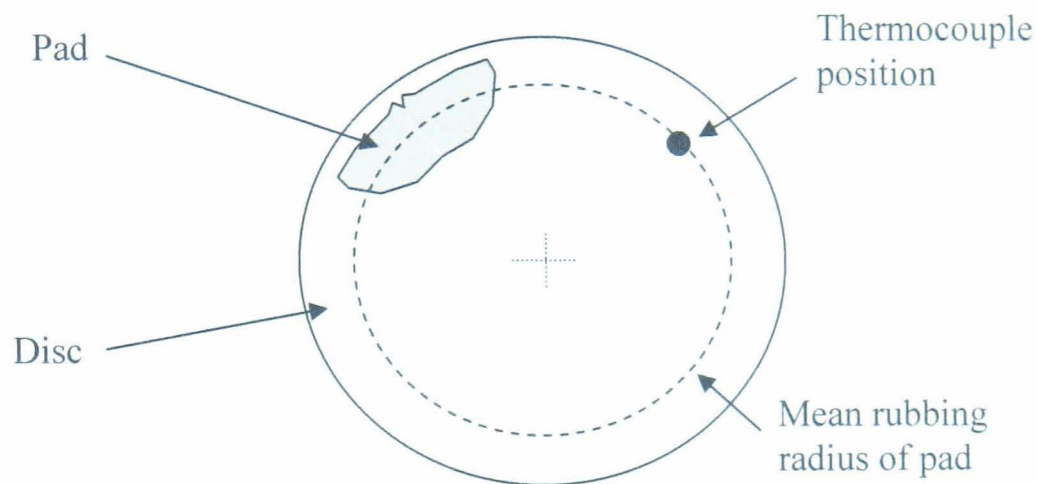


Figure 4.8 Position of the thermocouple on the disc

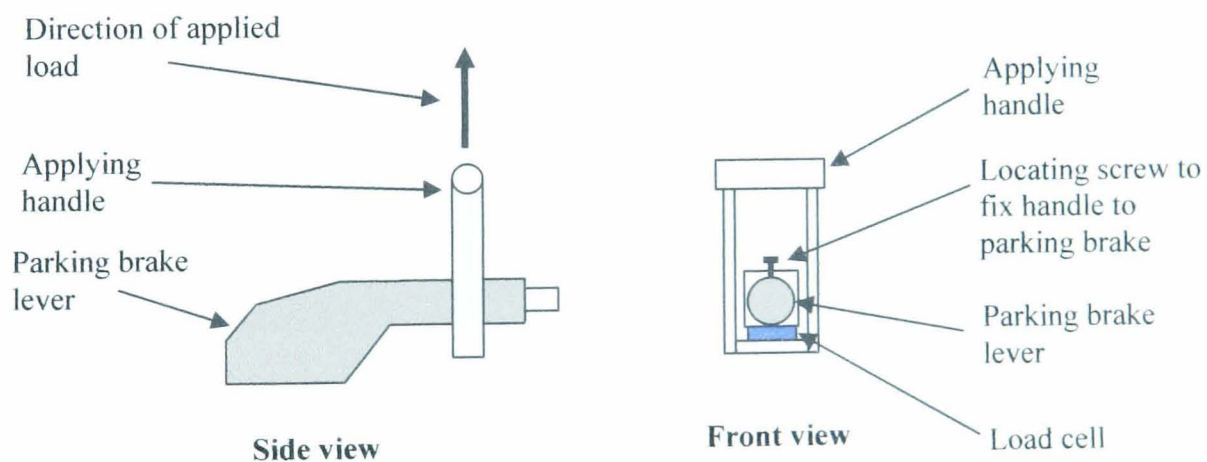


Figure 4.9 Diagram of parking brake applying bracket



Figure 4.10 Parking brake lever with load cell and accelerometer attached.



Figure 4.11 Microphone positioned inside the cabin

4.4. Results

This section presents the results from all of the on-vehicle tests conducted as part of this research. The movement of the vehicle down the gradient recorded during all of the on-vehicle tests can typically be described by one of four outcomes which are summarized in Table 4.2. An example of each type of movement is shown in Figures 4.12 to 4.15 along with any noise associated with the movement. The vehicle movement has been described by the four types of behaviour so that a description of each on-vehicle test can be given without the need for a graphical representation of every test.

Type	Description	Example
1	No stick/slip, no noise, no rollaway	Figure 4.12
2	Stick/slip, noise, no rollaway	Figure 4.13
3	Stick/slip, noise, followed by rollaway	Figure 4.14
4	Stick/slip, noise, followed by a period of movement, then stick/slip and noise continues, then rollaway	Figure 4.15

Table 4.2 Description of the on-vehicle results

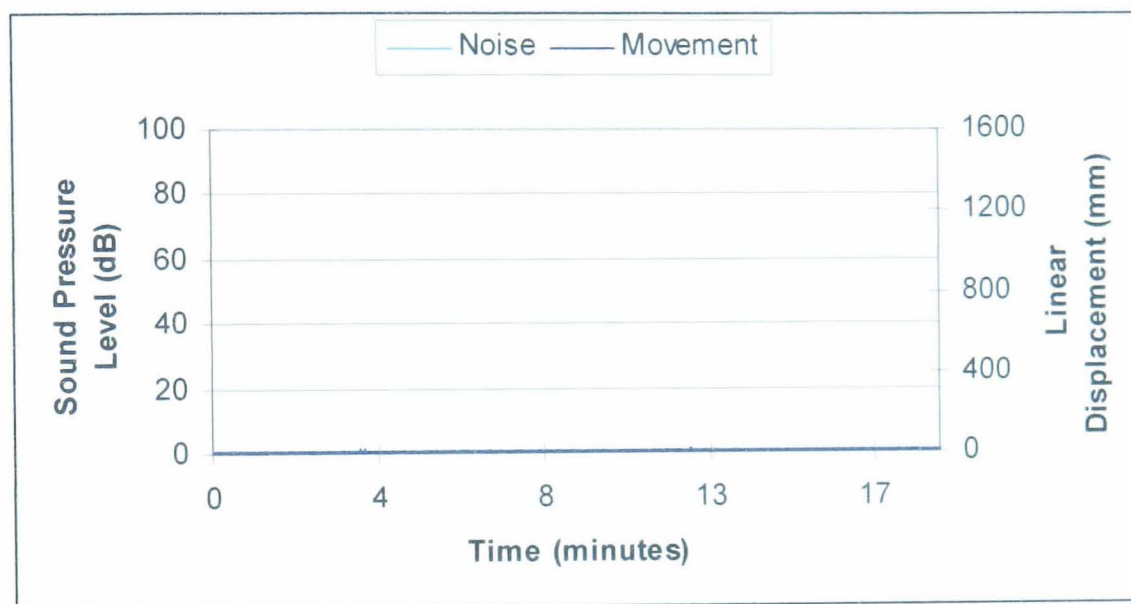


Figure 4.12 Test type 1 - No movement no rollaway. Taken from the on-vehicle result for Pad 3 bedded facing up the 8% gradient with brake cooling down from 50°C.

The test result shown in Figure 4.12 indicates that the vehicle remained stationary for the duration of the test with no movement or groan noise recorded. This is the behaviour that is expected of a vehicle while parked and is designated Type 1. This vehicle passed the rollaway test.

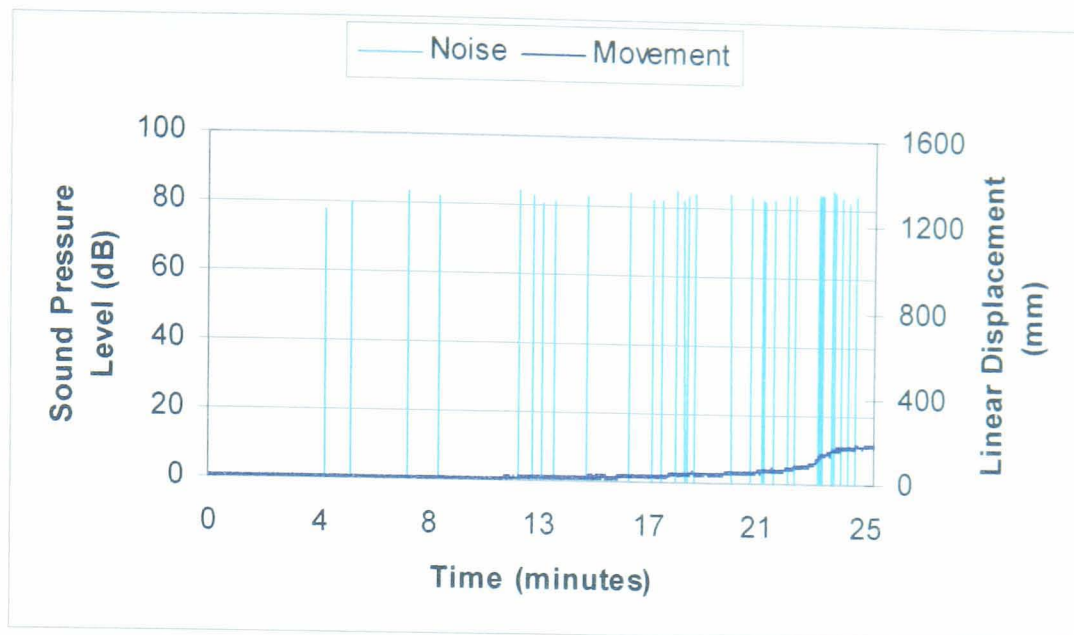


Figure 4.13 Test type 2 - Stick/slip, noise, no rollaway. Taken from the on-vehicle result for Pad 2 bedded facing down the 8% gradient with brake cooling down from 50°C.

The type 2 result shown in Figure 4.13 shows that the vehicle began to move down the slope with a stick/slip motion. Some groan noise was associated with this movement. The vehicle did not rollaway in this case and it would have passed the rollaway test as it did not move more than one metre.

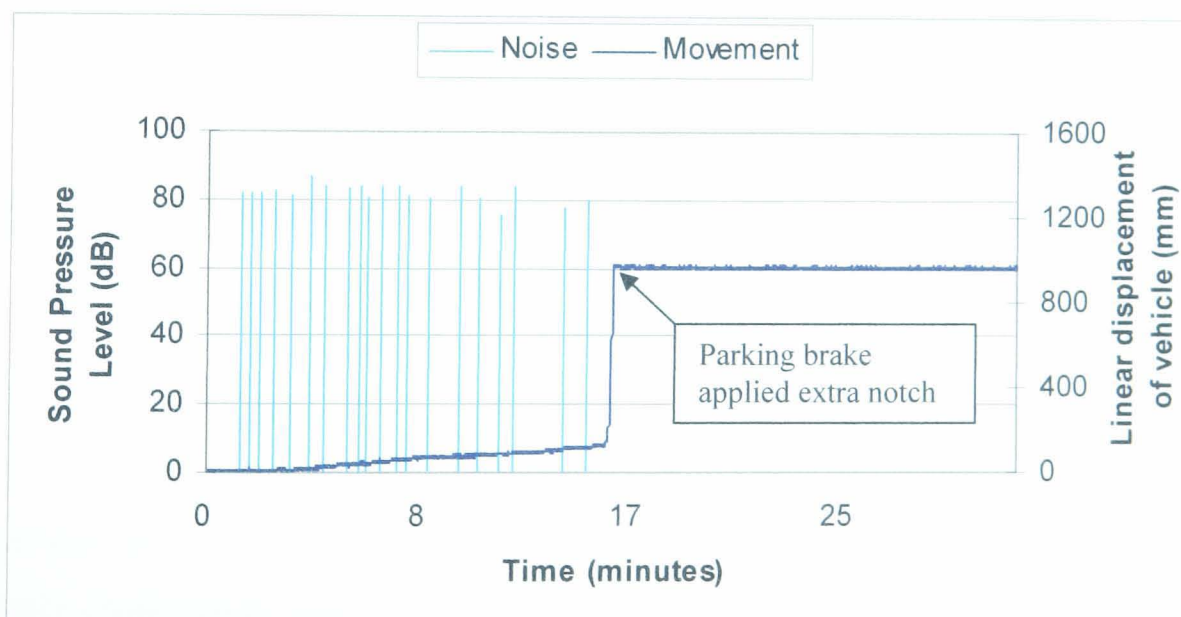


Figure 4.14 Test type 3 - Stick/slip, noise, followed by rollaway. Taken from the on-vehicle result for Pad 1 bedded facing up the 8% gradient with brake cooling down from 100°C.

The test type 3 result in Figure 4.14 shows that the vehicle slowly moved down the gradient over a period of around 16 minutes. The movement was a stick/slip motion

and a low frequency groan noise was typically recorded during the slip events. After a period of stick/slip movement the brake failed and the vehicle began to accelerate down the slope. After the vehicle had moved more than one meter the handbrake lever was applied to the next notch on the ratchet mechanism and this extra force was sufficient to keep the vehicle stationary for the remainder of the test with no additional movement or noise recorded.

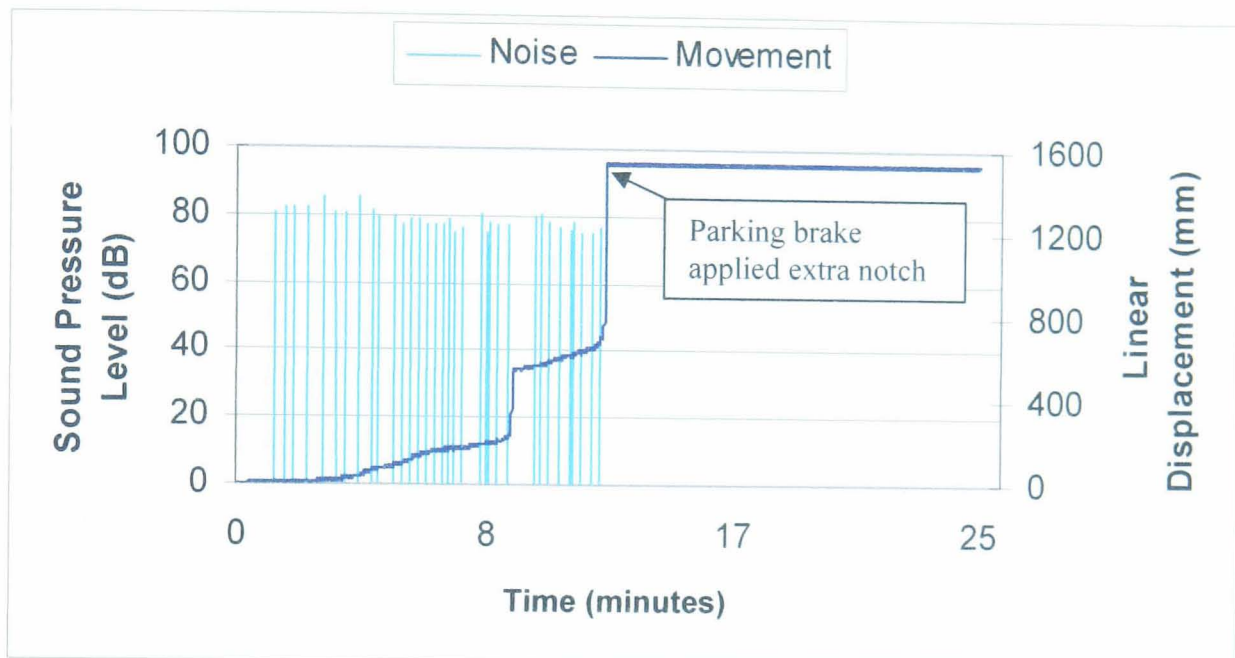


Figure 4.15 Test type 4 - Stick/slip, noise, followed by a period of movement, then stick/slip and noise continues, then rollaway. Taken from the on-vehicle result for Pad 1 bedded facing down the 8% gradient with brake cooling down from 100°C.

The type 4 result shown in Figure 4.15 shows that the vehicle slowly moved down the gradient with a stick/slip motion and a groan noise was generated during the slip event. After a period of stick/slip the brake failed and the vehicle began to accelerate down the slope. After a short period of acceleration the vehicle slowed and stopped without any input from the driver. The vehicle then continued to exhibit the stick/slip motion with the groan noise until the brake failed again. This time the vehicle continued to accelerate down the slope indicating that the brake had failed completely. The handbrake lever was then applied an extra notch on the ratchet mechanism and this was sufficient to keep the vehicle stationary for the remainder of the test with no movement or noise recorded.

4.4.1. Performance of the OE parking brake system

Tests were conducted to characterise the performance of the Jaguar S-Type OE parking brake system. The tests were conducted on three different gradients of 8%, 16.6%, and 25% with the pads in a bedded and un-bedded condition. The gradients were chosen because they were available at the Federal Mogul proving ground and gradients of more than 25% are not typically found on public roads. The un-bedded tests were conducted at a temperature of 50°C and 100°C. The temperature was not allowed to go higher than this as it could have affected the properties of the un-bedded pads. The bedded pads were tested at temperatures of 50°C, 100°C, 200°C and 300°C as these are temperatures that can be achieved at the rear brakes by normal vehicle usage. The tests were conducted with the vehicle facing up and down the gradient because vehicles can be parked in either direction. The results using the un-bedded pads are shown in Table 4.3 and the results using the bedded pads are shown in Table 4.4.

Grad (%)	Temp (°C)	Direction	Hold (N)	Notch (No)	Park (N)	Notch (No)	Result	Time (min:sec)	Result type
8	50	Up	170	3	180	4	Held		2
8	50	Down	170	3	180	4	Held		2
16.6	50	Up	230	4	230	5	Rolled	03:35	3
16.6	50	Down	220	4	230	5	Rolled	17:06	3
25	50	Up	290	6	320	7	Held		1
25	50	Down	280	5	280	6	Held		2
8	100	Up	150	3	210	4	Rolled	18:17	3
8	100	Down	140	3	190	4	Held		1
16.6	100	Up	180	4	210	5	Rolled	05:00	3
16.6	100	Down	180	3	200	4	Rolled	01:02	4
25	100	Up	240	5	260	6	Rolled	00:31	3
25	100	Down	250	5	290	6	Rolled	09:29	3

Table 4.3 Un-bedded results for Jaguar S-Type OE pad (Pad 1)

Grad (%)	Temp (°C)	Direction	Hold (N)	Notch (No)	Park (N)	Notch (No)	Result	Time (min:sec)	Result type
8	50	Up	170	3	190	4	Held		2
8	50	Down	140	3	180	4	Held		1
16.6	50	Up	200	5	270	6	Held		1
16.6	50	Down	190	4	230	5	Held		1
25	50	Up	240	5	260	6	Rolled	03:50	3
25	50	Down	210	5	270	6	Held		1
8	100	Up	150	3	190	4	Rolled	08:05	3
8	100	Down	150	3	190	4	Held		1
16.6	100	Up	230	5	260	6	Rolled	05:45	3
16.6	100	Down	170	3	180	4	Rolled	01:00	4
25	100	Up	280	6	330	7	Rolled	04:00	3
25	100	Down	200	5	270	6	Rolled	08:00	3
8	200	Up	160	3	190	4	Rolled	05:45	3
8	200	Down	160	3	200	4	Rolled		2
16.6	200	Up	220	5	260	6	Rolled	07:00	3
16.6	200	Down	190	3	210	4	Rolled	01:30	4
25	200	Up	320	6	320	7	Rolled	04:00	4
25	200	Down	250	5	300	6	Rolled	10:15	3
8	300	Up	200	3	220	4	Rolled	05:10	3
8	300	Down	200	3	210	4	Rolled	09:50	3
16.6	300	Up	260	5	270	6	Rolled	09:50	3
16.6	300	Down	220	4	250	5	Rolled	11:25	3
25	300	Up	350	7	380	8	Held		2
25	300	Down	280	5	300	6	Rolled	12:40	3

Table 4.4 Bedded results for Jaguar S-Type OE pad (Pad 1)

The results in Table 4.3 and 4.4 show that the vehicle rolled away on all of the gradients tested with the pad in both a bedded and un-bedded state. The results suggest that the vehicle was more likely to roll away with an increased test temperature. This is because the pads and discs will undergo a greater amount of thermal contraction as the brake cools. The amount of excess applied force that was required to move the parking brake lever from the ‘just hold’ to the ‘park’ condition had an influence on the likelihood of rollaway occurring. The higher the amount of excess force that was applied, the less likely the vehicle was to roll away as the excess stored load could compensate for the load lost due to the thermal contractions of the brake components.

The only condition in which the vehicle held consistently was the 8% gradient with the brakes cooling from 50°C. This could be due to the small amount of thermal

contraction occurring in the pads and disc, and also that there is only a small amount of brake torque required to hold the vehicle on this gradient.

4.4.2. Rollaway propensity as a function of friction pair

Tests were conducted on the Jaguar S-Type with Pads 1 to 4 installed in bedded and un-bedded conditions. All of the tests were conducted on an 8% gradient with the vehicle facing both up and down the slope. The 8% gradient was chosen as it required the least amount of applied load to achieve the 'hold' condition. This reduced variations in the measured loads and enabled the 'hold' and 'park' loads to be recorded more accurately. The 8% gradient also produced the lowest levels of force down the incline thereby reducing the acceleration of the vehicle and giving more detailed stick/slip results. The results from the four different friction materials are shown in Tables 4.5 to 4.12.

Grad (%)	Temp (°C)	Direction	Hold (N)	Notch (No)	Park (N)	Notch (No)	Result	Time (min:sec)	Result type
8	50	Up	120	4	150	5	Held		2
8	50	Down	120	4	150	5	Held		1
8	100	Up	140	3	140	4	Rolled	11:56	4
8	100	Down	130	3	140	4	Rolled	09:33	3

Table 4.5 Un-bedded results from Jaguar S-Type OE pad (Pad 1)

Grad (%)	Temp (°C)	Direction	Hold (N)	Notch (No)	Park (N)	Notch (No)	Result	Time (min:sec)	Result type
8	50	Up	110	3	130	4	Held		1
8	50	Down	90	2	100	3	Rolled	03:29	3
8	100	Up	100	3	130	4	Held		1
8	100	Down	90	3	140	4	Held		1
8	200	Up	90	2	100	3	Rolled	03:03	3
8	200	down	100	2	100	3	Rolled	03:42	3
8	300	Up	110	3	150	4	Rolled	12:00	4
8	300	Down	120	3	150	4	Held		2

Table 4.6 Bedded results from Jaguar S-Type OE pad (Pad 1)

Grad (%)	Temp (°C)	Direction	Hold (N)	Notch (No)	Park (N)	Notch (No)	Result	Time (min:sec)	Result type
8	50	Up	120	3	130	4	Rolled	02:36	3
8	50	Down	130	3	130	4	Rolled	10:01	3
8	100	Up	120	3	130	4	Rolled	08:15	3
8	100	Down	110	3	140	4	Rolled	07:08	3

Table 4.7 Un-bedded results from Pad 2

Grad (%)	Temp (°C)	Direction	Hold (N)	Notch (No)	Park (N)	Notch (No)	Result	Time (min:sec)	Result type
8	50	Up	120	3	130	4	Held		2
8	50	Down	120	3	140	4	Held		2
8	100	Up	130	3	140	4	Rolled	23:25	3
8	100	Down	120	3	150	4	Held		2
8	200	Up	110	3	150	4	Rolled	06:32	4
8	200	Down	110	2	120	3	Rolled	01:40	3
8	300	Up	100	3	150	4	Rolled	08:06	3
8	300	Down	130	3	170	4	Rolled	01:38	3

Table 4.8 Bedded results from Pad 2

Grad (%)	Temp (°C)	Direction	Hold (N)	Notch (No)	Park (N)	Notch (No)	Result	Time (min:sec)	Result type
8	50	Up	150	4	200	5	Held		1
8	50	Down	110	3	130	4	Rolled	12:49	3
8	100	Up	140	4	180	5	Held		2
8	100	Down	120	3	140	4	Rolled	14:35	3

Table 4.9 Un-bedded results from Pad 3

Grad (%)	Temp (°C)	Direction	Hold (N)	Notch (No)	Park (N)	Notch (No)	Result	Time (min:sec)	Result type
8	50	Up	130	3	140	4	Rolled	03:40	3
8	50	Down	150	5	180	5	Held		1
8	100	Up	140	3	150	4	Rolled	16:30	3
8	100	Down	130	3	150	4	Rolled	12:19	4
8	200	Up	130	3	150	4	Rolled	18:07	4
8	200	Down	130	3	160	4	Rolled	22:40	3
8	300	Up	180	4	200	5	Held		2
8	300	Down	170	4	230	5	Held		1

Table 4.10 Bedded results from Pad 3

Grad (%)	Temp (°C)	Direction	Hold (N)	Notch (No)	Park (N)	Notch (No)	Result	Time (min:sec)	Result type
8	50	Up	80	2	80	3	Rolled	05:14	4
8	50	Down	90	2	100	3	Rolled	01:29	3
8	100	Up	110	3	140	4	Rolled	20:43	3
8	100	Down	100	2	100	3	Rolled	05:27	4

Table 4.11 Un-bedded results from Pad 4

Grad (%)	Temp (°C)	Direction	Hold (N)	Notch (No)	Park (N)	Notch (No)	Result	Time (min:sec)	Result type
8	50	Up	100	3	130	4	Held		1
8	50	Down	100	2	110	3	Held		2
8	100	Up	100	3	140	4	Held		1
8	100	Down	120	3	150	4	Held		1
8	200	Up	90	2	110	3	Rolled	02:59	3
8	200	Down	110	2	120	3	Rolled	02:18	3
8	300	Up	130	3	150	4	Rolled	17:10	3
8	300	Down	120	2	120	3	Rolled	03:12	3

Table 4.12 Bedded results from Pad 4

The results from the on-vehicle friction pair tests show that rollaway occurred for all of the four different pads. No significant variation between the pads was observed and therefore conclusions cannot be made as to which pad formulation performed the best.

The results did not show evidence that the pads performed differently if they were in a bedded or un-bedded condition and rollaway occurred for both conditions. The results show that the temperature of the brake did not have a significant effect on the results and that rollaway could occur at all of the temperatures tested.

The results illustrate that rollaway cannot be prevented by changing the friction material formulation within the range specified for these tests. This could be because the pads do not have a significant effect on rollaway or because the properties of the pads used during this test are within the range that can lead to rollaway.

4.4.3. Rollaway propensity as a function of calliper design

A Jaguar X-type was used to evaluate the performance of Callipers 2 and 3 because they would not fit onto the Jaguar S-type. The 20mm thick vented disc that was used on the Jaguar S-Type could not fit inside callipers 2 and 3 and so a solid disc of 12mm thickness was used. The calliper tests were conducted with the OE friction material formulation (Pad 1) installed. All the tests were conducted on a 16.6% gradient with the vehicle facing down the slope and the brake at an initial temperature of 300°C. The 16.6% gradient was used because the 8% gradient was not available at the time of the test due to maintenance work and the 25% gradient would provide less accurate hold and park loads and recorded stick/slip movements due to the higher accelerations down the slope. All of the tests were conducted with the vehicle facing down the slope as this was the easier direction to park due to the layout of the test circuit. An initial brake temperature of 300°C was chosen as this would produce the highest level of thermal contraction of the brake components. All of the tests followed the procedure described in Section 4.3. The test was repeated three times for each calliper and the results are shown in Tables 4.13 and 4.14.

Grad (%)	Temp (°C)	Direction	Hold (N)	Notch (No)	Park (N)	Notch (No)	Result	Time (min:sec)	Result type
16.6	300	Down	200	2	220	3	Rolled	13:54	3
16.6	300	Down	230	3	240	4	Rolled	03:00	3
16.6	300	Down	170	3	200	4	Rolled	05:30	3

Table 4.13 Results using Calliper 2.

Grad (%)	Temp (°C)	Direction	Hold (N)	Notch (No)	Park (N)	Notch (No)	Result	Time (min:sec)	Result type
16.6	300	Down	190	2	190	3	Rolled	01:30	3
16.6	300	Down	190	2	200	3	Rolled	02:15	3
16.6	300	Down	190	3	230	4	Held		1

Table 4.14 Results using Calliper 3.

The results show that the vehicle rolled away with both callipers installed. The vehicle rolled away for all of the tests using the cast iron calliper and rolled away for two of the tests using the aluminium calliper. This suggests that the aluminium calliper is less likely to cause rollaway under the test conditions. The load required to ‘just hold’ the vehicle and to ‘park’ the vehicle was generally lower for the aluminium calliper. The aluminium calliper has a higher thermal expansion coefficient than the cast iron calliper which could affect the results. If the calliper bridge is initially at an elevated temperature when the vehicle is parked then as the calliper cools the thermal contractions of the calliper bridge will result in an increase in the clamp load at the frictional interface. A higher thermal expansion would produce a greater increase in clamp load as the calliper cools which could explain why the aluminium calliper performed better than the cast iron calliper in the on-vehicle tests.

4.5. Summary

The on-vehicle tests have proven the existence of a rollaway problem on the two vehicles tested in this research. The vehicles both have an integrated parking brake mechanism and it is believed that rollaway can potentially occur on any vehicle using this type of parking brake system. A period of stick/slip motion was found to occur prior to the onset of rollaway.

Rollaway occurred on the vehicle with all of the different pads installed which indicates that rollaway cannot be eliminated by changing the friction material formulation within the range used for these tests. This suggests that rollaway may

not be prevented by the pads of friction material. It is more likely that rollaway is a system problem and the additional parking brake components have a significant effect on rollaway, which influenced the on-vehicle results. This highlights the need for the parking brake components to be analysed and evaluated. It is not possible to do this on the vehicle, and therefore a laboratory based dynamometer was required to conduct further evaluations.

Rollaway was less likely to occur when a larger amount of excess load was applied going from the 'just hold' condition to the 'park' condition. This is because the excess energy stored in the parking brake system is used to overcome the lost force from the thermal contractions of the pads and disc. The amount of excess load is dependant on the position of the handbrake notch relative to the 'just hold' condition. If the 'just hold' condition is close to the next notch on the ratchet mechanism a low lever of excess force will be applied. If the 'just hold' condition is a long way from the next notch on the ratchet mechanism then a larger amount of excess force will be developed. The level of excess force could generally be increased if the number of notches on the ratchet mechanism was reduced. For example if there were only two notches on the ratchet mechanism it would be unlikely that the 'just hold' condition would be close to the next notch, and therefore a large amount of excess force would be applied reducing the likelihood of rollaway occurring. This may however result in poor handbrake feel and would be undesirable to the driver.

Rollaway was found to occur on all of the gradients tested in the evaluations. The results suggested that rollaway was more likely to occur with an increased brake temperature, but could also occur with lower temperatures. This is due to the higher thermal contractions of the pad and disc for the higher temperatures. However a small contraction can be sufficient to cause rollaway if the 'park' load is close to the 'just hold' load.

The on-vehicle tests have been successful in establishing the existence of the rollaway phenomenon on vehicles using an integrated rear calliper. To understand the mechanisms involved during a rollaway event further work was required to

characterise the behaviour of the parking brake components. To achieve this further laboratory based testing was required.

Chapter 5

Development of a Rollaway Dynamometer Experimental Facility

5.1. Introduction

A brake dynamometer is a testing machine that can be used to evaluate the performance of vehicle brakes. Typical dynamometers use an inertia flywheel to simulate the momentum of a moving vehicle and use the brakes to decelerate the flywheel. For this research, a dedicated dynamometer was required to assist in the characterisation of the behaviour of the parking brake system during a rollaway event. A dynamometer representing the Jaguar S-Type's parking brake system was available for use at the University of Leeds. The original machine was designed and produced by Mckinlay et al [2] as part of a fourth year MEng project. A detailed description of the design process used to develop the dynamometer is given in [2]. The dynamometer that was developed for this project differs from a typical design in that it does not decelerate inertia flywheels. Instead it employs a dragging method to heat the brakes.

This chapter discusses the process of developing the dynamometer facility to meet the demands of the current project. The operation and functionality of the original dynamometer facility that was developed during the fourth year MEng project are discussed in Section 5.2. The specifications of the dynamometer that were required for the current project and the work conducted to modify the existing dynamometer to meet these requirements are discussed in Section 5.3. A dedicated control and data acquisition system was developed for the dynamometer and is discussed in Section 5.5. Upon completion of the dynamometer modifications, commissioning tests were conducted to demonstrate the functionality of the test facility and ensure that the dynamometer satisfied the project specifications. These tests are discussed in Section 5.8.

5.2. Description of the original dynamometer

The original dynamometer facility was separated into two main sections, the drive rig and the apply rig. A description of each section is given below.

5.2.1. Drive rig

The drive rig housed the brake components from the vehicle including the two rear discs, two rear drive shafts, two spider mounting brackets (rear uprights), callipers, pads, the parking brake cables and apply lever. The drive rig also housed an electric motor, bearings to support the axle, a torque wheel used to apply a torque on the axle, an extraction system, a pneumatic actuator connected to a hydraulic actuator and hydraulic brake lines. A diagram of the drive rig layout is shown in Figure 5.1 and photographs of the drive rig components are shown in Figures 5.2 and 5.3.

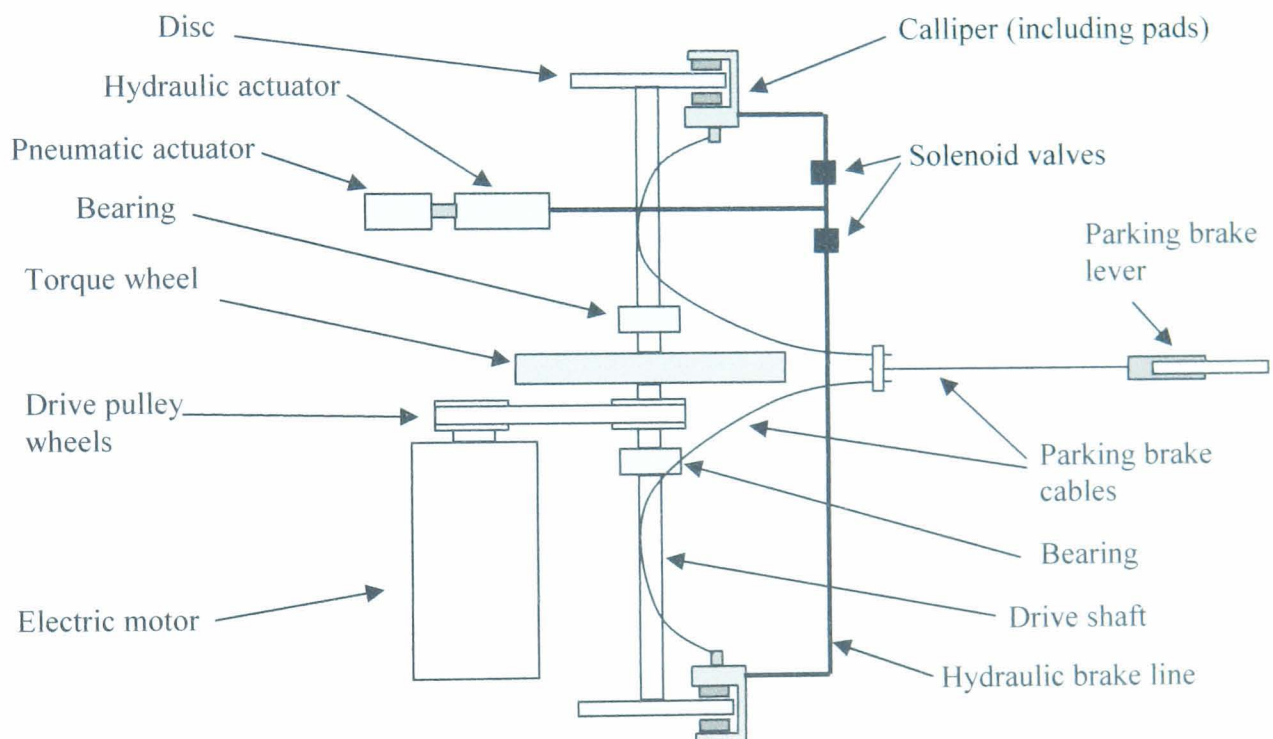


Figure 5.1 Schematic of drive rig (top view)

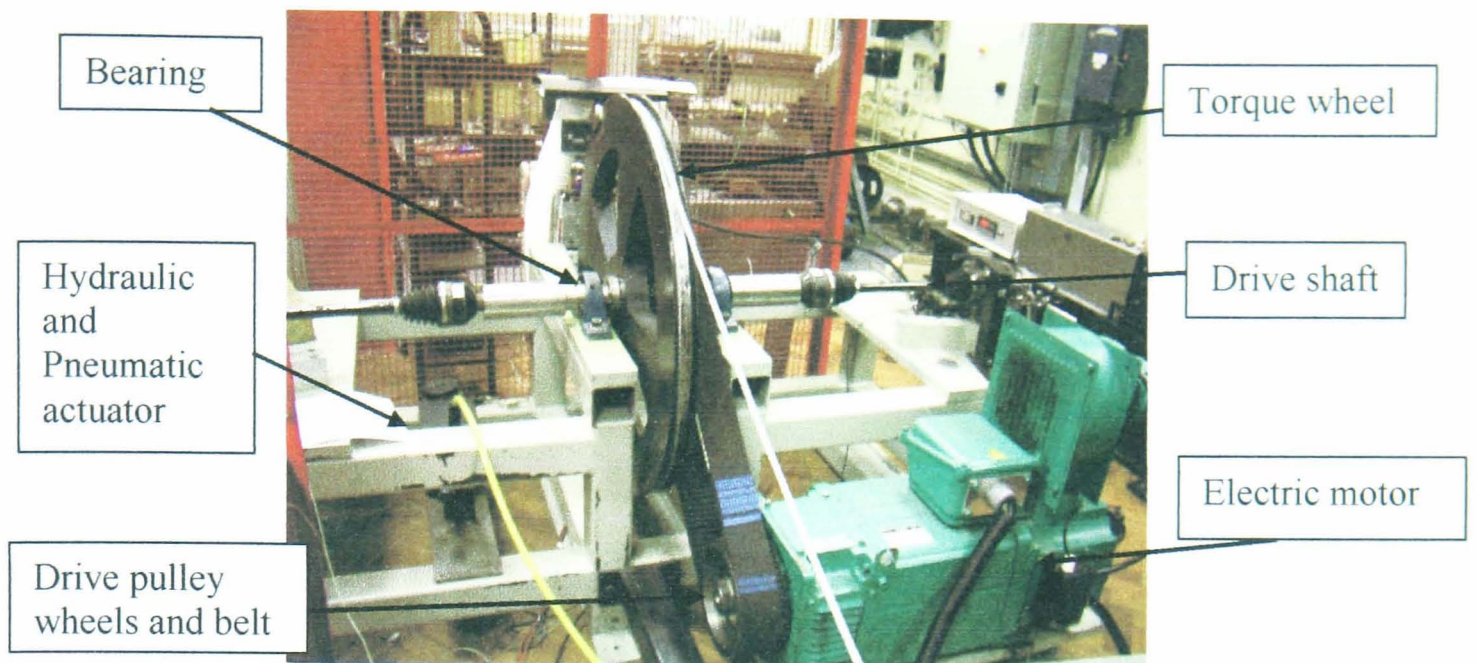


Figure 5.2 End view of drive rig



Figure 5.3 Side view of drive rig

5.2.2. Apply rig

The apply rig is used to apply a torque on the dynamometer axle via the torque wheel, a second hydraulic actuator and the cable pulley arrangement. The cable is attached to the outer radius of the torque wheel on the drive rig using a connecting bracket as shown in Figure 5.4. When the hydraulic actuator is applied, a force is generated in the cable system which results in a torque on the dynamometer axle that simulates the vehicle parked on a gradient. The layout of the hydraulic actuator and

cable pulley arrangement on the apply rig is shown in Figure 5.5 and a photograph of the system is shown in Figure 5.6.



Figure 5.4 Cable connecting bracket

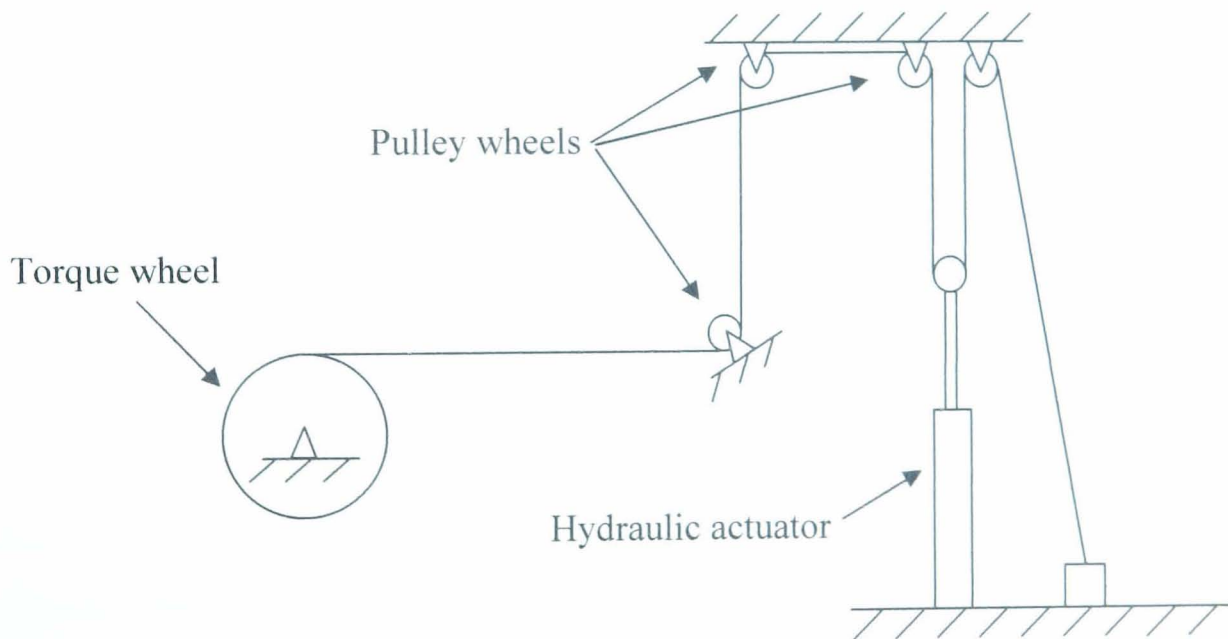


Figure 5.5 Layout of apply rig (side view)

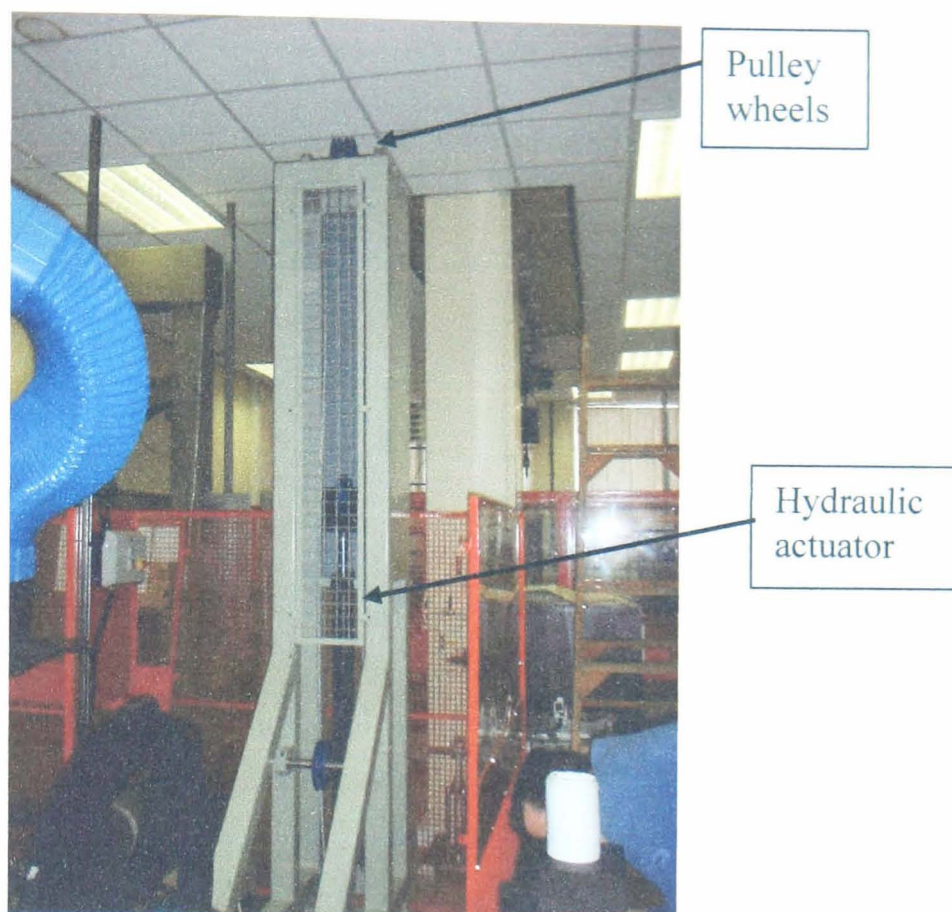


Figure 5.6 End view of apply rig

5.2.3. Operation

The dynamometer used a dragging method to heat the brakes to the required test temperature. This was achieved by rotating the discs using a Leroy Somer LSK1604M04 45kW DC electric motor and Control Techniques Mentor II DC drive, while simultaneously applying the brakes. The speed of the motor was manually controlled using a potentiometer that varied the voltage signal that was sent to the drive controller. The brake was manually controlled using a pneumatic actuator which was connected to a hydraulic cylinder via a rigid link and used to vary the hydraulic brake fluid pressure inside the calliper. Two solenoids valves were included in the brake lines so that the two brakes could be tested together or an individual brake could be isolated and tested independently. A diagram of the hydraulic brake circuit is given in Figure 5.7.

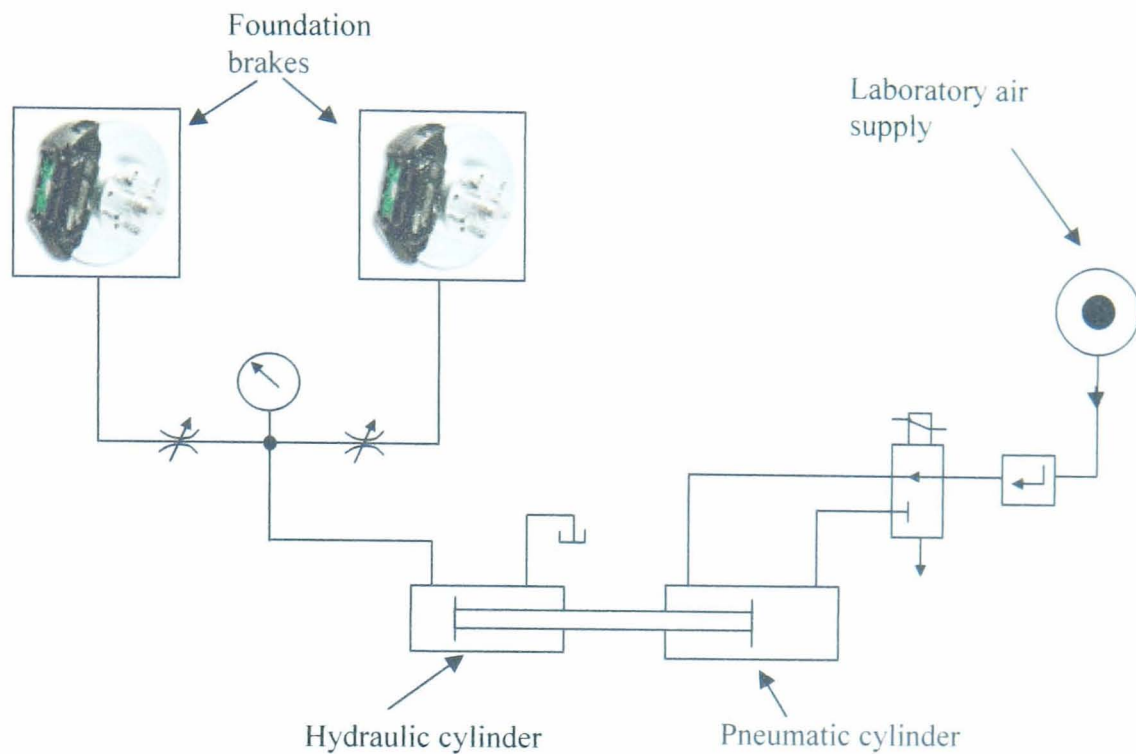


Figure 5.7 Schematic of hydraulic circuit

Once the brakes are at the correct temperature, the drive is stopped and the axle torque apply system is connected to simulate a vehicle parked on a gradient. Hydraulic fluid is pumped into the actuator using a Europack Hydraulics Ltd power pack and controller. The fluid is pumped using a 7.5kW electric pump which is capable of producing pressures up to 200bar. The magnitude of the torque produced on the dynamometer axle is determined by the pressure used in the hydraulic actuator, which is set according to the torque required for any given test. The hydraulic actuator is controlled from outside of a protective cage which was installed to comply with the University of Leeds Health and Safety regulations. The flow of hydraulic fluid in the actuator can be set to forward, reverse or zero using a three position switch connected to a directional solenoid control valve. The control valve has an exhaust system which allows the fluid to return to the reservoir via a filter. A schematic of the hydraulic actuator system is shown in Figure 5.8.

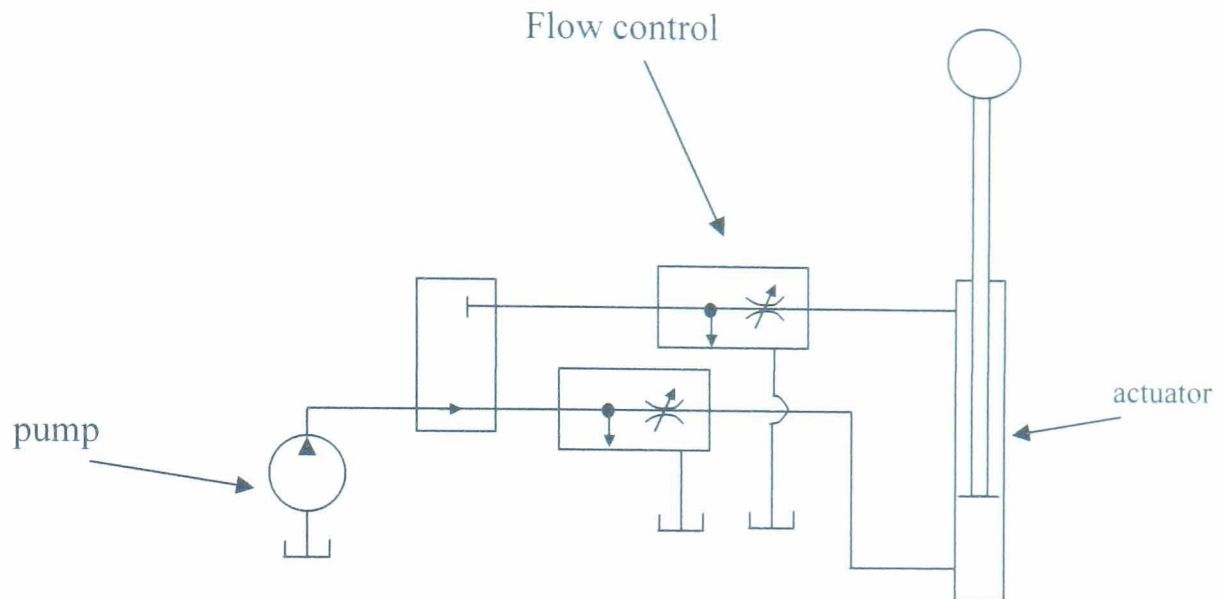


Figure 5.8 Schematic of the hydraulic actuator circuit

The parking brake is applied using the vehicle handbrake lever and cable system connected to the rear callipers as shown in Figure 5.9. The handbrake is isolated from the dynamometer by a protective cage to comply with the University of Leeds Health and Safety regulations.



Figure 5.9 Jaguar S-Type handbrake mounted on the dynamometer

The temperature of the brakes is measured using a contacting K-type thermocouple positioned at the mean rubbing radius of the pad on the disc as shown in Figure 5.10.

The thermocouple is connected to a handheld digital amplifier which allows the operator to monitor the brake temperature.

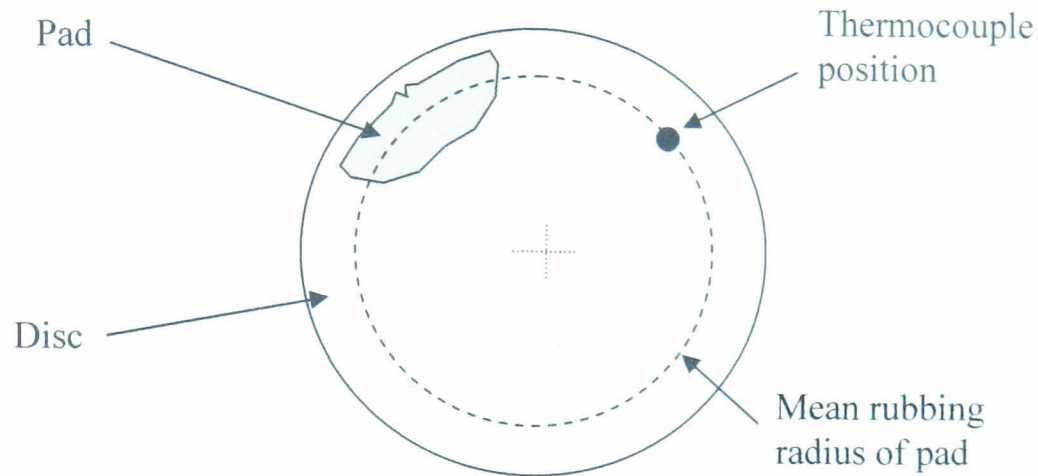


Figure 5.10 Position of the thermocouple on the disc

Rotation of the dynamometer axle is measured using a proximity sensor that monitors movement of the teeth on an anti-lock braking system (ABS) component on the vehicle drive shaft. The sensor outputs a voltage of 1v if a peak on the tooth is detected and 0v if a trough is detected as shown in Figure 5.11. The voltage signal is read by a computer program which counts the number of teeth that pass the sensor. The rotation of the axle is calculated from the number of teeth detected. A photograph of the system is shown in Figure 5.12.

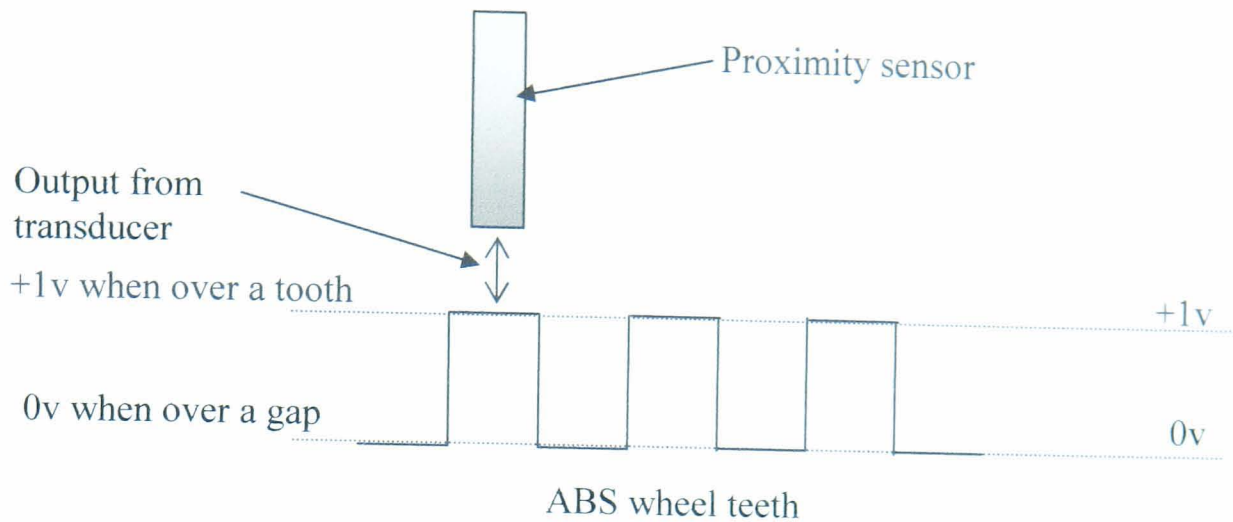


Figure 5.11 ABS wheel speed measurement

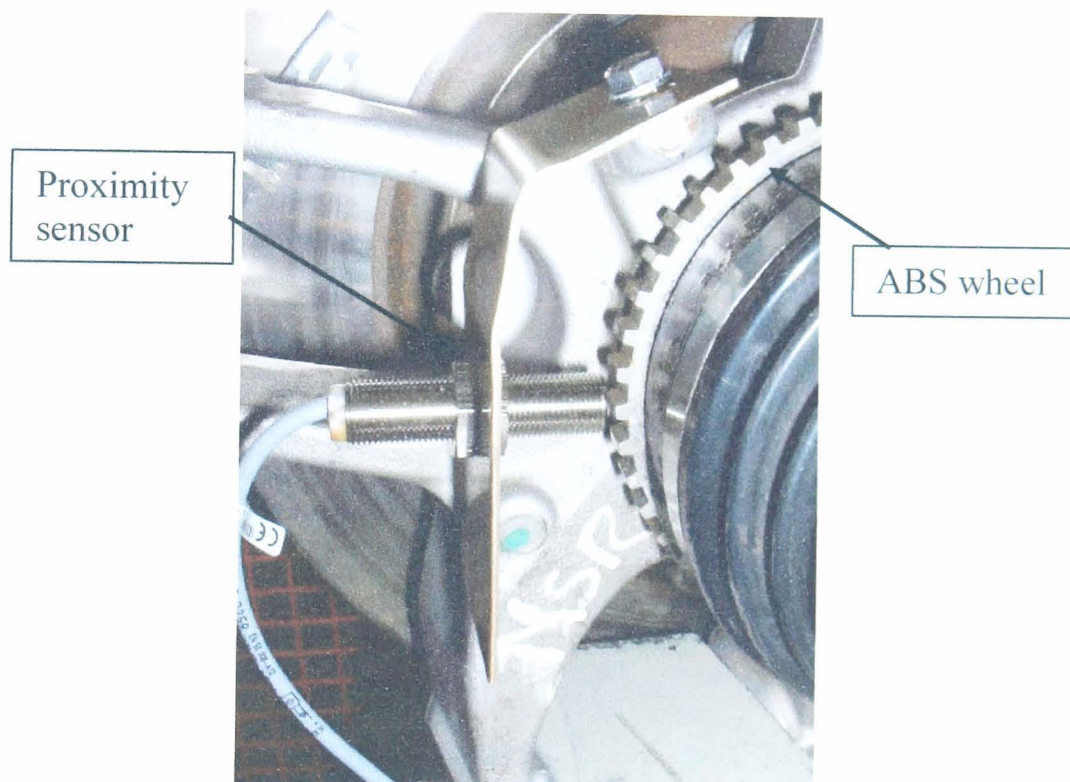


Figure 5.12 Photograph of proximity sensor on the ABS wheel

The force in line with the parking brake cable is measured at the calliper attachment point using a 2kN Novatech load cell mounted between the calliper lever and the cable end using two brackets as shown in Figure 5.13. A photograph of the load cell in line with the parking brake cable is shown in Figure 5.14. The output from the load cell is read by an amplifier unit which also displays the data.

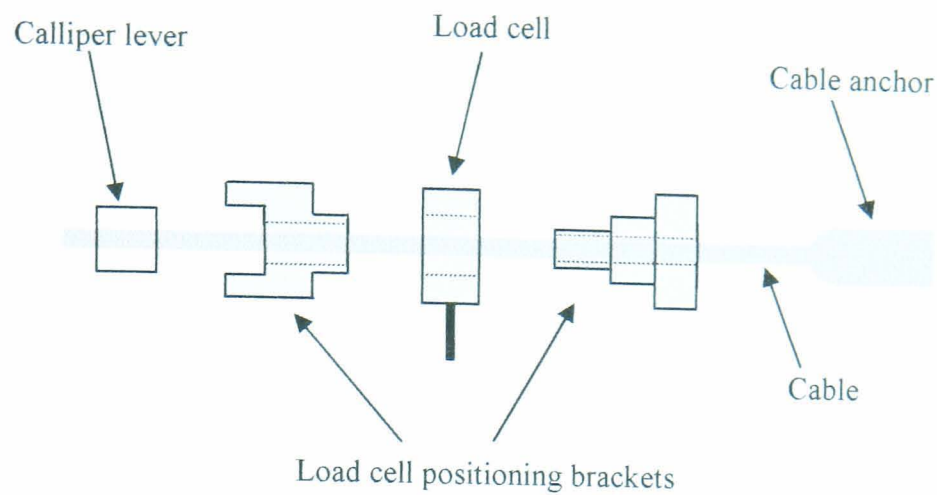


Figure 5.13 Schematic of load cell in line with parking brake cable

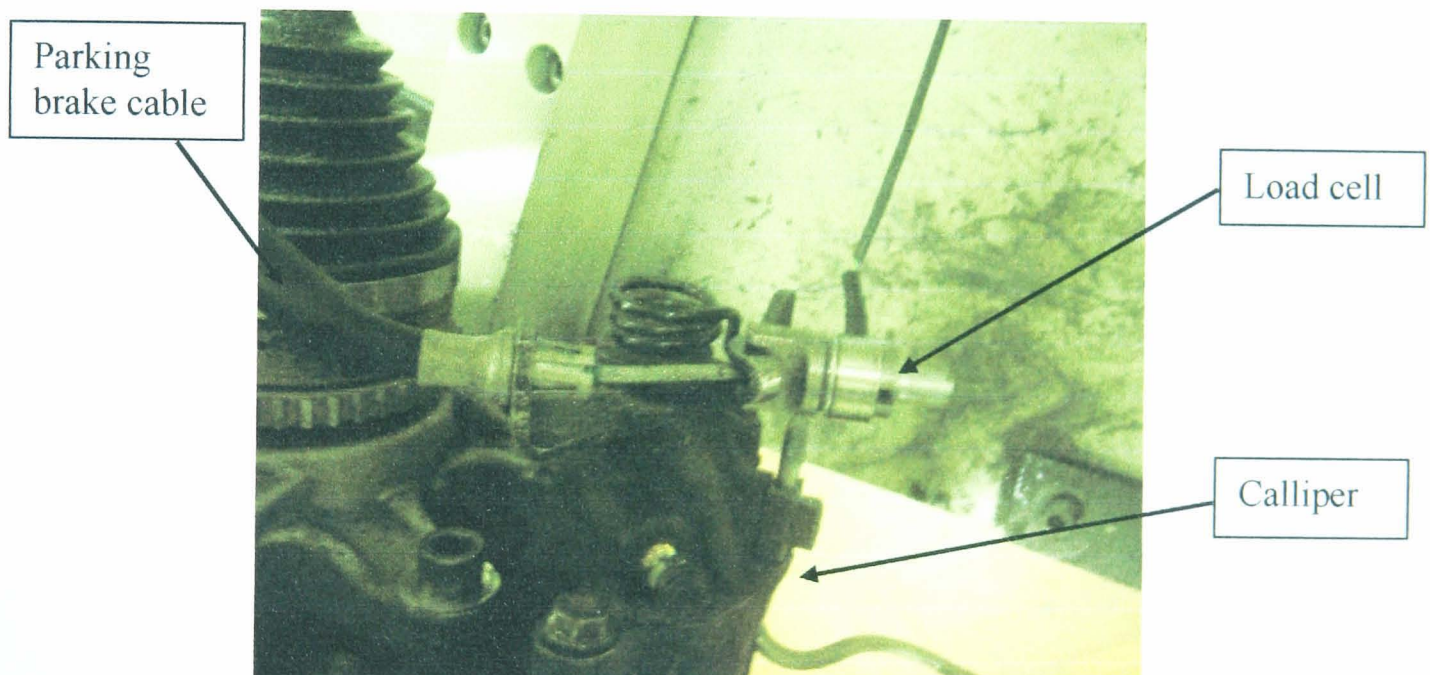


Figure 5.14 Load cell in line with parking brake cable

5.3. Dynamometer requirements

To meet the demands of the current project, the dynamometer must:

- Heat the brakes to a specified temperature.
- Apply a specified constant torque to the dynamometer axle.
- Actuate the parking brake system to produce a specified clamp force at the frictional interface.

- Contain a dedicated control and data acquisition system to control the test procedure and record data from each test.
- Measure the parking brake clamp force as a function of temperature.
- Measure the static coefficient of friction as a function of temperature.

5.4. Preliminary test programme

Preliminary tests were conducted to demonstrate the functionality of the original dynamometer and determine whether the project specifications, described in Section 5.3, could be satisfied with the current setup. The following section discusses the tests that were conducted and identifies issues with the original dynamometer that required modification.

5.4.1. Heating the brakes to a specified temperature

The project specifications require the dynamometer to be capable of heating the brakes to a specified temperature. This was achieved through the dragging method described in Section 5.2 with the motor speed and brake line pressure controlled manually by the dynamometer operator. A preliminary test was conducted to heat the brakes to a temperature of 250°C to investigate the heating process. The result is shown in Figure 5.15.

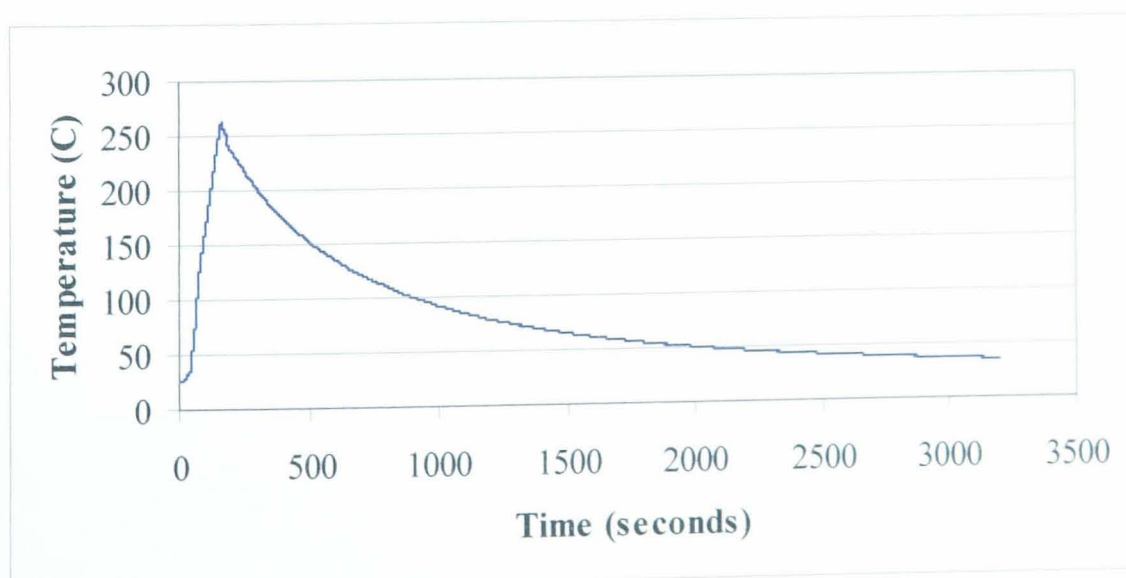


Figure 5.15 Temperature of brake during preliminary heating test

The result in Figure 5.15 proved that the dragging method used on the dynamometer is capable of heating the brakes to a specified temperature. The maximum temperature that was achieved during the test was above 250°C as it took a short period of time to reduce the brake pressure to zero. The rate of heating is dependant on the speed of disc rotation and the brake line pressure which is controlled by the operator. With the current configuration the heating rates are prone to variations due to operator variability, which could significantly influence the test results. The requirements for the research state that the rollaway tests should be automated in order to eliminate any variations produced by the operator and so the manual controllers were deemed to be unsuitable.

5.4.2. Application of a specified constant torque

The hydraulic actuator used to apply the torque failed during the final stage of the level four MEng project [2] and did not function at the start of this project. The actuator was stripped, cleaned and the seals replaced before the preliminary tests commenced. Once working, the hydraulic actuator was found to produce operating pressures exceeding those required for the rollaway tests. After discussions with Airdale Tubes and Fittings Ltd, it was decided that a pressure reducing valve, installed in line with the hydraulic circuit, would enable the required pressure levels to be developed. This work was carried out and enabled the preliminary torque measurement test to be conducted. The load in the cable produced by the hydraulic actuator was measured using a Graham and White DSCRA 20kN load cell in line with the cable system. The measured cable force was multiplied by the radius of the large pulley wheel to calculate the applied torque on the dynamometer axle. The measured torque during a preliminary test is shown in Figure 5.16.

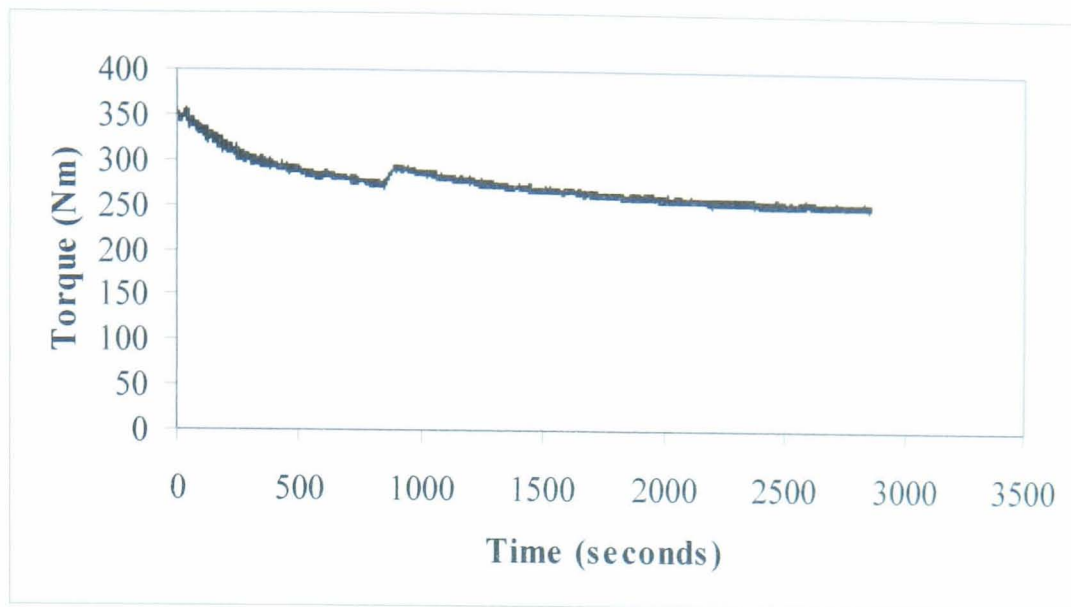


Figure 5.16 Torque produced by the hydraulic actuator system

It can be seen from Figure 5.16 that the torque fluctuated and generally reduced over time. The dynamometer is required to produce a constant torque over time to simulate the vehicle parked on a gradient and therefore the torque application method was deemed to be unsuitable for the rollaway tests.

The test also highlighted a problem with the bracket used to attach the cable to the large pulley wheel, shown in Figure 5.4. The dimensions of the bracket restricted the cable from passing it on the large pulley wheel. Therefore the rotation of the dynamometer axle was limited to one revolution which equates to a vehicle linear displacement of 2m. The vehicle is deemed to fail a rollaway test if it moves more than 1m down the slope, but during the on-vehicle rollaway tests described in Chapter 4, the vehicle was found to exhibit a stick/slip motion which could result in the vehicle moving more than 2m down the slope. To capture this displacement the dynamometer needs to be capable of simulating more than one revolution of the large pulley wheel. The design of the bracket also meant that it was awkward to attach to the large pulley wheel which took more time than necessary. It was decided that the original cable attachment bracket was not suitable for use on the dynamometer.

5.4.3. Actuating the parking brake

The parking brake on the original dynamometer was actuated using the Jaguar S-Type's parking brake lever, shown in Figure 5.9. The lever fixed the cable

displacement at one of eleven positions determined by the notches on the lever's ratchet mechanism. A test was conducted to measure the cable load, and the clamp load produced by the handbrake lever mechanism. The cable load was measured using the 2kN Novatech load cell described in Section 5.2 and the clamp load was measured using a 10kN Novatech load cell. The 10kN load cell was held inside the calliper using two ball bearings fixed to back plates. The back plates had small indentations drilled into them to fix the position of the ball bearings and the 10kN load cell was cylindrical with a hollow centre which enabled it to be held between the ball bearings as shown in Figure 5.17. The back plates were used so that the mechanism would fit inside the calliper. The results from the tests are shown in Figure 5.18.

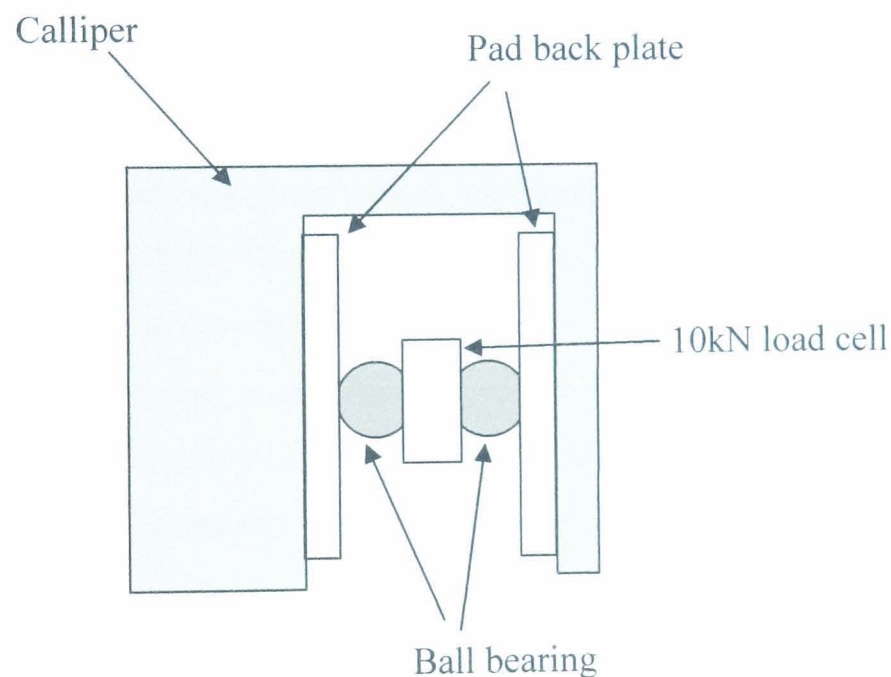


Figure 5.17 Layout of clamp load cell mechanism

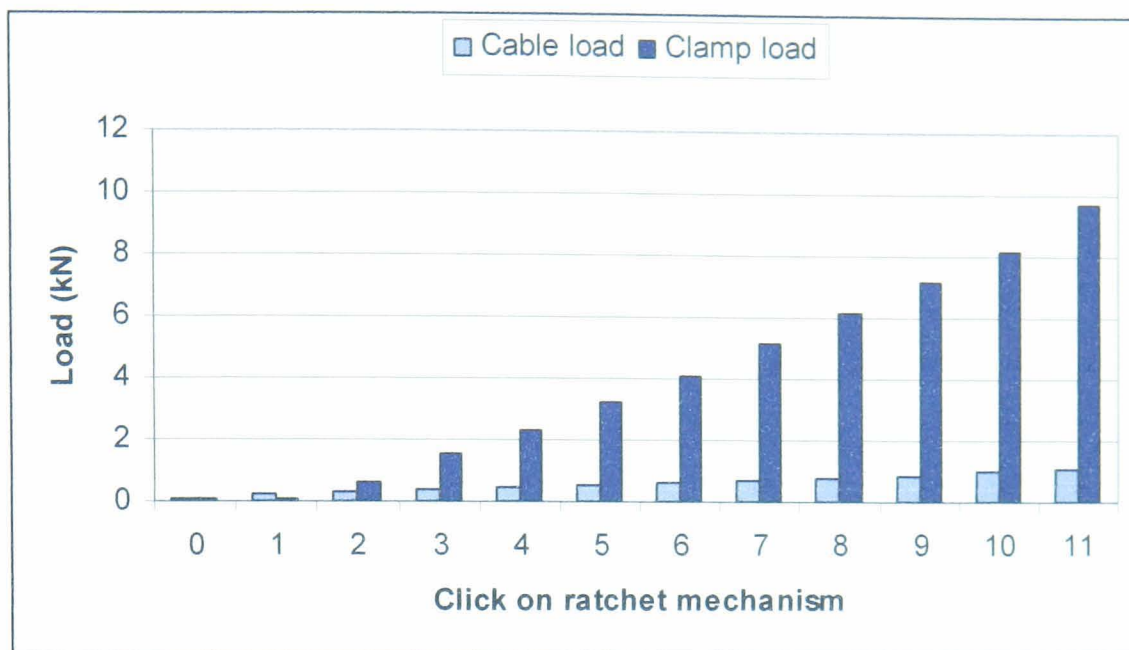


Figure 5.18 Cable load and clamp load for each click on the Jaguar S-Type handbrake mechanism

The result in Figure 5.18 shows that the loads produced by the handbrake lever are constrained by the location of the notches on the ratchet mechanism. This is a useful result as it shows the operation of the vehicle parking brake, but it is not possible to achieve a clamp load between the finite values set by the ratchet mechanism. This does not comply with the requirements of the project that state the dynamometer must be capable of producing a specified clamp load at the frictional interface. It was decided that an alternative method of applying the clamp load would be developed and used in conjunction with the parking brake lever.

5.5. Control and data acquisition system design and development

5.5.1. Introduction

A dedicated control and data acquisition (DAQ) system is the most significant contributory component to the successful development of the dynamometer experimental facility. This section discusses the design and development of the system used on the rollaway dynamometer.

5.5.2. Hardware

National Instruments (NI) was chosen as the main supplier for the system hardware due to the simple ‘plug and play’ type modules and the compatibility with the system software. The NI modules allow data from the dynamometer to be streamed quickly and reliably to a desktop PC with a 600MHz Pentium 3 processor, 392MB of RAM and running Windows NT. The PC has a NI PCI-6040E card installed into one of the PCI slots which connects the PC to a NI BNC-2090 rack module using a 68 pin cable. The rack module has BNC connectors and spring terminal blocks that can read data from the dynamometer sensors and output signals to drive the instrument controllers. Two K-type thermocouples are connected to the NI BNC-2090 module via two AD595AD amplifiers to measure temperature of the brake components. Rotation of the dynamometer axle is measured using a Hohoner quadrature shaft encoder that is connected directly to the NI BNC-2090 module. A NI SCXI 1000 chassis is connected to the NI BNC-2090 module via a 68 pin cable. The NI SCXI 1000 chassis is a low noise chassis that can hold up to four SCXI modules providing them with power and handling the signal routing between the modules and the NI BNC-2090 module. The NI SCXI 1000 chassis has three modules installed. A NI SCXI 1102 module is used to control the stepper motor which applies the park brake cable on the modified dynamometer. A NI SCXI 1180 module is used to connect the stepper motor wiring to the NI SCXI 1000 chassis and a NI SCXI 1121 module is used to amplify the signal from the four load cells on the dynamometer. Two Novatech 2kN load cells are mounted between the parking brake cable and the calliper attachment point to measure loads in the cable. A 10kN Novatech load cell can be mounted inside the calliper to measure the clamp load. A 20kN Graham and White DSCRA load cell is positioned in line with the apply cable to measure the torque on the dynamometer axle. An NI SCXI 1321 terminal block module is used to connect the load cells to the NI SCXI 1121 module. An NI SCXI 1302 terminal block module is used to connect wires from the stepper motor to the NI SCXI 1180 module. The NI SCXI 1302 module connects to a safety circuit and stepper motor driver, which is used to drive the stepper motor. The Control Techniques Mentor II DC drive which is used to control the Leroy Somer LSK1604M04 45kW DC electric motor is connected to the BNC-2090 chassis and controlled by the software outputs. The hydraulic pressure used to apply the brake is

controlled by a Hymid Hydraulics controller connected to the BNC-2090 module and the pressure is measured using a Sensotec pressure sensor in line with the hydraulic circuit. A diagram of the dynamometer hardware components is given in Figure 5.19

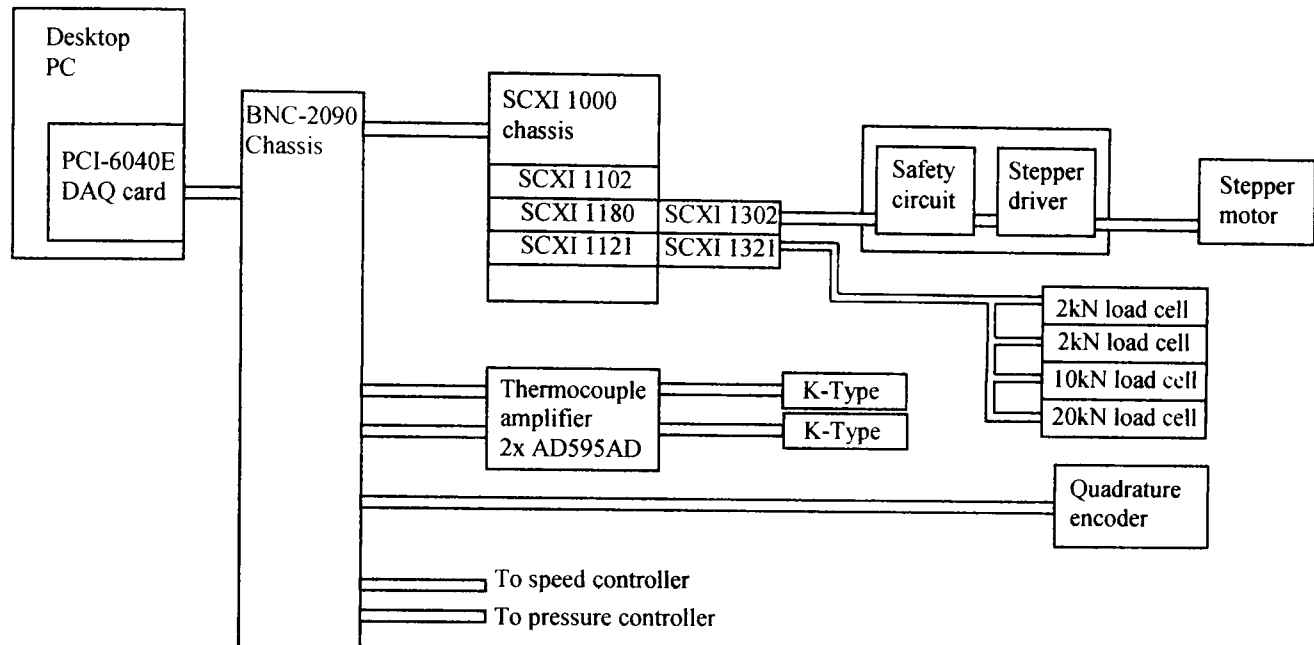


Figure 5.19 Schematic of dynamometer control and DAQ system hardware

5.5.3. Software

National Instruments LabVIEW is a graphical programming language that is widely used throughout industry and academia. It uses a programming language called “G” which allows the user to create block diagrams of the program rather than the traditional text based code. The block diagrams are used to build a program called a Virtual Instrument (VI) which is operated by the user from a front panel on the desktop PC. Numerous VI’s can be created and run simultaneously from the front panel enabling multi-channel data logging and post processing.

The rollaway control and DAQ system uses a command script process whereby the dynamometer performs a series of commands for a given test. The commands used by the dynamometer are given in Table 5.1. The command script used to heat one brake to a temperature of 250°C and then allow it cool to 30°C is given in Table 5.2.

The hydraulic brake pressure inside the calliper at the start of the test is set to 0bar. The hydraulic pressure in the hydraulic system is initially at 20bar and is isolated from the calliper by two solenoid valves. The command script is paused at step 4 to allow the operator to turn one of the solenoid valves off and allow the hydraulic pressure to reach the calliper and apply the brake. This procedure is used because the pressure controller is not capable of producing pressures below 5bar.

Command	Description
Ignore	Ignore the current command line and move on to the next line.
Heat	Wait for the temperature of a specified thermocouple to reach above a specified temperature and then proceed to the next line.
Cool	Wait for the temperature of a specified thermocouple to drop below a specified temperature and then proceed to the next line.
Wait	Wait for a specified period of time before proceeding to the next line.
Pause	Pause the script until the operator presses the 'proceed' button on the software front panel then proceed to the next line.
Ramp speed	Change the speed of the motor to a specified value in a specified period of time.
Ramp pressure	Change the hydraulic brake pressure to a specified value in a specified period of time.
Rotate stepper clockwise	Rotate the stepper motor in a clockwise direction at a specified speed until a specified load is achieved in the parking brake cable.
Rotate stepper anti-clockwise	Rotate the stepper motor in an anti-clockwise direction at a specified speed until a specified load is achieved in the parking brake cable.

Table 5.1 Description of the software commands

Step	Command	Time (seconds)	Speed (rpm)	Pressure (bar)	Thermocouple 1 Temp (°C)
1	Wait	2	0	20	
2	Ramp speed	30	400	20	
3	Ramp pressure	2	400	5	
4	Pause		400	5	
5	Wait	2	400	5	
6	Ramp pressure	2	400	10	
7	Heat		400	10	250
8	Ramp pressure	1	400	0	
9	Ramp speed	20	0	0	
10	Cool		0	0	30

Table 5.2 Command script to heat a brake to 250C then allow it to cool to 30C

The software is activated when the operator starts the script by pressing the 'start script' button on the front panel. Once running the software starts logging data from the dynamometer sensors which is also plotted in the front panel so that the operator can monitor the test. 100 samples per second are recorded which are averaged every $1/10^{\text{th}}$ of a second to produce 10 data points per second for every channel. The software has safety alarms built into the program which shut down the dynamometer if the value measured by one of the sensors exceeds a predefined safety limit. The shaft encoder logging system has a limit of $\pm 2 \times 10^{22}$ measurements. If the data logging system reaches this limit the encoder counter is reset so that the data can continue to be logged. The software executes all of the command scripts and then the dynamometer is shut down, the logging stops and the program ends. A flow chart of the rollaway control and DAQ system program can be seen in Figures 5.20 and 5.21.

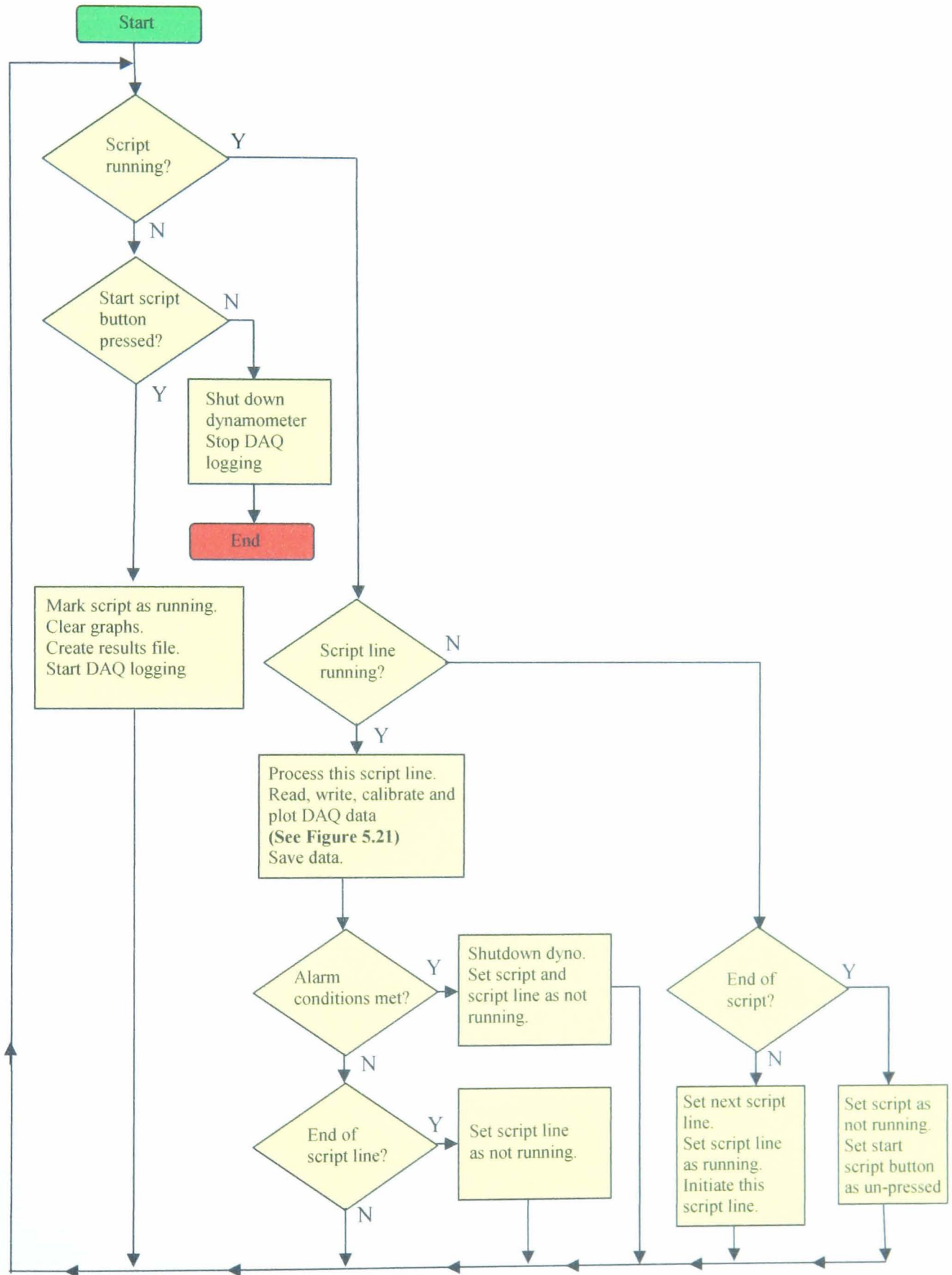


Figure 5.20 Operation of rollaway program

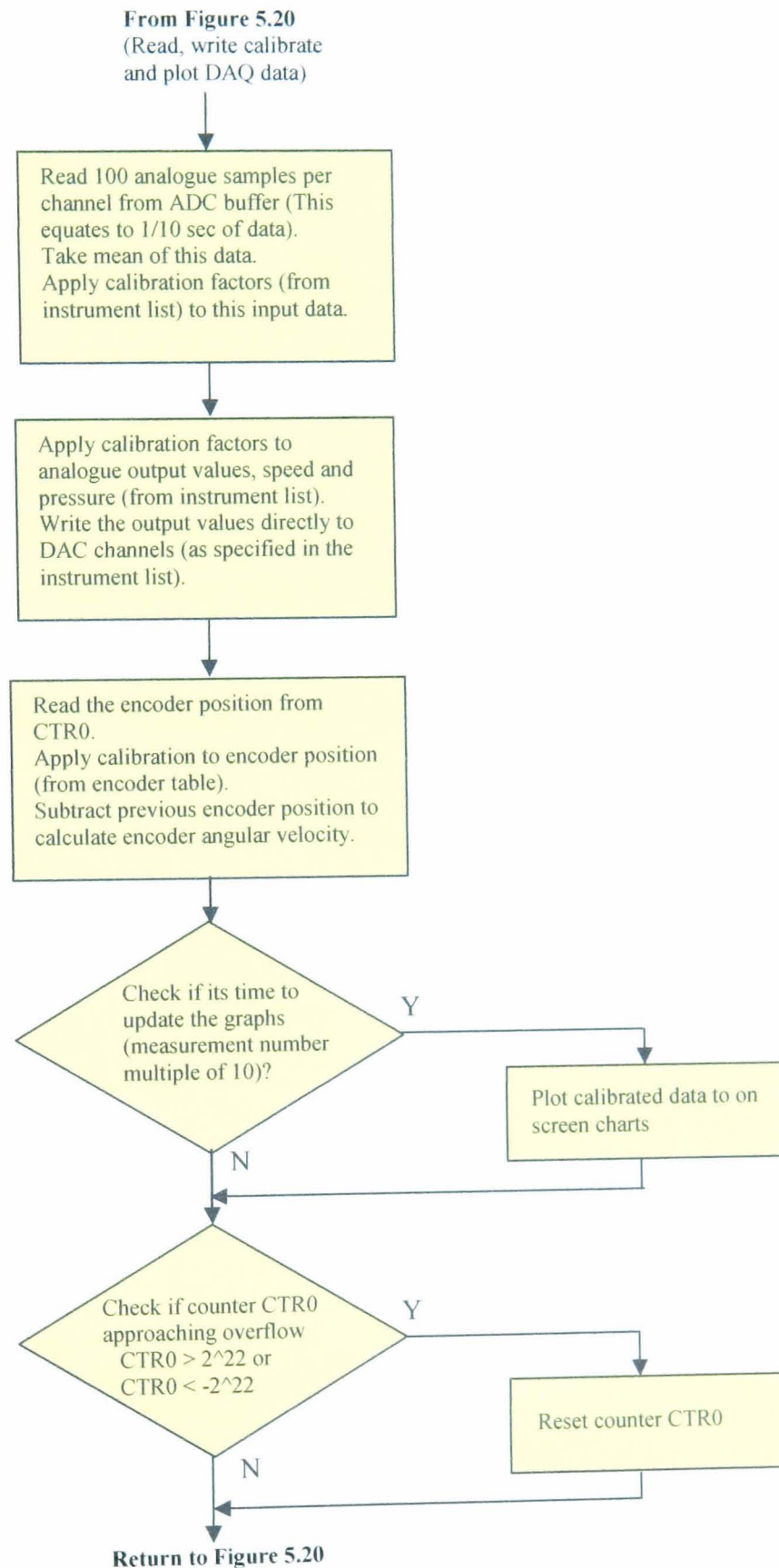


Figure 5.21 Read, write, calibrate and plot DAQ data subsystem of rollaway program

5.6. Modifications to dynamometer

This section describes the modifications that were made to the original dynamometer to develop it into a suitable testing facility for this project.

5.6.1. Dead weight system

The preliminary tests identified the hydraulic actuator as being unsuitable for applying the torque on the dynamometer axle. It was decided that a dead weight system that uses steel weights hung on the cable system would be a cost effective and reliable alternative method of applying a constant torque on the dynamometer axle. The number of weights that are hung on the cable can be varied to develop the required cable load and torque on the dynamometer axle for the test. The hydraulic actuator was retained and used to lift the weights into position to produce the required torque. A diagram of the dead weight system layout is shown in Figure 5.22.

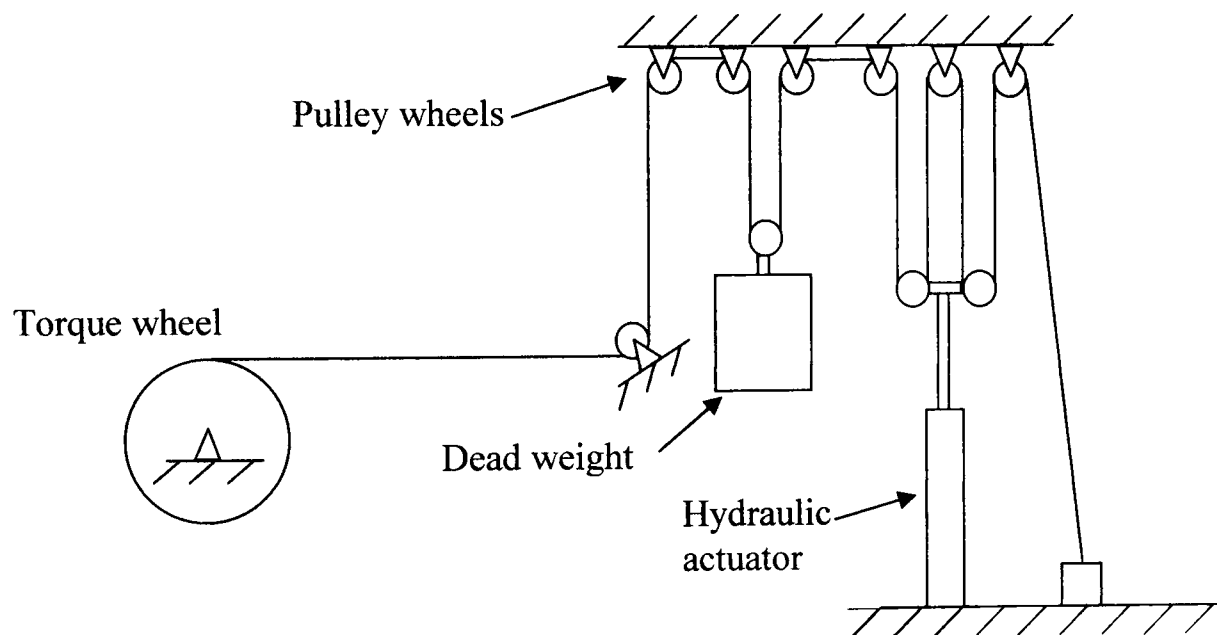


Figure 5.22 Diagram of the dead weight apply system

The framework of the original apply rig was modified so that it could be used to house the dead weight system. The actuator was moved to a newly designed section of framework which was fixed to the original apply rig frame. The new section was designed using AutoCAD 2000 and manufactured by Lambert Engineering Ltd. A photograph of the modified apply rig is shown in Figure 5.23.

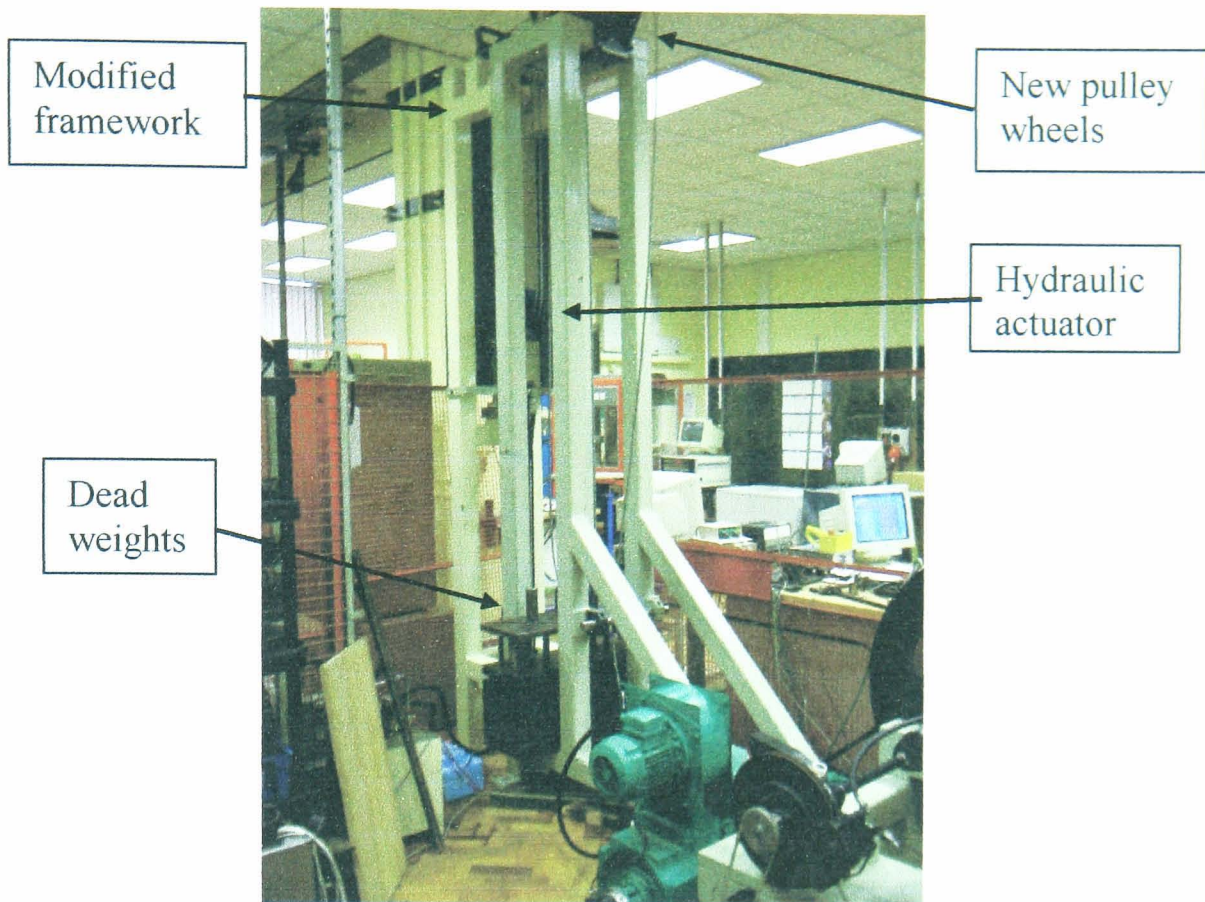


Fig 5.23 Side view of the modified apply rig

The dead weight apply system required additional pulley wheels to those on the original apply rig and so new bearing blocks were designed to fix the pulley wheels to the framework. The pulley wheel assemblies were manufactured by Lambert Engineering Ltd and can be seen in Figure 5.24.

A new cable was required for the apply rig and was supplied by Peter Cassidy Lifting Equipment.



Figure 5.24 Pulley bearing blocks

The preliminary tests discussed in Section 5.4 found the bracket which attached the cable to the large pulley wheel to be unsuitable for use on the dynamometer. A new bracket, shown in Figure 5.25, was designed and manufactured at the University of Leeds that allowed the cable to make more than one revolution on the large pulley wheel and was easy to attach.

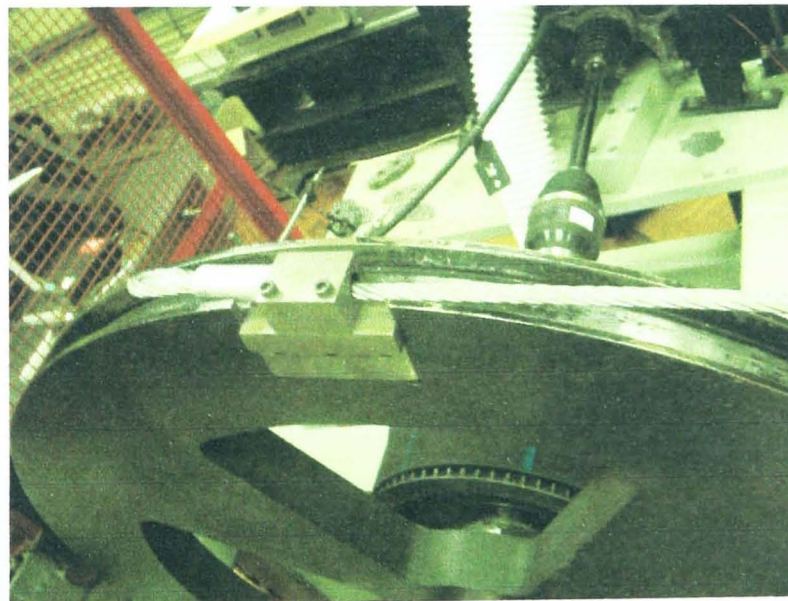


Figure 5.25 Cable attachment bracket

The weights were designed to be located on a weight hanger that was attached to the cable system via a pulley wheel fixed to the hanger. The number of weights attached to the hanger could be varied depending on the required test torque and ensured that

the dynamometer could simulate a vehicle with a mass up to 1900kg parked on a gradient up to 25%. Each of the weights have a mass of 35kg and are held in position on the hanger using a locking pin which passed through the weights and the hanger. The width of the weight hanger and the weights was less than the internal dimensions of the apply rig framework to ensure that the mechanism could be positioned inside the rig. A diagram of the weight hanger assembly is shown in Figure 5.26.

Alken Engineering was selected to manufacture the weight hanger and weights; the pulley wheel assembly that was fixed to the hanger was supplied by Lambet Engineering Ltd.

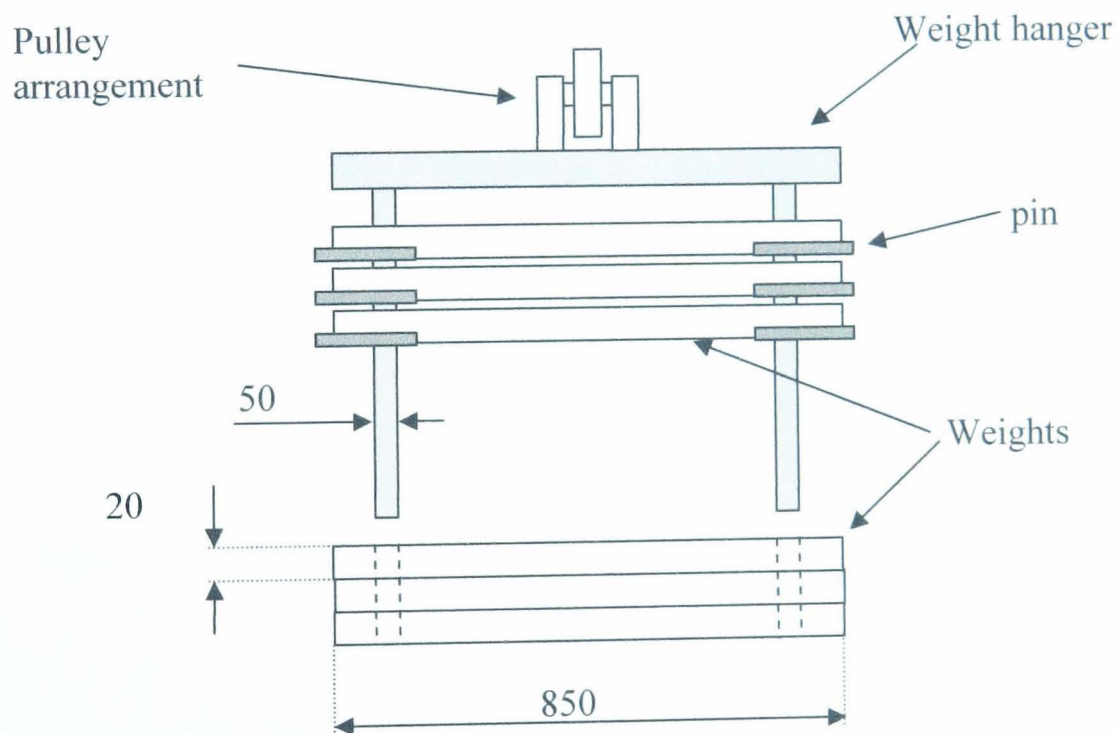


Figure 5.26 Diagram of the weight hanger arrangement

5.6.2. Parking brake apply system

The test described in Section 5.3 showed that the clamp load produced by the Jaguar S-Type's handbrake lever was fixed at finite values determined by the lever's ratchet mechanism. The project requirements state that the dynamometer must be capable of developing a specified clamp load at the frictional interface. To achieve this, a McLennon electric stepper motor was used in conjunction with a worm gear system to pull a shaft attached to the parking brake cable. A 10kN load cell is mounted in line with the actuation system so that the cable loads can be monitored and controlled. A diagram of the electrical parking brake system is shown in Figure 5.27 and a photograph of the system is shown in Figure 5.28.

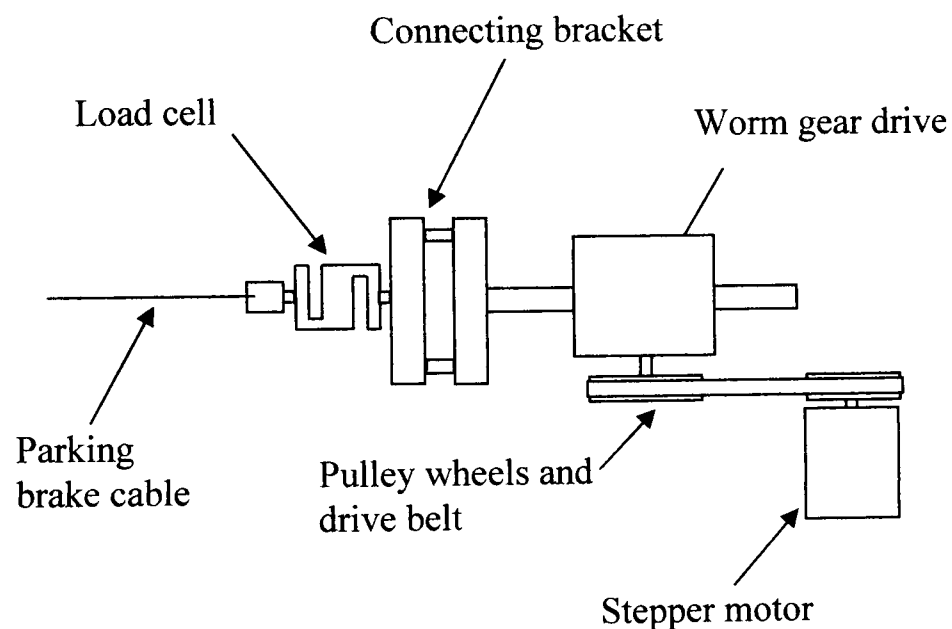


Figure 5.27 Diagram of the electrical parking brake actuation system

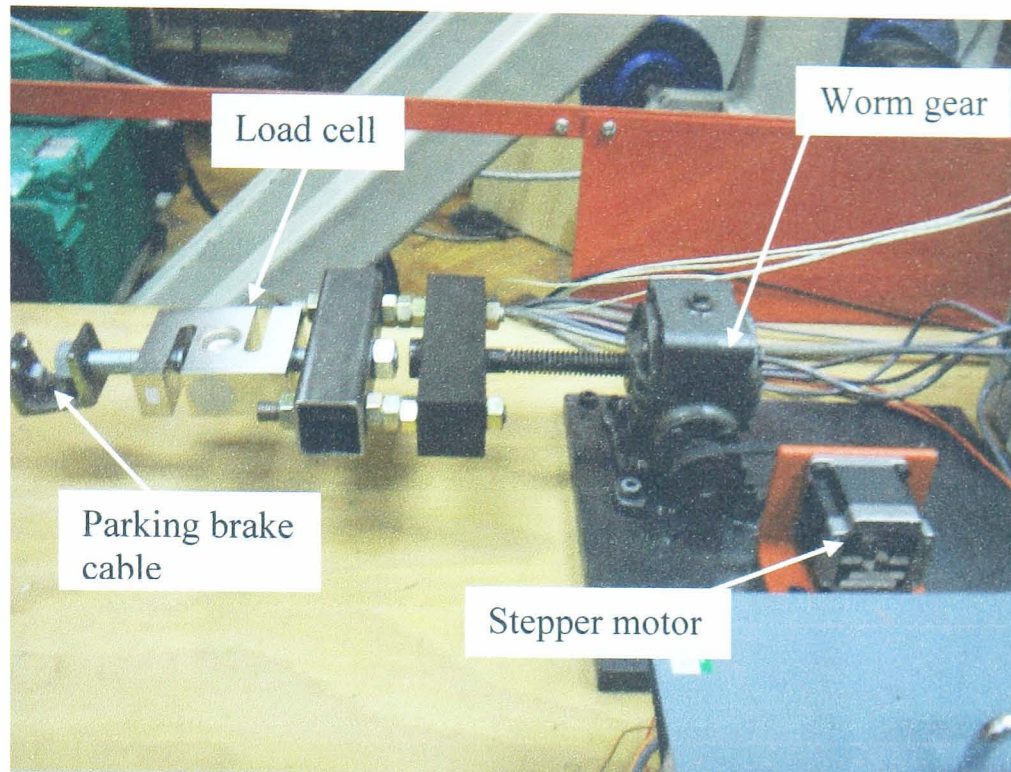


Figure 5.28 Electrical parking brake actuation system

5.6.3. Axle rotation measurement

The proximity sensor used to measure the axle rotation, described in Section 5.2.3, was deemed to be unsuitable for the rollaway dynamometer because the rotation of the axle could only be measured at finite points defined by the teeth on the ABS wheel. A more accurate axle rotation measurement is required for this research because the control software requires an accurate interpolation of the axle speed in order to control the electric motor driving the rig. A Hohoner quadrature shaft encoder that has 720 measurement locations was used to measure the rotation of the dynamometer axle. The shaft encoder was connected to the axle using two gears and a belt. The gear on the axle has double the number of teeth as the gear connected to the shaft encoder. This system doubles the accuracy of the measurements. A photograph of the shaft encoder connected to the dynamometer axle is shown in Figure 5.29.

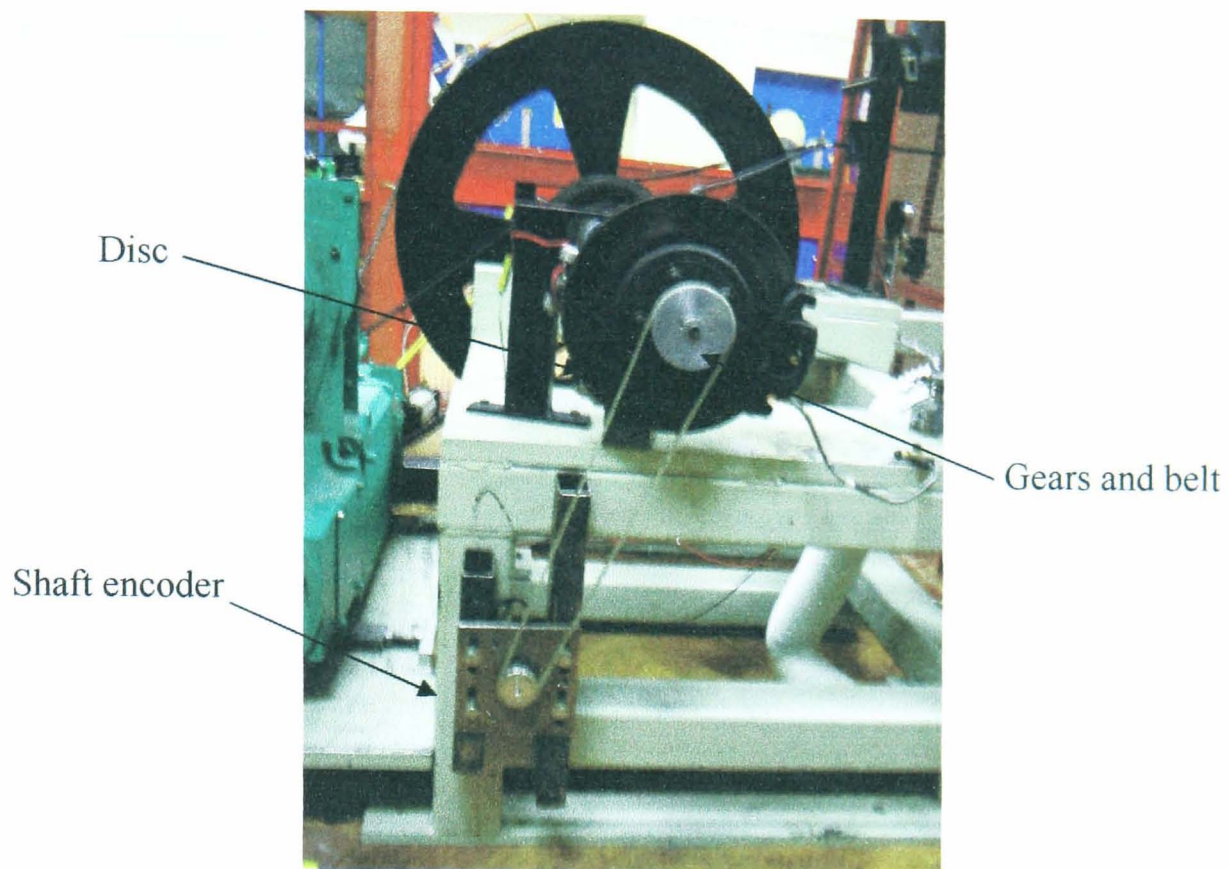


Figure 5.29 Shaft encoder on drive axle of the dynamometer

5.7. Dynamometer operation

The dynamometer is required to conduct two main types of test for the current research project, a normal load test and a static friction test. The normal load test is used to measure the normal load at the frictional interface as a function of temperature. The static friction test is used to measure the static coefficient of friction between the pads and disc as a function of temperature. Before either of these tests can be conducted, the dynamometer is setup according to the procedure described in Appendix A. Once the dynamometer has been correctly setup, the normal load procedure, described in Appendix B, or the static friction procedure, described in Appendix C, is followed.

5.8. Commissioning tests

A series of commissioning tests was conducted to confirm that the modified dynamometer fulfilled the requirements of the project described in Section 5.3. A brief description of these tests and their outcomes is given below in Sections 5.8.1 to 5.8.4.

5.8.1. Heating the brakes to a specified temperature

A test was designed to heat a brake on the dynamometer to a temperature of to 250°C and allow the brake to cool to a temperature of 30°C. The test was controlled by the Labview program described in Section 5.5 and the result from the test is shown in Figure 5.30.

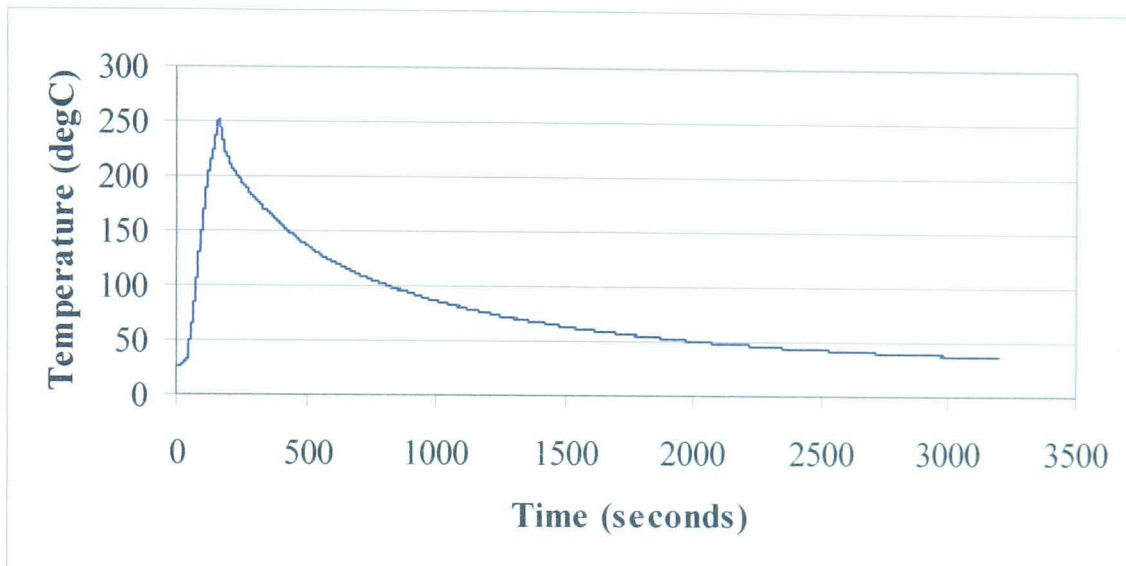


Figure 5.30 Temperature of the brake during commissioning test

The result in Figure 5.30 shows that the dynamometer is capable of heating the brake to a specified temperature. The maximum temperature achieved was 251°C, which is closer to the target temperature of 250°C than the temperature achieved during the manual test operation described in Section 5.4.1. The test was controlled by the rollaway program and is therefore repeatable. This ensures that the brakes are heated consistently during the dynamometer experiments.

5.8.2. Application of a constant torque

A test was designed to investigate the capacity of the dead weight system to apply a constant torque on the dynamometer axle. A 20kN Graham and White DSCRA load cell positioned in line with the cable system was used to measure the force in the cable. The torque on the dynamometer axle was calculated by multiplying the measured force by the radius of the large pulley wheel. Figure 5.31 shows the torque on the dynamometer axle produced by the original hydraulic apply system and the modified dead weight system.

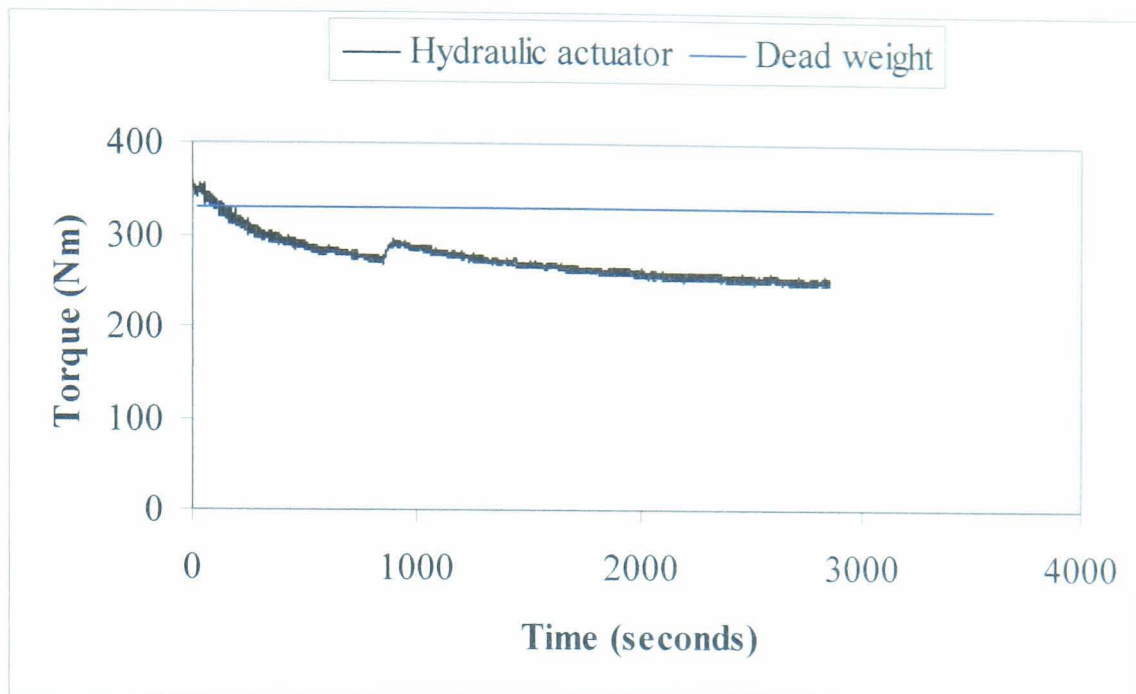


Figure 5.31 Torque on the dynamometer axle during commissioning test

The result in Figure 5.31 shows that the torque produced by the dead weight system remained constant for the duration of the test whereas the torque produced by the hydraulic actuator varied and generally decreased with time. The torque values produced by the dead weight system prior to 18 seconds were neglected as the weights were raised into position during this time. The test has shown that the modified dynamometer is capable of simulating a vehicle parked on a gradient. The test also demonstrated the functionality of the new cable attachment bracket, which allowed the cable to complete more than one revolution of the large pulley wheel and was easily attached during the test.

5.8.3. Actuating the parking brake and measuring the clamp load

During a rollaway test it is not possible to measure the clamp load at the frictional interface using the 10kN load cell because the pads and disc are located at the load cell position. The clamp load is measured indirectly using the 2kN load cell in line with the parking brake cable. A test was conducted to measure the clamp load as a function of the cable load when the maximum cable load of 1.1kN was applied and then released. The test was conducted 5 times and the results were repeatable and can be seen in Figure 5.32. The maximum cable load of 1.1kN was not applied during the on-vehicle tests as discussed in Chapter 4 and so a cable load of 0.6kN

was selected for the dynamometer evaluations. During the dynamometer tests, it was expected that the cable load would reduce over time. A test was conducted to measure the clamp load as the cable load reduced from 0.6kN to 0kN. The result was repeatable and is plotted in Figure 5.33.

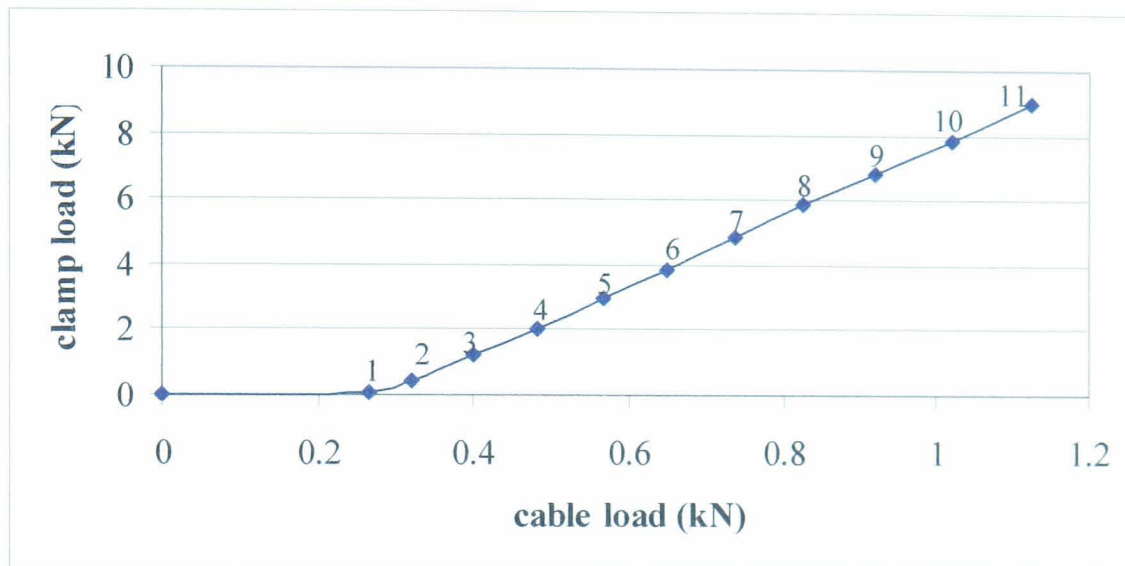


Figure 5.32 Cable load and clamp load produced by Jaguar S-Type parking brake system with the location of the 11 ratchet positions

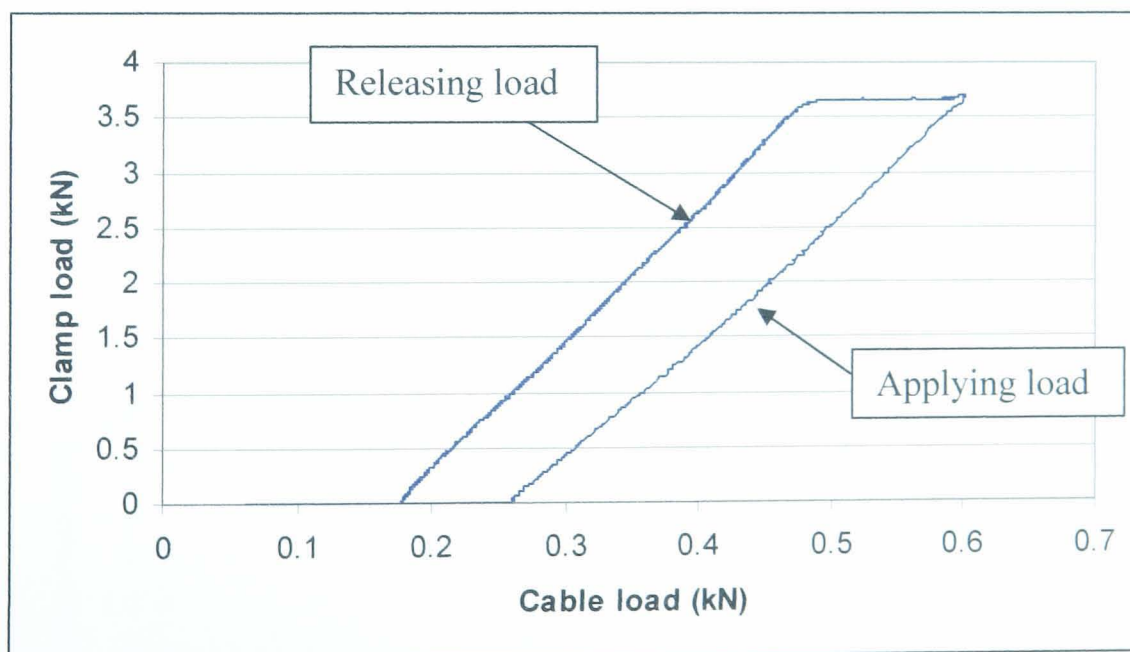


Figure 5.33 Cable load and Clamp load produced by the Jaguar S-Type parking brake system with a load of 0.6kN applied and released

The result in Figures 5.32 and 5.33 shows that no clamp load was achieved for cable loads below 0.25kN because the calliper is designed to have a threshold load below which no piston displacement is produced. Once the threshold load has been

overcome, the clamp load follows a linear relationship with cable load. The result in Figure 5.33 shows that when the cable load was released to 0.48kN the system contained sufficient stored energy to prevent the clamp load from reducing by more than 0.1kN. For cable loads between 0.48 and 0.2kN the clamp load followed a linear relationship.

The result in Figure 5.33 was used to establish an approximate relationship between cable load and clamp load as the cable load reduced from 0.6kN. The result can be used to calculate the clamp load in the dynamometer experiments. The approximation is defined as:

$$\begin{aligned} F_{cp} &= 3.66 & \text{for} & & 0.48 < F_{cb} < 0.6 \\ F_{cp} &= 11.8F_{cb} - 2 & \text{for} & & 0.2 < F_{cb} < 0.48 \end{aligned} \quad (5.1)$$

Where:

F_{cp} = Clamp load (kN)

F_{cb} = Cable load (kN)

The approximate relationship is plotted in Figure 5.34 along with the experimental result recorded during the test.

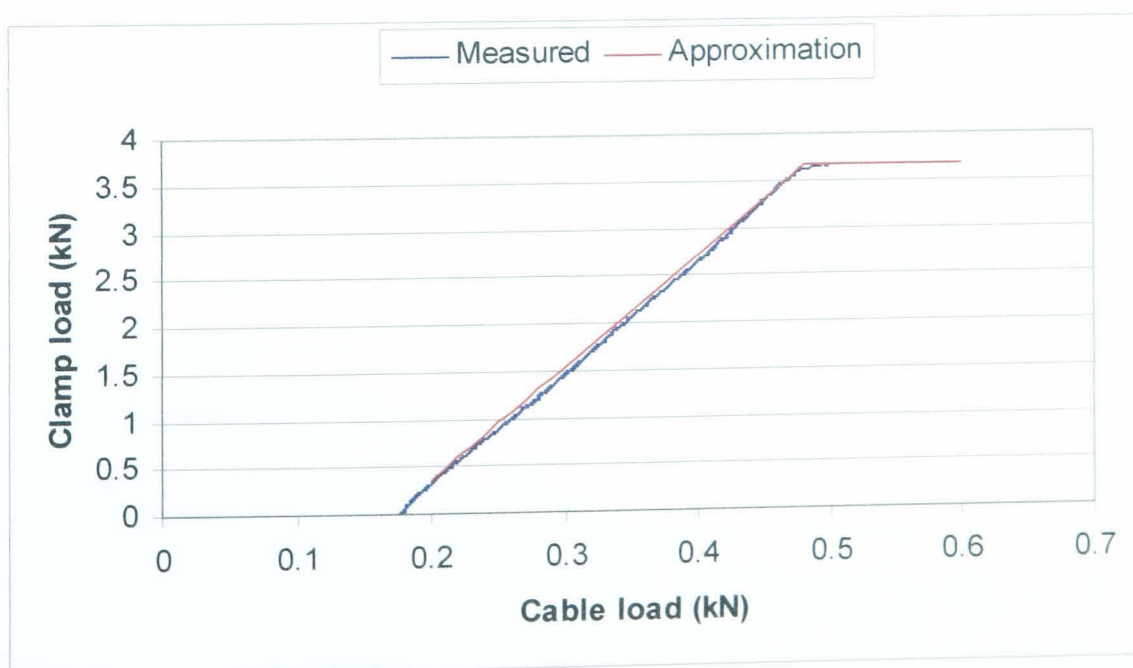


Figure 5.34 Clamp load measured on the dynamometer and the mathematical approximation

Figure 5.34 shows that the approximation can be used to calculate the clamp load for cable loads between 0.2 and 0.6kN.

5.8.4. Clamp force measurement as a function of temperature

A commissioning test was conducted to measure the clamp force at the frictional interface as a function of temperature. The test followed the procedure described in Appendix B.

The load in the cable attached to the calliper was measured using the 2kN NovaTech load cell as the brake cooled from 250°C to 30°C. The clamp load was calculated from Equation 5.1 and the result is plotted in Figure 5.35.

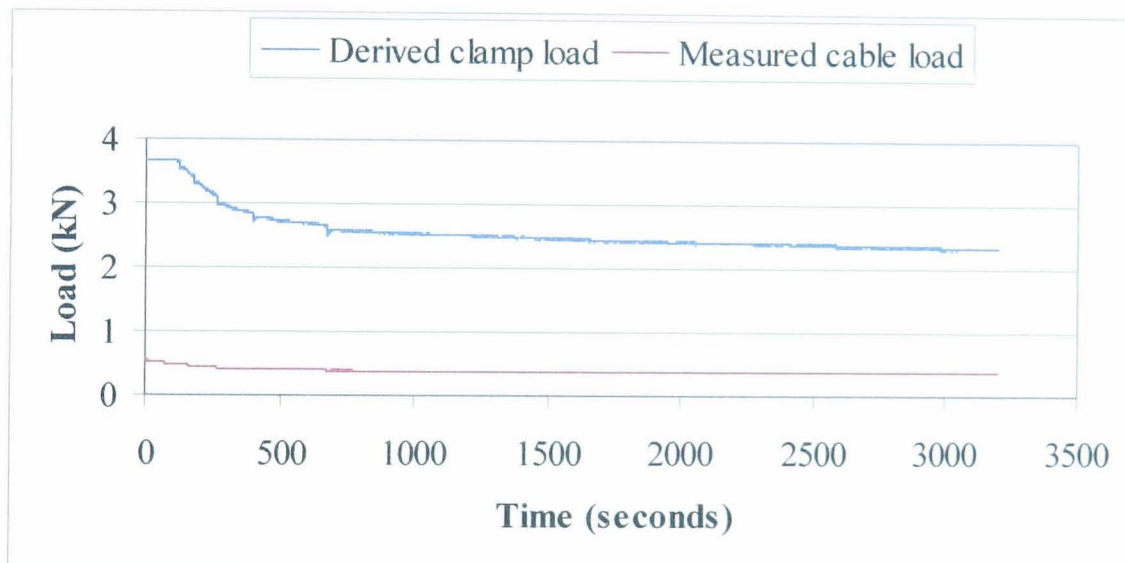


Figure 5.35 Measured cable load and derived clamp load as the brake cools from 250°C to 30°C

Figure 5.35 shows that once the hysteresis in the system had been overcome the clamp force at the frictional interface reduced as the brake cooled. The test demonstrates that the dynamometer is capable of measuring the reduction in clamp load at the frictional interface as a function of temperature.

5.8.5 Measuring the static coefficient of friction as a function of temperature

A commissioning test was conducted to measure the static coefficient of friction between the pad and disc as a function of temperature. The test followed the procedure described in Appendix C and was repeated for the disc at temperatures

between 20°C and 300°C to establish a relationship between the static coefficient of friction and temperature. The result is plotted in Figure 5.36.

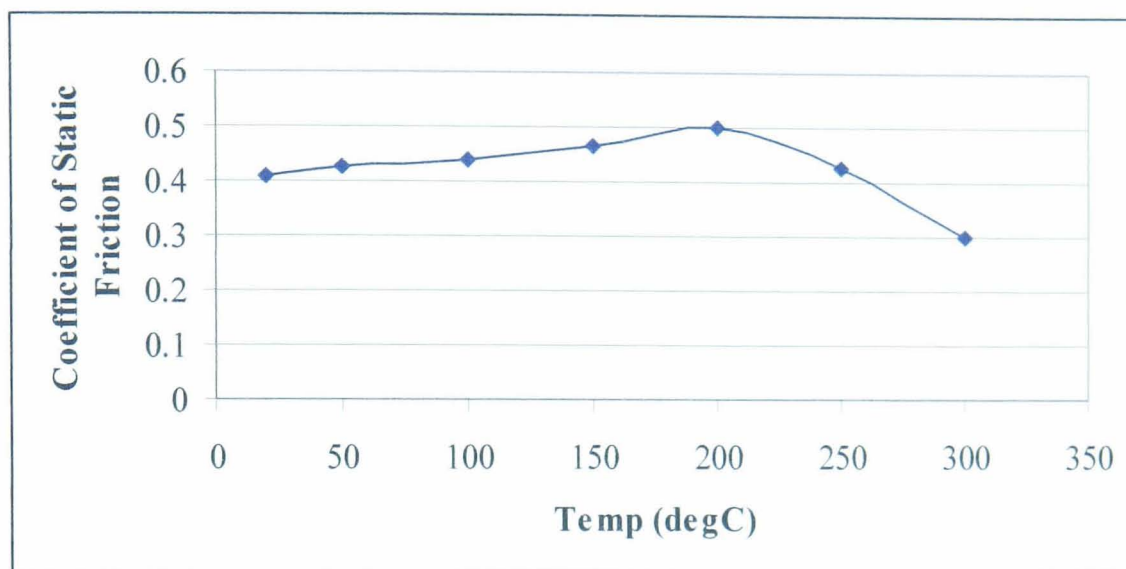


Figure 5.36 Coefficient of static friction of Pad 1 as a function of temperature

The result in Figure 5.36 shows that the static coefficient of friction between the pad and disc generally increases up to a temperature of 200°C and then decreases between temperatures of 200°C and 300°C. This result shows that the dynamometer is capable of measuring the static friction level as a function of temperature. The test was not repeated because it was a set-up test. The measured values used in this research are taken from repeat readings and are described in Chapter 6.

5.9. Summary

A novel dynamometer test facility dedicated to the study of vehicle rollaway has been developed. This faithfully represents the Jaguar S-Type's parking brake system layout and is capable of simulating automotive operating conditions. The dynamometer can be used to measure the change in the parking brake force as the brake cools from an elevated temperature. The dynamometer is capable of measuring the static coefficient of friction at the brake frictional interface as a function of temperature.

Chapter 6

Experimental characterisation of rollaway

6.1. Introduction

This chapter discusses the laboratory based experimental evaluations that have been conducted for this research. The foundation brake components investigated are described in Section 6.2. The testing methods employed to characterise the performance of the parking brake system are described in Section 6.3. The performance of the Jaguar S-Type OE parking brake system is discussed in Section 6.4. Sections 6.5 to 6.9 discuss the results from the Jaguar S-type components that have been investigated for this research.

6.2. Foundation brake components

This section describes the foundation brake components that have been used during the present study. Sections 6.2.1 to 6.2.4 discuss the brake pads that have been tested. Sections 6.2.5 and 6.2.6 discuss the discs and callipers that have been used.

6.2.1. On-vehicle pads

The performance of the four different pads that were tested during the on-vehicle tests, labelled Pads 1 to 4, was characterised during the experimental evaluations. The pads include the original equipment pad (Pad 1) and three additional pads (Pads 2, 3 and 4) designed by Federal Mogul formulators. A full description of the pads is given in Chapter 4.

6.2.2. Pressure scorched pads

The literature review in Chapter 3 identified that the properties of the pads have a significant influence on the brake performance. Vehicle rollaway is thought to be caused by a reduction in clamp load at the frictional interface which occurs when the brake cools, due to thermal contractions of the pad and disc. Therefore the thermal expansion coefficient of the friction material is believed to have a significant effect on the clamp load variations with temperature. The brake is assumed to behave like a spring system that is capable of storing energy and so the stiffness of the materials

is also believed to have a significant effect on the clamp load variations with temperature.

Pressure scorching is a method that is sometimes used in the manufacture of friction materials so that they require less bedding and exhibit optimal properties off the production line. Pressure scorching is believed to change the thermal expansion coefficient and the stiffness of the friction materials and so was used for this research to attempt to vary the properties of the OE pad. Four new sets of pads, labelled Pads 5 to 8, were produced and then treated on a Leinweber pressure scorching machine housed at the Federal Mogul technical centre. The machine works by compressing a pad at a temperature of 600°C for 4 minutes then compressing the pad at a temperature of 15°C for a period of 4 minutes. The pads are compressed using a hydraulic actuator which when under load moves the pad into contact with the counter surface. The pressure applied to compress the pad can be varied between 0 and 5.7bar. The heat is provided by two hotplates set to 150°C and 600°C. The 600°C hotplate is located above the pad facing the friction surface. The back plate faces the 150°C hotplate which moves upwards and presses the pad against the 600°C hotplate generating the required pressure. Once the pad has been scorched it is then cooled down using two water cooled plates at a temperature of 15°C which apply a pressure in the same way to the scorching phase. A schematic of the pressure scorching machine is shown in Figure 6.1, along with a photograph of the machine in Figure 6.2.

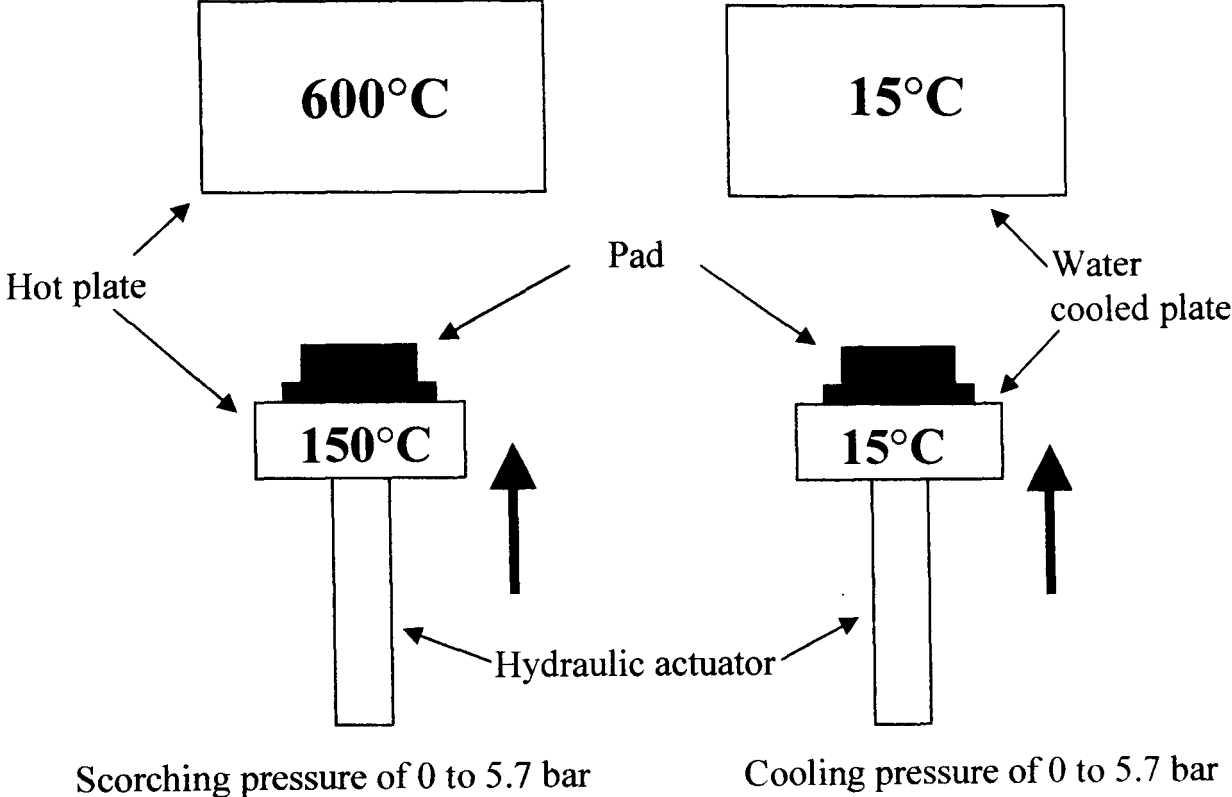


Figure 6.1 Schematic of the pressure scorching machine



Scorching draw

Cooling draw

Figure 6.2 Photograph of the pressure scorching machine

The four pads were subjected to different pressure scorching treatments. Table 6.1 lists the hot and cold pressures that were applied to the pads. A pressure of 0bar indicates that a nominal pressure was applied during this period so that the pad was in contact with the hot plate or water cooled plate.

Pad number	Hot pressure (bar)	Cold pressure (bar)
5	0	5.7
6	5.7	5.7
7	1.6	1.6
8	5.7	0

Table 6.1 List of pad numbers and pressure scorch conditions

6.2.3. Modified formulation pads

The properties of a friction material are primarily governed by the elements used within the formulation. Two friction materials, labelled Pads 9 and 10, were developed by formulators at Federal Mogul that would have varying stiffness and thermal expansion values. This was done to see how the properties of the pad affect the clamp load variations with temperature. Pad 9 was designed to have a high stiffness and low thermal expansion coefficient and Pad 10 was designed to have a low stiffness and a high thermal expansion coefficient.

6.2.4. Modified Original Equipment Formulations

The literature review in Chapter 3 suggests that the level of hard abrasives in the friction material formulation is directly linked to the coefficient of friction between the pad and disc. It is hypothesised that the friction level can be changed by varying the amount of hard abrasive in the formulation. A significant hard abrasive in the Jaguar S-Type OE pad is fused alumina. Discussions with the formulators at Federal Mogul revealed that the pad contains 0.29% fused alumina by weight in the formulation. This formulation was modified by the formulators to produce three new pads labelled Pads 11 to 13, containing 0%, 0.6% and 1.2% fused alumina by weight respectively in the formulation. Inert filler additions were used to compensate for the changing percentage of fused alumina in the pad formulations.

6.2.5. Disc

Five different disc designs have been investigated during the present study. They include the Jaguar S-Type OE disc, which is a vented disc with a 20mm thickness and 288mm diameter. Four additional discs were also tested, which are solid discs with a diameter of 288mm and a thickness of 12mm, 10mm, 8mm and 6mm. The discs were produced by machining the inboard side of a 12mm thick disc down to the required size. The discs were machined by Federal Mogul technicians to ensure that the surface finish of the disc was kept to the same standard as the un-machined disc. The discs were produced to investigate the effect of disc thickness on the propensity of rollaway. A cross sectional photograph of one of the machined discs is shown in Figure 6.3.

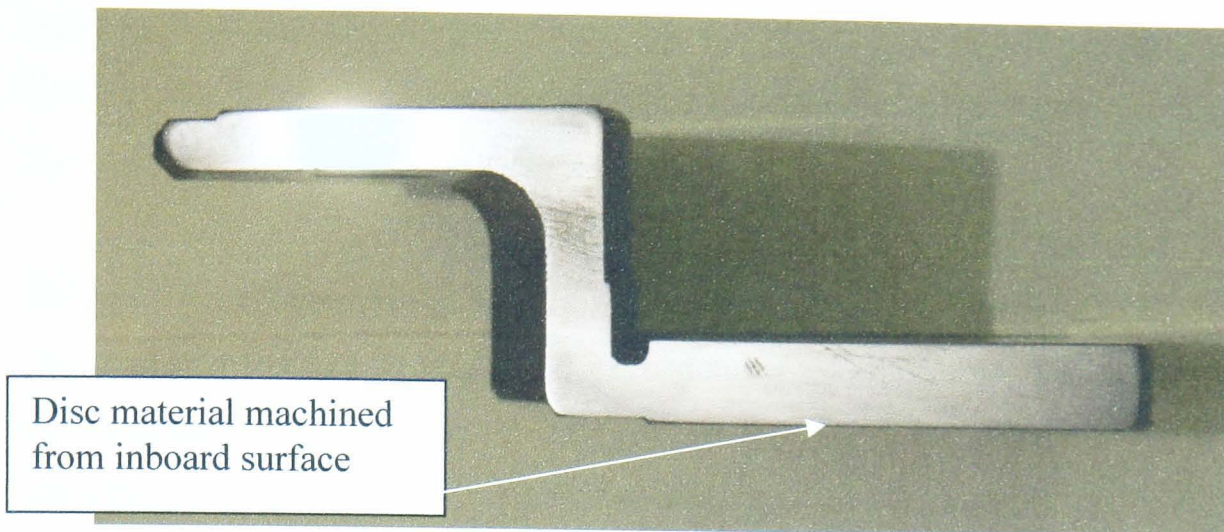


Figure 6.3 Cross sectional photograph of the disc machined down to 9mm thickness.

6.2.6. Calliper

Three calliper designs, labelled Callipers 1 to 3, were used during the study: a cast iron TRW Jaguar S-Type OE calliper, a cast iron Bosch BIR3 calliper and an aluminium Bosch BIR3 calliper. The Bosch BIR3 callipers were selected to compare the performance of the two different calliper materials. The callipers are discussed in detail in Chapter 4.

6.3. Methods

This section describes the testing methods that have been used during the experimental characterisation of rollaway. The friction materials used in this study are composed of varying properties of either the same or different constituents or are subjected to varying manufacturing processes, which influence the characteristics of the material. An accurate interpretation of the material characteristics is required to successfully develop a mathematical model of the parking brake system. Tests have been conducted to measure the properties of the friction materials used in this project and are discussed in Section 6.3. Section 6.4 discusses the results from tests conducted to characterise the behaviour of the Jaguar S-Type OE parking brake system.

Hildred [28] states that the material properties of a friction material cannot be generalised by a simple law of mixtures because certain constituents in the

formulation interact with the matrix material on an almost atomic level. The resulting material properties of the composite system are therefore highly complex. This section describes the mechanical tests conducted to describe the properties of the materials used during the current project.

6.3.1. Compression tests

The friction material is composed of a number of different elements with each contributing to the overall compressibility of the material. Compression tests were conducted to accurately describe the stiffness and Young's modulus of the friction material for temperatures between 20°C and 400°C and pressures between 40bar and 160bar. The pad stiffness (k) and Young's modulus (E) of the material are calculated from the compression results using Equations 6.1 and 6.2.

$$F = k\Delta l \quad (6.1)$$

$$E = \frac{kl}{A} \quad (6.2)$$

Where:

F = applied load (N)

k = stiffness (N/m)

Δl = compression (m)

l = original thickness of the pad (m)

A = area of the pad (m^2)

The compression tests were conducted by placing a pad inside a Jurid compression tester and measuring the deflection of the pad while under varying loads and at different temperatures. The full test procedure used to obtain the pad compression is described in Appendix G.

6.3.2. Thermal Expansion tests

The thermal contraction of the brake components that occurs when the brake cools is believed to have a significant effect on the clamp load variation at the frictional interface. A successful mathematical model of the parking brake system requires an accurate interpretation of the thermal expansion coefficients of the materials within

the model. Tests were conducted to measure the thermal expansion coefficient of the materials used in the brake system using a Perkin Elmer Dynamic Mechanical Analyzer (DMA).

The success of the results depends of the preparation of the samples used and the DMA dictates that the samples must be no wider than 6mm by 6mm with a height less than 12mm. The top and bottom faces of the sample must be parallel to obtain an accurate result. The samples were cut by hand from the brake pad because attempts to machine the samples resulted in the destruction of the material. It was difficult to obtain the required sample geometry due to the composite nature of the material. The samples were polished by hand using varying grades of polishing paper to obtain the required finish with the surfaces as smooth and parallel as possible.

The test consisted of heating the sample inside a helium filled oven and measuring the deflection of the samples with a contacting displacement transducer. The full test procedure used for the DMA thermal expansion tests is given in Appendix H.

An electrical fault occurred during the tests which meant that the DMA could not be used to measure the thermal expansion coefficient of Pads 5 to 8. An alternative method of measuring the thermal expansion coefficient was developed using the Jurid testing machine that was used for the compression tests. The machine was used to measure the thermal expansion coefficient of Pads 5 to 8. The test was also conducted on Pads 1 to 4 and Pads 9 and 10 to compare the results from the DMA and the Jurid tester. The Jurid tester measured the thermal expansion coefficient of the pad by placing it on a hotplate at ambient temperature then increasing the hotplate temperature to 400°C. A contacting displacement transducer was used to measure the deflections of the pad as it was heated. A full description of the test procedures used to obtain the thermal expansion coefficient using the DMA and Jurid tester are given in Appendices H and I.

6.3.3. Dynamometer clamp load evaluations

The clamp load evaluations were conducted on the rollaway dynamometer, described in Chapter 5, to measure the clamp load at the frictional interface as a function of time. A full description of the test is given in Chapter 5 and the test procedure is described in Appendix E.

6.3.4. Dynamometer static friction tests

The static friction tests were conducted on the rollaway dynamometer, described in Chapter 5, to quantify the friction level as a function of temperature. A full description of the test is given in Chapter 5 and the test procedure is described in Appendix F.

6.3.5. Surface characterisation

The friction coefficient is influenced by the real area of contact at the frictional interface. A smooth pad surface will produce a larger real contact area than a rough surface due to the protruding asperities and undulations on the rough surface. Only the peaks of the undulations on the rougher pad will come into contact with the counter surface producing a lower contact area. The surface profile of the pad is dependant on the ingredients within the friction material formulation and also the conditions which the pad has been subjected to. Hildred [25] has shown that a bedded pad has a smoother surface than a virgin pad, which is due to the reduction of protruding particles on a bedded pad because they are effectively polished and worn down by the disc and a third body layer is produced. Surface profile tests were conducted using a Taylor-Hobson Talysurf contacting stylus which traces a path across the surface of the pad. The stylus can measure variations in the surface to a level of $\pm 0.01 \mu\text{m}$ which is used to calculate the center line average roughness, R_a , of the pad using Equation 6.3.

$$R_a = \frac{1}{L} \int_0^L |z(x)| dx \quad (6.3)$$

Where: x = position along the sample from 0 to L
 z = deviation from mean surface
 L = length of the sample

During the test, roughness samples were taken from Pad 1 in a bedded and un-bedded condition at three positions, P1, P2 and P3, which are indicated on Figure 6.4, with the pad at a temperature of 20°C, 100°C and 200°C.

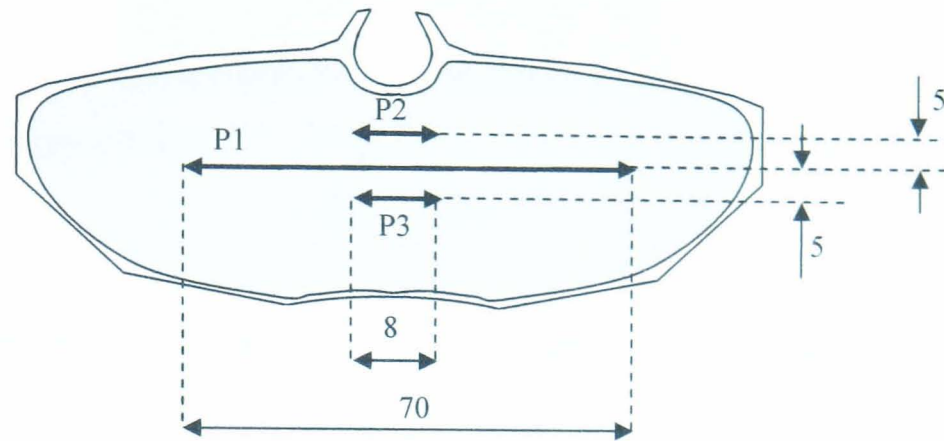


Figure 6.4 Position of the surface profile measurements on the pad (not to scale)

6.3.6. Calliper tests

Tests were conducted on the Jaguar S-Type OE calliper, Calliper 1, to measure the deflection of the calliper fingers under loads produced by the hydraulic system and loads produced by the parking brake system. The deflection of the calliper fingers can be used to calculate the stiffness of the calliper assembly which may have an influence on the propensity of the parking brake system to rollaway. The tests were conducted at temperatures of 30°C to 90°C in increments of 10°C to investigate the calliper stiffness as a function of temperature. The calliper was heated on the Jaguar S-Type by driving the vehicle on the Federal Mogul proving ground and applying brake stops. The brake stops were repeated until the calliper had reached the required temperature. The bulk calliper temperature was measured using a contacting K-type thermocouple located on the calliper bridge. The point on the calliper finger where the deflections were measured is shown in Figure 6.5. The displacement was measured using a linear variable differential transformer (LVDT). The brake line pressure was controlled by manually applying the foot brake pedal. The load from the parking brake system was controlled by manually applying the vehicle hand brake lever.

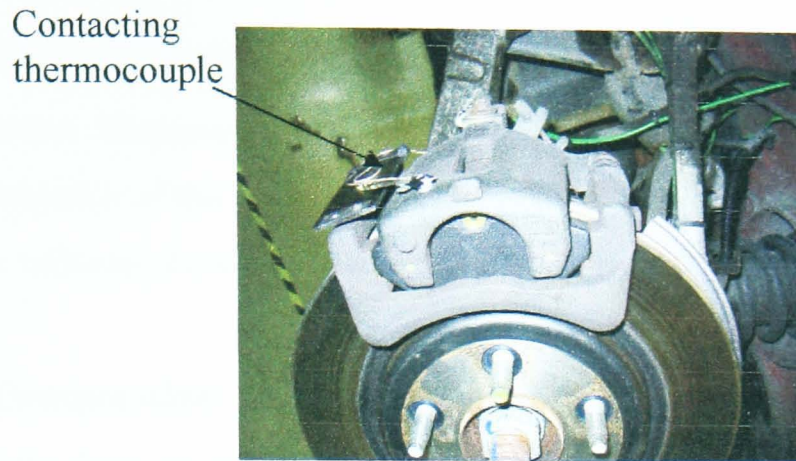


Figure 6.5 S-Type calliper with deflection measurement point 15mm from tip of calliper finger.

Tests were conducted on Callipers 2 and 3 to compare the deflections produced by the cast iron and the aluminium callipers. The deflections were measured at ambient temperature from three positions on the calliper finger, shown in Figure 6.6, to investigate how the calliper fingers deflected at varying locations on the finger.

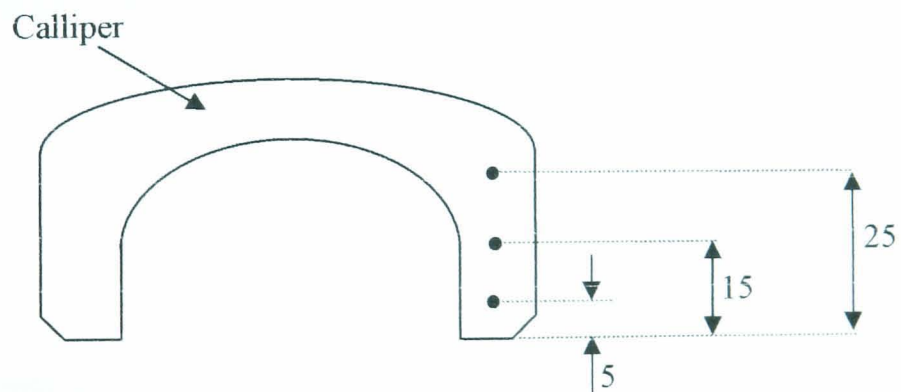


Figure 6.6 Locations of the measurement positions on the calliper finger

6.4. Original Equipment Performance Results

This section discusses the tests that have been conducted to contribute to the characterisation of the behaviour of the Jaguar S-Type OE brake system components during a rollaway event.

6.4.1. Compression

The results from the compression tests conducted on Pad 1 are shown in Table 6.2 and Figures 6.7 and 6.8. The test was repeated twice and the values shown in Table 6.2 are the average of the two values. The maximum variation in all of the results was $\pm 11\mu\text{m}$.

Temp (°C)	Compression (μm)				
	40 bar	60 bar	80 bar	100 bar	160 bar
20	42	61	80	96	140
50	40	60	79	95	145
100	41	61	81	98	148
200	44	66	87	105	159
300	55	81	105	127	193

Table 6.2 Pad 1 compression at varying applied load and temperature.

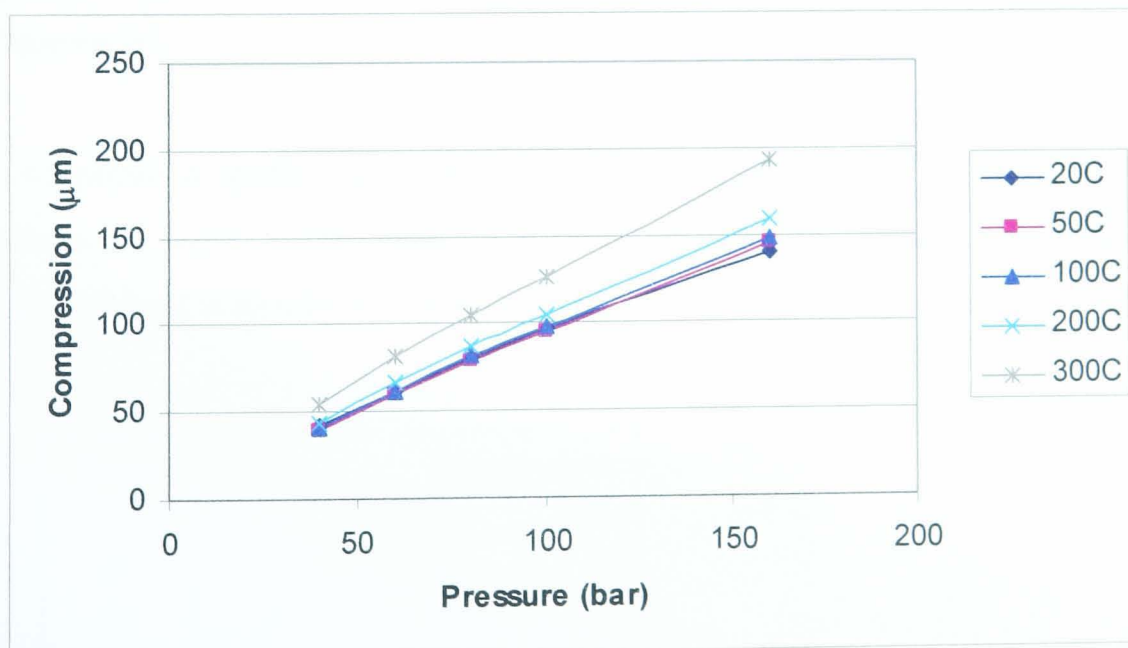


Figure 6.7 Compression of Pad 1 at varying pressures and constant temperatures

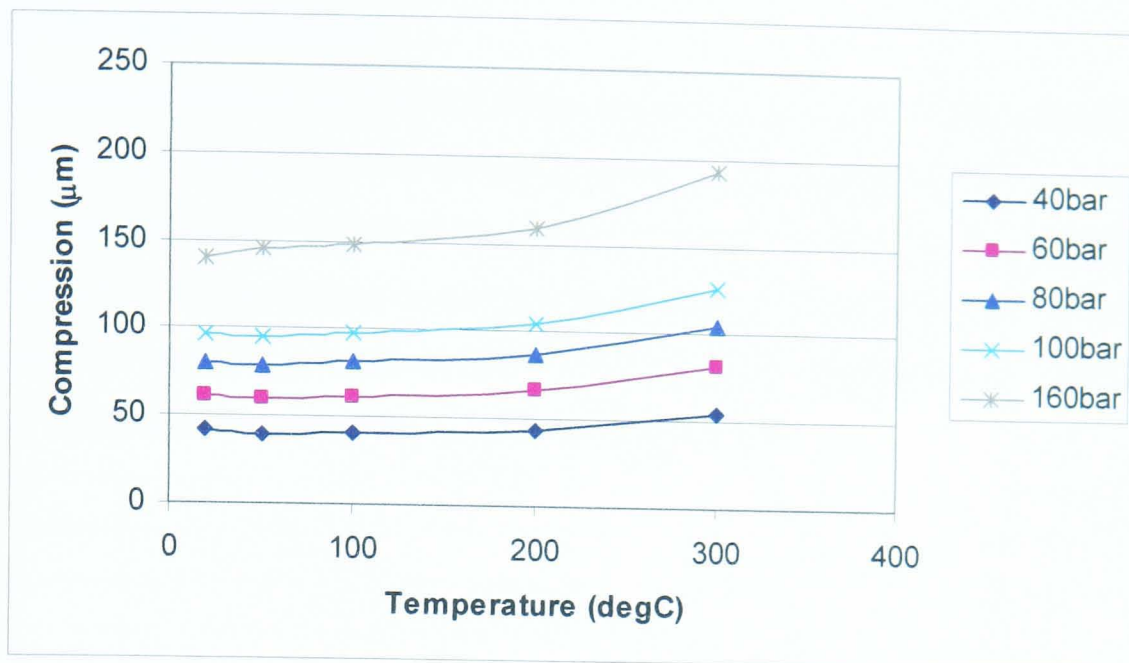


Figure 6.8 Compression of Pad 1 at varying temperatures and constant pressures

The results show that the compressibility of the pad increases with an approximately linear relationship with pressure at a constant temperature for the temperatures tested. The compressibility of the pad increased with temperature in a non-linear manner for the different applied pressures. The results suggest that the compressibility of the friction material will reduce as the brake cools and the normal load decreases.

The compression results were used to derive the Young's modulus of Pad 1 using Equations 6.1 and 6.2. The Young's modulus of Pad 1 as a function of temperature and applied load is plotted in Table 6.3.

Temp (°C)	Young's modulus ($\times 10^6$ Pa)				
	40 bar	60 bar	80 bar	100 bar	160 bar
20	518	357	272	227	155
50	544	363	275	229	150
100	530	357	269	222	147
200	494	330	250	207	137
300	395	269	207	171	113

Table 6.3 Pad 1 Young's modulus at varying applied pressure and temperature

6.4.2. Thermal expansion

The thermal expansion coefficients of the Jaguar S-Type OE pad and cast iron disc were measured using the DMA testing machine. Three samples of the pad and disc were measured and the height of the sample during the test is plotted in Figures 6.9 to 6.14. The average thermal expansion coefficient was calculated for the samples between the start temperature of 30°C and the final temperature of 300°C. The results along with the variations are plotted in Table 6.4.

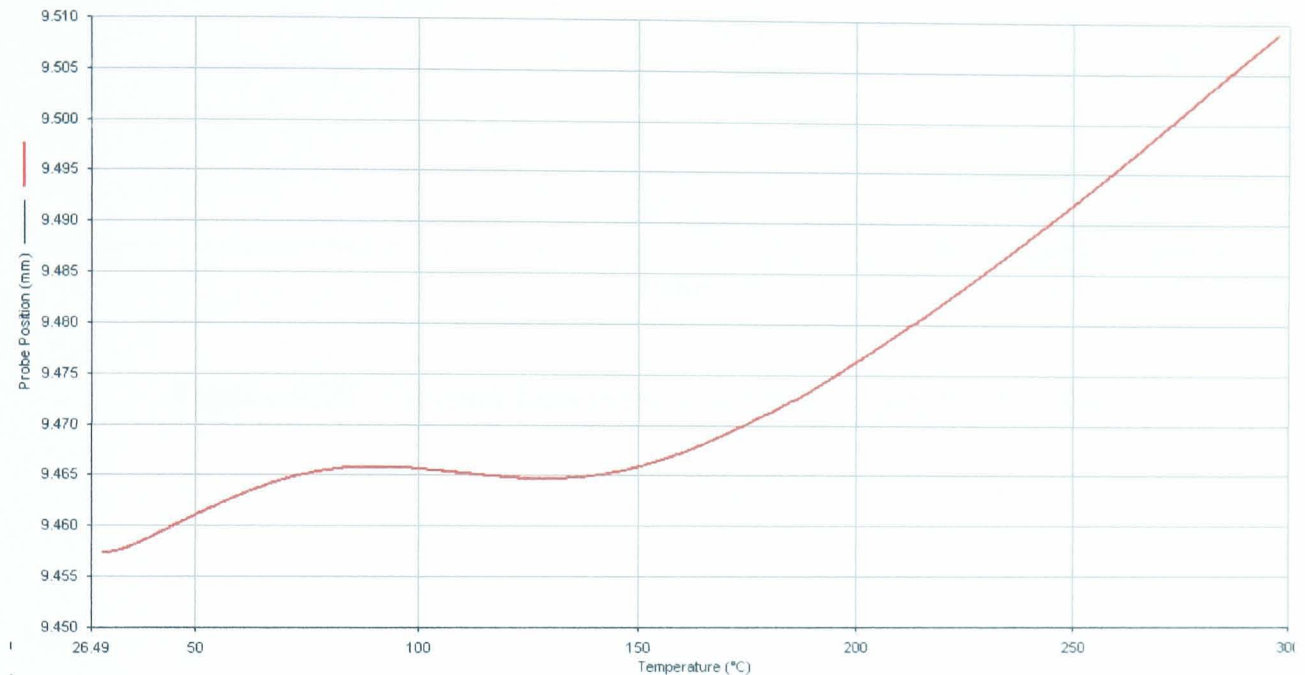


Figure 6.9 Thermal expansion of a sample from Pad 1 – test 1

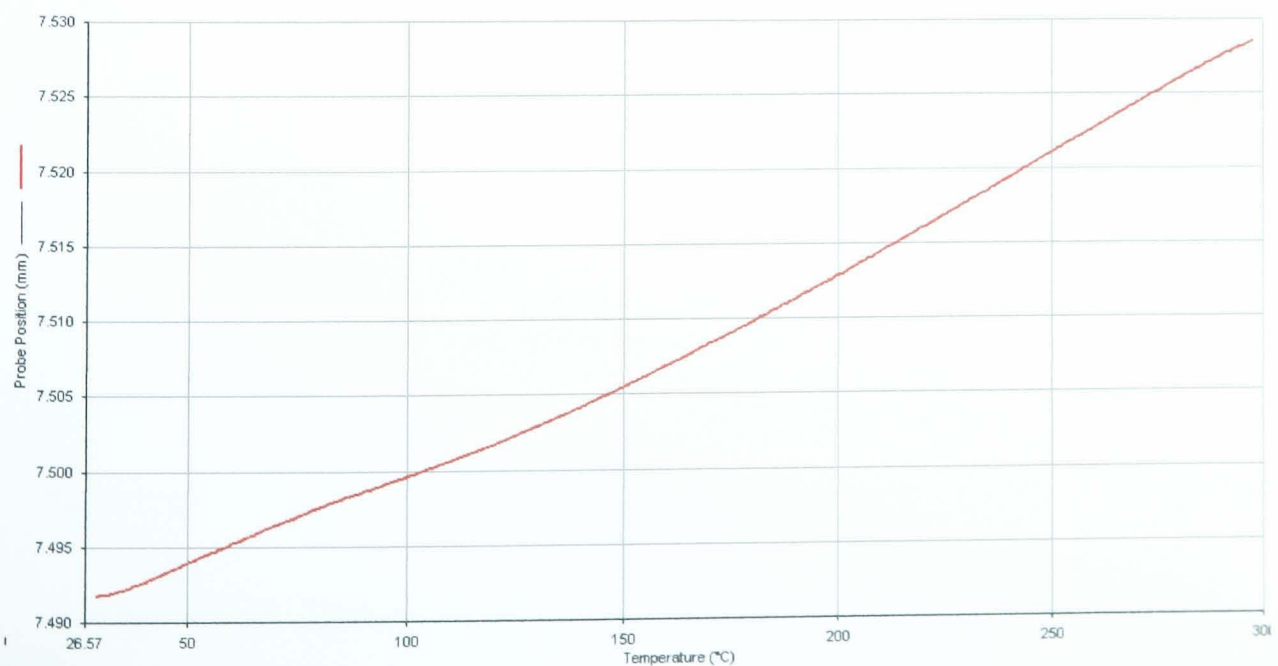


Figure 6.10 Thermal expansion of a sample from Pad 1 – test 2

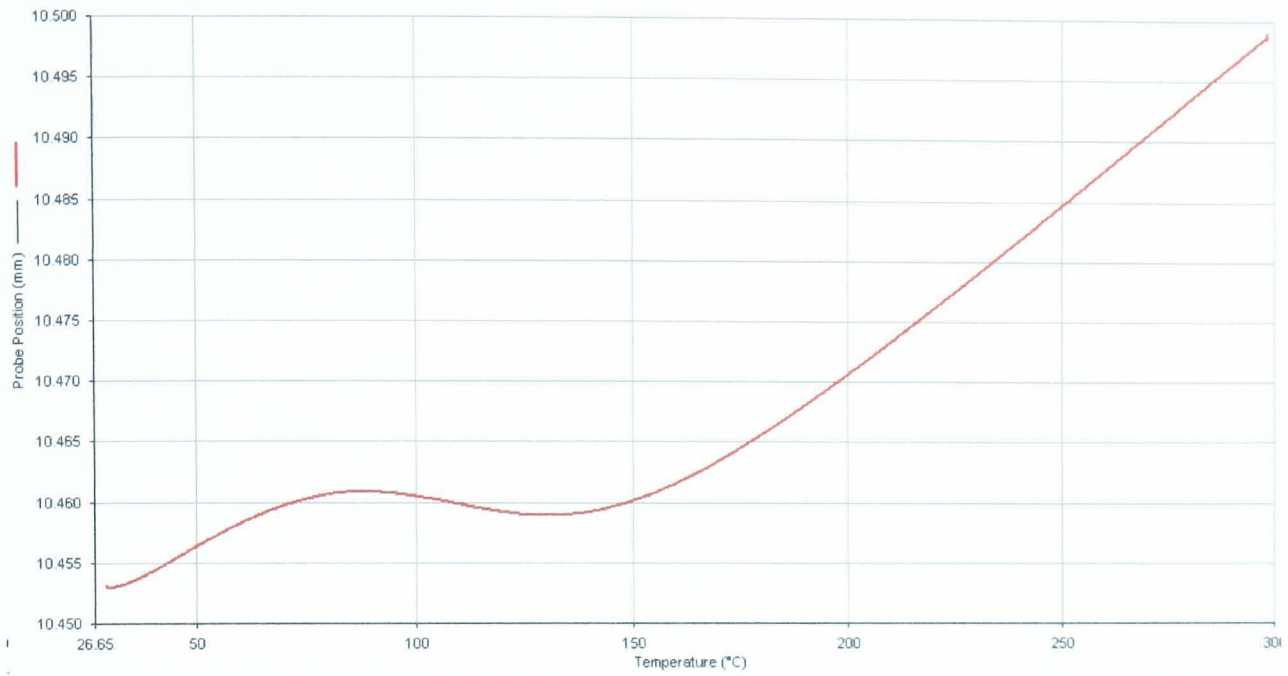


Figure 6.11 Thermal expansion of a sample from Pad 1 – test 3

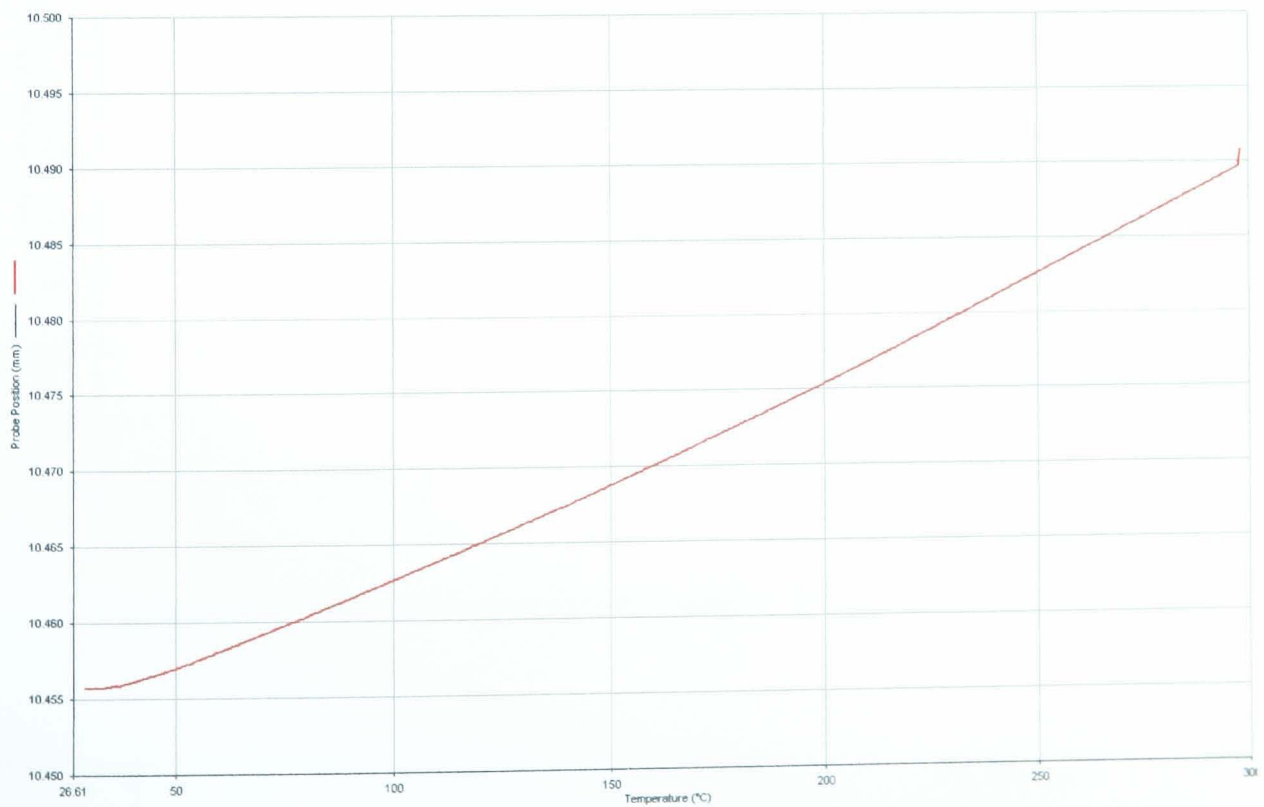


Figure 6.12 Thermal expansion of a sample from a cast iron disc – test 1

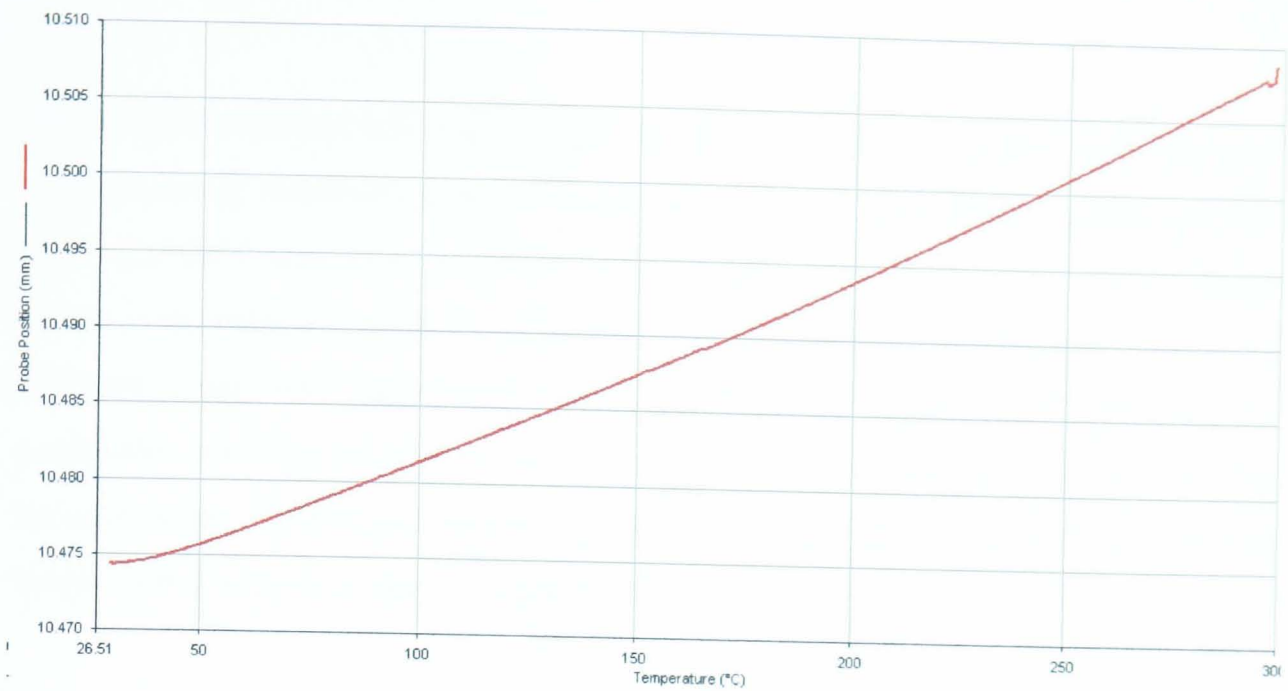


Figure 6.13 Thermal expansion of a sample from a cast iron disc – test 2

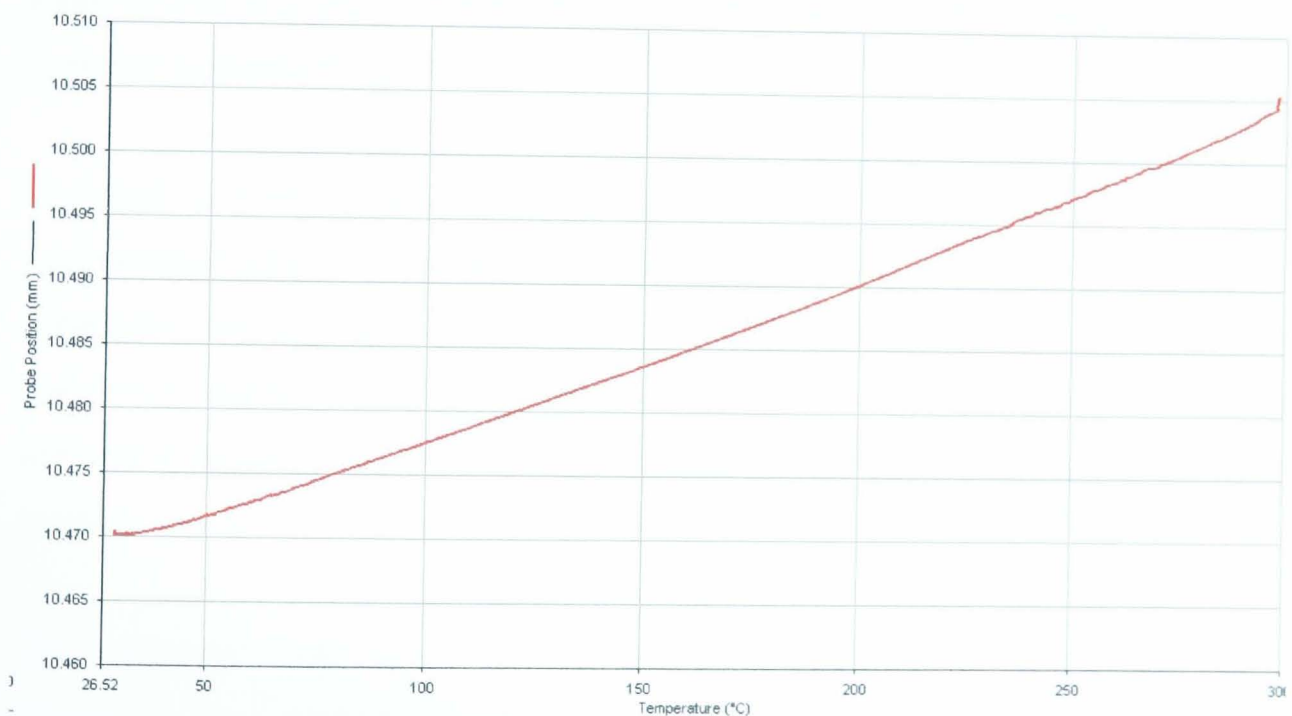


Figure 6.14 Thermal expansion of a sample from a cast iron disc – test 3

Sample	Thermal expansion coefficient ($\times 10^{-6} \text{ } ^\circ\text{C}^{-1}$)				Maximum variation in results	
	1	2	3	average	plus	minus
Pad 1	18.3	16.1	20.3	18.3	2.05	2.13
Disc	12.4	12.2	12.4	12.4	0.0751	0.126

Table 6.4 Thermal expansion coefficient values of the OE pad and disc

The results in Figures 6.9 to 6.11 show that the expansion of the pad samples did not follow a linear relationship with temperature. The pad expands up to a temperature of around 80°C and then contracts until a temperature of around 130°C is reached before continuing to expand for Pad 1 tests 1 and 3. This could be caused by the different constituent ingredients within the material expanding at different rates potentially creating cavities within the matrix. As the material heats up the resin becomes more fluid which allows it to flow into the cavities which could reduce the height of the sample as seen in Figures 6.9 to 6.11.

The results in Figures 6.12 to 6.13 show that the disc expands with an approximately linear relationship with temperature. This is to be expected because the disc is made from solid cast iron. The results tend to be slightly non-linear below 40°C, but it is expected that this could be reduced if a slower heating rate was used during the test to ensure a homogenous temperature.

The result in Table 6.4 shows that the thermal expansion coefficient of the different pad samples varies more than the disc samples. This is because the pad is a composite material and the samples used in the tests were small and so the mix of constituent ingredients in each sample is expected to vary. The variations could be reduced if larger samples were tested or the friction material mixing process could produce a more even distribution of constituent ingredients.

The variations could be reduced further if the sample preparation method was improved. The samples tested were produced by hand using a hacksaw and polishing paper. This coupled with the granular nature of the friction material meant that variations occurred in the sample geometry which could have affected the results.

6.4.3. Dynamometer clamp load

The cable load was measured on the dynamometer as the brake cooled from 250°C to 30°C with all of the OE components installed. The test was repeated 3 times and the results were found to be similar for all 3 tests. A typical result from the tests is

plotted in Figure 6.15 and the details of all of the tests are given in Table 6.5. The clamp load at the frictional interface was calculated using Equation 5.1.

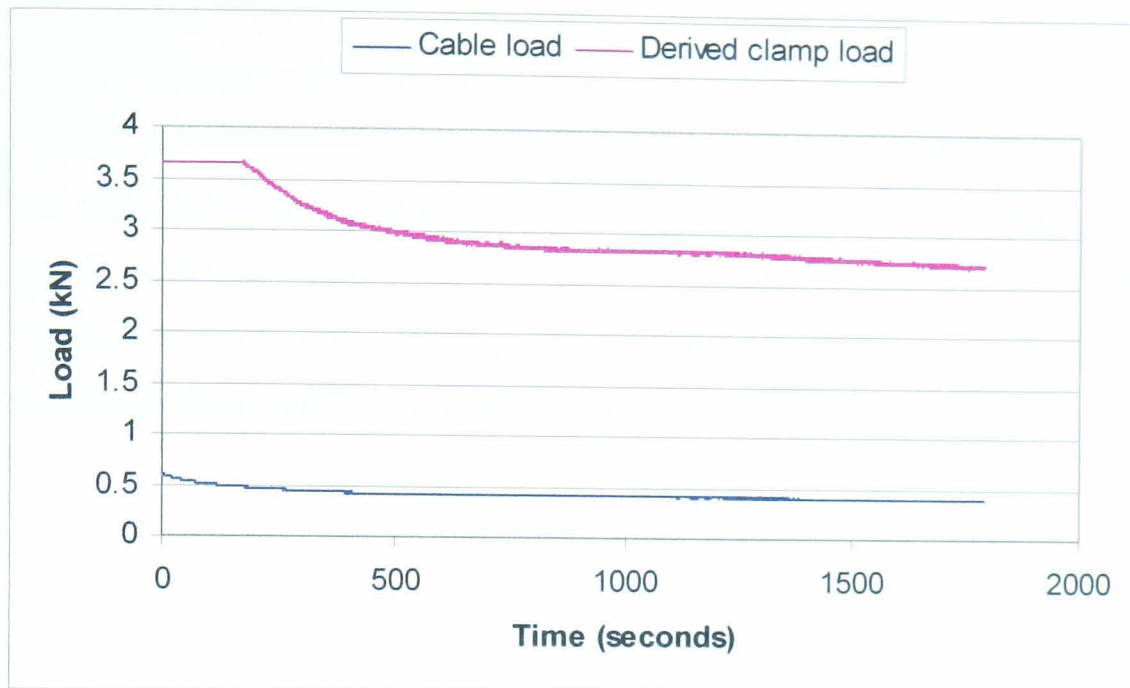


Figure 6.15 Cable load and derived clamp load from the OE parking brake system.

Test Repeat	Cable load (kN)			Derived clamp load (kN)		
	start	end	% lost	start	end	% lost
1	0.6	0.39	34.5	3.66	2.64	28.0
2	0.6	0.40	33.9	3.66	2.68	26.8
3	0.6	0.38	37.4	3.66	2.43	33.6

Table 6.5 Cable load and derived clamp load for the Jaguar S-Type OE parking brake system.

The result in Figure 6.15 and Table 6.5 shows that the cable load decreases over time losing around 33% of the initially applied load for all of the tests. The clamp load, which is derived from the cable load using Equation 5.1, was found to lose around 26% of the initial applied load. The amount of lost clamp load is lower than the amount of lost cable load because the equation used to calculate the clamp load takes the hysteresis of the system into consideration.

6.4.4. Varying test temperature

The temperature of the brake is believed to have a primary effect on the likelihood of rollaway occurring with a hotter brake being more likely to result in rollaway. It is expected that the amount of lost clamp load at the frictional interface will increase as a function of temperature. To investigate this hypothesis, tests were conducted on the Leeds handbrake dynamometer with the OE parking brake components installed. The test was conducted at temperatures of 50°C to 300°C with increments of 50°C. This would enable the performance of the parking brake clamp load to be evaluated as a function of temperature. The test was repeated five times for each temperature and the results along with the measured variations are given in Figure 6.16.

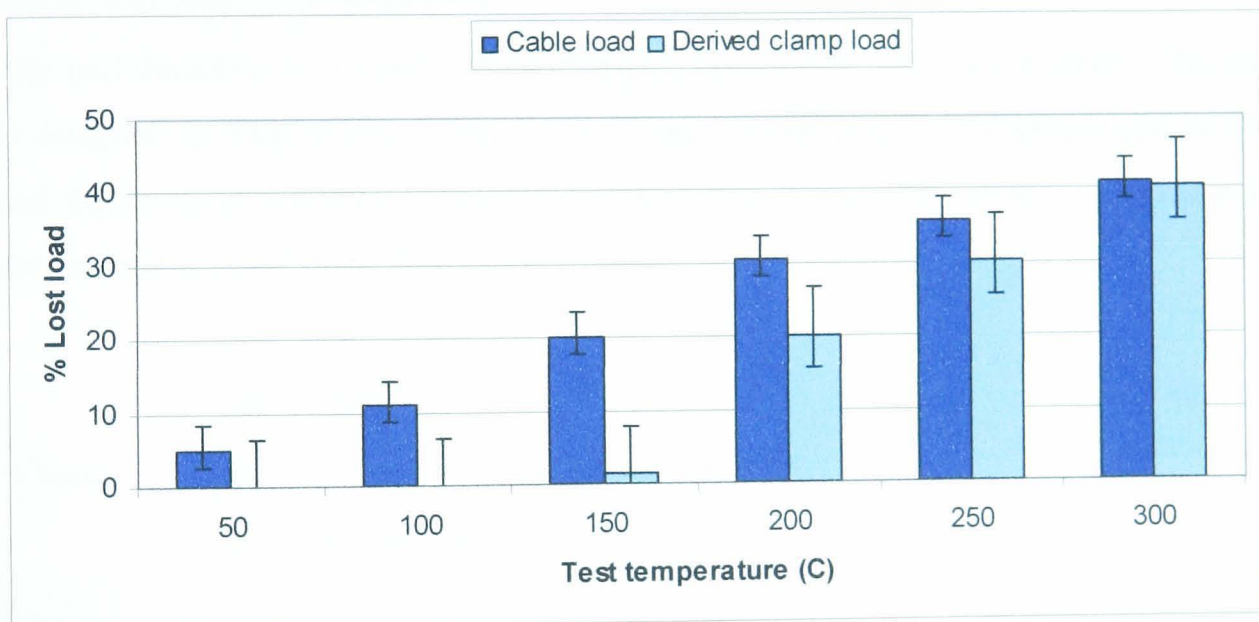


Figure 6.16 Percentage of lost cable load and derived clamp load produced by the Jaguar S-Type OE parking brake system cooling from various temperatures.

The result in Figure 6.16 shows that the amount of lost clamp load is approximately linearly proportional to the temperature of the brake. The results are used to obtain an expression for the percentage of lost cable load as a function of the initial test temperature, which is given in Equation 6.4.

$$\text{Percentage of lost cable load} = 0.151 \text{ test temperature} - 2.53 \quad (6.4)$$

The approximation given in Equation 6.4 has an R^2 correlation with the measured results of 0.986. The squared correlation coefficient, R^2 , is the proportion of variance in one test variable that can be accounted for by knowing the other in a test with two variables. The high R^2 value in Equation 6.4 indicates that the results follow a linear relationship.

The result shows that the lost clamp load is influenced by the reduction in temperature that occurs as the brake cools. The brake would lose less than 5% of the initial applied load if it is heated to a temperature less than 50°C. This result shows that the likelihood of rollaway occurring can be significantly reduced if the temperature of the brake remains low.

6.4.5. Varying pad thickness

The pad thickness is a variable that changes constantly with vehicle usage. The pad is designed to wear which results in a reduction of the material thickness and so the pad thickness is a relevant parameter to investigate. The pad thickness is linked to the thermal expansion of the pad by Equation 6.5.

$$\Delta l = l_0 \alpha \Delta T \quad (6.5)$$

Where:

- Δl = Change in length or thickness (m)
- l_0 = Original length or thickness (m)
- α = Thermal expansion coefficient ($^{\circ}\text{C}^{-1}$)
- ΔT = Change in temperature ($^{\circ}\text{C}$)

Equation 6.5 assumes a uniform temperature change in the pad which is unlikely to occur due to the way the pad is heated and convects heat to the surroundings. Equation 6.4 implies that a smaller pad thickness (l_0) will result in a reduced change in thickness (Δl), which will produce a smaller change in clamp load.

Tests were conducted on five sets of virgin Jaguar S-Type OE pads with thicknesses of 9mm, 11mm, 13mm, 15mm and 17mm. The thickness of the pads was modified by grinding the pads to the correct size. The five sets of pads were tested on the

Leeds parking brake dynamometer with the brake cooling from 250°C to 30°C following the procedure described in Section 5.3.3. The test was repeated five times for each set of pads and the results along with the corresponding measured variations are plotted in Figure 6.17.

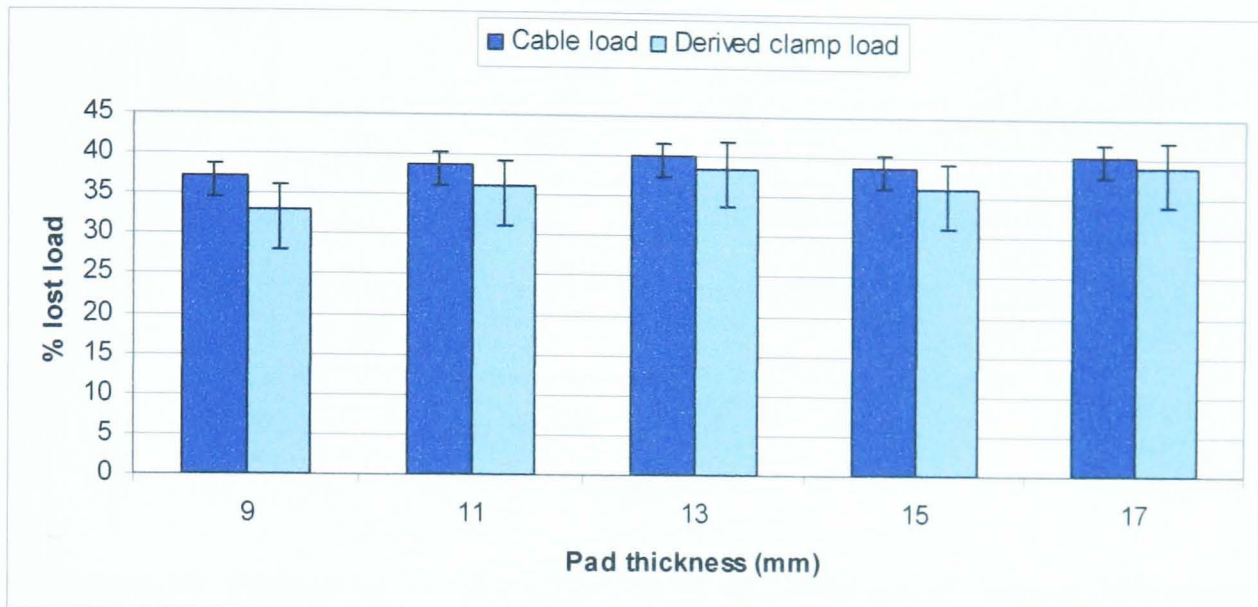


Figure 6.17 Percentage of lost cable load and derived clamp load produced by the Jaguar S-Type OE parking brake system with pads of varying thickness.

The result in Figure 6.17 does not show any correlation between the pad thickness and the lost clamp load. This could be due to the thermal insulation of the friction material preventing the whole pad reaching a uniform temperature with only the material close to the pad surface reaching an elevated temperature. The results suggest that the pad thickness is not a significant factor in rollaway.

6.4.6. Calliper tests

The deflection of the Jaguar S-Type OE calliper was measured when the parking brake was applied and when the hydraulic brake was applied with the calliper at temperatures between 30°C and 90°C. The results are plotted in Figures 6.18 and 6.19 respectively. The test was only conducted once for each measurement because a skilled Federal Mogul test driver was required to heat the calliper to the required temperature and was only available for a limited period of time.

The test was not conducted for temperatures above 90°C because this was difficult to achieve on the Federal Mogul proving ground. There is also a risk that the brake fluid might boil at higher temperatures which could result in brake failure.

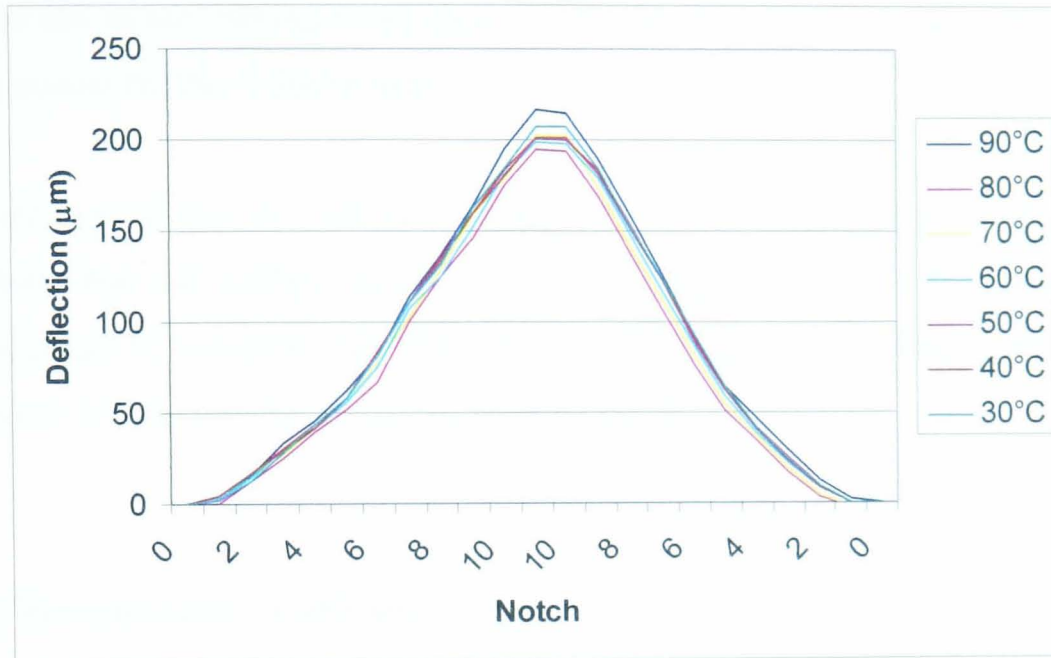


Figure 6.18 Deflections of the calliper finger for different notches on the parking brake ratchet mechanisms at different constant temperatures

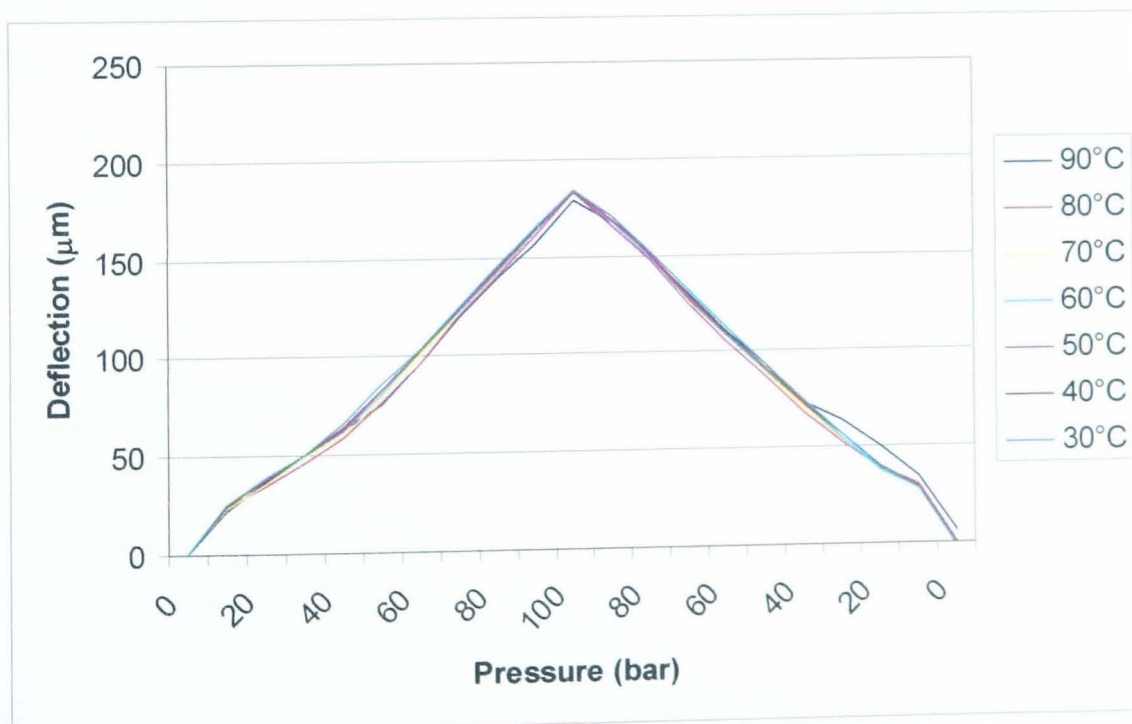


Figure 6.19 Deflections of the calliper finger with different applied pressures at different constant temperatures

The result in Figures 6.18 and 6.19 shows that the deflection of the calliper finger is not affected by temperature for the range of temperatures tested. The result in Figure 6.18 shows that the parking brake system produces a greater variation in deflection measurements at different temperatures than the hydraulic system. These variations could be due to the parking brake apply system producing varying amounts of cable displacements for the different tests.

The tests showed that the calliper is capable of reaching temperatures up to 90°C. It is unlikely that the calliper would reach temperatures above 90°C during normal vehicle usage. It is possible that the calliper could achieve temperatures above 90°C in extreme driving conditions such as a mountain descent.

6.4.7. Dynamometer static friction

The static friction level of the OE brake system was measured on the dynamometer as a function of temperature. One brake was isolated on the dynamometer and used with a virgin set of pads and a new disc installed for the test. The brake underwent a bedding procedure on the dynamometer which consisted of dragging the brake up to a temperature of 300°C and allowing it to cool to 30°C which was repeated 50 times. The torque used to simulate the vehicle parked on a gradient was applied in the opposite direction to the drive used to drag the brakes to the test temperature. This simulates a vehicle parked facing up a gradient. The test procedure described in Appendix C was used and all of the tests were repeated 5 times. The results along with the corresponding variations in the measurements are plotted in Figure 6.20.

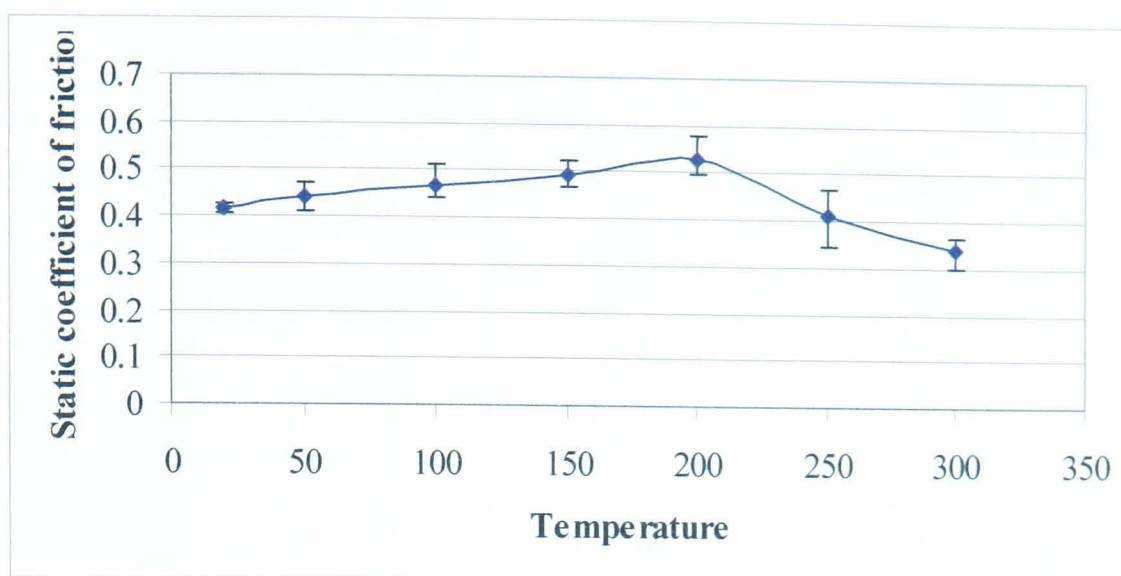


Figure 6.20 Static friction level variation with temperature for the Jaguar S-Type OE parking brake system.

The result in Figure 6.20 shows how the coefficient of static friction varies with temperature for Pad 1. The friction level increases up to a temperature of 200°C and then decreases for temperatures between 200°C and 300°C. The result suggests that if the Jaguar S-Type was parked facing up a gradient with the rear brakes at a temperature of 200°C, then as the brakes cooled the coefficient of static friction would reduce. This would lead to a drop in the frictional force produced at the frictional interface, which if large enough would result in parking brake failure and rollaway.

6.4.8. Surface characterization

Two of the Jaguar S-Types OE pads were used for the tests with one in an unbedded state and one in a bedded condition. The bedding procedure took place on the vehicle and consisted of 200 brake stops from 60 km/h to 0 km/h at a pressure of 30bar. The rubbing surface profile was measured at a temperature of 20°C, 100°C and 200C for each pad and the roughness, Ra, was calculated. The results from the test are given in Table 6.6 and Figures 6.21 to 6.26. The location of the measurement positions is defined in Figure 6.4.

Temperature (°C)	Position	Bedded pad Ra (μm)	Un-Bedded pad Ra (μm)
20	1	5.20	6.90
20	2	4.88	6.06
20	3	4.71	4.08
100	1	5.47	5.99
100	2	5.74	7.23
100	3	4.83	7.33
200	1	5.60	6.71
200	2	7.45	3.92
200	3	5.30	2.76

Table 6.6 Roughness values from the bedded and un-bedded pads

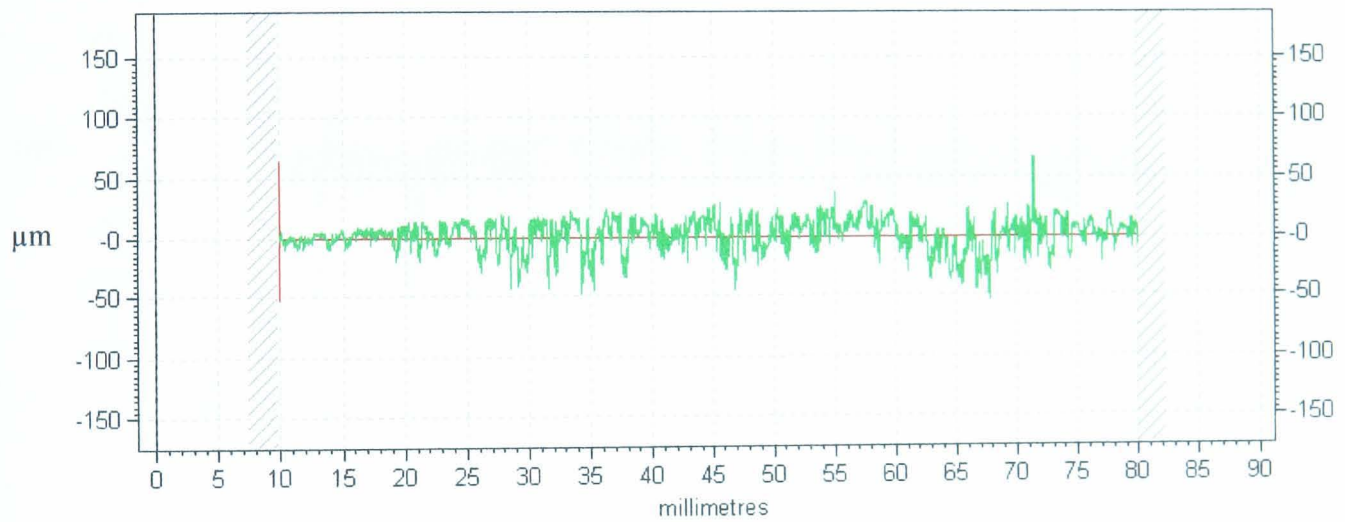


Figure 6.21 Surface profile of the bedded pad at 20°C from position 1

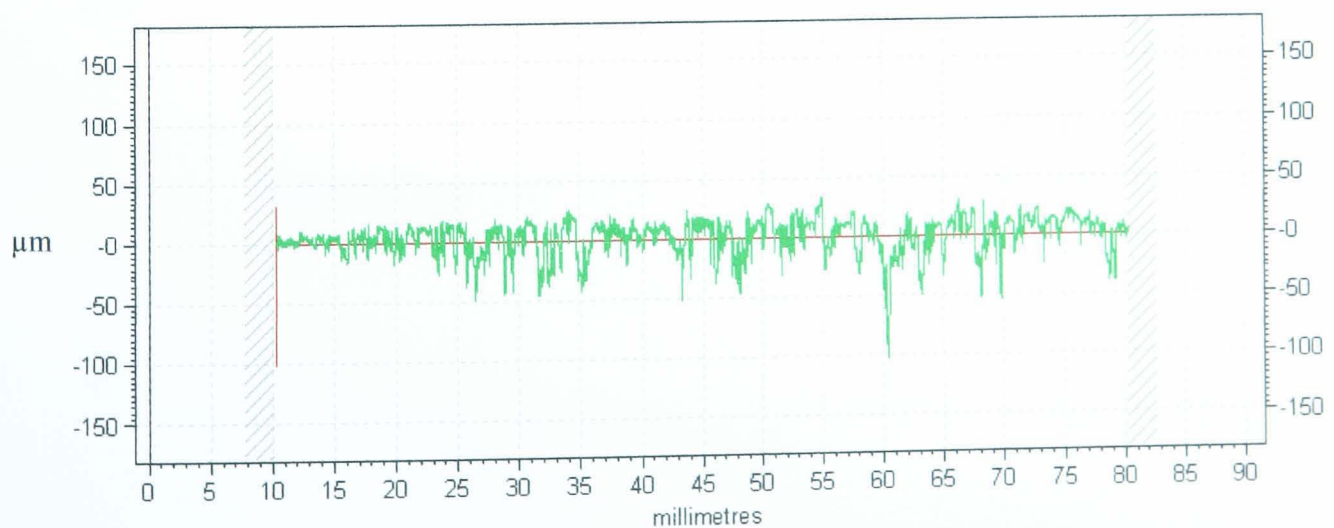


Figure 6.22 Surface profile of the bedded pad at 100°C from position 1

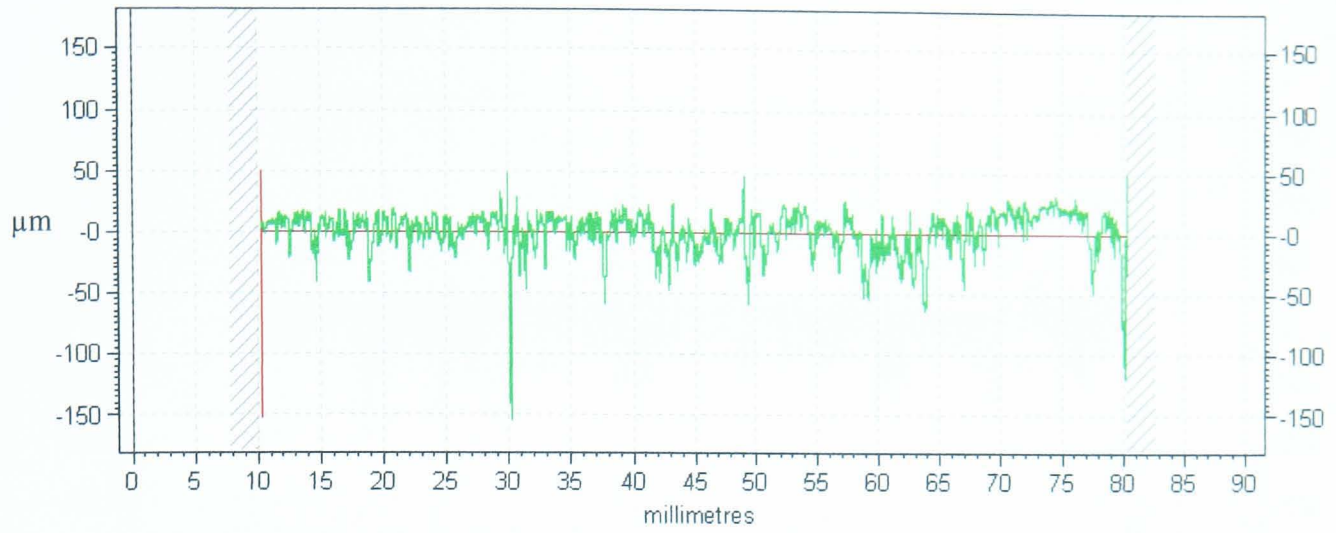


Figure 6.23 Surface profile of the bedded pad at 200°C from position 1

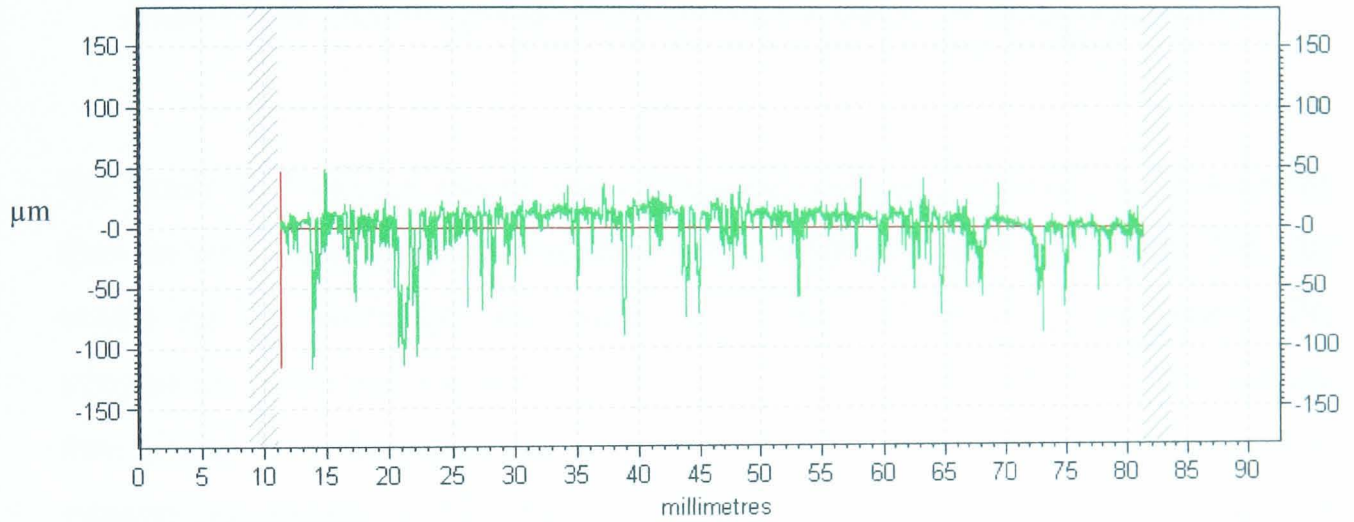


Figure 6.24 Surface profile of the un-bedded pad at 20°C from position 1

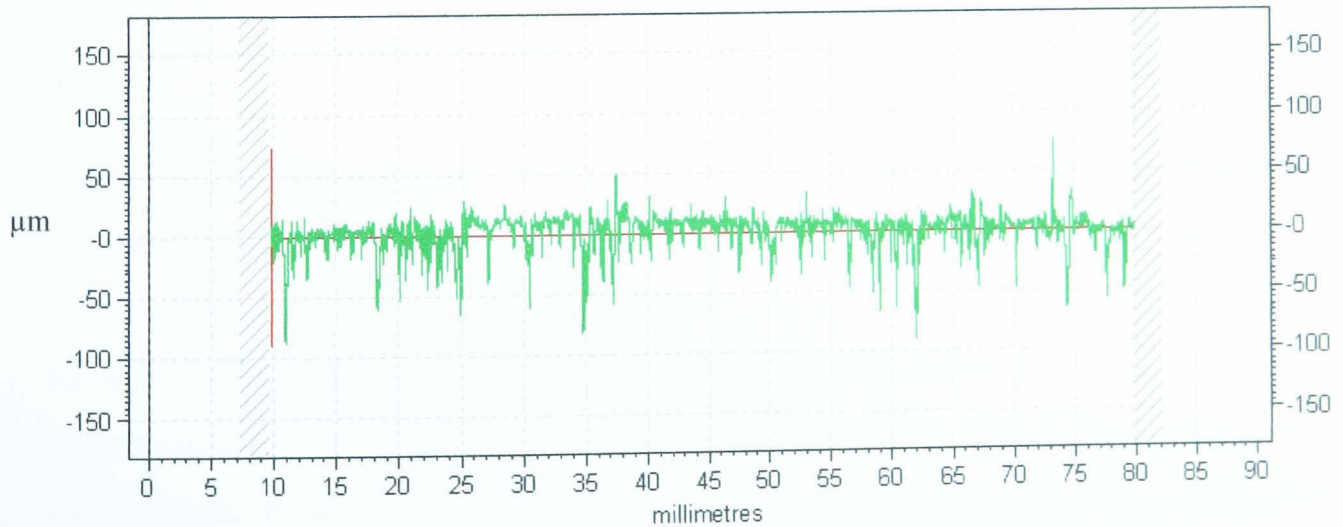


Figure 6.25 Surface profile of the un-bedded pad at 100°C from position 1

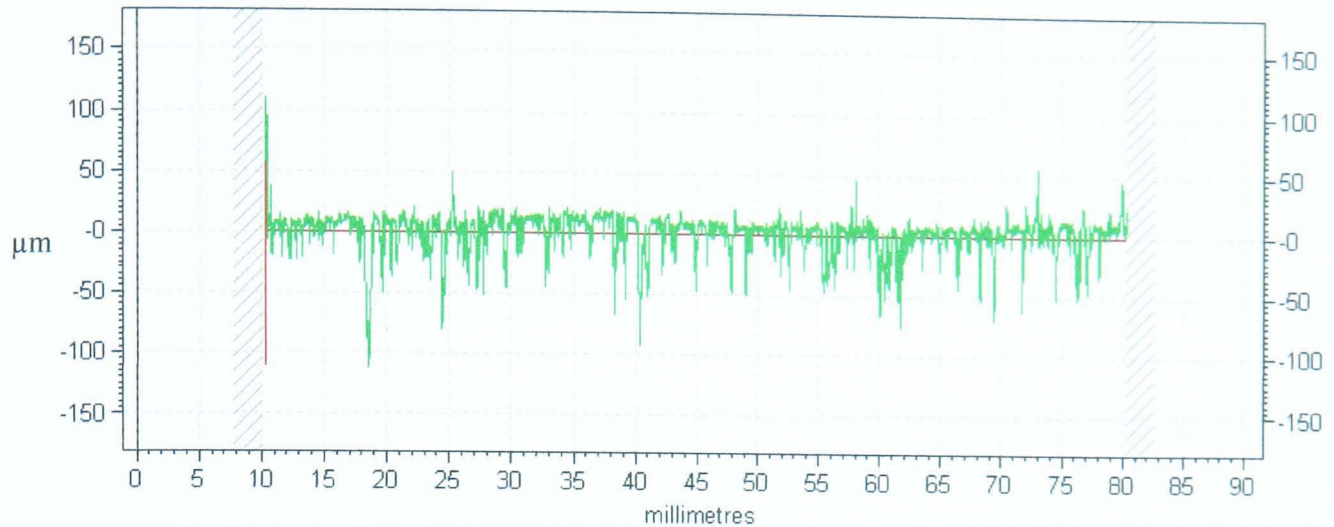


Figure 6.26 Surface profile of the un-bedded pad at 200°C from position 1

The result in Table 6.6 shows that the bedded pad has a smoother surface profile than the un-bedded pad, which agrees with the work conducted by Hildred [25]. The results do not show that the surface roughness varies with temperature. The temperature of the pad was raised to 200°C by heating it on a hot plate. The pad was then placed onto the measuring surface so that the Taylor-Hobson Talysurf could measure the surface profile. The temperature of the pad will decrease while it is transferred to the test location and during the time taken to measure the surface profile. This could have affected the results and the temperature at which the results were obtained could have been lower than 200°C.

The results in Figures 6.21 to 6.26 show that the bedded pad had fewer asperities protruding from the surface than the un-bedded pad. The bedded pad had a small number of large depressions in the surface, which could be due to hard particles having been dislodged, whereas the un-bedded pad tended to have a larger number of smaller depressions. There were no obvious variations in the surface profiles with temperature. It is expected that the pad would become smoother with further bedding.

6.5. Stiffness results

The compressive stiffness of pads 1 to 4 was measured for pressures of 40bar, 60bar, 80bar, 100bar and 160bar applied to the pads at temperatures of 20°C, 50°C, 100°C, 200°C and 300°C. The compression results of these tests are plotted in Tables 6.7 to 6.10 and Figures 6.27 and 6.28. The tests were repeated twice and the maximum variations for the results are given.

The compression of pads 1 to 10 was measured with an applied pressure of 40bar at a temperature of 20°C and at an elevated temperature. The elevated temperature was 300°C for pads 1 to 4 and 400°C for pads 5 to 10. It was intended for all of the pads to be tested at 300°C, but this had to be modified because the Jurid compression tester was designed to operate at 400°C and it was difficult to use the tester at a temperature of 300°C. The compression results of pads 1 to 10 with 40bar of pressure applied were used to calculate the stiffness, k , and Young's modulus, E , of the pads using Equations 6.1 and 6.2. The results are plotted in Tables 6.11 and 6.12. The maximum variation in all of the measured results is $\pm 13\mu\text{m}$.

Temp (°C)	Compression (μm)				
	40 bar	60 bar	80 bar	100 bar	160 bar
20	42	61	80	96	140
50	40	60	79	95	145
100	41	61	81	98	148
200	44	66	87	105	159
300	55	81	105	127	193

Table 6.7 Pad 1 compression(max error in these results = + 11 μm – 7 μm)

Temp (°C)	Compression (μm)				
	40 bar	60 bar	80 bar	100 bar	160 bar
20	39	56	71	84	121
50	45	66	85	102	150
100	51	75	96	115	168
200	65	94	120	143	208
300	78	110	139	163	229

Table 6.8 Pad 2 compression (max error in these results = + 5 μm – 6 μm)

Temp (°C)	Compression (μm)				
	40 bar	60 bar	80 bar	100 bar	160 bar
20	61	88	112	131	178
50	63	92	116	136	189
100	68	98	123	144	199
200	76	108	135	158	216
300	85	121	149	173	238

Table 6.9 Pad 3 compression (max error in these results = + $9\mu\text{m}$ – $9\mu\text{m}$)

Temp (°C)	Compression (μm)				
	40 bar	60 bar	80 bar	100 bar	160 bar
20	44	64	82	96	136
50	46	68	86	102	146
100	51	73	93	110	155
200	55	80	101	119	167
300	63	90	113	132	187

Table 6.10 Pad 4 compression (max error in these results = + $10\mu\text{m}$ – $13\mu\text{m}$)

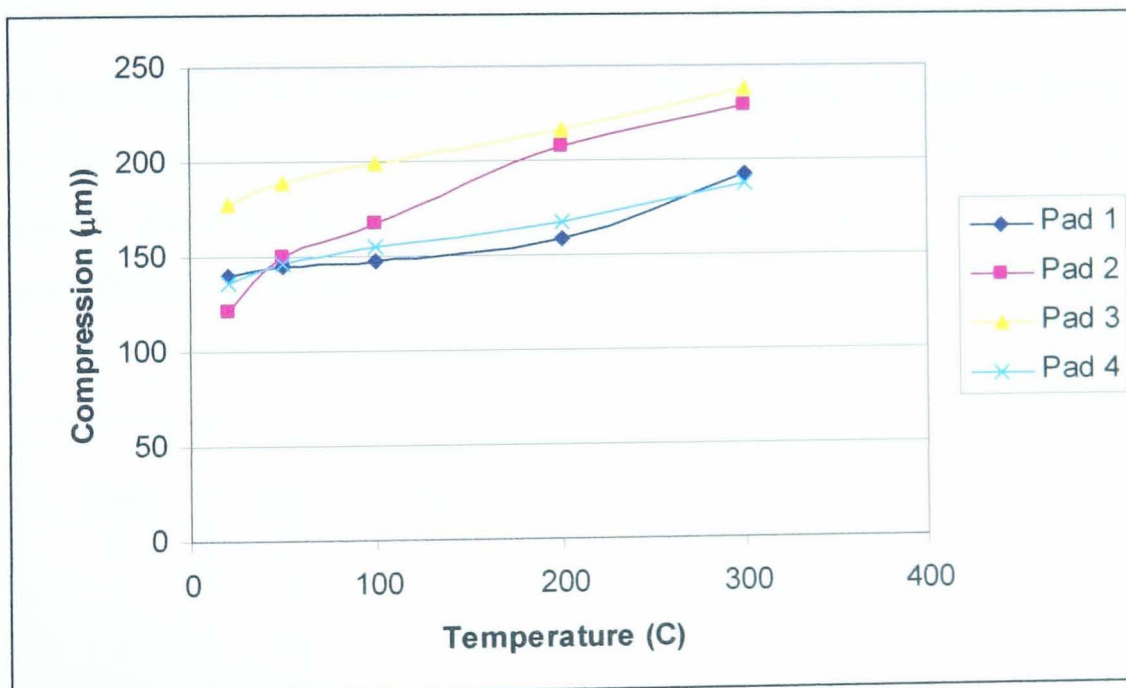


Figure 6.27 Compression of pads 1 to 4 with varying temperature and an applied constant pressure of 160bar

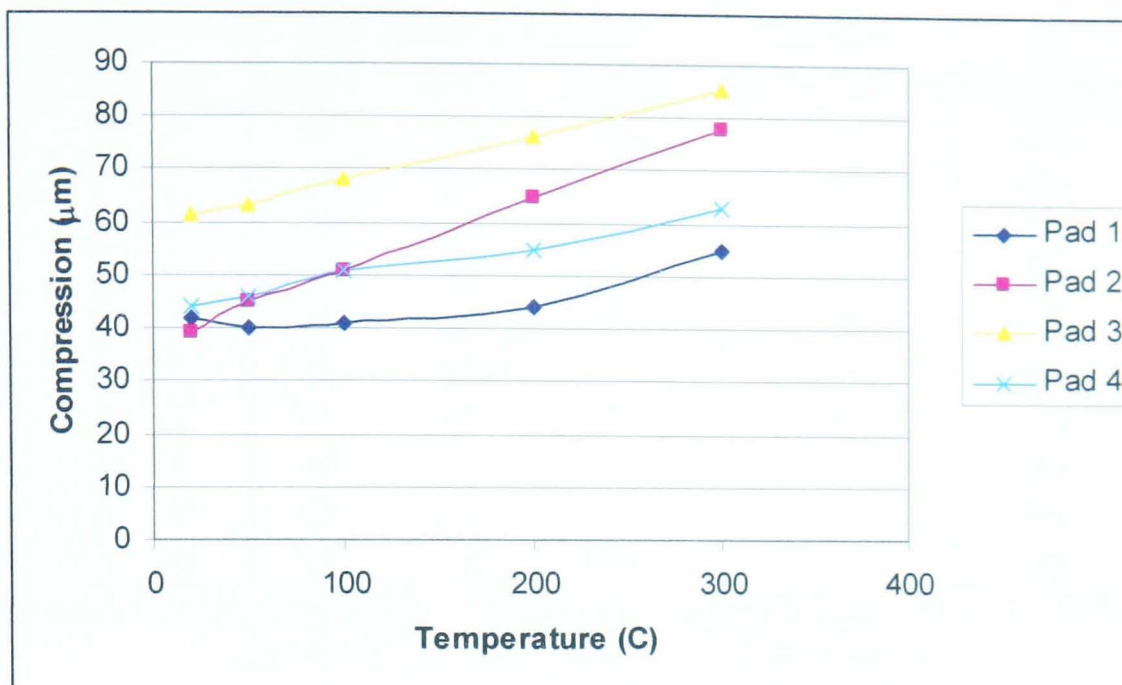


Figure 6.28 Compression of pads 1 to 4 with varying temperature and an applied constant pressure of 40bar

The result in Figures 6.27 and 6.28 shows that Pad 3 has the highest compressibility of the four pads tested. Pad 2 has the largest variation in compressibility with temperature. Pad 1 has the lowest compressibility with an applied pressure of 40bar and generally has the lowest compressibility with an applied pressure of 160bar.

Pad	Ambient compression (µm)			Stiffness ($\times 10^6 \text{ Nm}^{-1}$)	E ($\times 10^6 \text{ Pa}$)
	test 1	test 2	average		
1	45	42	43.5	133	500
2	38	42	40	145	544
3	66	68	67	86	325
4	54	50	52	112	418
5	40	48	44	132	494
6	44	41	42.5	137	512
7	41	44	42.5	137	512
8	47	44	45.5	128	478
9	29	23	26	223	837
10	50	53	51.5	113	422

Table 6.11 Compression results at ambient temperature with 40bar applied

Pad	Hot compression (μm)			Stiffness ($\times 10^6 \text{ Nm}^{-1}$)	E ($\times 10^6 \text{ Pa}$)
	test 1	test 2	average		
1	64	59	61.5	94	354
2	68	80	74	78	294
3	95	101	98	59	222
4	74	78	76	76	286
5	49	48	48.5	120	448
6	48	42	45	129	483
7	47	44	45.5	128	478
8	48	45	46.5	125	468
9	31	24	27.5	211	791
10	91	88	89.5	65	243

Table 6.12 Compression results at an elevated temperature of 300°C for Pads 1 to 4 and 400°C for Pads 5 to 10 with 40bar applied

The result in Tables 6.11 and 6.12 shows that the stiffness and Young's modulus values are different for the different pads and significantly reduce with temperature. The pressure scorching treatment did not affect the ambient compressive stiffness but significantly increased the hot compressive stiffness. A linear interpolation of the results in Tables 6.11 and 6.12 was used to obtain the stiffness and Young's modulus of the pads at a temperature of 30°C and 250°C. These result are presented in Table 6.13. The values at these temperatures will be used in the mathematical models of the system to simulate the dynamometer rollaway tests, described in Chapter 5, in which the vehicle brakes cooled from a temperature of 250°C to 30°C.

Pad	Stiffness at 30°C ($\times 10^6 \text{ Nm}^{-1}$)	Stiffness at 250°C ($\times 10^6 \text{ Nm}^{-1}$)	Young's modulus at 30°C ($\times 10^6 \text{ Pa}$)	Young's modulus at 250°C ($\times 10^6 \text{ Pa}$)
1	132	101	495	380
2	143	90	535	339
3	86	64	321	240
4	110	83	413	310
5	131	124	493	466
6	136	132	511	494
7	136	131	511	491
8	127	126	478	472
9	223	216	836	809
10	111	84	417	314

Table 6.13 Stiffness and Young's modulus of Pads 1 to 10 at a temperature of 30°C and 250°C.

6.6. Thermal expansion results

The thermal expansion coefficient of the friction materials used in Pads 1, 2, 3, 4, 9 and 10 was measured using the DMA. The results were obtained from 3 different samples of the same friction material and are presented in Table 6.14. The Jurid compression tester was used to calculate the thermal expansion coefficients of Pads 1 to 10 and the results are presented in Table 6.15.

Pad	Thermal expansion coefficient ($10^{-6} \text{ } ^\circ\text{C}^{-1}$)				Maximum variation (10^{-6})	
	1	2	3	average	plus	minus
1	18.35	16.15	20.32	18.27	2.05	2.13
2	14.36	13.03	10.89	12.76	1.60	1.87
3	8.28	11.02	4.76	8.02	2.99	3.26
4	10.13	11.56	9.74	10.48	1.08	0.73
9	6.74	5.66	6.13	6.18	0.57	0.52
10	16.53	14.58	16.41	15.84	0.69	1.26

Table 6.14 Results from the DMA test

Pad	Test 1			Test 2			Mean	Variation
	ΔT ($^\circ\text{C}$)	Δl (10^{-6} m)	α ($10^{-6} \text{ } ^\circ\text{C}^{-1}$)	ΔT ($^\circ\text{C}$)	Δl (10^{-6} m)	α ($10^{-6} \text{ } ^\circ\text{C}^{-1}$)	Mean α ($10^{-6} \text{ } ^\circ\text{C}^{-1}$)	Variation (10^{-6})
1	370	50	9.01	370	58	10.45	9.73	0.72
2	370	65	11.71	370	59	10.63	11.17	0.54
3	370	64	11.53	370	50	9.01	10.27	1.26
4	370	47	8.47	370	56	10.09	9.28	0.81
5	370	127	22.88	370	99	17.84	20.36	2.52
6	370	89	16.04	370	99	17.84	16.94	0.90
7	370	82	14.77	370	82	14.77	14.77	0.00
8	370	67	12.07	370	61	10.99	11.53	0.54
9	370	46	8.29	370	28	5.05	6.67	1.62
10	370	69	12.43	370	62	11.17	11.80	0.63

Table 6.15 Results from the Jurid testing machine

The result in Table 6.14 shows that the samples produced relatively high variations in the measurements taken on the DMA. The measured variations could be due to variations in the sample geometries and the varying constituent ingredients in the samples. The variations could be reduced if an improved method was developed to

manufacture the samples with a greater geometric tolerance. The variation could also be reduced if the distribution of constituents in the friction material was made more uniform.

The results in Table 6.15 from the Jurid testing machine have smaller variations than the results from the DMA tester. The results from the 6 pads tested on the DMA and the Jurid compression tester are within the measured variation ranges of the tests except for pads 1 and 10.

Different sets of the OE pad (Pad 1) were produced by Federal Mogul at different times throughout the research project. The pads tested on the DMA and Jurid testing machines for Pad 1 came from different batches. The manufacturing process or constituent ingredients could have varied between the production of each set of pads. This could have varied the properties of the pads which could explain the variations in the measured expansion coefficients.

The samples tested on the Jurid compression tester were heated using a hotplate in contact with the pad frictional surface. The samples tested on the DMA were heated in a helium filled oven. Therefore the samples tested on the DMA are likely to have a more uniform temperature distribution than the samples tested on the Jurid compression tester. The thermal expansion coefficients used in the mathematical models, discussed in Chapters 7 and 8, will be taken from the DMA measurements for Pads 1, 2, 3, 4, 9 and 10. The thermal expansion coefficients used in the mathematical models for Pads 5, 6, 7 and 8 will be taken from the measurements on the Jurid compression tester because these pads were not tested on the DMA.

6.7. Dynamometer clamp load results

The dynamometer clamp load tests were conducted to investigate the change in clamp load at the frictional interface as the brake cooled from 250°C to 30°C for Pads 1 to 10. The test was repeated five times for Pads 1, 2, 3, 4, 9 and 10 but only one test was conducted for Pads 5 to 8. This was because the testing method could vary the properties of the pressure scorched pads and therefore the test was not repeatable. Repeat testing could vary the properties of the pad measured in the

laboratory and hence affect the model results. The tests used with Pads 1, 2, 3, 4, 9 and 10 are repeatable because the pads had undergone a bedding period consisting of 200 brake stops prior to the tests. The results from the tests are plotted in Figure 6.29.

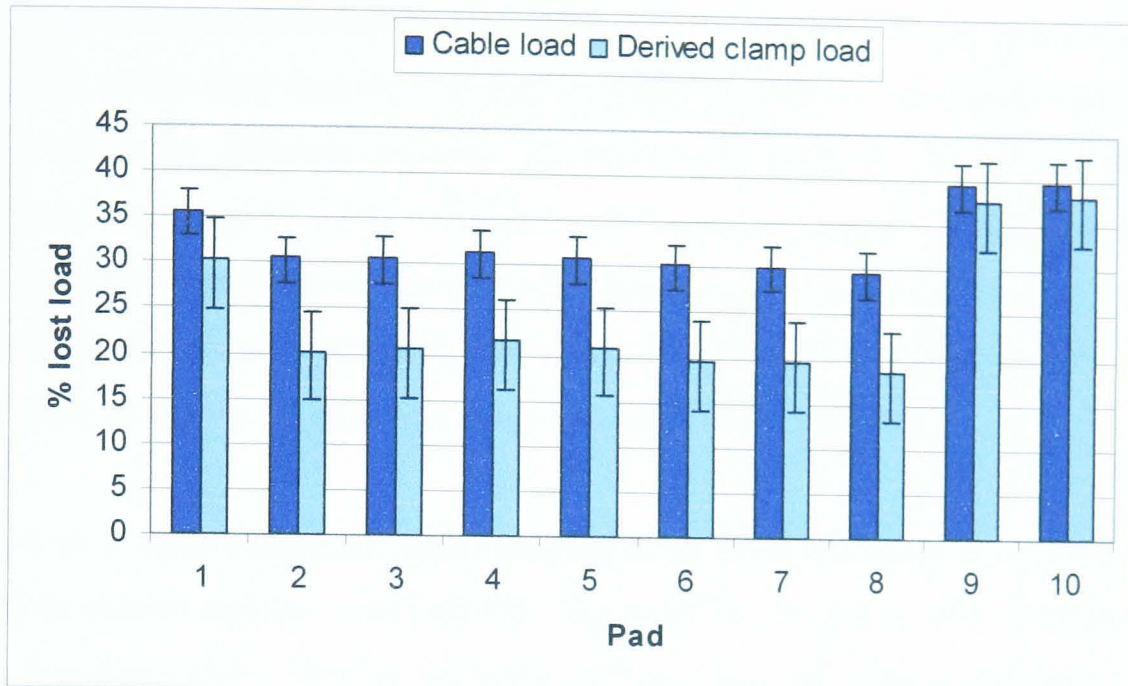


Figure 6.29 Percentage of lost cable load and derived clamp load during the dynamometer clamp load evaluations.

The result in Figure 6.29 shows the percentage of the initially applied cable load that was lost as the brake cooled from 250°C to 30°C and the percentage of the derived clamp load that was lost. The result shows that the percentage of initial load that was lost varies for the parking brake system with the different pads installed. The result suggests that the pad can influence the likelihood of rollaway occurring. All of the pads tested lost over 29% of the initially applied cable load as they cooled which indicates that the parking brake is liable to fail a rollaway test with any of the tested pads installed. This suggests that rollaway on the Jaguar S-Type cannot be prevented by changing the properties of the pads within the range of properties of the pads used for this research.

The OE pad (Pad 1) has the highest percentage of lost cable and clamp load out of the four pads tested on the vehicle (Pads 1 to 4) as shown in Figure 6.29. Pad 1 has the highest stiffness values and the highest thermal expansion coefficient of Pads 1 to 4. Pad 3 has the highest compressibility and the lowest thermal expansion

coefficient and lost the least amount of cable and clamp load out of Pads 1 to 4. The results from Pads 1 to 4 suggest that pads with a low thermal expansion coefficient and a high compressibility will lose less clamp load as the brake cools.

All of the pressure scorched pads (Pads 5 to 8) produced a lower amount of lost cable and clamp load than the OE pad without any pressure scorching, Pad 1. The results from the different pressure scorched pads are very similar and have a maximum variation of 1.3% which is lower than the typical variations measured during repeat measurements from the other pads. This suggests that the performance of the different pressure scorched pads cannot be distinguished from each other and the results lie within the expected range of experimental variation.

Pads 5 to 8 were examined upon completion of the dynamometer tests and were found to exhibit similar wear patterns. The pads on the piston side of the calliper were found to exhibit wear at the inner radius of the pad whereas the pads on the finger side of the calliper exhibited wear on the outer radius of the pad, as shown in Figures 6.30 and 6.31. The wear produced during the rollaway tests on the other pads used in this research could not be accurately examined because the pads had undergone a period of bedding prior to the rollaway tests. Therefore the wear produced during the rollaway test could not be distinguished from the wear produced by the bedding procedure. The wear in Figures 6.30 and 6.31 indicates that either the calliper is rotating when it is under load due to the tolerances in the calliper design or the disc is coning during the tests. The results suggest that not all of the pad surface is uniformly in contact with the disc. The location of the contact area will affect the developed torque with the pad on the piston side of the calliper producing a lower level of torque than the pad on the finger side of the calliper.

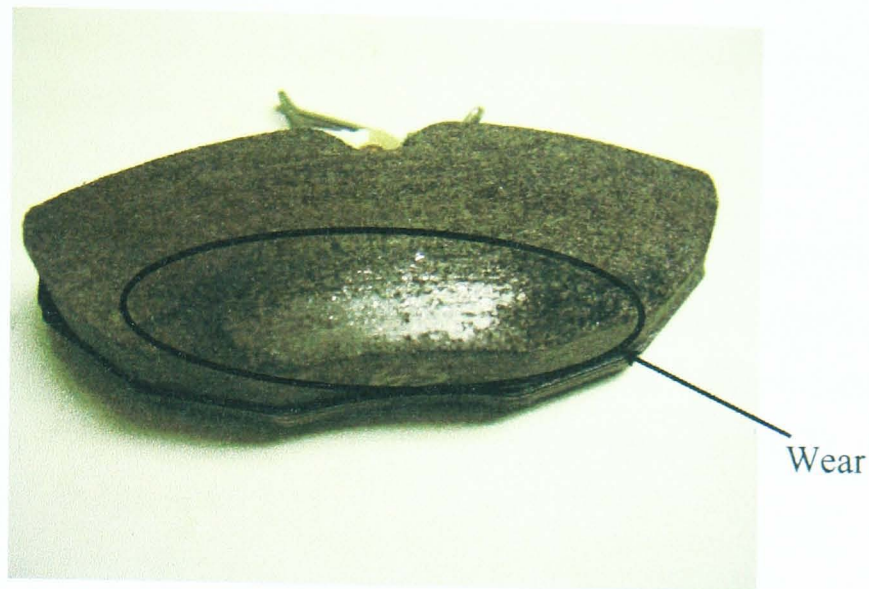


Figure 6.30 Wear on pad from piston side of calliper



Figure 6.31 Wear on pad from finger side of calliper

The results in Figure 6.29 show that Pads 9 and 10 lost the highest percentage of the initially applied load as they cooled out of all the pads tested. This could be due to the stiffness of the friction material as a function of temperature.

6.7.1. Investigating the effect of disc thickness

The thickness of the disc was varied to see if it affected the amount of lost clamp load as the brake cooled. Equation 6.1 states that the amount of thermal expansion/contraction is governed by the original thickness of the disc. Therefore a thinner disc will result in a lower thermal contraction as the brake cools and a smaller amount of lost clamp load. The thickness of the disc varies in service as the

disc is worn by the pads. The disc is designed to produce low wear and is replaced if significant wear is detected.

Four solid cast iron discs were manufactured that would fit the Jaguar S-Type rear assembly. The discs were turned down to thicknesses of 12mm, 10mm, 8mm and 6mm. The discs were tested on the dynamometer with the Jaguar S-Type OE pad, Pad 1. The tests were repeated five times for each disc, and their results and variations are given in Figure 6.32.

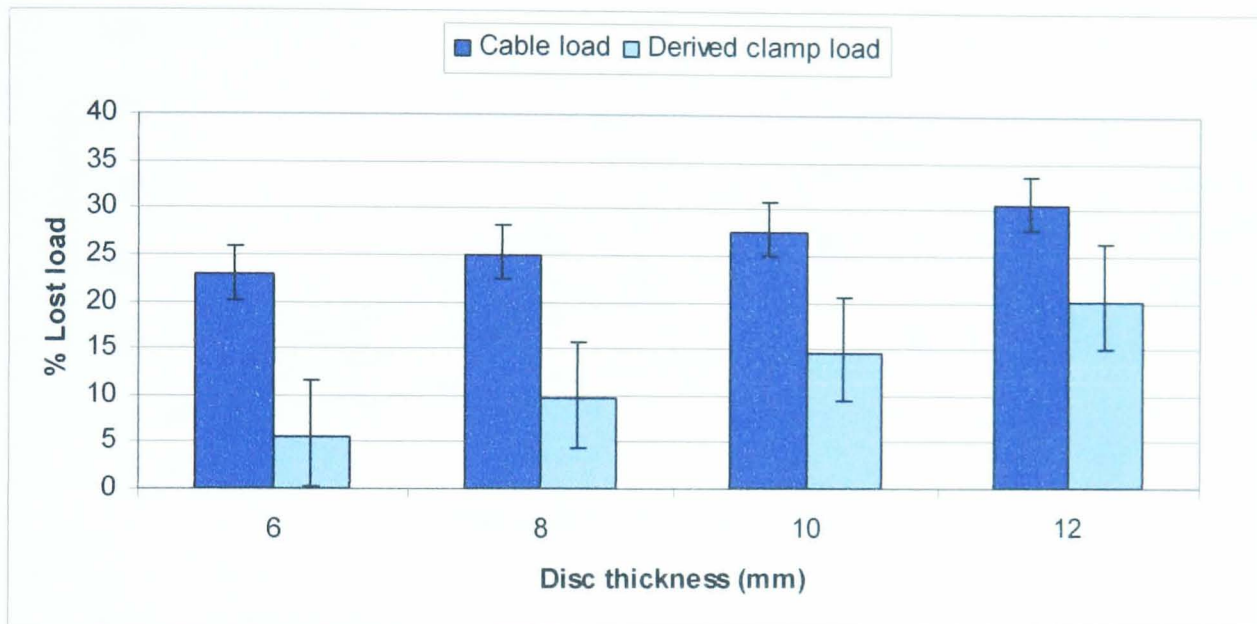


Figure 6.32 Percentage of lost cable load and derived clamp load produced by the Jaguar S-Type OE parking brake system with discs of varying thickness

The result in Figure 6.32 shows that the thickness of the disc does have a significant effect on the amount of lost clamp load. The four solid discs with thickness from 6mm to 12mm have an approximately linear relationship with the percentage of lost clamp load. The percentage of lost cable load is expressed as a linear variation with disc thickness in Equation 6.6.

$$\% \text{ lost cable load} = 1.27 \times \text{disc thickness} + 15.04 \quad (6.6)$$

Equation 6.6 has an R^2 correlation with the measured data of 0.996. This suggests that the thermal contraction of the disc is directly related to the amount of lost clamp load.

6.8. Calliper results

The deflection of the calliper fingers at three locations on Callipers 2 and 3 was measured on the dynamometer. The deflection was measured 5 times for each measurement location with the calliper at ambient temperature. The results are plotted in Figures 6.33 and 6.34. The maximum variation in all of the measurements was $\pm 3\mu\text{m}$.

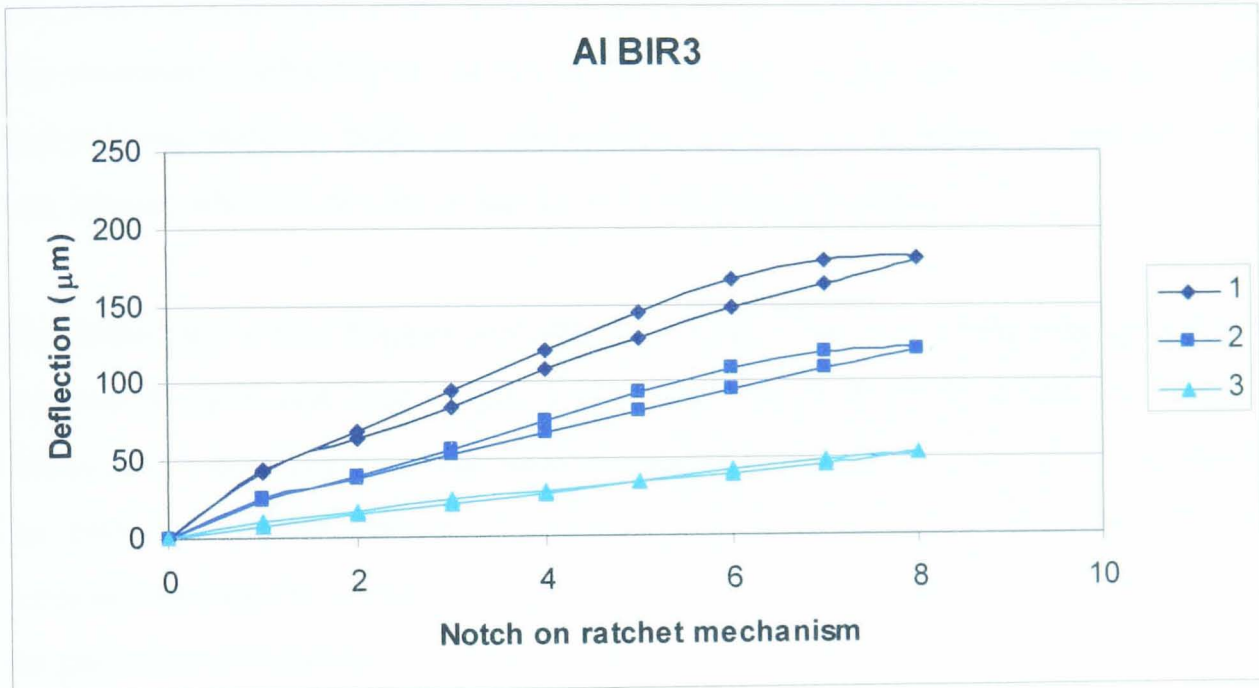


Figure 6.33 Deflections of the aluminium BOSCH BIR3 calliper finger

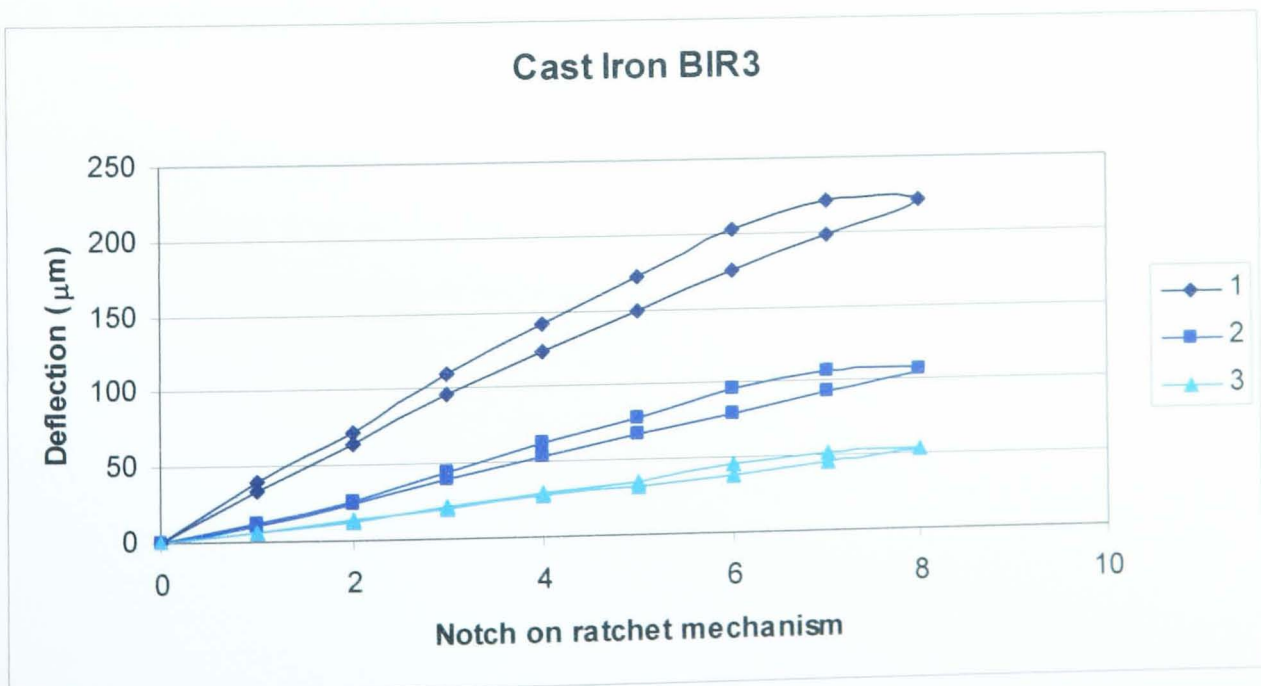


Figure 6.34 Deflections of the cast iron BOSCH BIR3 calliper finger

The results in Figures 6.33 and 6.34 show that both callipers exhibited similar deflections along the calliper finger. The similar results could be due to the modifications in the calliper design between the two materials which were designed to produce the same stiffness. The aluminium calliper had fingers with a thickness of 25mm and the cast iron had fingers with a thickness of 13mm. The calliper deflections increased towards the tip of the calliper fingers due to the bending moment acting on the fingers causing them to deflect. The deflections could also be due to the calliper assembly rotating because of the tolerances in the calliper design. The maximum deflection of the finger on Calliper 1 at position 1 produced by fully applying the parking brake at ambient temperature, as described in Section 6.4.6, was 200 μ m which is similar to the results of Callipers 2 and 3.

The deflected calliper fingers will alter the location and size of the real contact area between the pad and disc which could affect the braking force and the level of torque developed. If the contact area is initially at the outer radius of the pad due to the deflected fingers, then as the clamp load decreases the deflections will also decrease moving the location of the centre of pressure towards the inner radius of the pad. This will reduce the level of torque developed by the brake.

6.9. Dynamometer Static friction results

6.9.1. On-vehicle pads

The level of static friction for the pads used during the on-vehicle tests (Pads 1 to 4) was measured as a function of temperature on the dynamometer. Figure 6.35 shows the results from all four pads.

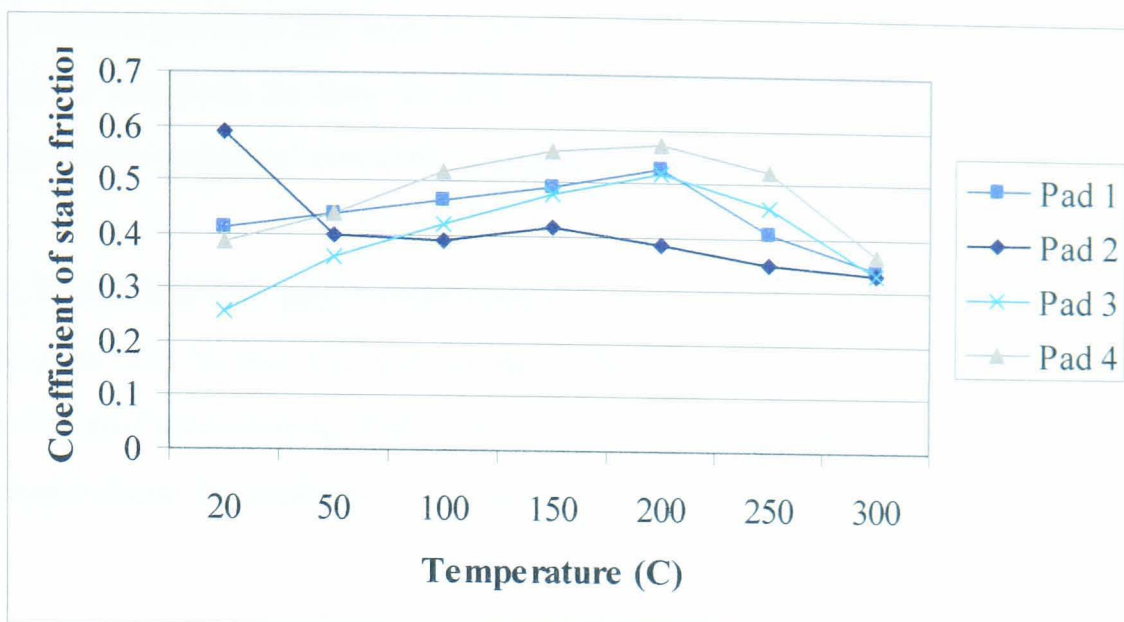


Figure 6.35 Static friction level variation with temperature for Pads 1 to 4

The result in Figure 6.35 shows that the static friction level of pad 1 increases with temperature up to a temperature of 200°C and then decreases for temperatures above 200°C. This suggests that if these pads were used on a Jaguar S-type parked on a gradient with the rear brakes at 200°C, then as the brakes cooled the torque produced by the parking brake system would reduce, which could potentially lead to the vehicle rolling away.

Figure 6.35 shows that Pad 2 has a higher static friction level at ambient temperature than at an elevated temperature. The static friction level tends to decrease with increasing temperature. This result suggests that if these pads were used on a vehicle parked on a gradient with hot brakes, then as the brakes cooled the torque produced by the parking brake system would increase if the normal clamp load remained constant. Pad 2 is less likely to produce rollaway than Pad 1 if both pads were subjected to the same clamp loads as the brake cooled.

The static friction level of Pad 3 follows a similar trend as Pad 1. The static friction level increases with temperature up to a temperature of 200°C, and then reduces above this temperature. Pad 4 has a similar static friction with temperature variation as Pads 1 and 3. The static friction level is generally higher than for the other pads.

Pad 2 would perform the best in a rollaway test if a constant normal load was applied to the pads as they cooled. This is because the friction level generally increases with reducing temperature producing an increasing brake torque.

6.9.2. Modified OE pad formulations

Three pads (11, 12 and 13) were produced by modifying the level of fused alumina in the OE pad formulation, Pad 1, and were tested on the dynamometer. The test was repeated 5 times for each data point and the results are plotted in Figure 6.36.

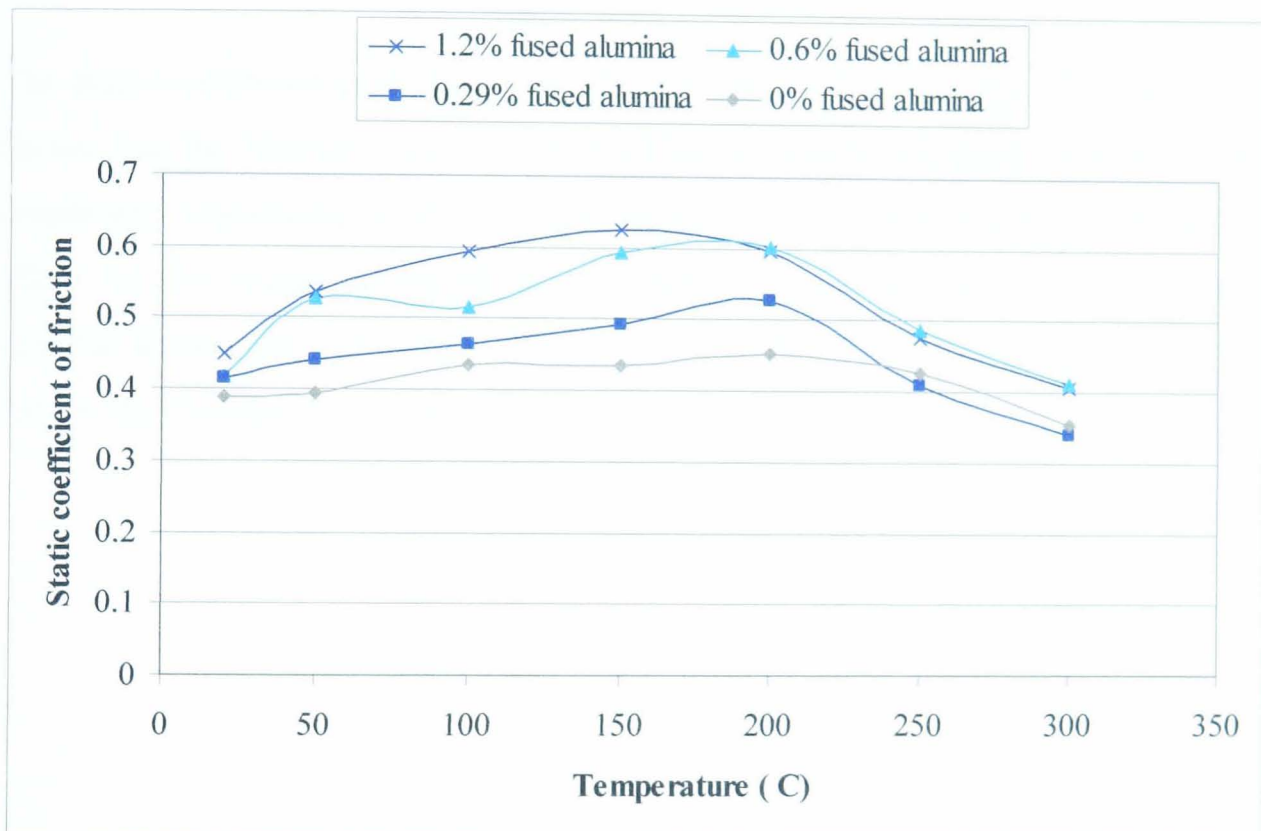


Figure 6.36 Static friction level variation with temperature for Pads 1, 11, 12 and 13

The result in Figure 6.36 shows that the pads with increased levels of fused alumina generally produce a higher level of static friction. The pads with increased levels of fused alumina also produce a greater variation in the static friction level with temperature. The maximum variation in the measured results was 0.066.

6.10. Summary

The experimental characterisation of rollaway described in this chapter has determined the material properties of the components used in the parking brake

system. The results from the experiments can be used in a mathematical model of rollaway to accurately describe the characteristics of the system. The results in Section 6.4.4 have shown that the reduction in clamp load at the frictional interface is directly related to the initial temperature of the brake. This means that the likelihood of rollaway occurring is reduced if the brake is at a lower temperature when the vehicle is parked. The results in Section 6.7.4 have shown that the thickness of the disc has a direct influence on the likelihood of rollaway occurring. This suggests that the thermal contractions of the disc have a primary effect of the likelihood of rollaway.

The static coefficient of friction was found to vary with temperature. The tests have shown that the friction variation with temperature can be modified by changing the constituent ingredients in the friction material. The varying friction level has an effect on the torque produced by the parking brake and therefore the friction material developers may be able to produce a pad that has characteristics which will reduce the likelihood of rollaway.

Chapter 7

Rollaway simulation using the finite element method

7.1. Introduction

A mathematical model of vehicle rollaway is required to investigate the performance of components within parking brake systems and predict the behaviour of modified parking brake systems. The model requires the material properties of the brake components measured in Chapter 6 to accurately describe the mechanisms involved in a rollaway event. This chapter describes the finite element model developed to simulate a parking brake system during a rollaway test.

7.2. Methodology

Finite element analysis (FEA) is a tool widely used throughout the brake industry mainly for conducting structural and noise, vibration and harshness (NVH) analyses. A finite element model has been developed for this research to simulate a parking brake system under rollaway conditions. ANSYS V8.0 was chosen since it is widely used within the braking industry and finite element models, when developed using the ANSYS Parametric Design Language (APDL), are ideally suited to parametric sensitivity studies of the type required by this research. Ioannidis [44] states that, “APDL is a scripting language that is very similar to Fortran77 which allows the customization of the software’s standard input and output numerical tools, introducing flexibility and increased productivity to the engineer”. The APDL code allows parameters within the model to be easily varied which is useful for investigating different geometries and material properties.

The finite element model was developed to simulate the torque developed by a vehicle parking brake system during an on-vehicle rollaway event. The challenge of the finite element model was to recreate the on-vehicle thermal and structural conditions. To achieve this a decoupled thermal-mechanical analysis was used whereby the thermal and structural analyses are conducted separately.

The thermal analysis predicts the temperature distribution of the brake as it cools from a uniform temperature of 250°C to an ambient temperature of 30°C. The temperature distribution at different time points is saved to a file and used as boundary conditions in the subsequent structural analysis. The structural analysis is conducted in two stages, known as load steps. During the first load step a normal load is applied to the back of the pads to simulate the parking brake application. During the second load step, disc rotation is used to generate a reaction torque that is equivalent to the static torque produced by the parking brake. As the brake cools the ability of the parking brake to generate this torque is reduced which can lead to rollaway. An overview of the FE model is given in Figure 7.1 with the model sub-systems discussed in the remainder of this section.

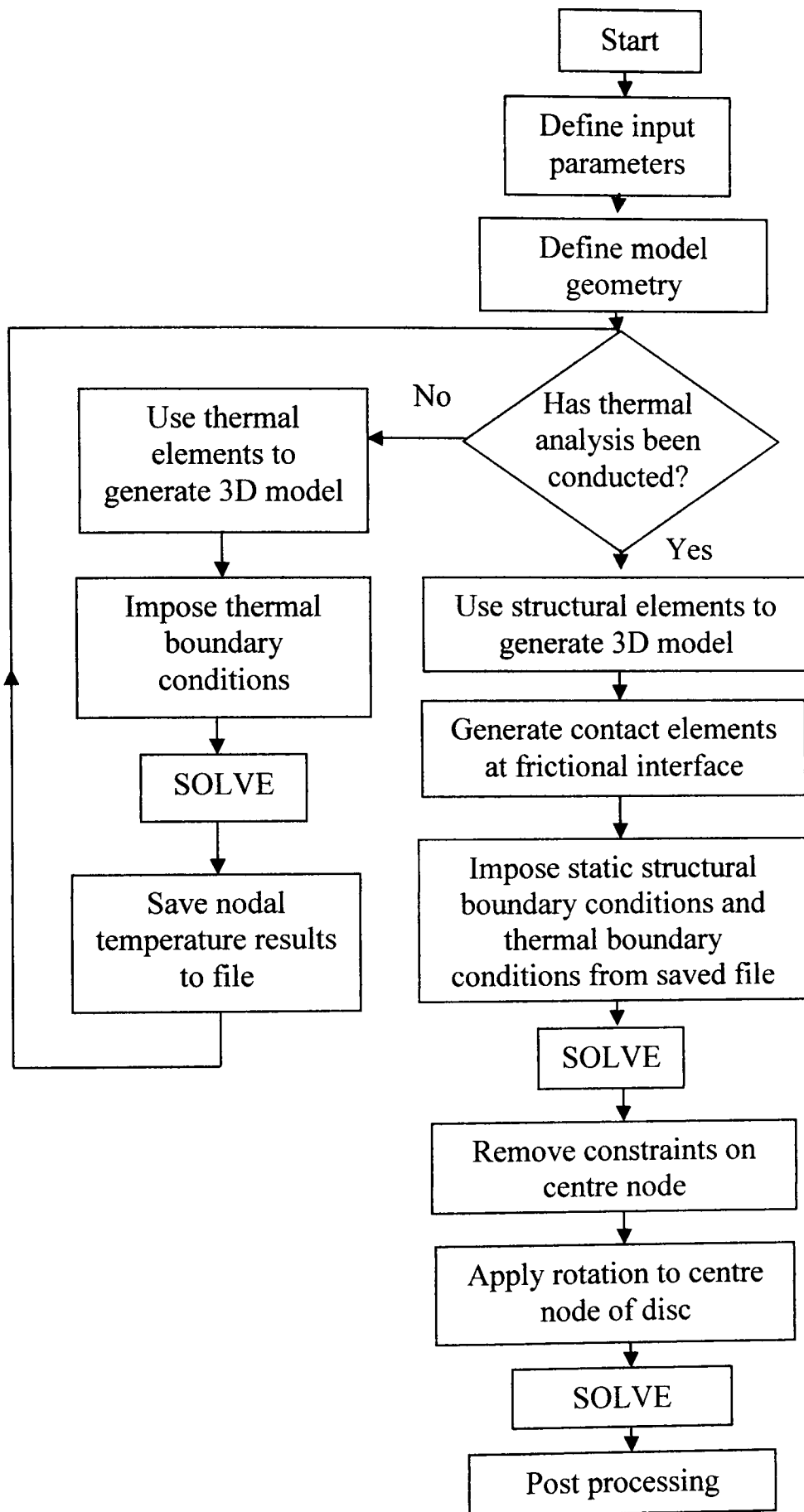


Figure 7.1 Overview of the finite element model

7.2.1. Define input parameters

The initial stage of the model requires the user to define the input variables for the test. This research has investigated the performance of the Jaguar S-Type parking brake system with different pads installed with the brake cooling from 250°C to 30°C. The input parameters varied for this research were the thermal expansion coefficient of the friction material, the temperature dependent Young's modulus of the friction material and the coefficient of friction between the pad and disc. The values used in the model have been estimated through the experimental work described in Chapter 6 where possible. The value of the conductive heat transfer coefficient was selected so that the model results agreed with the experimental measurements. The value used is higher than that typically expected because the model assumes a free convection but in reality a forced convection may be present due to prevailing weather conditions. The remainder of the material property values have been obtained from the work conducted by Ioannidis [44]. The fixed values are given in Table 7.1 and the pad dependent values are given in Table 7.2.

Parameter	Value	Unit
Young's modulus of disc	2.00×10^{11}	<i>Pa</i>
Poisson's ratio of disc	0.3	
Density of disc	7850	<i>kgm³</i>
Thermal conductivity of disc	54	<i>Wm⁻¹°C⁻¹</i>
Thermal expansion coefficient of disc	1.24×10^{-5}	<i>°C⁻¹</i>
Specific heat capacity of disc	440	<i>Jkg⁻¹°C⁻¹</i>
Convective heat transfer coefficient of disc	80	<i>Wm⁻²°C⁻¹</i>
Young's modulus of back plate	2.00×10^{11}	<i>Pa</i>
Poisson's ratio of back plate	0.3	
Density of back plate	7850	<i>kgm³</i>
Thermal conductivity of back plate	54	<i>Wm⁻¹°C⁻¹</i>
Thermal expansion coefficient of back plate	1.24×10^{-5}	<i>°C⁻¹</i>
Specific heat capacity of back plate	440	<i>Jkg⁻¹°C⁻¹</i>
Heat transfer coefficient of back plate	80	<i>Wm⁻²°C⁻¹</i>
Poisson's ratio of friction material	0.3	
Density of friction material	3000	<i>kgm³</i>

Table 7.1 Fixed values used in the FE model

Pad	E at 30°C (x 10 ⁶ Pa)	E at 250°C (x 10 ⁶ Pa)	α (x 10 ⁻⁶ °C ⁻¹)
1	495	380	15.8
2	535	339	12.8
3	321	240	8.0
4	413	310	10.5
5	493	466	20.4
6	511	494	16.9
7	511	491	14.8
8	478	472	11.5
9	836	809	6.2
10	417	314	15.8

Table 7.2 Properties of pads 1 to 10 used in FE simulation.

The static coefficient of friction as a function of temperature is required in the model to predict the torque developed by the parking brake system as a function of time. A third order polynomial has been used to approximate the results from the dynamometer tests, described in Chapter 6, to obtain the coefficient of friction as a function of temperature. The polynomials were obtained by using an interpolation function within MS Excel. The coefficients of the third order used to approximate the static coefficient of friction as a function of temperature for Pads 1 to 4 are given in Table 7.3 and the equations are plotted along with the corresponding dynamometer results in Figure 72.

Pad	$\mu = \alpha_3 T^3 + \alpha_2 T^2 + \alpha_1 T + \alpha_0$			
	α_3	α_2	α_1	α_0
1	-2×10^{-8}	3×10^{-6}	0.0007	0.398
2	-6×10^{-8}	3×10^{-5}	-0.0049	0.6417
3	-2×10^{-8}	-1×10^{-6}	0.0024	0.2201
4	-3×10^{-8}	3×10^{-6}	0.0015	0.3558

Table 7.3 Static coefficient of friction approximations as a function of temperature

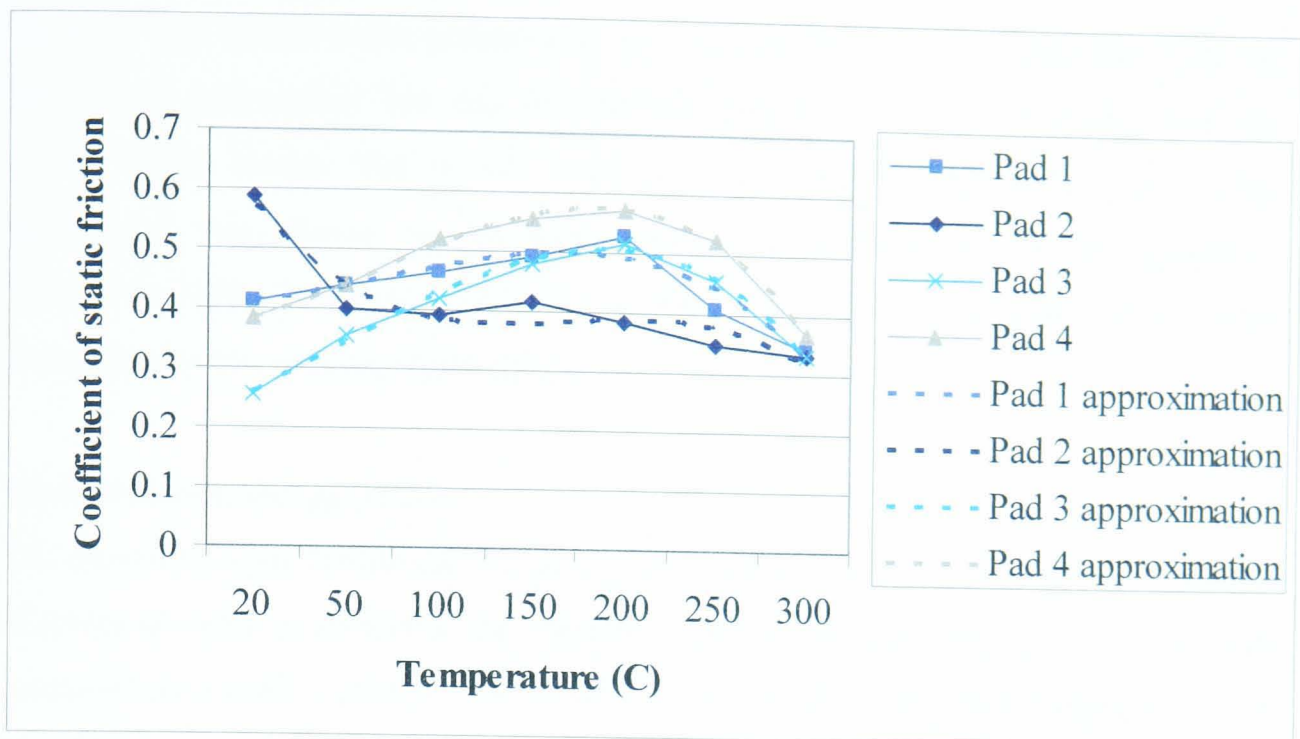


Figure 7.2 Coefficient of static friction as a function of temperature for Pads 1 to 4 as measured on the dynamometer and approximated by the mathematical model polynomial

The result in Figure 7.2 shows that the third order polynomial is a good approximation for the coefficient of static friction as a function of temperature for the pads tested. An R^2 correlation coefficient has been derived for the results given in Figure 7.2. The R^2 values from the third order polynomials are given in Table 7.4 along with the R^2 values for second and fourth order polynomials.

Pad	Second order polynomial	Third order polynomial	Fourth order polynomial
1	0.8128	0.8926	0.9122
2	0.7482	0.8999	0.9959
3	0.9453	0.9921	0.9936
4	0.9025	0.9964	0.997
Mean R^2 value	0.8522	0.9453	0.9747

Table 7.4 R^2 values from the polynomial approximations

The result in Table 7.4 shows that the third order polynomial has a mean R^2 coefficient of 0.95. This was deemed suitable for the mathematical model. The second order polynomial has a mean R^2 coefficient of 0.85 which was deemed to be

too low. The fourth order polynomial has a higher mean R^2 coefficient than the third order polynomial but this polynomial introduces more complexity into the model which means that it will take a longer time to solve. The third order polynomial was chosen as the most suitable approximation and the equations defined in Table 7.3 were used in the mathematical model to calculate the torque developed by the parking brake system.

7.2.2 Define model geometry

The geometry used within the FE model was simplified to reduce the total number of nodes in order to minimise the complexity and computational time. The disc was modelled as a solid cylinder with a hollow centre. The pads were modelled with a simplified geometry and include the back plate and the friction material. The finite element model and the pad and disc dimensions are shown in Figure 7.3 and 7.4 respectively. The 3D model was created by defining the location of key points within the ANSYS working environment. Lines were created between the key points and areas created from the lines. The disc volume was generated by rotating a 2D cross section of the disc through 360° about the centre of the disc. The pad model was created by extruding the 2D surface of a pad outwards away from the disc to generate the friction material volume and the back plate volume. The different material properties of the brake components were assigned to the corresponding volumes within the model.

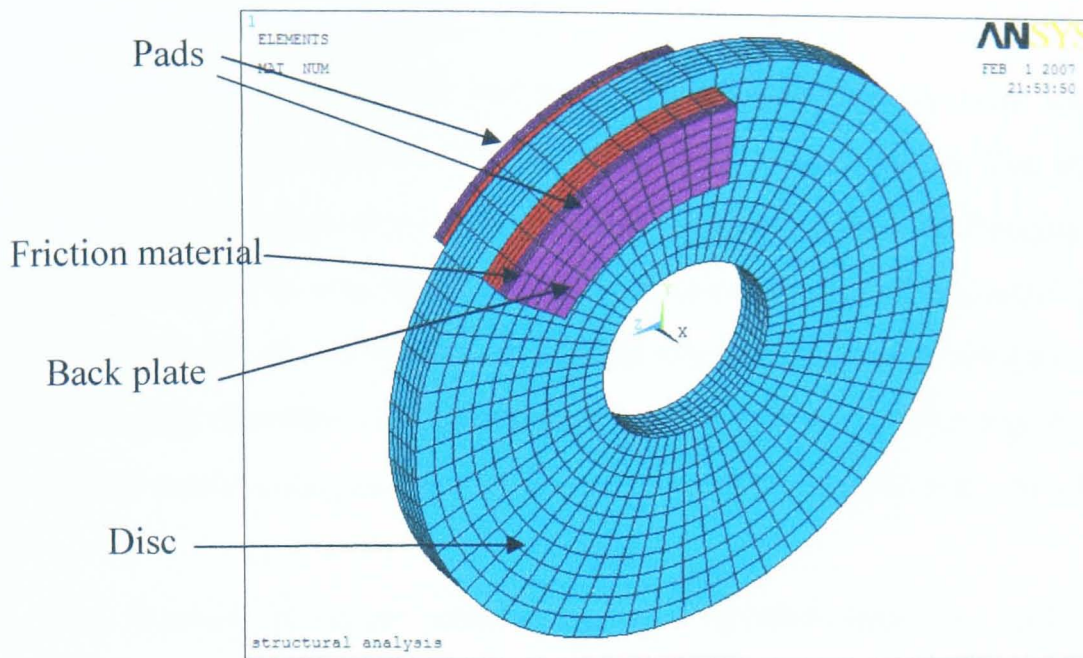


Figure 7.3 Simplified finite element model of the brake disc and pad with the pad comprising a back plate and friction material.

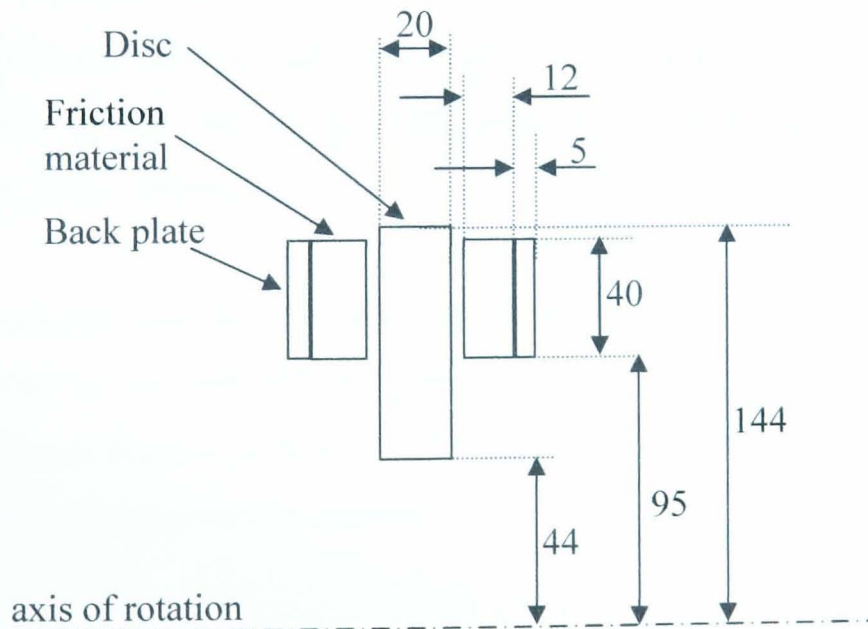


Figure 7.4 Dimensions (mm) of the brake disc and pads used in the FE model

7.2.3. Thermal analysis

Once the model geometry had been defined, the volumes were filled with thermal elements known as SOLID70 in the ANSYS nomenclature. The SOLID70 element is an 8-node brick element with 8 temperature degrees of freedom that allow heat conduction. The number of elements in each volume of the brake is defined by the mesh density of the model. A suitable mesh density was selected for the model to accurately describe the brake thermal behaviour without having too many elements which would increase the computational time required to solve the model.

The thermal boundary conditions were applied once the model geometry and element had been generated. Convection was applied to all of the free surfaces and a uniform temperature of 250°C applied to the disc and pads. The temperature/time history for all nodes within the model were saved to a file which can be re-read by ANSYS for the structural analysis.

7.2.4. Structural analysis

The structural analysis was conducted in two load steps. The first load step to apply the parking brake and the second load step to measure the torque produced by the parking brake system.

The elements used for the structural analysis are 8-node brick elements known as SOLID45 in the ANSYS nomenclature. Each node within the element has three translational degrees of freedom in the x, y and z direction. The nodes can also have a temperature specified to simulate thermal swelling of the materials.

The elements were created within the model using the same mesh density as for the thermal analysis. It is vital that the same mesh density is used so that all of the nodes are at the same location in both the structural and thermal analyses.

The SOLID45 elements used in the model do not have the capability to simulate contact between two bodies. Therefore contact elements were required at the frictional interface to model the contact between the pad and disc. The contact elements work in pairs requiring a contact surface and a target surface. The target

surface was assigned to the disc rubbing surface and the contact surface was assigned to the rubbing surface of the pad. The target surface is required to be larger than the contact surface to take into account any deformation of the pad during the simulation.

TARGE170 elements were used on the target surface and CONTA174 elements on the contact surface. The contact and target elements were attached to the surface of the SOLID45 elements and contact occurs when a contact element penetrates a target element during the simulation. The contact pairs require a coefficient of friction and a contact stiffness. The contact stiffness controls the conformability and amount of penetration between the contact and target surfaces. In reality no penetration would occur between the pad and disc and therefore an infinite stiffness should be specified. This would however potentially lead to convergency difficulties in the solution and therefore a compromise is required with a user specified contact stiffness that permits a minimum amount of penetration for reasonable solution times.

The structural model aims to simulate the constraints imposed on the actual vehicle park brake system. The disc on the vehicle is constrained by the wheel hub which has been simulated in the model using 3D beam elements known as BEAM4. The beam elements connect the inner surface of the disc to a central node on the brake axis. Constraints are applied to the central node to prevent movement in all degrees of freedom. The beam elements have a high stiffness to ensure that the constraints on the central node are transmitted to the inner radius of the disc. The beam elements in the centre of the disc representing the vehicle hub can be seen in Figure 7.5.

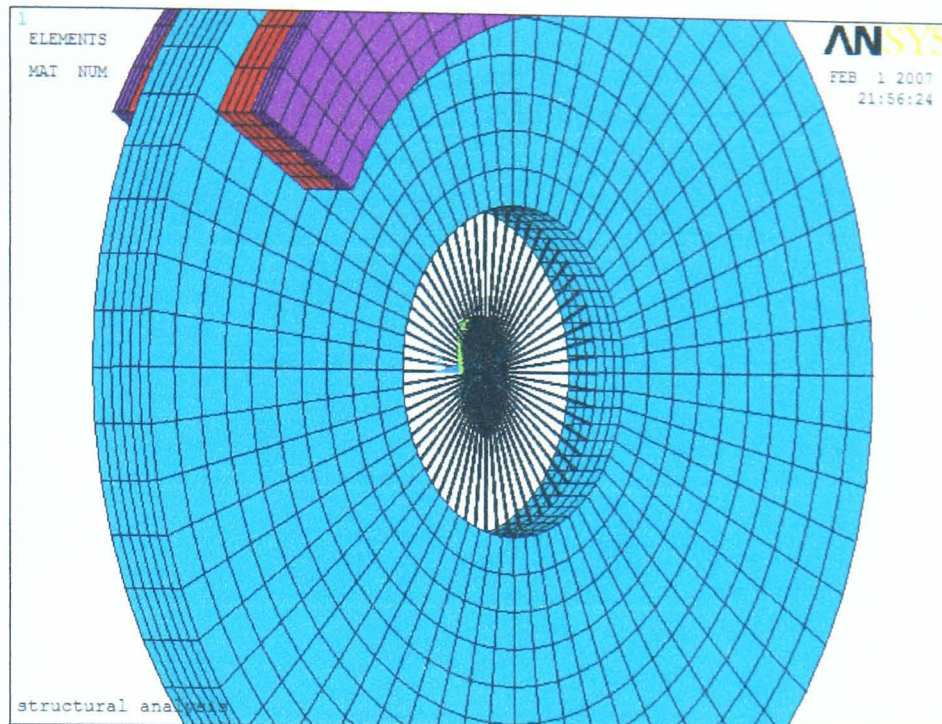


Figure 7.5 Beam elements in the centre of the disc

The pads are constrained on the vehicle by the abutments within the calliper. This was simulated in the model by constraining the side of the back plates facing the direction of disc rotation. Constraints were only applied to one side of the back plates to allow the pad to swell due to the thermal expansion. The constraints ensure that the pad can move in a direction perpendicular to the disc surface yet it can expand in the circumferential and radial directions.

Springs were used to apply a displacement to the pad which allows the stiffness of the parking brake apply system to be simulated. The springs are arranged on the pad back plate so as to simulate the loading of the calliper piston and calliper fingers. The apply springs are constrained so that they can only move in a direction perpendicular to the disc surface. The position of the apply springs is shown in Figure 7.6.

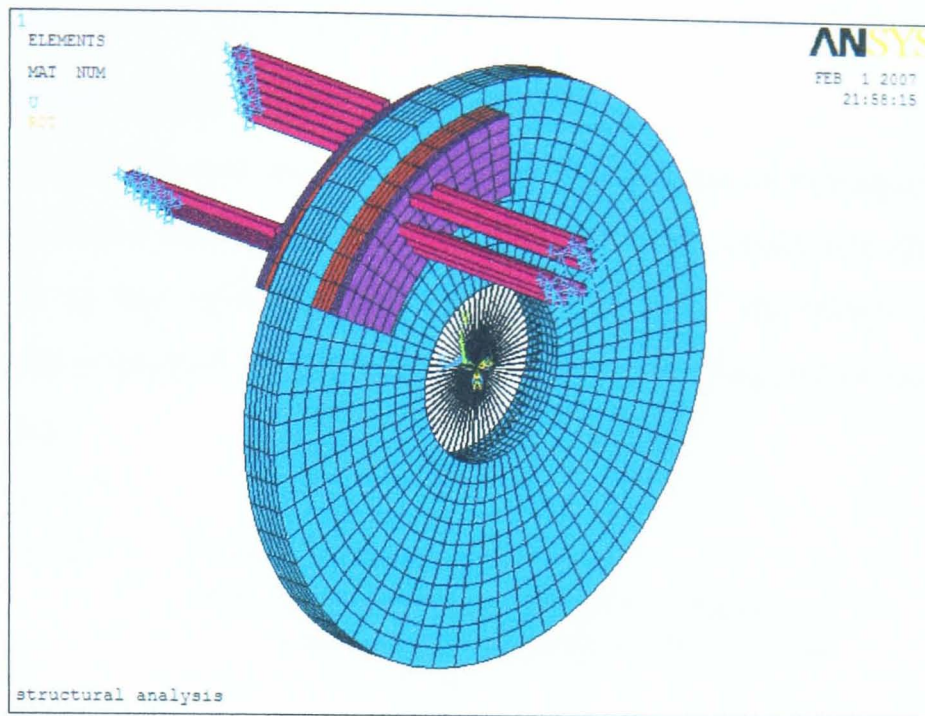


Figure 7.6 Location of the apply springs on the back plate of the pads

The temperatures of the nodes within the model were assigned a value read from the thermal analysis results file. This allowed the required temperature distribution to be generated within the brake.

With the first load step solved and the pads applied against the disc, the analysis was modified so that the disc could rotate. To achieve this, the boundary conditions on the central node were removed and replaced with new boundary conditions which allowed the central node to rotate about the axis of disc rotation. The central node was constrained so that it could not move in any other degrees of freedom. A rotation of 0.05 degrees about the axis of disc rotation was applied to the central node.

The reaction torque on the centre node at the time when the disc begins to rotate was recorded. The structural analysis was conducted with the temperature of the mean rubbing radius of the disc at 250°C, 200°C, 150°C, 100°C, 50°C and 30°C respectively. The results were used to obtain the torque produced by the parking brake system as a function of time.

7.3. Results

7.3.1. Thermal results

The thermal analysis was used to predict the temperature of the brake as a function of time as it cooled from 250°C to 30°C. The predicted temperature of a node on the disc surface at the same position as the location of the thermocouple on the dynamometer is plotted in Figure 7.7 along with the temperature measured on the dynamometer.

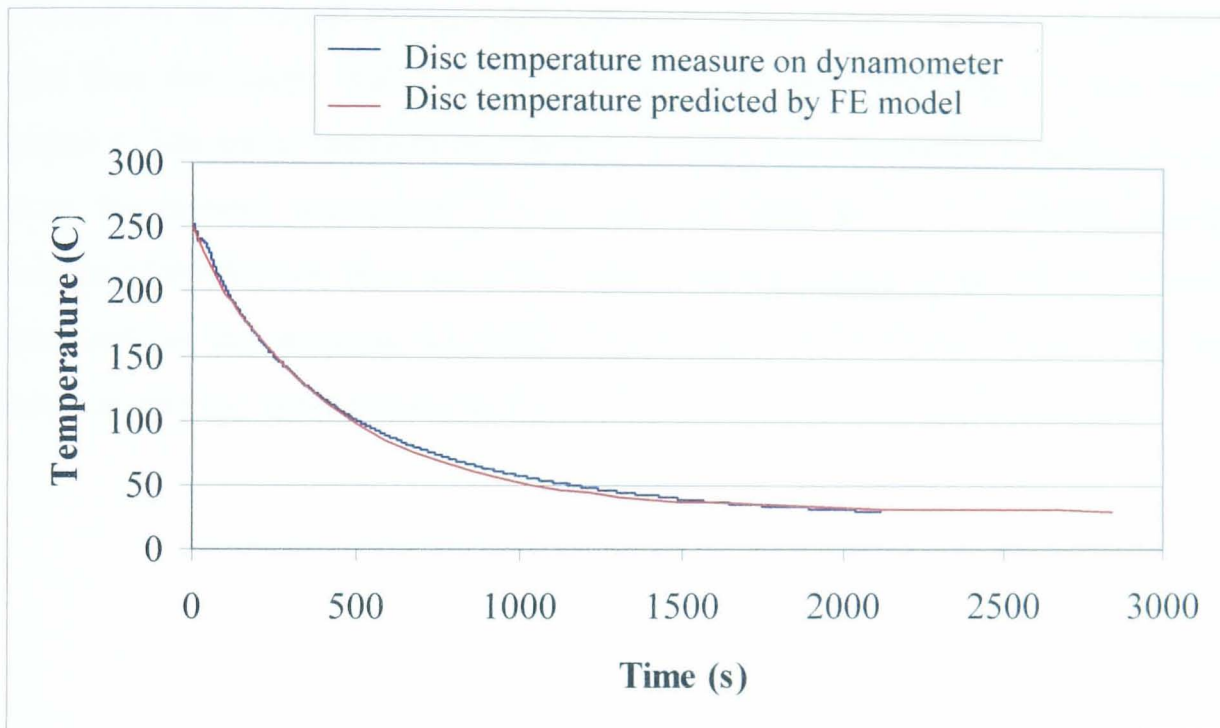


Figure 7.7 Cooling of the brake disc predicted by the FE model and measured on the dynamometer

The results in Figure 7.7 show that the finite element model is very accurate in simulating the temperature of the brake as it cools from 250°C to 30°C.

7.3.2. Clamp load

The finite element model was used to calculate the change in normal clamp load at the frictional interface as a function of time. This was done to compare the results predicted by the model to those measured on the dynamometer. The clamp load, N , at the frictional interface was calculated from the torque, T , predicted by the simulation using Equation 7.1.

$$N = \frac{T}{\mu r_{brake}} \quad (7.1)$$

Where: μ = coefficient of friction

r_{brake} = mean rubbing radius of the pad

The finite element model does not include hysteresis losses that may be present in the parking brake system and therefore it is more appropriate to compare the results predicted by the model to the cable load measured directly on the dynamometer rather than the clamp load derived from the measured cable load as described in Chapter 6. The model predicts that the clamp load will decrease as a function of time due to the thermal contraction of the brake components and the varying Young's modulus of the friction material. The torque produced by the parking brake system is dependant on the pressure distribution at the frictional interface which has been plotted at varying temperatures in Figure 7.8.

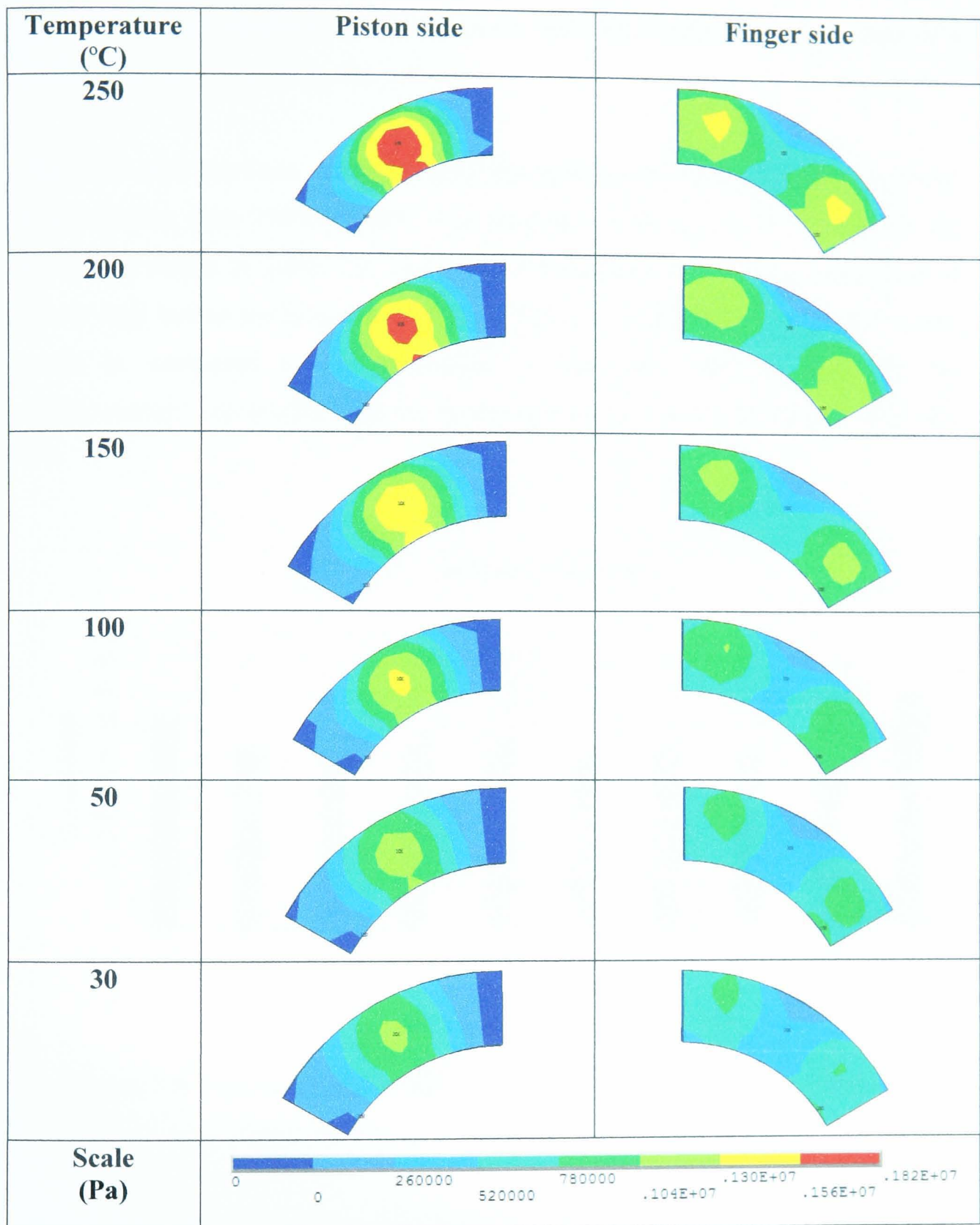


Figure 7.8 Pressure distribution of the contact pressure produced at the pad surface for the parking brake system with Pad 1 installed when cooling from 250°C to 30°C.

The results in Figure 7.8 show how the pressure distribution at the frictional interface varies as a function of temperature. Initially the pressure is concentrated at the location of the calliper piston and fingers. This is less apparent as the brake cools

towards ambient temperature. The pressure could be distributed more evenly if a stiffer material was used for the pad.

The FE model has been used to predict the performance of Pads 1 to 10 with the brake cooling from 250°C to 30°C. The properties of Pads 1 to 10 used within the model are shown in Table 7.2. The model was used to calculate the percentage of clamp load lost as the brakes cooled from 250°C to 30°C so that the model results could be compared to the percentage of lost cable load measured on the dynamometer. The results from the model and dynamometer are plotted in Figure 7.9.

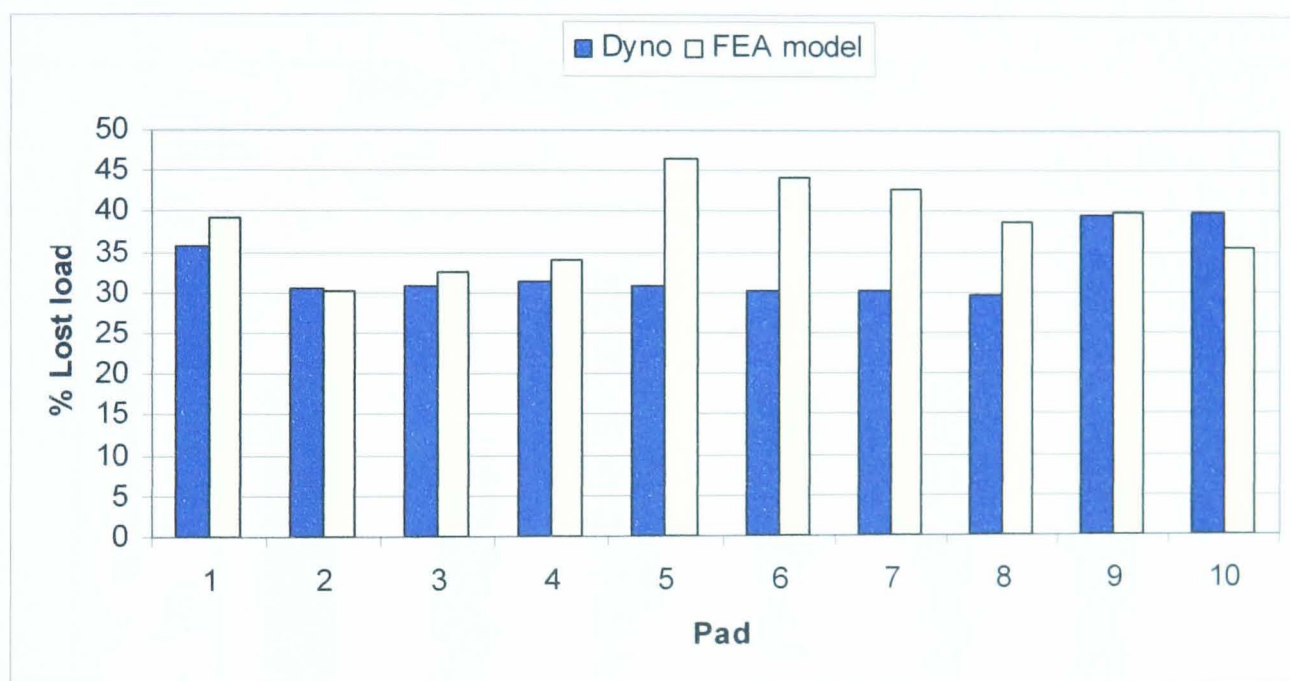


Figure 7.9 Percentage of lost clamp load of Pads 1 to 10 as measured on the dynamometer and predicted by the FE model.

The results in Figure 7.9 show that the percentage of lost clamp load predicted by the model has very a good correlation to the percentage of lost cable load measured on the dynamometer except for Pads 5 to 8. The large errors in the results for Pads 5 to 8 could be because the dynamometer test was not repeated and the properties of the pads measured in the laboratory could have varied during the dynamometer tests.

The simulation results predict that the properties of the pads can affect the percentage of clamp load lost as the brake cools. The analysis was therefore used to

investigate if the properties of Pad 1 could be modified so that the brake would lose less clamp load. Five additional pads were simulated, labelled Pads 1a to 1e, with the properties of the pads given in Table 7.5. The percentage of the initial applied clamp load that was lost as the brake cooled from 250°C to 30°C with Pad 1 and Pads 1a to 1e installed is plotted in Figure 7.10.

Pad	E at 30°C (x 10 ⁸ Pa)	E at 250°C (x 10 ⁸ Pa)	α (x 10 ⁻⁶ °C ⁻¹)
1	4.95	3.8	15.8
1a	4.95	3.8	7.9
1b	4.95	3.8	31.6
1c	2.475	1.9	15.8
1d	9.9	7.6	15.8
1e	4.95	1.9	15.8

Table 7.5 Properties of Pads 1a to 1e.

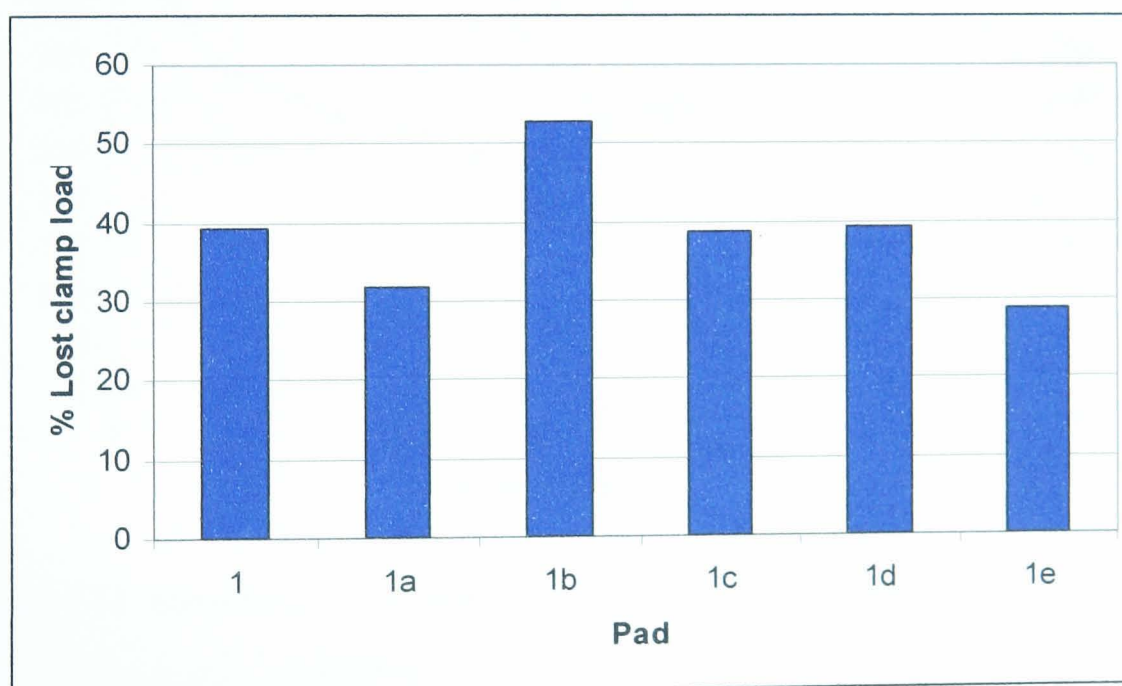


Figure 7.10 Percentage of lost clamp load predicted by the FE model for Pads 1a to 1e.

The results in Figure 7.10 show that the FE model predicts that the coefficient of thermal expansion has a significant effect on the percentage of lost clamp load. The model shows that doubling or halving the Young's modulus values at 250°C and 30°C does not have a significant effect on the percentage of lost clamp load although it does show that a lower Young's modulus somewhat reduces the percentage of lost clamp load. The model predicts that increasing the difference between the Young's

modulus at 250°C and 30°C, as with Pad 1e, reduces the percentage of lost clamp load.

The finite element model was used to predict the torque produced by the parking brake for Pads 1 to 4 with the vehicle parked on a 12% gradient and the brake cooling from 250°C to 30°C. The static coefficient of friction for Pads 1 to 4 specified as a function of temperature within the finite element model was obtained from the dynamometer test results described in Chapter 6. The results from the finite element simulation are plotted in Figure 7.11 along with the torque required to hold the vehicle on the gradient.

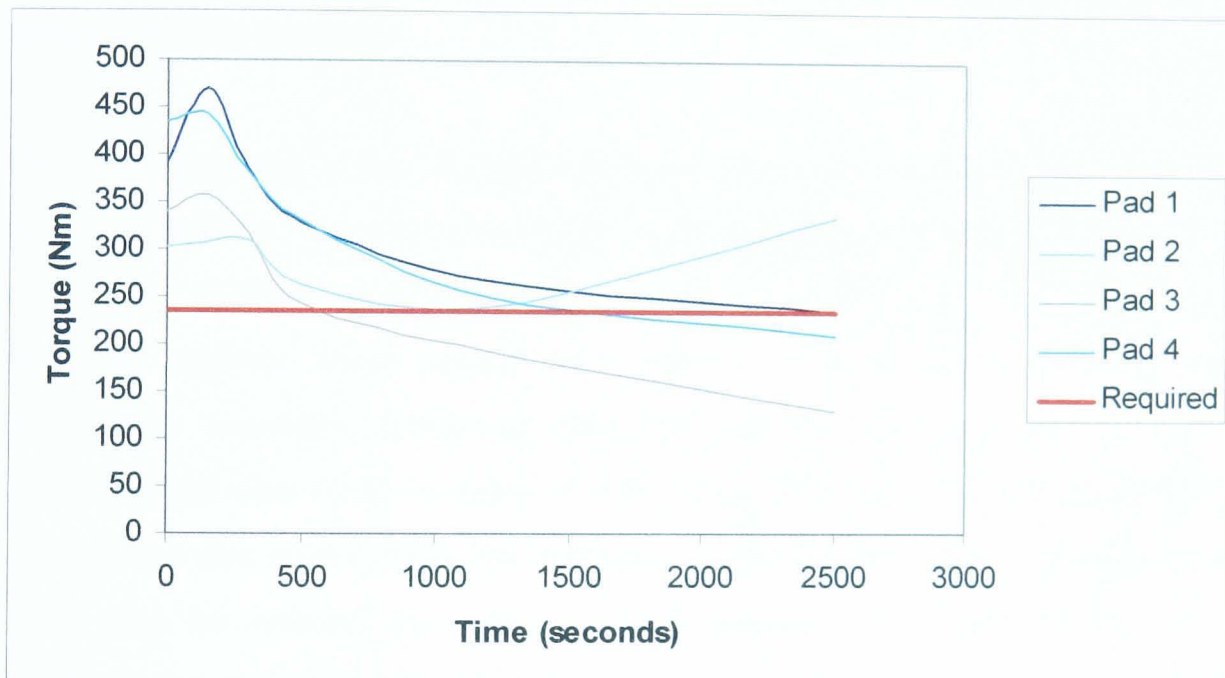


Figure 7.11 Simulated torque produced by the parking brake system with Pads 1 to 4 installed cooling from 250°C to 30°C.

The results in Figure 7.11 show that the torque produced by the parking brake system with Pads 1 to 4 installed varies as a function of temperature. The model runs under displacement control so the initial applied torque values vary for the different pads due to the varying stiffness values. The torque values in the model can increase due to the changing friction level.

7.4. Summary

A finite element model has successfully been developed which simulates the performance of a parking brake system during a rollaway event. The model has been validated against the dynamometer results and has shown to have a good correlation with the measured rate of cooling and loss of clamp load. The model shows that the properties of the friction material affect the percentage of lost clamp load at the frictional interface and that carefully selected properties for the friction material can reduce the amount of clamp load that is lost as the brakes cool. However the percentage of lost clamp load cannot be made negligible by changing the properties of the pad alone due to the thermal contractions of the disc and the behaviour of the apply system. To fully understand the behaviour of the apply system a more detailed model would be required.

The main drawback of the FE model is the computational time required to solve the complete problem. The thermal analysis has a computational time of five minutes on a PC using an Intel Pentium 4 with a 3 GHz processor and 1 GB of RAM. The structural analysis takes around ten minutes to solve but loading the nodal temperature boundary conditions into the model takes over five hours. The computational time could be reduced if the number of nodes within the model was reduced but this might affect the accuracy of the results. The computational time could also be reduced by using a faster computer but there would be cost implications associated with this solution. An alternative method would be to use a different finite element software package which has elements with both structural and thermal degrees of freedom.

Chapter 8

Rollaway simulation using Matlab/Simulink

8.1. Introduction

The finite element method has the potential to be an excellent tool for predicting the performance of parking brake systems. However it is not currently a viable desktop design tool for the brake engineer due to the computational time required to conduct the analysis. Therefore an alternative mathematical model has been developed to investigate the effects of the brake system parameters on the likelihood of rollaway. This model allows for the inclusion of the calliper and the parking brake apply system. The model has been written using the Matlab and Simulink software. This chapter describes the methodology behind the model and presents the results that it has generated.

8.2. Methodology

Vehicle rollaway occurs when the torque produced by the parking brake system drops below the torque required to hold the vehicle on a gradient. The torque produced by the parking brake system is dependent on the normal clamp load at the frictional interface and the associated coefficient of friction. The mathematical model calculates the torque required by the parking brake system to hold a vehicle on a given gradient and the torque produced by the parking brake as the brake and apply system cools from an elevated temperature. The results are used to predict if a vehicle will rollaway and the effect that brake system parameters have on the likelihood of rollaway occurring. An overview of the model is given in Figure 8.1 and the sub-systems are explained in the remainder of this section.

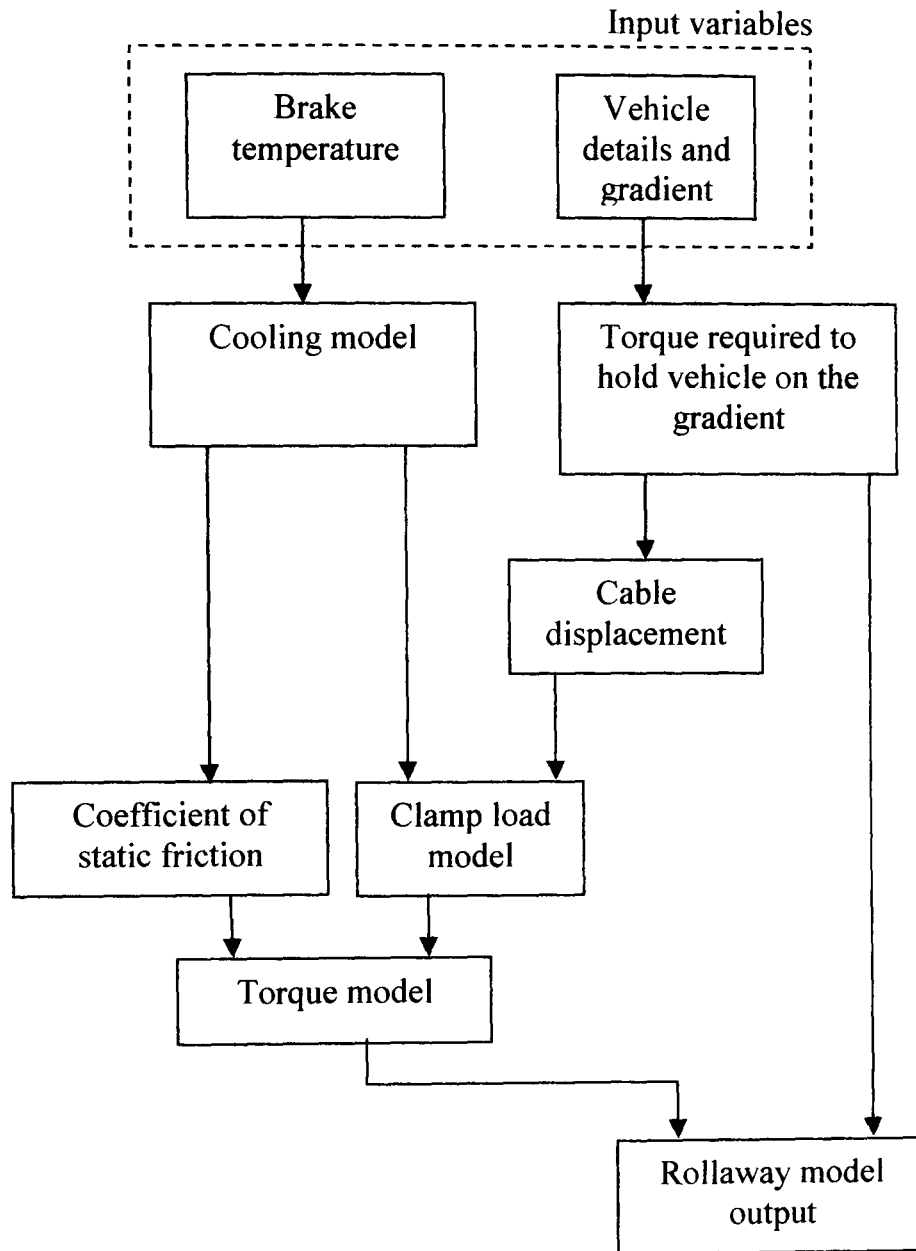


Figure 8.1 Overview of mathematical model

8.2.1. Input variables

The parameter values used within the model have been obtained from the experimental work described in Chapter 6. The fixed system values are given in Table 8.1. The pad dependant parameters are given in Table 8.2. The values used in Table 8.1 have been obtained from measurements taken during the work conducted in Chapter 6 or from the work published by Ioannidis [44].

Parameter	Symbol	Value	Units
Disc stiffness	K_d	2×10^{11}	Nm^{-1}
Pad thickness	l_{0p}	0.012	m
Half disc thickness	l_{0d}	0.01	m
Disc thermal expansion coefficient	α_d	12.4×10^{-6}	$^{\circ}C^{-1}$
Length of Cable 1	l_{0cab1}	0.5	m
Cable 1 thermal expansion coefficient	α_{cab1}	12.4×10^{-6}	$^{\circ}C^{-1}$
Calliper stiffness	K_{cal}	1×10^9	Nm^{-1}
Calliper bridge length	l_{0cal}	0.1	m
Calliper thermal expansion coefficient	α_{cal}	12.4×10^{-6}	$^{\circ}C^{-1}$
Stiffness of Cable 1	K_{cab1}	5×10^6	Nm^{-1}
Stiffness of Cable 2	K_{cab2}	5×10^6	Nm^{-1}
Calliper lever ratio	R_c	11	
Initial displacement	u_1	0.001	m
Specific heat capacity of the disc	C_{pdisc}	440	$Jkg^{-1}^{\circ}C^{-1}$
Volume of the disc	V_d	5.21×10^{-3}	m^3
Area of the disc	A_d	0.261	m^2
Convective heat transfer coefficient of the disc	h_d	80	$WC^{-1}m^{-2}$
Density of the disc	ρ_d	7850	kgm^{-3}
Specific heat capacity of the pad	C_{ppad}	440	$Jkg^{-1}^{\circ}C^{-1}$
Volume of the pad	V_p	0.00068	m^3
Area of the pad	A_p	0.004	m^2
Heat transfer coefficient of the pad	h_p	80	$W^{\circ}C^{-1}m^{-2}$
Density of the pad	ρ_p	3000	kgm^{-3}
Specific heat capacity of the calliper	C_{pcal}	440	$Jkg^{-1}^{\circ}C^{-1}$
Volume of the calliper	V_{cal}	0.0005	m^3
Area of the calliper	A_{cal}	0.2	m^2
Heat transfer coefficient of the calliper	h_{cal}	80	$WC^{-1}m^{-2}$
Density of the calliper	ρ_{cal}	7850	kgm^{-3}
Specific heat capacity of Cable 1	C_{ppad}	440	$Jkg^{-1}^{\circ}C^{-1}$
Volume of Cable 1	V_{cab1}	5×10^{-5}	m^3
Area of Cable 1	A_{cab1}	0.025	m^2
Heat transfer coefficient of Cable 1	h_{cab1}	80	$W^{\circ}C^{-1}m^{-2}$
Density of Cable 1	ρ_{cab1}	7850	kgm^{-3}

Table 8.1 Values of the system parameters used in the model

Pad	Stiffness at 30°C ($K_p 30$) ($\times 10^6 \text{ Nm}^{-1}$)	Stiffness at 250°C ($K_p 250$) ($\times 10^6 \text{ Nm}^{-1}$)	Thermal expansion coefficient (α_p) ($\times 10^{-6} \text{ }^\circ\text{C}^{-1}$)
1	132	101	18.3
2	143	90.3	12.8
3	85.6	64.1	8.0
4	110	82.6	10.5
5	131	124	20.4
6	136	132	16.9
7	136	131	14.8
8	127	126	11.5
9	223	216	6.2
10	111	83.7	15.8

Table 8.2 The stiffness of Pads 1 to 10 at 30°C and 250°C

8.2.2. Cooling model

The cooling model is used to predict the temperature of the brake components within the system. The model simulates the temperature of the disc, pads, calliper and the parking brake apply cable.

The temperature of the disc is an important parameter because it affects the thermal contractions of the disc and it has been measured on the dynamometer allowing the model results to be validated. The disc is assumed to have an initial uniform temperature at the start of the simulation. The subsequent temperature of the disc as a function of time has been modelled using the lumped heat capacitance method [45], which assumes convection is the dominant cooling regime and is given by the negative exponential curve of Equation 8.1:

$$T(t) = (T_{0d} - T_{\infty}) \exp\left[\frac{-h_d A_d}{\rho_d c_d V_d} t\right] + T_{\infty} \quad (8.1)$$

Where: $T(t)$ = Instantaneous temperature ($^\circ\text{C}$)

T_0 = Initial temperature ($^\circ\text{C}$)

T_{∞} = Ambient temperature ($^\circ\text{C}$)

h = Heat transfer coefficient ($\text{Wm}^{-2}\text{C}^{-1}$)

A = Area (m^2)

ρ = Density (kgm^{-3})

c = Specific heat capacity ($Jkg^{-1}C^{-1}$)

V = Volume (m^3)

The temperature of the pad is assumed to have an initial uniform temperature and has been modelled as a function of time using Equation 8.2.

$$T(t) = (T_{0p} - T_{\infty}) \exp \left[\frac{-h_p A_p}{\rho_p c_p V_p} t \right] + T_{\infty} \quad (8.2)$$

The on-vehicle tests described in Chapter 4 have shown that the temperature of the calliper could have a significant effect on the level of clamp load generated at the frictional interface as a function of time. As the calliper bridge cools from an elevated temperature it contracts increasing the clamp load at the frictional interface. The temperature of the calliper was not measured during the on-vehicle rollaway and dynamometer clamp load tests because the data acquisition system was developed for use with two thermocouples. These thermocouples were used to measure the temperature of the disc as this was considered to be the most significant component. The thermocouples were used to measure the calliper temperature during the calliper stiffness evaluations described in Chapter 6. The bulk calliper temperature was found to achieve temperatures up to 90°C during these tests. The calliper temperature is determined by the thermal conduction of heat through the brake pad away from the frictional interface, the heat radiating from the brake components and the convection of heat from the calliper to the surrounding air. The thermal conductivity of the pads used in this research is reported by Federal Mogul engineers to vary between the formulations used [23]. This means that the calliper temperature may be different for every pad used in the research. The calliper temperature can affect the variation of the clamp load at the frictional interface as a function of temperature and was therefore included in the model. The temperature of the calliper as a function of time has been modelled using Equation 8.3.

$$T(t) = (T_{0cal} - T_{\infty}) \exp \left[\frac{-h_{cal} A_{cal}}{\rho_{cal} c_{cal} V_{cal}} t \right] + T_{\infty} \quad (8.3)$$

The vehicle parking brake system is comprised of 3 cables. The first cable, Cable 1, connects the hand brake lever to a simple yolk and this is parallel and in close

proximity to the engine exhaust. The other cables, Cables 2 and 3, connect the yolk to the rear foundation brakes. The temperature of Cable 1 has been included in the model to investigate the effect of cable temperature on clamp load. The location of Cable 1 on the Jaguar S-Type means that it could potentially be heated by the engine exhaust system. If Cable 1 was at an elevated temperature when the vehicle was parked then as the cable cools, the thermal contractions will increase the cable load which will affect the clamp load at the frictional interface. The cable temperature has been included in the model to investigate if it is feasible to develop sufficient thermal contraction of the cable to prevent rollaway. Cables 2 and 3 are assumed to have a uniform ambient temperature in the simulation because there is no potential for them to be heated on the vehicle. The temperature of Cable 1 as a function of time has been modelled using Equation 8.4.

$$T(t) = (T_{0cab} - T_{\infty}) \exp\left[\frac{-h_{cab} A_{cab}}{\rho_{cab} c_{cab} V_{cab}} t\right] + T_{\infty} \quad (8.4)$$

8.2.3. Torque required to hold the vehicle

The torque required to hold the vehicle on the gradient is calculated from the forces produced by the weight of the vehicle on the slope and the radius of the vehicle wheels shown in Figure 8.2. The rolling resistance of the vehicle's wheels and tyres has been neglected for this analysis in order to reduce the complexity.

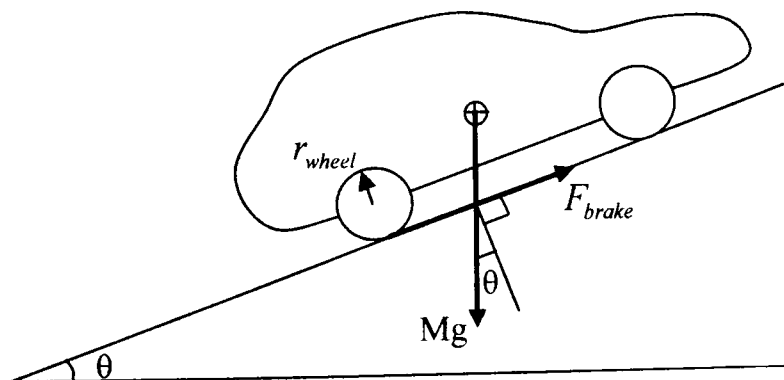


Figure 8.2 Diagram of vehicle parked on a gradient

The torque required to hold the vehicle on the gradient, T_r , is given by:

$$T_r = Mgr_{wheel} \sin \theta \quad (8.5)$$

Where: T_r = Torque required to hold vehicle on the gradient (Nm)
 M = Mass of the vehicle (kg)
 θ = Angle of the gradient ($^\circ$)
 r_{wheel} = Radius of the vehicle wheel (m)

The tangential brake force required for each of the rear brakes to hold the vehicle on the gradient is given by:

$$F_{brake} = \frac{T_r}{2r_{brake}} \quad (8.6)$$

Where: F_{brake} = Force produced by the brake (N)
 r_{brake} = Mean rubbing radius of the brake (m)

The normal clamp load at the frictional interface required by the rear brakes to hold the vehicle on the gradient is given by:

$$F_{Nrequired} = \frac{F_{brake}}{\mu} \quad (8.7)$$

Where: $F_{Nrequired}$ = Minimal normal load required to hold the vehicle on the gradient (N)
 μ = Static coefficient of friction at the pad-disc interface

The values used in the calculations were obtained from the input variables described in Section 8.2.1.

8.2.4. Description of the clamp load model

The change in normal clamp load that occurs during a cooling cycle is modelled using an essentially 1-D quasi-static system that has five degrees of freedom. An overview of the system modelled is given in Figure 8.3. The model includes the brake calliper, pad, half of the disc and the parking brake apply system, incorporating the yoke, the cable connecting the parking brake lever to the yoke, Cable 1, and the two cables connecting the yoke to the two rear callipers, Cable 2 and 3. The yoke has been modelled as a rigid link because symmetrical operation has been assumed for the foundation brakes connected to each side of the yoke. The model has been simplified to represent one pad and half of one disc to reduce the complexity of the simulation because the other half of the disc and pad are assumed to be identical. Consequently, only one wheel station has been modelled in detail and the stiffness of the other wheel station has been embedded within the stiffness of Cable 3. The parking brake apply system, disc and calliper have been modelled using simple linear spring elements whilst the stiffness of the pad includes temperature dependence. The thermal deformations of the pad, disc, calliper and Cable 1 are also described by a coefficient of thermal expansion. The model runs under displacement control in the sense that when the parking brake is actuated, a displacement, u_1 , is applied to the parking brake lever. This results in a displacement, u_4 , being generated at the back of the pad producing a load at the frictional interface. The magnitude of the load is governed by the initial displacement, u_1 , the stiffness of the elements within the model and the calliper ratio, R_c . As the brake cools the load at the frictional interface is dependant on the thermal contractions of the brake components and the stiffness of the system. The model assumes that the apply system has no inefficiencies which could occur from friction in the cable system. A schematic diagram of the model is given in Figure 8.4.

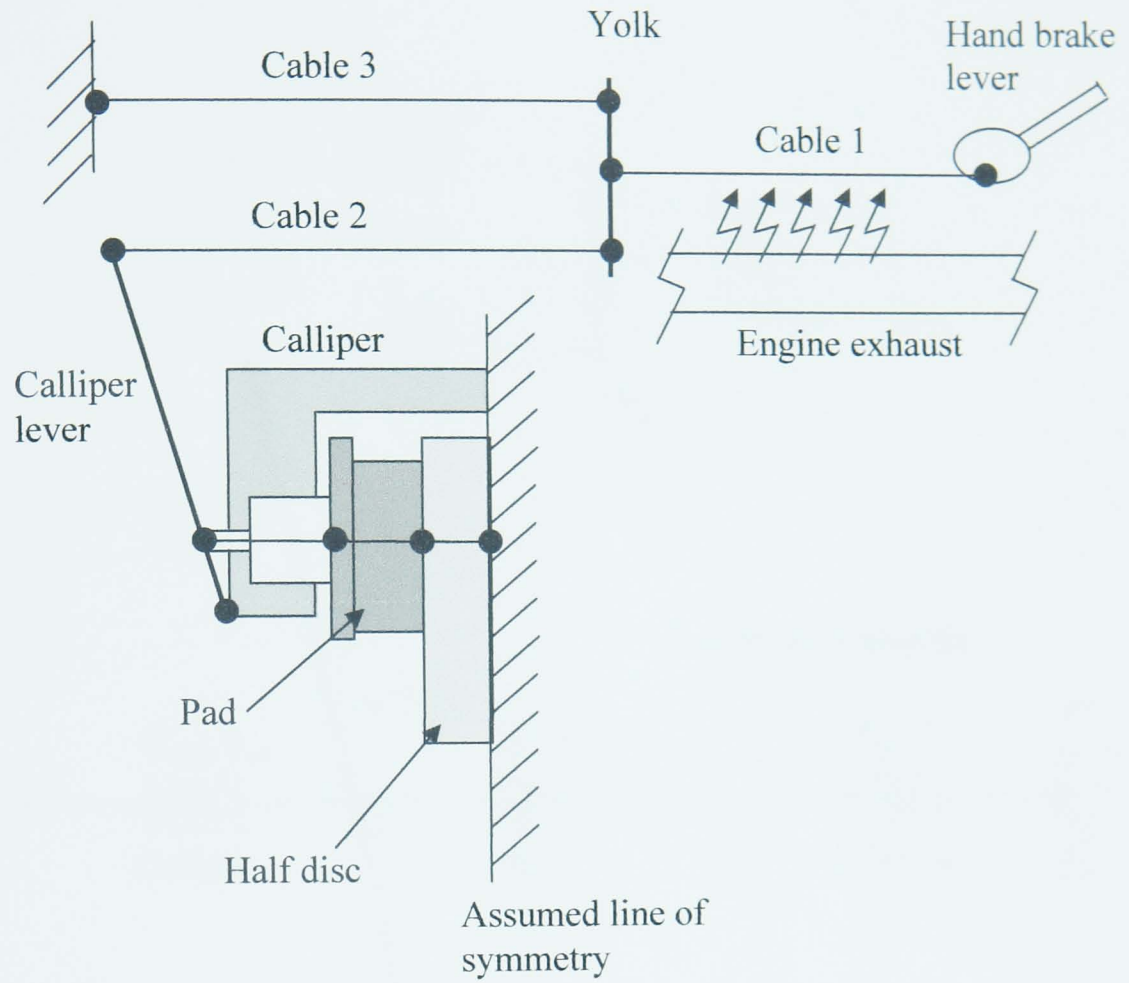


Figure 8.3 Overview of the system modelled

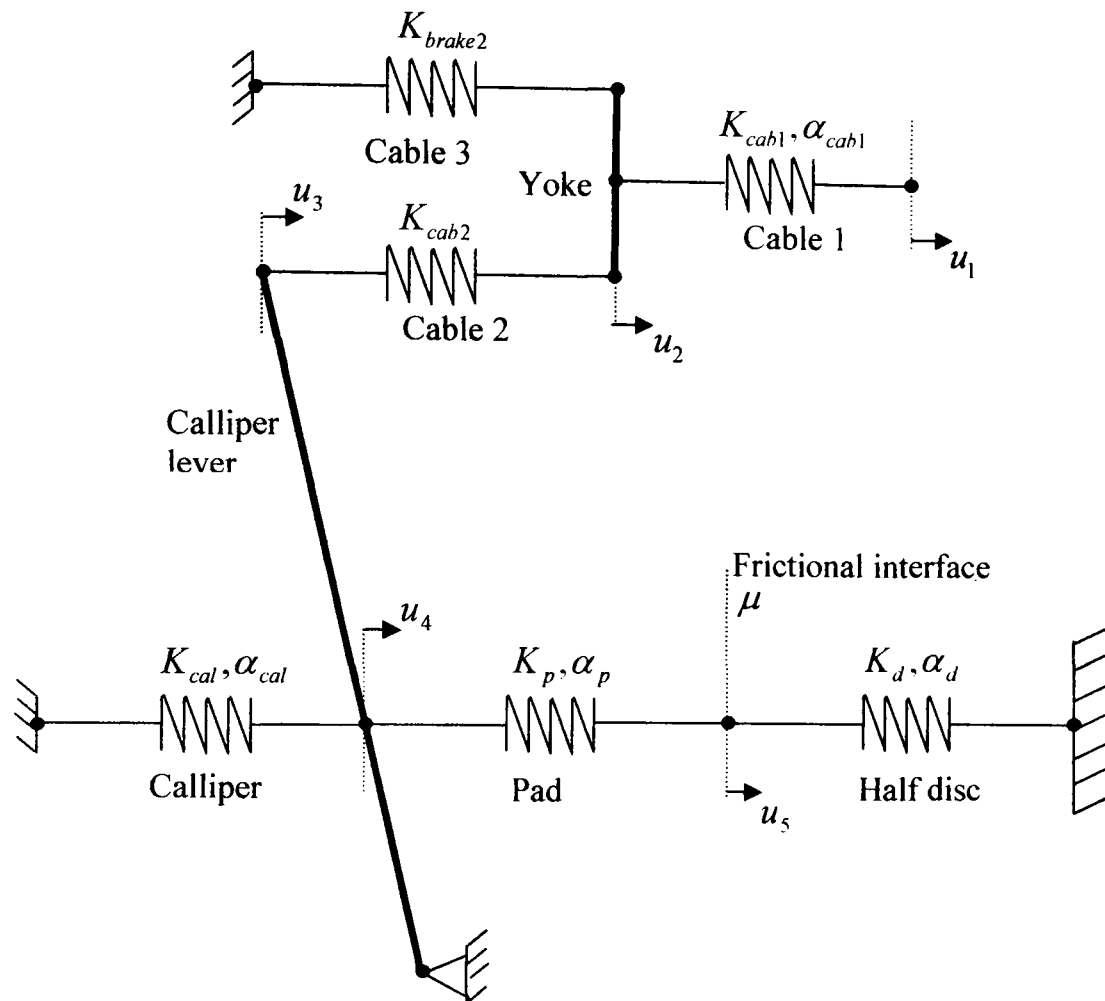


Figure 8.4 Schematic of clamp load model

The loads in the elements within the model are calculated using Hooke's law and are given in Equations 8.8 to 8.13.

$$\text{Cable 1: } F_{a1} = K_{cab1}(u_1 - u_2 + \Delta l_{cab1}) \quad (8.8)$$

$$\text{Cable 2: } F_{a2} = K_{cab2}(u_2 - u_3) \quad (8.9)$$

$$\text{Cable 3: } F_{a3} = K_{brake2}u_2 \quad (8.10)$$

$$\text{Pad: } F_i = K_p(u_5 - u_4 - \Delta l_p) \quad (8.11)$$

$$\text{Half disc: } F_i = K_d(u_5 - \Delta l_d) \quad (8.12)$$

$$\text{Calliper: } F_i = K_{cal}(u_4 + \Delta l_{cal}) \quad (8.13)$$

The thermal contractions of the pad, half disc, calliper and apply cable 1 are given by equations 8.14 to 8.17.

$$\Delta l_p = l_{0p} \alpha_p \Delta T_p \quad (8.14)$$

$$\Delta l_d = l_{0d} \alpha_d \Delta T_d \quad (8.15)$$

$$\Delta l_{cal} = l_{0cal} \alpha_{cal} \Delta T_{cal} \quad (8.16)$$

$$\Delta l_{cab} = l_{0cab} \alpha_{cab} \Delta T_{cab} \quad (8.17)$$

The stiffness of the calliper, pad, half disc and Cable 2 are combined to give the equivalent stiffness of brake 1, K_{brake1} . This is done to simplify the later calculations of the load at the frictional interface.

$$\frac{1}{K_{brake1}} = \frac{1}{K_{cab2} R_c^2} + \frac{1}{K_p} + \frac{1}{K_d} + \frac{1}{K_{cal}} \quad (8.18)$$

Which becomes:

$$K_{brake1} = \frac{K_{cab2} R_c^2 K_{cal} K_p K_d}{K_{cal} K_p K_d + K_{cab2} R_c^2 K_p K_d + K_{cab2} R_c^2 K_{cal} K_d + K_{cab2} R_c^2 K_{cal} K_p} \quad (8.19)$$

The stiffness of the calliper, pad and half disc are combined to give the equivalent stiffness of the wheel station of brake 1, K_{wheel1} .

$$\frac{1}{K_{wheel1}} = \frac{1}{K_p} + \frac{1}{K_d} + \frac{1}{K_{cal}} \quad (8.20)$$

$$K_{wheel1} = \frac{K_{cal} K_p K_d}{K_{cal} K_p + K_{cal} K_d + K_p K_d} \quad (8.21)$$

The calliper ratio, R_c , is used to describe the relationship between the displacements and loads in the system by Equations 8.22 and 8.23.

$$F_i = R_c F_{a2} \quad (8.22)$$

$$u_5 = R_c u_4 \quad (8.23)$$

To ensure symmetry of operation the load produced in Cable 1, F_{a1} , is assumed to be divided equally between Cable 2 and Cable 3 giving Equations 8.24 and 8.25.

$$F_{a1} = F_{a2} + F_{a3} \quad (8.24)$$

$$F_{a2} = F_{a3} \quad (8.25)$$

The load at the frictional interface, F_i , is derived as a function of the initial parking brake displacement, u_1 , from Equation 8.8. Combining this with Equation 8.22 gives:

$$\frac{2F_i}{R_c} = K_{cab1}(u_1 - u_2 + \Delta l_{cab1}) \quad (8.26)$$

$$F_i = \frac{R_c K_{cab1}}{2}(u_1 - u_2 + \Delta l_{cab1}) \quad (8.27)$$

$$u_2 \frac{R_c K_{cab1}}{2} = \frac{R_c K_{cab1}}{2}(u_1 + \Delta l_{cab}) - F_i \quad (8.28)$$

$$u_2 = u_1 + \Delta l_{cab} - \frac{2F_i}{R_c K_{cab1}} \quad (8.29)$$

From Equation 8.9, 8.22 and 8.23:

$$\frac{F_i}{R_c} = K_{cab2}(u_2 - R_c u_4) \quad (8.30)$$

Substituting Equation 8.29 into 8.30 gives:

$$F_i = R_c K_{cab2} \left[\left(u_1 + \Delta l_{cab} - \frac{2F_i}{R_c K_{cab1}} \right) - R_c u_4 \right] \quad (8.31)$$

$$F_i + R_c^2 u_4 K_{cab2} = R_c K_{cab2} \left(u_1 + \Delta l_{cab} - \frac{2F_i}{R_c K_{cab1}} \right) \quad (8.32)$$

$$u_4 = \frac{1}{R_c} \left(u_1 + \Delta l_{cab} - \frac{2F_i}{R_c K_{cab1}} \right) - \frac{F_i}{R_c^2 K_{cab2}} \quad (8.33)$$

The equivalent stiffness of the calliper, pad and half disc from Equation 8.21 is used to calculate the load at the frictional interface, F_i .

$$F_i = K_{Wheel1} (u_4 - \Delta l_p - \Delta l_d + \Delta l_{cal}) \quad (8.34)$$

Using Equation 8.33:

$$F_i = K_{Wheel1} \left[\frac{1}{R_c} \left(u_1 + \Delta l_{cab} - \frac{2F_i}{R_c K_{cab1}} \right) - \frac{F_i}{R_c^2 K_{cab2}} - \Delta l_p - \Delta l_d + \Delta l_{cal} \right] \quad (8.35)$$

$$F_i = -\frac{K_{Wheel1}}{R_c} \frac{2F_i}{R_c K_{cab1}} - \frac{K_{Wheel1} F_i}{R_c^2 K_{cab2}} + K_{Wheel1} \left[\frac{1}{R_c} (u_1 + \Delta l_{cab}) - \Delta l_p - \Delta l_d + \Delta l_{cal} \right] \quad (8.36)$$

$$F_i \left[1 + \frac{2K_{Wheel1}}{R_c^2 K_{cab1}} + \frac{K_{Wheel1}}{R_c^2 K_{cab2}} \right] = K_{Wheel1} \left[\frac{1}{R_c} (u_1 + \Delta l_{cab}) - \Delta l_p - \Delta l_d + \Delta l_{cal} \right] \quad (8.37)$$

$$F_i = \frac{K_{Wheel1} \left[\frac{1}{R_c} (u_1 + \Delta l_{cab}) - \Delta l_p - \Delta l_d + \Delta l_{cal} \right]}{\left[1 + \frac{2K_{Wheel1}}{R_c^2 K_{cab1}} + \frac{K_{Wheel1}}{R_c^2 K_{cab2}} \right]} \quad (8.38)$$

8.2.5. Static coefficient of friction

The static coefficient of friction as a function of temperature is required in the model to predict the torque developed by the parking brake system as a function of time. A third order polynomial has been used to approximate the results as in the work described in Chapter 7. The coefficients of the third order used to approximate the static coefficient of friction as a function of temperature for Pads 1 to 4 and Pads 11 to 13 are given in Table 8.3 and the equations are plotted along with the corresponding dynamometer results in Figures 8.5 and 8.6.

Pad	$\mu = \alpha_3 T^3 + \alpha_2 T^2 + \alpha_1 T + \alpha_0$			
	α_3	α_2	α_1	α_0
1	-2×10^{-8}	3×10^{-6}	0.0007	0.398
2	-6×10^{-8}	3×10^{-5}	-0.0049	0.6417
3	-2×10^{-8}	-1×10^{-6}	0.0024	0.2201
4	-3×10^{-8}	3×10^{-6}	0.0015	0.3558
11	-2×10^{-8}	5×10^{-6}	8×10^{-5}	0.3846
12	-6×10^{-9}	-6×10^{-6}	0.0023	0.3871
13	2×10^{-8}	-2×10^{-5}	0.0041	0.3734

Table 8.3 Static coefficient of friction approximations as a function of temperature

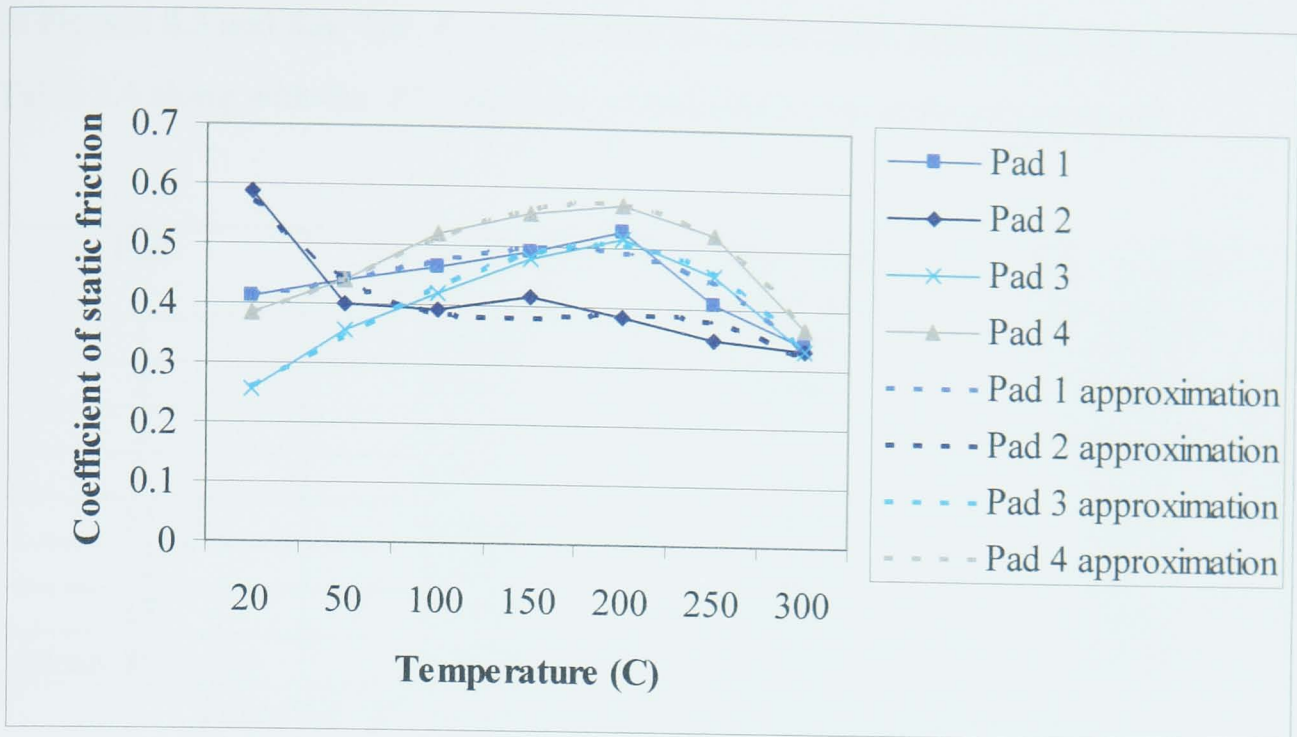


Figure 8.5 Coefficient of static friction as a function of temperature for Pads 1 to 4 as measured on the dynamometer and approximated by the mathematical model polynomial

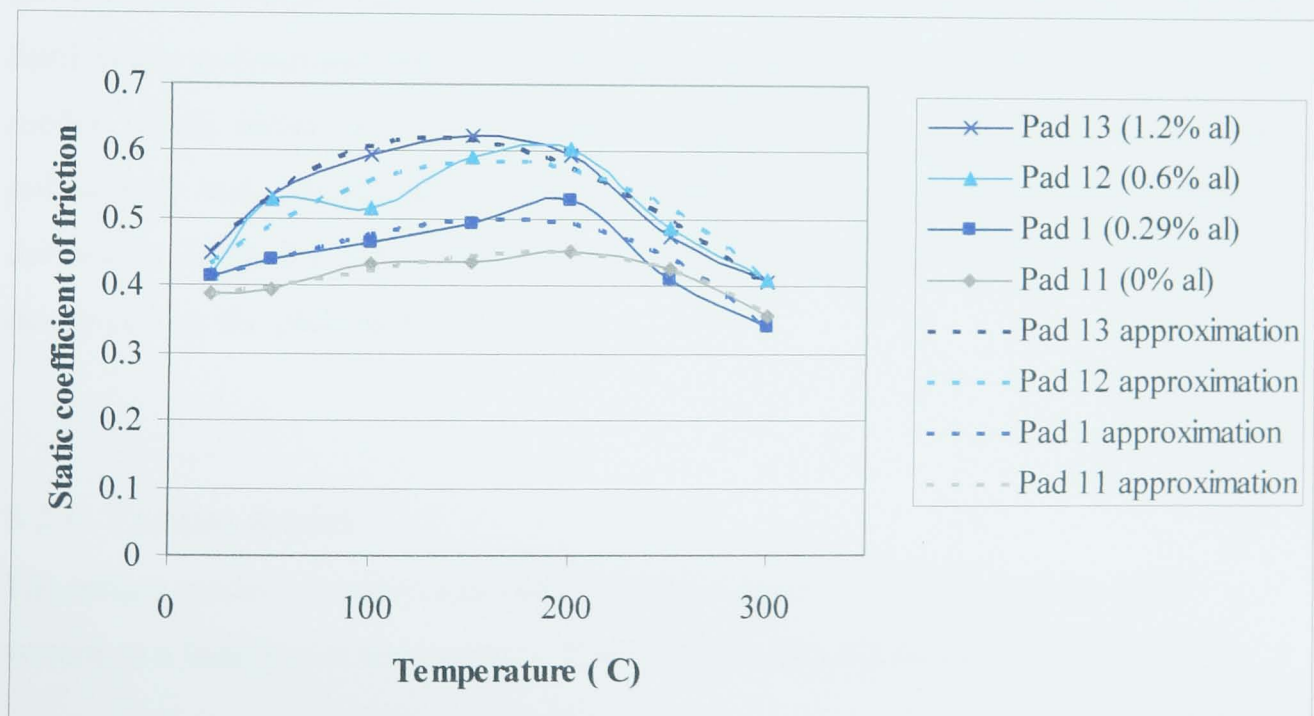


Figure 8.6 Coefficient of static friction as a function of temperature for Pads 1, 11, 12 and 13 as measured on the dynamometer and approximated by the mathematical model polynomial

The results in Figures 8.5 and 8.6 show that the third order polynomial is a good approximation for the coefficient of static friction as a function of temperature for the pads tested. An R^2 correlation coefficient has been derived for the results given

in Figures 8.5 and 8.6. The R^2 values from the third order polynomials are given in Table 8.4 along with the R^2 values for second and fourth order polynomials.

Pad	Second order polynomial	Third order polynomial	Fourth order polynomial
1	0.8128	0.8926	0.9122
2	0.7482	0.8999	0.9959
3	0.9453	0.9921	0.9936
4	0.9025	0.9964	0.997
11	0.8626	0.9612	0.9633
12	0.8532	0.8552	0.8559
13	0.9498	0.9706	0.9815
Mean R^2 value	0.8678	0.9383	0.9571

Table 8.4 R^2 values from the polynomial approximations

The result in Table 8.4 shows that the third order polynomial has a mean R^2 coefficient of 0.94. This was deemed suitable for the mathematical model. The second order polynomial has a mean R^2 coefficient of 0.87 which was deemed to be too low. The fourth order polynomial has a higher mean R^2 coefficient than the third order polynomial but this polynomial introduces more complexity into the model which means that it will take a longer time to solve. The third order polynomial was chosen as the most suitable approximation and the equations defined in Table 8.3 were used in the mathematical model to calculate the torque developed by the parking brake system.

8.2.6. Torque model

The torque model is used to calculate the torque produced by the parking brake system as a function of temperature. The torque is calculated using Equation 8.39.

$$T = \mu F_i r_{brake} \quad (8.39)$$

Where: T = Brake torque (Nm)

μ = static coefficient of friction

F_i = Clamp load at the frictional interface (N)

r_{brake} = mean rubbing radius of the brake (m)

The normal clamp load at the frictional interface and the associated coefficient of friction are calculated from the previous sub systems within the model.

8.2.7. Rollaway model output

The rollaway model output is displayed in graphical form. The output displays the torque required to hold the vehicle on the gradient and the torque produced by the parking brake system as a function of time. The results show if the simulation predicts that the vehicle will rollaway or remain stationary on the gradient.

8.3. Simulation and Results

8.3.1. Cooling results

The model was used to predict the temperature of the brake components as a function of time. In this particular example, the pad and half disc were allowed to cool from an initial temperature of 250°C to 30°C. The calliper was assumed to cool from an initial temperature of 50°C and Cable 1 cooled from an initial temperature of 80°C. The calliper and Cable 1 temperatures were selected as they are typical temperatures that can be expected. The results obtained from the model are plotted in Figure 8.7 along with measurements of the disc temperature obtained from the dynamometer tests.

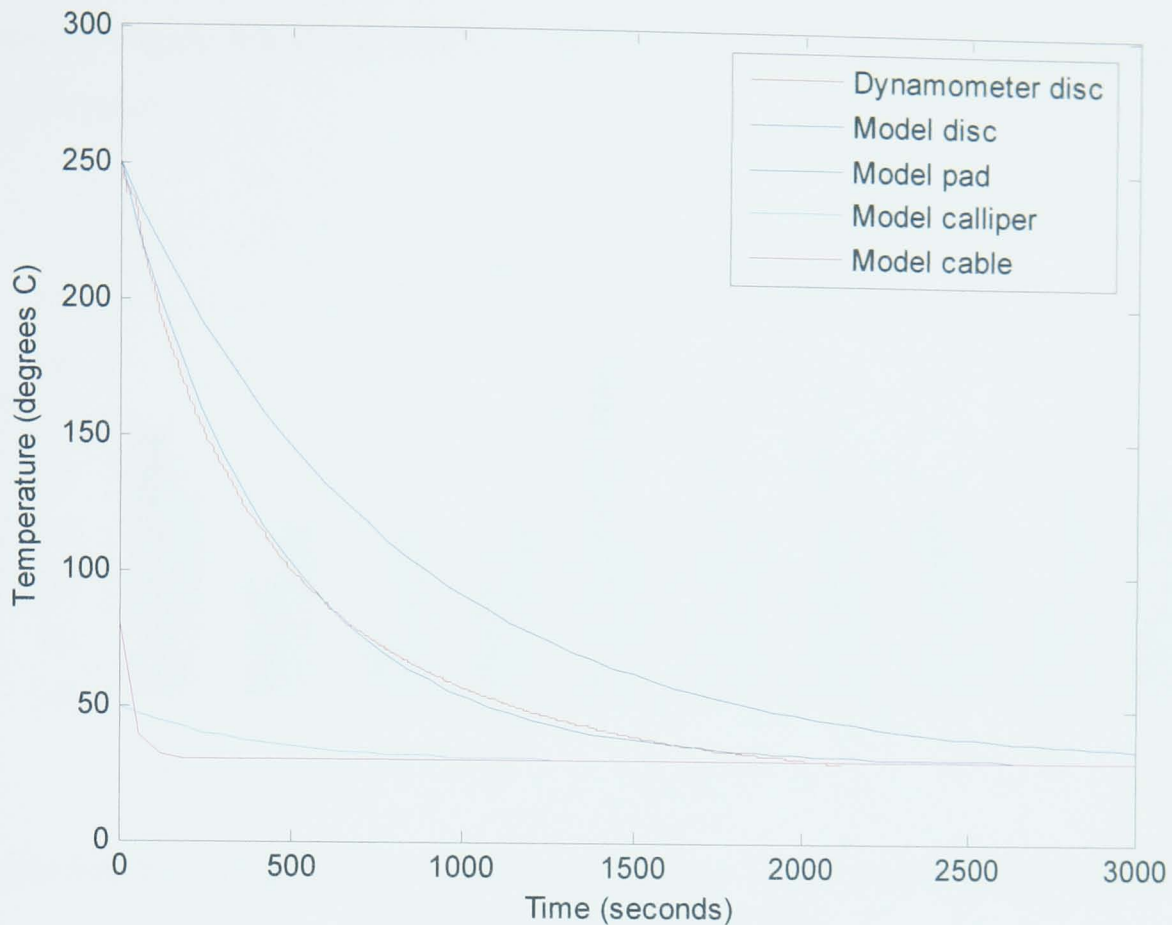


Figure 8.7 Temperature of the brake components as predicted by the mathematical model and the disc temperature measured on the dynamometer

The result in Figure 8.7 shows that the model is capable of simulating the temperature of the disc as a function of time. The model also predicts how the temperatures of the other brake components vary as a function of time. The pad cools more slowly than the disc as it has a smaller surface area. Conversely the cable cools more quickly than the disc and other components due to its relatively large surface area and low volume.

8.3.2. Dynamometer clamp load

The model was used to investigate clamp load variation at the frictional interface as a function of time while the brake pad and disc cooled from 250°C to 30°C. The initial temperature of the calliper was set at 50°C and Cable 1 was at an ambient temperature of 30°C throughout the simulation.

The percentage of lost clamp load predicted by the model with Pads 1 to 10 installed with the pad and half disc cooling from an initial temperature of 250°C, the calliper

at an initial temperature of 50°C and Cable 1 at ambient temperature of 30°C is plotted in Figure 8.8 along with the percentage of lost cable load measured on the dynamometer.

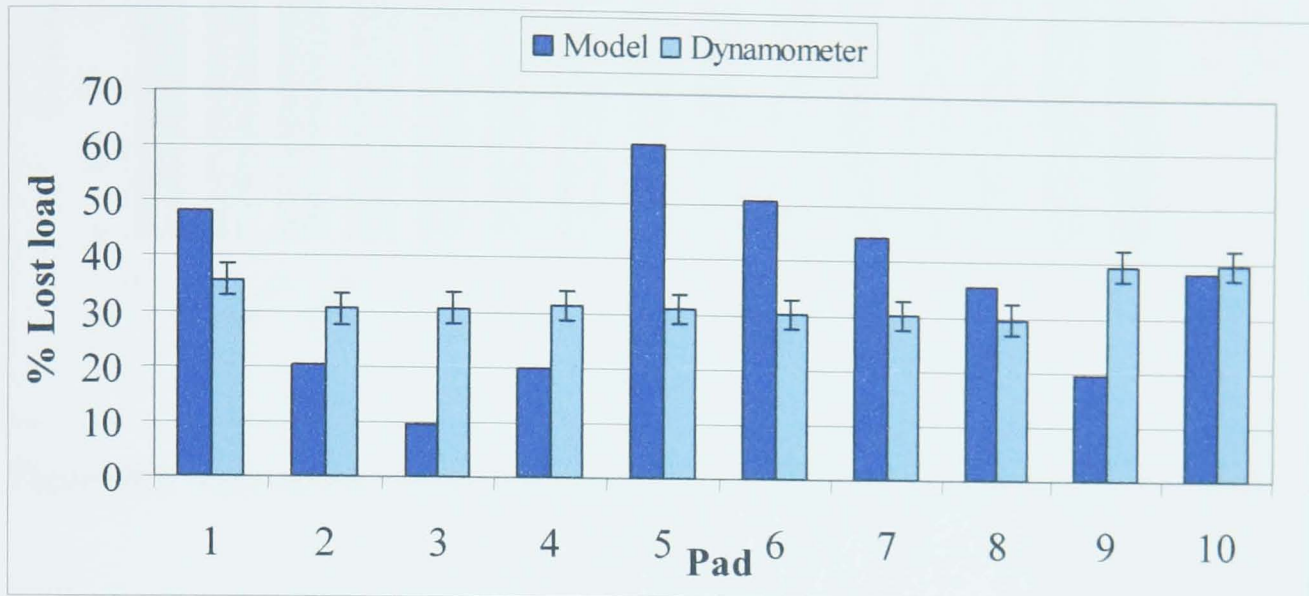


Figure 8.8 Percentage of lost clamp load predicted by the model and lost cable load measured on the dynamometer

The result in Figure 8.8 shows that the model predicts that the parking brake will lose varying amounts of clamp load with the different pads installed. The results predicted by the model have large variations compared to the results measured on the dynamometer. This could be due to inaccurate parameters used within the model. The model parameters measured in Chapter 6 had variations in the results which can accumulate together within the model. This can produce the discrepancies shown in Figure 8.8.

A sensitivity study was conducted on the model parameters for Pad 1 cooling from 250°C to 30°C to see the effect of the different parameters on the results. The result of varying each of the model parameters by $\pm 10\%$ is given in Figure 8.9.

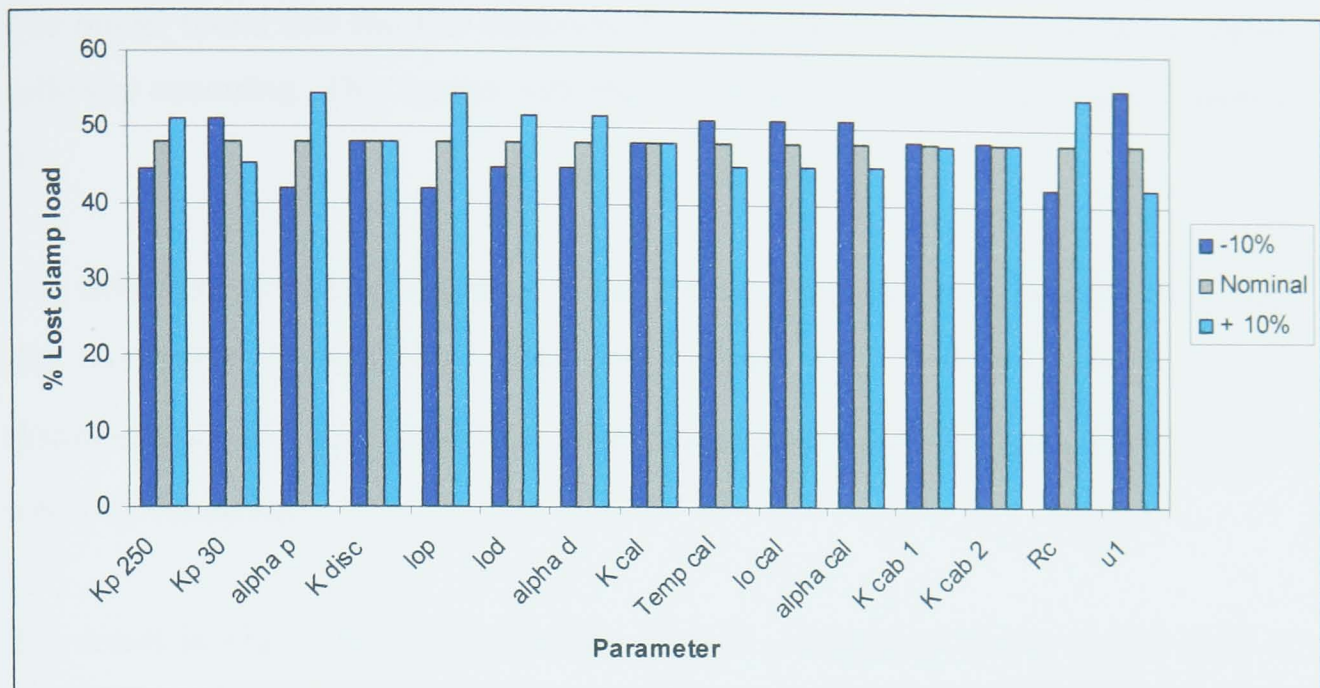


Figure 8.9 Varying the system parameters by $\pm 10\%$ for Pad 1 cooling from 250°C to 30°C

The result in Figure 8.9 shows the sensitivity of the lost clamp load to changes in the model parameters. The result presents ways of minimising the percentage of lost clamp load through a series of changes to the system. The result shows that the model predicts that the pad stiffness parameters at different temperatures have a significant effect on the percentage of lost load. The pad stiffness can be varied by changing the constituent ingredients in the friction material. This suggests that a friction material chemist can design a pad with stiffness values that will reduce the likelihood of rollaway occurring.

The result in Figure 8.9 shows that the thermal expansion coefficient of the pad and disc has a significant affect on the likelihood of rollaway occurring. Varying the stiffness parameter of the disc and calliper by $\pm 10\%$ was found to have no effect on the likelihood of rollaway occurring.

The sensitivity study also found that the pad thickness has a significant affect on the percentage of lost clamp load. This does not agree with the experimental evaluations described in Chapter 6. This may be because the model assumes that the pad has a uniform temperature whereas the pad on the dynamometer may have an uneven temperature distribution.

The model found that the disc thickness has a significant affect on the likelihood of rollaway occurring. This agrees with the experimental results described in Chapter 6.

The stiffness parameters of Cables 1 and 2 were found to have a minimal affect on the likelihood of rollaway. The calliper ratio, R_c , and the initial applied displacement, u_1 , were found to have a significant affect on the likelihood of rollaway occurring.

The result in Figure 8.9 shows that the thermal contractions of the calliper have a significant affect on the percentage of lost clamp load. The thermal contractions of the calliper are directly related to the initial calliper temperature. The calliper was found to achieve temperatures up to 90°C during the calliper stiffness evaluations described in Chapter 6. The temperature of the calliper was not measured during the dynamometer clamp load evaluations. It is expected that the calliper temperature would vary for each of the pads tested due to the thermal conductivity of the friction material transferring the heat from the frictional interface to the calliper. The initial calliper temperature used in the analysis was varied to correlate the model results to the results measured on the dynamometer. The optimised calliper temperatures that were selected are given in Table 8.5. The model results using the optimised calliper temperatures are shown in Figure 8.10 along with the percentage of lost clamp load measured on the dynamometer.

Pad	Calliper temperature (°C)
1	58
2	43
3	36
4	42
5	70
6	64
7	60
8	54
9	36
10	49

Table 8.5 Optimal temperature of the calliper when used with Pads 1 to 10

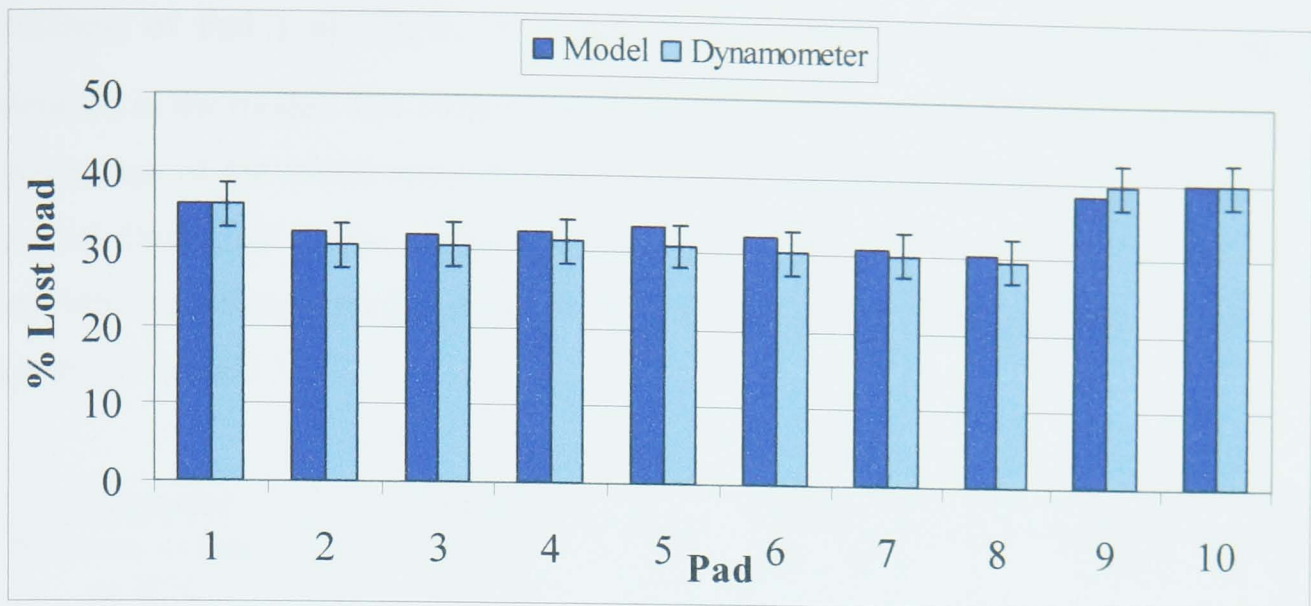


Figure 8.10 Percentage of clamp load that is lost as the brake cools from 250°C to 30°C for Pads 1 to 10 as predicted by the model and measured on the dynamometer

The result in Figure 8.10 shows that the optimised model results agree well with those that have been measured on the dynamometer. The initial calliper temperatures used, shown in Table 8.5, are within the expected temperature range of the calliper. The results suggest that the calliper temperature has a significant effect on the change in clamp load at the frictional interface. The model predicts that by increasing the initial calliper temperature and therefore the thermal contraction of the calliper bridge, the amount of clamp load that is lost as the brake cools can be reduced. The calliper cools more slowly than the pad and disc because it has a relatively small surface area compared to its mass. Therefore the clamp load will be lost at a faster rate due to the thermal contractions of the pad and disc than the rate of gain in clamp load resulting from the calliper contraction. This implies that rollaway is still liable to occur on the vehicle. It is critical that the calliper temperature remains relatively low because if the calliper becomes too hot the brake fluid inside the calliper could boil leading to a system failure and so a trade off exists.

The sensitivity study showed that the properties of the friction material can affect the percentage of the initial clamp load that is lost as the brake cools. The properties of Pad 1 were modified within the model to investigate how the modified pads would perform. The stiffness of Pad 1 as a function of temperature was modified by changing the stiffness of the pad at temperatures of 250°C and 30°C. The measured

stiffness of Pad 1 at 250°C, $K_{p1}250C$, and at 30°C, $K_{p1}30C$, was halved and doubled in the model. The values of the parameters used are given in Table 8.6. The percentage of the initial applied clamp load that was lost as the pad and half disc cooled from 250°C, the calliper cooled from 58°C and the cable remained at ambient temperature predicted by the model using the modified stiffness values is given in Figure 8.11.

Parameter	Symbol	Value	Units
Stiffness of Pad 1 at 30°C	$K_{p1}30$	1.32×10^8	Nm^{-1}
Half of the stiffness of Pad 1 at 30°C	$\frac{1}{2} K_{p1}30$	6.6×10^7	Nm^{-1}
Double the stiffness of Pad 1 at 30°C	$2 K_{p1}30$	2.64×10^8	Nm^{-1}
Stiffness of Pad 1 at 250°C	$K_{p1}250$	1.01×10^8	Nm^{-1}
Half of the stiffness of Pad 1 at 250°C	$\frac{1}{2} K_{p1}250$	5.05×10^7	Nm^{-1}
Double the stiffness of Pad 1 at 250°C	$2 K_{p1}250$	2.02×10^8	Nm^{-1}

Table 8.6 Modified stiffness values of Pad 1 at 30°C and 250°C

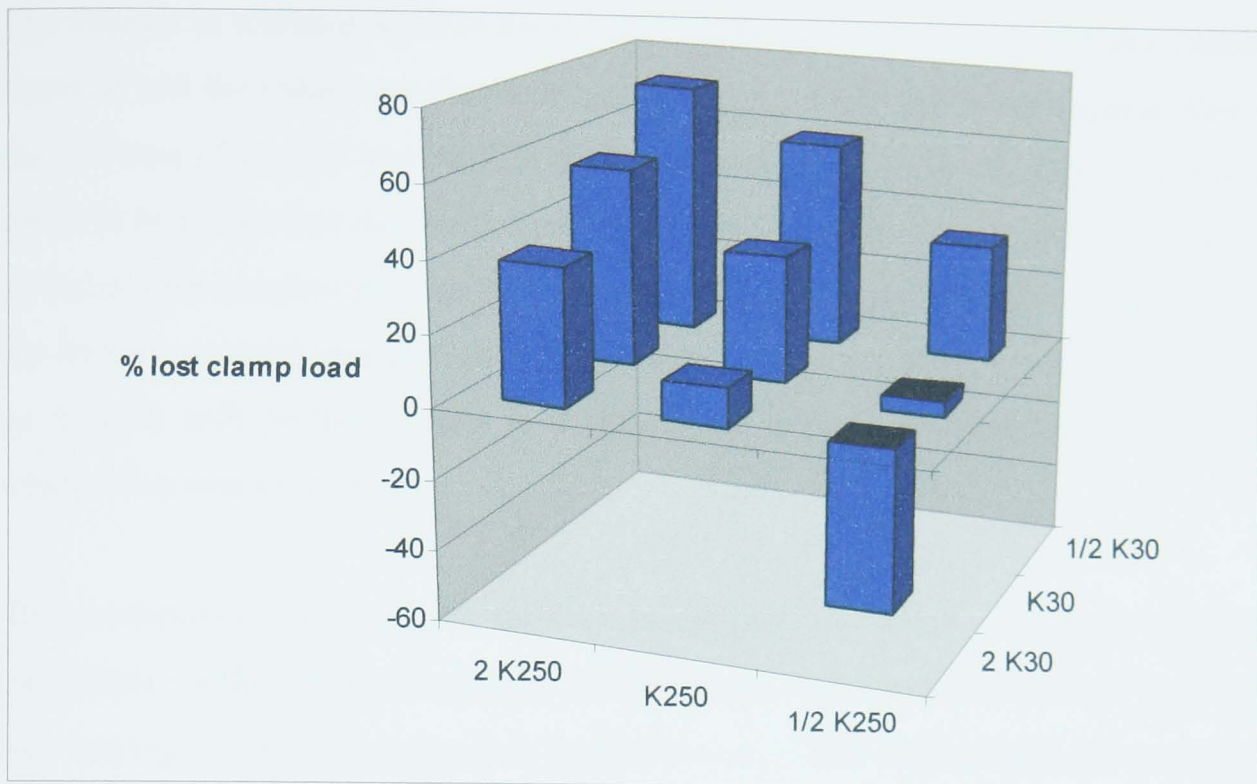


Figure 8.11 Percentage of lost clamp load produced by changing the stiffness of pad 1 at 250°C and 30°C.

The result in Figure 8.11 shows how the stiffness of the pad as a function of temperature affects the percentage of lost clamp load. The results show that if the stiffness of the pad at 250°C and 30°C is doubled then the model predicts that the percentage of lost clamp load increases. If the stiffness values at 250°C and 30°C are halved the model predicts that the percentage of lost clamp load is reduced. This suggests that lower stiffness values for the pad will reduce the amount of lost clamp load at the frictional interface.

The model predicts that the variation of stiffness as a function of temperature has a significant effect on the percentage of lost clamp load. A large variation with temperature as produced by doubling the stiffness at 250°C and halving the stiffness at 30°C, produces a larger decrease in the clamp load. A small variation with temperature, produced by halving the stiffness at 250°C and doubling the stiffness at 30°C, reduces the percentage of clamp load that is lost. The model predicts that the clamp load will increase as the brake cools when the stiffness value of $\frac{1}{2} K_{p1} 250C$ is used with stiffness values of $K_{p1} 30C$ and $2 K_{p1} 30C$.

The change in stiffness used in the model is difficult to achieve for a brake friction material and the values are therefore unrealistic. However the result suggests that if the stiffness of the pad increases as the brake cools the amount of clamp load that is lost will be reduced or the clamp load will actually increase. The variation of the pad stiffness with temperature can be changed by varying the constituent ingredients in the friction material formulation. A pad designed to have a large increase in stiffness as it cools will perform better in a rollaway test than an equivalent pad with a smaller increase in stiffness.

The mathematical model was used to investigate the effect of the pad thermal expansion coefficient on the change in clamp load. Pad 1 was modified by doubling and halving the thermal expansion coefficient, α_{p1} . The model was used to predict the percentage of the initial applied clamp load that was lost as the pad and half disc cooled from 250°C, the calliper cooled from 58°C and Cable 1 remained at an ambient temperature. The values used in the simulations are given in Table 8.7 and the results are plotted in Figure 8.12.

Parameter	Symbol	Value	Units
Thermal expansion coefficient of Pad 1	α_{p1}	18.3×10^{-6}	$^{\circ}C^{-1}$
Half of the thermal expansion coefficient of Pad 1	$\frac{1}{2}\alpha_{p1}$	9.15×10^{-6}	$^{\circ}C^{-1}$
Double the thermal expansion coefficient of Pad 1	$2\alpha_{p1}$	36.6×10^{-6}	$^{\circ}C^{-1}$

Table 8.7 Different values of the thermal expansion coefficient of Pad 1 used in the simulation

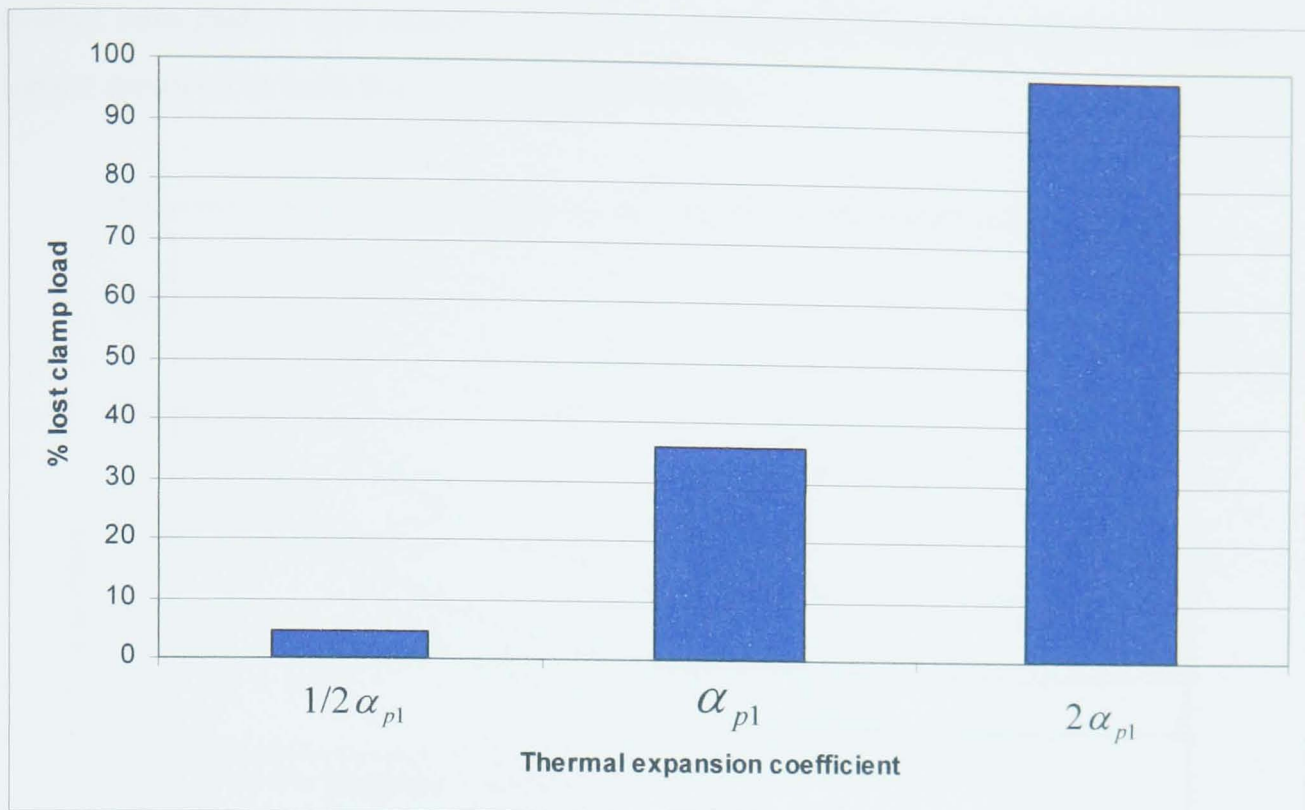


Figure 8.12 Percentage of lost clamp load as the brake cools with Pad 1 installed with modified thermal expansion coefficients.

The result in Figure 8.12 shows that the thermal expansion coefficient of the pad has a significant effect on the percentage of clamp load that is lost as the brake cools. The model predicts that a pad with a lower thermal expansion coefficient will lose less clamp load than an equivalent pad with a higher thermal expansion coefficient. The model confirms that the thermal expansion coefficient of the pads is an important parameter of the parking brake system for reducing the likelihood of rollaway occurring.

8.3.3. Rollaway output model

The rollaway model was used to predict the torque produced by the parking brake system as a function of time with Pads 1 to 4 installed. The disc and pads cooled from an initial temperature of 250°C, the calliper cooled from the corresponding initial temperature for each pad given in Table 8.4 and the cable remained at ambient temperature of 30°C. The model was used to simulate the Jaguar S-Type parked on a 16.6% gradient and the initial displacement produced at the parking brake lever was the same for each test. The torque produced by the parking brake

system with Pads 1 to 4 installed is plotted in Figure 8.13 together with the constant torque required to hold the vehicle on the gradient.

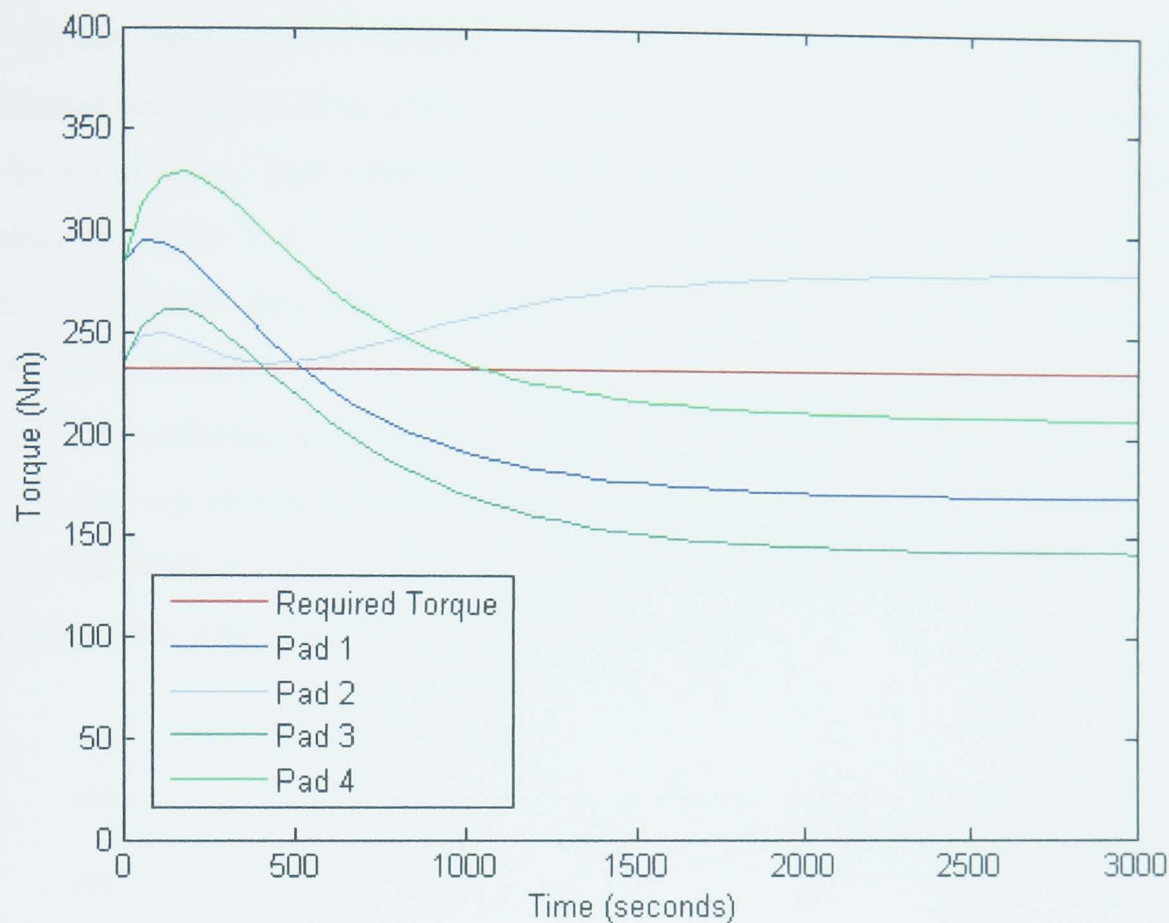


Figure 8.13 Torque produced by the parking brake system with pads 1 to 4 installed

The result in Figure 8.13 shows how the torque produced by the parking brake system varies with Pads 1 to 4 installed. The initial torque values are different for each pad because the model is run with the same initial displacement which will develop varying clamp loads dependant on the pad stiffness and the initial coefficient of friction will also vary for each pad. The model predicts that the torque produced by Pads 1, 3 and 4 will drop below that required to hold the vehicle on the gradient resulting in rollaway. The time at which rollaway is predicted to occur is different for each pad. The model predicts that the torque produced by Pad 2 does not drop below that required to hold the vehicle on the gradient and the vehicle will not rollaway. However the torque produced drops to a value close to that required to hold the vehicle on the gradient which could result in the stick/slip behaviour that was observed during the on-vehicle tests discussed in Chapter 4. The clamp load produced by Pad 2 decreases over time as can be seen in Figure 8.9 but the torque value generally increases due to the increase in static friction with reducing

temperature. This suggests that the coefficient of static friction between the pad and disc can have a significant effect on the likelihood of rollaway occurring.

The static coefficient of friction of Pad 1 was modified by producing three additional pads (Pads 11 to 13) with levels of fused alumina of 0%, 0.6% and 1.2% in the formulation. Pad 1 has 0.3% fused alumina in the formulation. The torque produced by Pads 1, 11, 12 and 13 was modelled using the static friction variation with temperature described in Table 8.7 with the clamp load variation with temperature of Pad 1. The clamp load variation with temperature of Pad 1 was used for all of the rollaway evaluations because the constituent ingredients of Pads 11, 12 and 13 are very similar to those of Pad 1 and the changes made are believed to only affect the friction level resulting in similar thermal expansion and stiffness characteristics. The results are plotted in Figure 8.14.

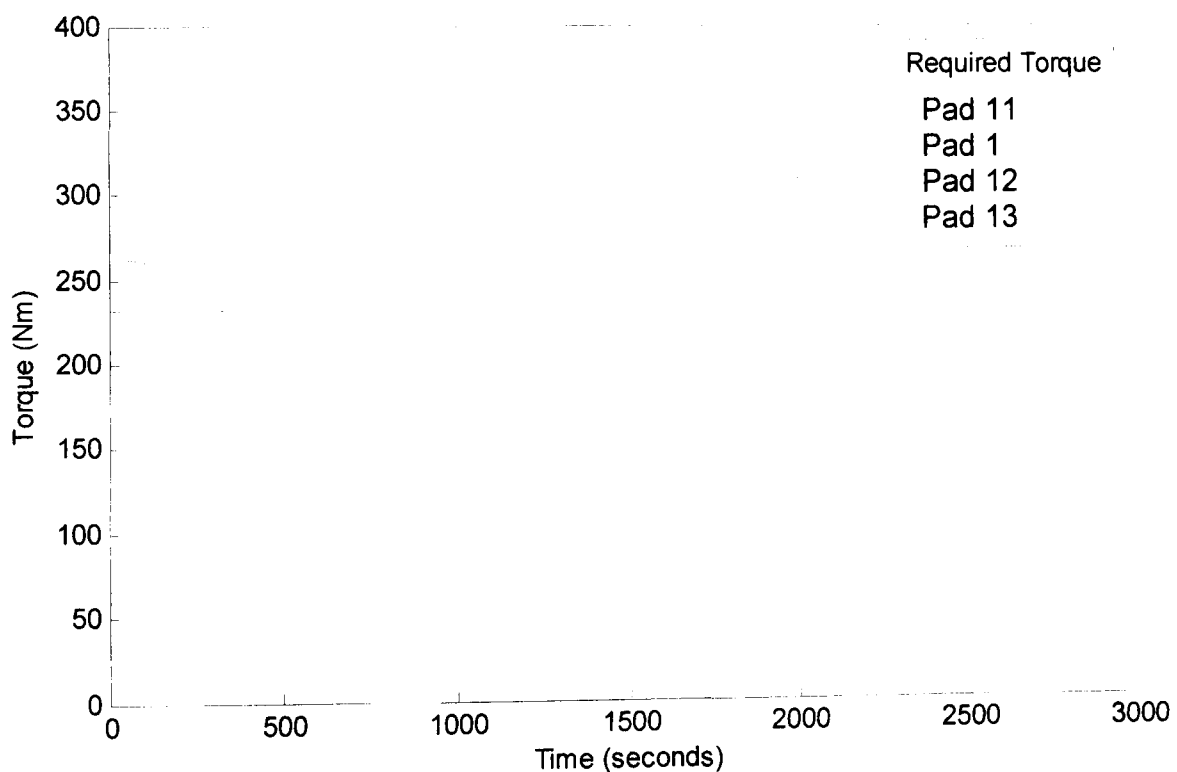


Figure 8.14 Torque produced by Pad 1 with varying levels of fused alumina

The result in Figure 8.14 shows the torque produced by the parking brake system with Pads 1, 11, 12 and 13 installed as a function of time. The initial torque produced by each pad is different because the coefficient of friction produced by each pad is different. The initial cable displacement and clamp load is the same for each of the pads. The model predicts that Pad 11 will produce the lowest initial

torque because it has the lowest coefficient of friction at the initial temperature of 250°C.

The model suggests that the formulations with varying levels of fused alumina affect the torque produced by the parking brake system. Pad 11 with 0% fused alumina lost the least amount of torque as the brake cooled. This is because the pad had the most consistent level of static friction with temperature. Pad 13 with 1.2% fused alumina produced the highest torque at ambient temperature because it has the highest friction level at this temperature. The torque produced by all of the pads dropped below the level required to keep the vehicle stationary on the gradient. The amount of torque that was lost varied for each of the pads suggesting that the formulations can be modified to reduce the likelihood of rollaway occurring.

8.3.4. Cable temperature variation

The model was used to investigate the effect of cable temperature on the clamp load produced at the frictional interface. The location of Cable 1 on the vehicle enables it to potentially be heated by the vehicle exhaust system. If the cable is at an elevated temperature when the vehicle is parked then as the cable cools the thermal contractions will increase the load in Cable 1 which in turn will increase the clamp load at the frictional interface. The predicted clamp load at the frictional interface has been calculated using the model with Pad 1 and the half disc cooling from 250°C, the calliper cooling from 58°C and half of a metre of Cable 1 cooling to ambient from temperatures ranging from 30°C to 90°C. The predicted torque from the results as a function of time is plotted in Figure 8.15.

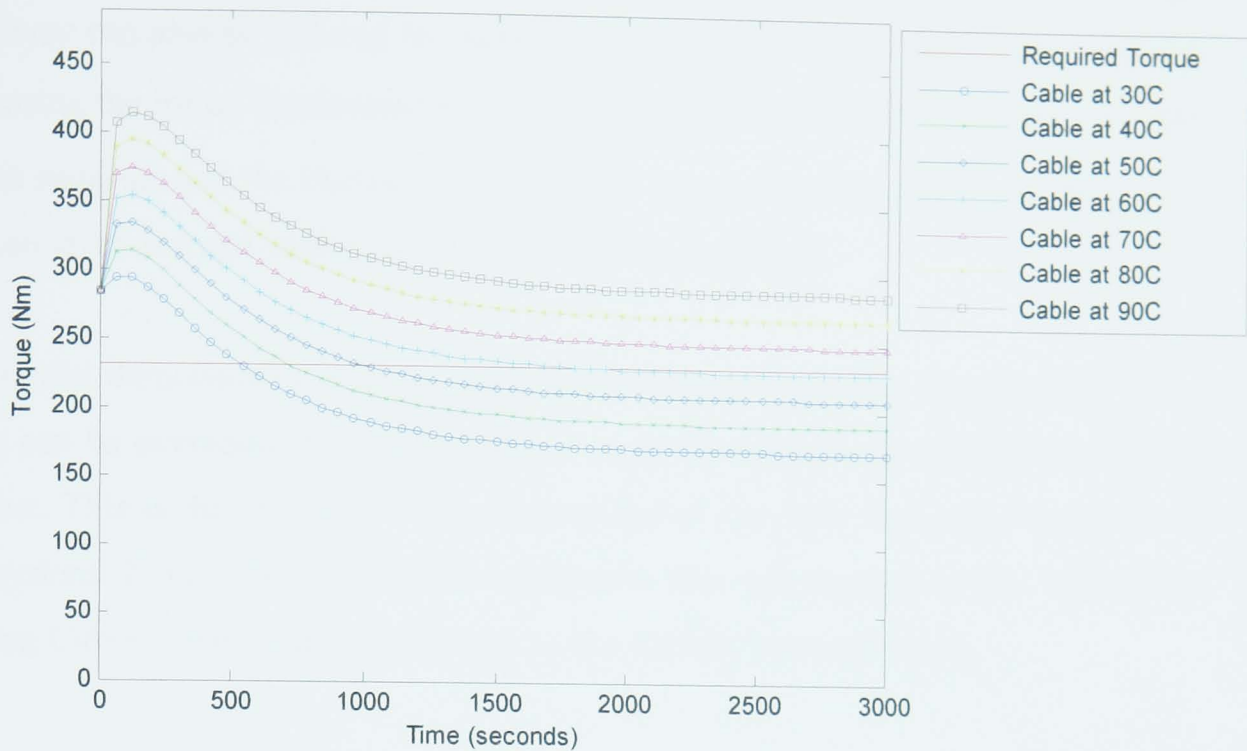


Figure 8.15 Clamp load produced by Pad 1 with cable at varying initial temperatures

The result in Figure 8.15 shows how the initial cable temperature affects the clamp load as a function of time. The cable temperature cools to ambient quicker than the other brake components as shown in Figure 8.5. Therefore the increased load developed by the cable contraction occurs within the first 200 seconds of the test. After this period the torque decreases due to the thermal contractions and stiffness variations of the other brake components and the friction variation. The results show that the amount of the initially developed torque that is lost can be reduced or the initial torque can be increased as the brake cools by varying the initial temperature of Cable 1. For the simulation shown in Figure 8.15 the vehicle will not rollaway if Cable 1 is at an initial temperature of 70°C or higher.

8.4. Summary

A mathematical model has been developed that successfully captures the behaviour of the parking brake system during a rollaway test. The model has been validated against results obtained from the rollaway dynamometer. A study was conducted to investigate the sensitivity of the percentage of lost clamp load to changes in the model parameters. The sensitivity study showed that the likelihood of rollaway

occurring can be reduced by reducing the thermal contractions of the pad and disc. Rollaway can also be reduced by increasing the thermal contractions of the calliper, increasing the initial displacement, u_1 , and reducing the calliper lever ratio, R_c . The model suggests that the likelihood of rollaway can also be reduced by modifying the friction level and pad stiffness as a function of temperature.

The model demonstrates that the reduction in brake torque that occurs as the brake cools can be overcome by setting Cable 1 at an elevated temperature at the start of the test. This is due to the thermal contractions of the cable increasing the loads in the system. It may be possible to implement this mechanism on the vehicle by heating Cable 1 using heating elements or the vehicle exhaust system.

Chapter 9

Discussion

This chapter discusses the results and theories generated in this research.

A comprehensive literature survey has uncovered no published research in the area of vehicle rollaway other than that published by the author of this research. The lack of published research suggests the need for this study and was one of the motivations for this research project.

The on-vehicle tests, described in Chapter 4, have proven the existence of a rollaway problem on vehicles with an integrated rear calliper. The tests showed that the vehicle generally exhibits a period of stick/slip prior to the onset of rollaway. A low frequency groan noise is associated with the slip movement. The tests showed that the Jaguar S-Type rolled away with four different pads installed. This suggests that rollaway cannot be prevented by changing the properties of the pad friction material within the range of the pads tested in this research. The likelihood of rollaway is dependent on the other brake system components and therefore rollaway should be investigated as a system problem. Rollaway occurred on all of the gradients tested and at all of the temperatures tested.

The on-vehicle tests showed that rollaway generally occurred after a period of stick/slip which is due to changing frictional conditioning at the interface. As the brake cools the pads and discs contract back to their ambient dimensions. These contractions produce a reduction in the normal force at the frictional interface, which results in a drop in the level of brake torque. If the brake torque approaches the limit of that required to hold the vehicle on the gradient, the stick/slip movement begins to occur and a groan noise is associated with this movement. This stick/slip movement and noise indicate an instability at the frictional interface. The instability generates vibrations at the frictional interface which are then amplified by the brake system into the audible noise that was recorded during the tests. A possible mechanism that facilitates this problem is postulated below:

When the pad is initially in contact with the disc, there is a large real contact area with the frictional load being shared by the particles in the brake pad and the binding matrix of the pad as shown in Figure 9.1. As the pad cools, the thermal contractions of the matrix are higher than that of the large particles as shown in Figure 9.2.

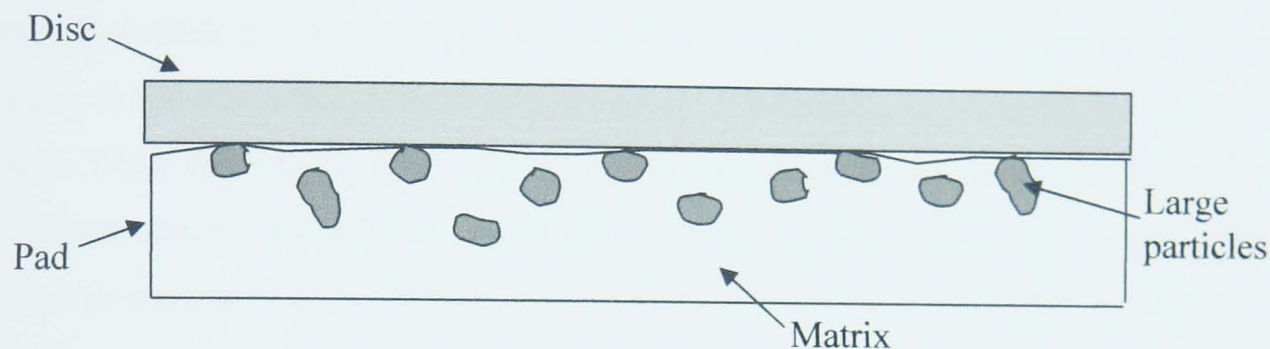


Figure 9.1 Frictional interface during stick slip event before cooling

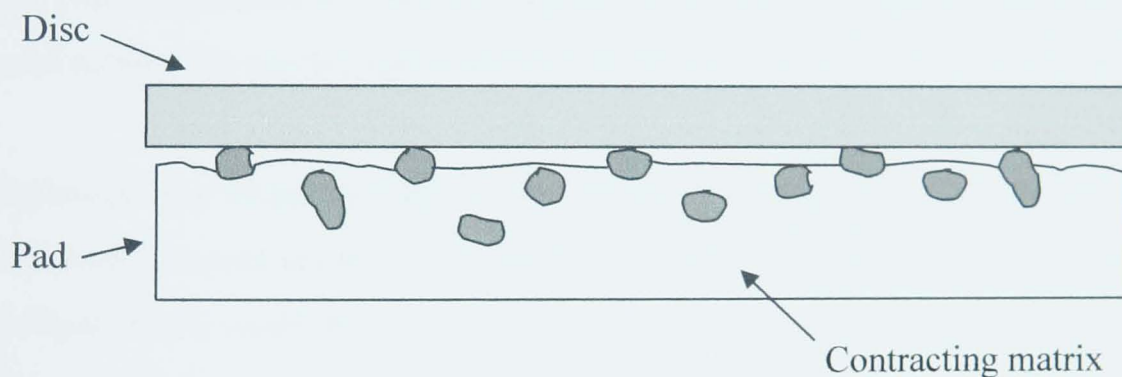


Figure 9.2 Frictional interface during stick slip event after cooling

This could be due to the matrix conducting the heat faster than the large particles or having a higher coefficient of thermal expansion. This results in the large particles protruding from the surface as the matrix contracts around them. The matrix will no longer be in contact with the disc surface and therefore the real contact area has been reduced and the load is being carried by the large particles. When the real contact area has reduced by a sufficient amount the frictional force will no longer be large enough to prevent the disc from rotating. The disc will begin to rotate, and this rotation will tear or realign the large, protruding particles out of the matrix. This in turn would increase the real contact area at the interface as the matrix comes into

contact with the disc. This continues until the frictional force is large enough to prevent the disc from rotating, and stick would result. The large particles that were removed would then fall away from the interface as wear particles or would get pressed back into the matrix at the surface. This process would continue as the brakes cooled down.

The on-vehicle test result ‘type 4’ shown in Figure 4.14 shows that the vehicle began to roll down the gradient after a period of stick/slip and then stop without any input from the driver. The vehicle subsequently continued to move down the gradient with a stick slip motion before rollaway occurred. The vehicle may have come to rest due to the variations in the disc thickness. If the disc began to rotate at a location with a low disc thickness then as the disc rotated the thickness may have increased. The increased thickness will increase the normal load at the brake interface due to Hooke’s law, described in Equation 8.5. The increase in normal load may have been sufficient to prevent the vehicle from rolling down the gradient. As the brake continued to cool and the disc continued to contract due to the thermal contractions the normal load continued to decrease until rollaway occurred.

Rollaway was found to occur on the Jaguar X-Type with both the aluminium and cast iron callipers installed. Rollaway was less likely to occur with the aluminium calliper which could be due to the thermal contractions of the calliper bridge. The thermal contractions of the calliper bridge will reduce the distance between the pad back plate and the disc. This will offset some of the thermal contractions of the pad and disc reducing the amount of lost clamp load. The aluminium calliper may also be at a higher initial temperature at the start of the test due to aluminium having a higher thermal conductivity than cast iron. The results from the Matlab model demonstrate that this would reduce the amount of lost clamp load at the frictional interface as the brake cooled.

A novel dynamometer test facility has been developed at the University of Leeds that is capable of testing vehicle park brake systems. The dynamometer was developed from an existing rig and has been modified into a fully functional testing facility. The dynamometer and software is adaptable and can be modified to conduct different brake system tests. This is because the software was written using Labview

and is easy to modify. The hardware on the rig can also be easily upgraded due to the modular nature of the National Instruments equipment. The dynamometer is capable of testing different brake systems. This can be achieved by installing different uprights on the rig and changing the coupling from the vehicle drive shaft and the dynamometer drive. The dynamometer was designed this way to ensure that it can be used for future research projects. The dynamometer has demonstrated that it is capable of:

- Heating the brakes to a specified temperature.
- Measuring the static coefficient of friction as a function of temperature.
- Measuring the change in cable load as a function of temperature.

The dynamometer showed that the normal clamp load at the brake frictional interface decreased as the brake cooled with all of the pads used in this research installed. All of the pads tested on the dynamometer lost over 29% of the initial applied cable load. This suggests that rollaway cannot be overcome by changing the properties of the pads within the range of pads tested for this research. The dynamometer cable load results did show that the pad can have an effect on the percentage of lost cable load as the brake cools. This suggests that the pad does influence the likelihood of rollaway occurring and that other brake system components have a significant affect on the likelihood of rollaway. It is therefore possible to produce a pad that will reduce the likelihood of rollaway.

All of the tests conducted for this research showed that the percentage of lost cable load is directly related to the initial test temperature. This result shows that the likelihood of rollaway occurring can be reduced if the initial brake temperature can be reduced. This can be achieved if the rear brake had an improved cooling mechanism. The brake temperature could also be reduced if the rear service brake was required to conduct less work. This could be achieved if the front brake conducted a larger proportion of the braking effort.

The increased temperature of the rear brake can lead to disc coning. The design of the Jaguar S-Type rear disc, shown in Figure 4.5, indicates that it may be prone to disc coning. If the disc was exhibiting significant coning it would affect the contact

pressure distribution at the frictional interface, which may explain the wear characteristics shown in Figure 6.30 and Figure 6.31. The varying contact pressure distribution as the disc cools may affect the friction level generated by the brake, which could lead to rollaway. No measurements of the disc deflection were taken for this research and it is therefore not possible to quantify the effect that disc coning has on rollaway.

The amount of excess applied force going from the just hold condition to the park condition had an affect on the likelihood of rollaway occurring. The higher the amount of excess force, the more stored energy would be in the parking brake system and the vehicle would be less likely to roll away. The amount of applied excess load would be increased if the driver of the vehicle applied the parking brake more than one extra notch when parking the vehicle. This could be achieved by educating the driver through instructions in the vehicle hand book.

The number of notches on the park brake ratchet mechanism could be reduced to reduce the likelihood that the ‘just hold’ condition is close to the ‘park’ condition. This would result in an increased probability that the amount of excess load would be higher reducing the likelihood of rollaway. This could however result in driver dissatisfaction due to poor lever feel.

The amount of excess applied load could also be increased by replacing the manual parking brake lever with an electronic park brake (EPB). The EPB can be set to apply sufficient excess load to reduce the likelihood of rollaway. The EPB is also capable of monitoring the rear brake temperature and the gradient on which the vehicle is parked. This information coupled with the results from this thesis can be used to program the EPB controller to ensure that the likelihood of rollaway is minimised.

The dynamometer tests and Matlab model results showed that rollaway can be reduced by reducing the disc thickness. This is because the thermal contractions of the disc are reduced. Reducing the disc thickness will however increase the disc temperature due to the reduced thermal mass. The thermal contractions of the disc can be reduced by reducing the thermal expansion coefficient of the disc material.

Alternative disc materials such as Carbon Ceramic (CSiC) brake discs might be able to achieve this.

The dynamometer tests showed that the thickness of the pad was found to have no correlation with the percentage of lost cable load. The Matlab model results suggest that the thickness of the pad does affect the percentage of lost clamp load. The model assumes that the pad has a uniform temperature whereas the pad on the dynamometer was unlikely to have a uniform temperature. The surface temperature of the pad is likely to have a higher temperature than the back plate. The result suggests that the thermal contractions of the pad can influence the likelihood of rollaway but to a lesser extent than that predicted by the mathematical model.

The dynamometer static friction results have shown that the coefficient of static friction varies with temperature for the pads tested. For Pads 1, 3 and 4 the friction level generally increases with temperature from 20C to 200C. This means that if the brake was cooling from 200C the friction level would decrease reducing the torque developed by the parking brake. This would increase the likelihood of rollaway occurring.

The tests discussed in Section 6.9.2 showed that it is possible to vary the static friction level of the pad as a function of temperature. This was achieved by modifying the amount of fused alumina in the friction material formulation. The results suggest that it is possible for the friction material chemist to design a pad that has a friction level that remains constant with temperature or increases as the temperature of the pad reduces. This will reduce the likelihood of rollaway occurring.

The measured thermal expansion results for the pad had a greater variation than the disc. This could be due to the composite nature of the friction material. The volume of each constituent material could vary between the samples tested, which could vary the measured results. A way to reduce the variations would be to use larger samples or to ensure that the constituent ingredients were dispersed evenly in the friction material. Friction material manufacturers are constantly improving their mixing techniques to ensure that the constituents are dispersed more evenly within

the friction material. This will reduce the variations between pads from the same formulation and will produce more consistent performance.

The finite element simulation, discussed in Chapter 7, was used to model the performance of a park brake system as the brake cooled from an elevated temperature. The model assumed a simplified geometry to reduce complexity and computational time. The model demonstrated how the contact pressure at the frictional interface varied as the brake cooled. The results predicted by the model have a good correlation to those measured on the dynamometer. The model predicts that the percentage of clamp load that is lost can be reduced by reducing the thermal expansion of the pad. The model predicts that pads with a greater variation between the Young's modulus at 30C and 250C will perform better than pads with a more constant Young's modulus with varying temperature. This suggests that friction material chemists can design a pad that has a large increase in Young's modulus as the brake cools to reduce the likelihood of rollaway.

The material property tests described in Chapter 6 showed that large variations are present in the measured material properties of the brake components. The accumulation of these variations is present in the mathematical model results discussed in Chapters 7 and 8. Therefore the models are not capable of giving precise predictions of rollaway. The models are however a good tool for predicting the trend of the parking brake performance with varying system parameters.

The Matlab model demonstrated that the amount of lost clamp load could be varied by changing the stiffness of the pads as a function of temperature. The compressibility of the pads can be used to overcome the thermal contractions of the pad and disc as the brake cools. This suggests that friction material chemists can design a pad to reduce the likelihood of rollaway occurring.

The Matlab simulation predicted that rollaway could be reduced by heating the front parking brake cable. The load in the cable increases as the cable cools due to the thermal contractions. The model assumed that the parking brake cables were 100% efficient, which would not be the case in reality. The efficiency of the cables would depend on the cable routing, the lubricity of the cables outer sheath and the loads in

the cable. The cable will become more in-efficient at higher loads due to the cable stretching and an increased frictional force between the cable and outer sheath.

The model did not take the efficiency of the cable system into consideration because the model was attempting to simulate the dynamometer conditions and results. The cable load on the dynamometer was measured at the cable attachment point on the calliper and therefore the cable inefficiency was not measured. The efficiency of the cable system is dependant on the cables used, the layout of the cable system and the loads in the cables. If the cable efficiency was taken into consideration the effect of the increase in clamp load generated by Cable 1 cooling from an elevated temperature would be reduced. This means that Cable 1 would have to be at a higher initial temperature to produce the same result. If the cable efficiency was taken into consideration the initial displacement u_1 would have to be increased to achieve the same clamp load.

The cooling rates used in the mathematical models have assumed that the brake components are cooling in still air. In reality the cooling rates will be affected by other components on the vehicle and the prevailing weather conditions. The brake cooling will be influenced by vehicle components such as the rear uprights, dirt shields and the geometry of the wheel arch. The cooling rate of Cable 1 will be influenced by the surrounding vehicle components. The cable on the vehicle may be affected by the engine exhaust which may slow the rate of cable cooling because the exhaust will take a period of time to cool.

Chapter 10

Conclusions and recommendations for further work

This Chapter discusses the main observations and findings of the research reported in the thesis. The chapter also includes a set of recommendations for areas of further work.

10.1. Conclusions

This research has investigated the phenomenon of vehicle parking brake rollaway. Many of the tests conducted were found to be of a fugitive nature with large variations in the results. This emphasises the complexity involved in studying vehicle parking brake systems. Experimental and computational approaches have been employed to study the system and the results have been collaborated to identify methods to reduce the likelihood of rollaway occurring. The main findings of the research can be summarised as follows:

- Rollaway is more likely to occur for higher initial brake temperatures. Therefore the likelihood of rollaway occurring can be reduced by reducing the temperatures generated in the rear brakes. This can be achieved by improving the cooling regime of the rear brakes or by reducing the level of braking conducted in the rear brakes.
- Rollaway is less likely to occur with a larger amount of stored elastic energy in the system. Stored elastic energy can be applied to the system by increasing the parking brake lever effort when parking.
- The thermal contractions of the disc were found to have a significant effect on the likelihood of rollaway. The thermal contractions of the disc can be reduced by reducing the initial temperature of the brake, reducing the thickness of the disc or by reducing the thermal expansion coefficient of the disc material.
- The thermal contractions of the pad have an effect on the likelihood of rollaway occurring. The thermal contractions of the pad are less significant than the thermal contractions of the disc in reducing the likelihood of rollaway.

- The static friction level at the pad/disc interface can vary as a function of temperature and directly influence the torque developed by the parking brake system. A friction pair that has a static friction level that remains constant with temperature or increases as the brake cools can be used to reduce the likelihood of rollaway occurring.
- The Young's modulus of the pad friction material as a function of temperature was found to have a significant affect on the likelihood of rollaway. The likelihood of rollaway occurring can be reduced by selecting a pad friction material that has a large increase in Young's modulus as the brake cools.
- Rollaway can be reduced by heating the front parking brake cable before the vehicle is parked. The thermal contractions will increase the load in the front cable and at the frictional interface.

10.2. Recommendations for further work

Knowledge in this research area can be improved by the following suggestions for further work:

(1) The static friction evaluations, described in Chapter 6, were conducted with the constant torque applied in the opposite direction to which the brake was dragged. This simulates a vehicle parked facing down a gradient. The friction level could be investigated further by conducting tests with the torque applied in the same direction to which the brake was dragged. The present dynamometer is capable of conducting these tests. The dynamometer is also capable of applying different constant torques on the dynamometer axle. This will enable the friction level to be investigated as a function of normal load and will simulate the vehicle parked on different gradients.

(2) The on-vehicle tests have proved that rollaway occurs on the Jaguar S-Type and the Jaguar X-Type. It is believed that rollaway is due to a particular type of parking brake system that uses an integrated floating rear calliper. Tests could be conducted on alternative vehicles using integrated rear callipers to investigate their

performance in a rollaway evaluation. These tests may identify system components that are sensitive to the rollaway results.

(3) The mathematical models could be further developed and improved with additional material property measurements. This could be achieved through further testing in the laboratory to measure the thermal parameter of the materials such as specific heat capacity and thermal conduction.

(4) The effect of disc coning on the likelihood of rollaway was not studied in detail during this research. Further work could be conducted to measure the deflections of the Jaguar S-Type disc as a function of temperature. These tests could be conducted using the dynamometer test facility or the FE model could be used to investigate disc coning. Other disc designs that have different tendencies to coning could also be used to quantify the effect of disc coning on the likelihood of rollaway.

References

1. **Pindar D (2004)**. Federal Mogul, Private communication
2. **Mckinlay A. J., Levitt A., Heald J., Hamilton O.** The Mystery of Vehicle Rollaway. Level 4 project. The school of Mechanical Engineering, The University of Leeds, 2003.
3. **Limpert R.** Brake design and safety, ISBN 1-56091-915-9, second edition, SAE, 1999
4. **Ma C.** Thermal buckling of automotive brake discs, Doctor of Philosophy thesis, The University of Michigan, 2004.
5. **Owen C. E.,** Today's technician: Automotive brake systems. Delmar Learning, 3rd edition, ISBN-10: 1401838901. 2003
6. **Gould P.,** Private communication, 2004, BOSCH Systemes de Freinage. France
7. **Harper G. A.,** Brakes and friction materials – the history and development of the technologies, John Wiley and sons, ISBN-10: 1860581277. 1998
8. **Smales H.,** Friction materials – black art or science? Proceedings of the Institution of Mechanical Engineers Part D. Vol 209 pp 151-157. 1994
9. **Mckinlay A. J., Brooks P. C., Barton D. C. Bissett A. Pindar D.** The Mystery of Vehicle Rollaway. Braking 2004, International conference. Leeds, Professional Engineering Publishing Ltd. ISBN 1 86058 464 0. 2004

10. **Mckinlay A. J. Brooks P. C. Barton D. C.** A study of Vehicle Handbrake Rollaway: a theoretical, numerical and experimental assessment, Braking 2006 International conference, York, ISBN 0 85316 245X, 2006
11. **Harding P. R. J., Day A. J.,** Instability in the hand-brake performance of cars and vans. Institute of mechanical engineers automobile division proceedings part D, volume 195 no. 27, p 315-323. 1981.
12. **Elvenkemper A.** Investigation of torque output variation in a duo-servo park brake system using six sigma tools and FE-Analysis. Proceedings of the 24th annual brake colloquium and exhibition. SAE international, 2006-01-3199. 2006
13. **Perkins S.** Electronic Parking Brake: Simple lever to safety critical system. 2004 SAE world congress. SAE technical paper series, 2004-01-1732.
14. **Balnus C.** Customer Orientation in the design process of an electromechanical parking brake – A vehicle manufacturer's point of view. 21st Annual brake colloquim and exhibition, SAE technical paper series 2003-01-3310 (2003).
15. **Eggleston D.,** EURAC Technical Bulletin Series, 00010433, www.eurac-group.com, 01/04/2006.
16. **Jacko M.G., Spurgeon R.M., Runsnak R.M., Catalano S.B.,** Thermal stability and fade characteristics of friction materials, SAE technical paper 680417 (1968)
17. **Chan D., Stachowiak G. W.,** Review of automotive brake friction materials. Proc. Institute of mechanical engineers. Vol 218 Part D. 2004.
18. **Spurr R. T.** Fillers in friction materials, Wear 22. pp 367-409. Elsevier sequoia S.A., Lausanne 1972.

19. **Yesnik M. A.** Friction material compromising powdered phenolic resin and method of making same. US Pat. 5529666, 1996 (United States Patent and Trademark office).
20. **Jang H., Lee J. S., Fash J.W.** Compositional effects of the brake friction material on creep groan phenomena. *Wear*, 2001, 251, 1477 – 1483.
21. **Gudmand-Hoyer L., Bach A., Nielsen G.T., Morgen P.**, Tribological properties of automotive disc brakes with solid lubricants. *Wear* 232 pp 168 – 175. 1999.
22. **Robinson J. W, Mogensen G.E., Packard K. D., Herman J.** Ceramic fibres for friction applications, *Automotive Engineering*, Volume 98. Number 12, pp 47 – 52, 1990
23. **Bissett A.** (2003), Federal Mogul. Private communication
24. **Watson C., Millsap T.** Friction Material; from Prototype to Production. SAE technical paper series 1999-01-3389.
25. **Hildred A. K.** Micro-mechanics of brake friction materials, Doctor of Philosophy thesis. The University of Leeds, 2002.
26. **Jang H., Kim S. J.**, The effects of antimony trisulfide (Sb_2S_3) and zirconium silicate ($ZrSiO_4$) in the automotive brake friction material on friction characteristics. *Wear* 239. (2000) 229-236
27. **Tarr W. R., Rhee S.K.**, Static friction of automotive friction materials. *Wear*, 33 (1975) 373 – 375.
28. **Jang H., Ko K., Kim S. J., Basch R. H., Fash J. W.** The effect of metal fibers on the friction performance of automotive brake friction materials. *Wear* 256 (2004) 406-414.

29. **Mace G., Bowler N., Goddard G., Morrey D.** Characterisation of Material Transformation during Cast Iron Brake Disc Bedding. Proceedings of the 24th annual brake colloquium and exhibition. 2006-01-3185.
30. **Metzler H.** The brake rotor – friction partner of brake linings. SAE technical paper series 900847, 1990.
31. **Wirth A. Stone K. Whitaker R.** A study of the relationship between transfer film chemistry and friction performance in automotive braking systems. SAE technical series 922541.
32. **Wirth A. Eggleston D. Whitaker R.** A fundamental tribochemical study of the third body layer formed during automotive friction braking, Tribology international, Volume 39 issue 5, pp 401-408. May 2006.
33. **Okamura T., Hiroyuki Y.** Fundamental Study on Thermal behaviour of brake discs. Proceedings of the 24th annual brake colloquium and exhibition. SAE international, 2006-01-3203. 2006
34. **Valvano T., Kwangjin L.,** An Analytical method to predict thermal distortion of a brake rotor. SAE 2000 world congress. SAE technical paper series, 2000-01-0445, 2000.
35. **Newcomb T.P. Spurr R.T.** Friction materials for brakes, Tribology volume 4 issue 2, pp 75-81, May 1971
36. **Dubensky R. G.** Experimental techniques for rotor performance measurements. SAE 0148-7191/85/0225-0078 (1985)
37. **Fieldhouse J. D., Ashraf N., Talbot C., Pasquet T. Franck P. Gabriel R.** Measurement of the Dynamic Center of Pressure of a Brake pad during a brake operation. Proceedings of the 24th annual brake colloquium and exhibition. SAE international, 2006-01-3208. 2006

38. **Yuhas D. E., Ding J., Venkatesan S.** Non-linear aspects of friction material elastic constants. Proceedings of the 24th annual brake colloquium and exhibition. SAE international, 2006-01-3193. 2006
39. **ECE Regulations.** ECE Regulation 13H Harmonised Braking Regulation. 2005
40. **Weiming Liu, Greg M., Vyletel Li. Jerry Li.** A rapid design tool and methodology for reducing high frequency brake squeal. Proceedings of the 24th annual brake colloquium and exhibition. SAE international, 2006-01-3205. 2006
41. **Aleksendric D., Duboka C.** A neural model of friction material behaviour. Proceedings of the 24th annual brake colloquium and exhibition. SAE international, 2006-01-3200. 2006
42. **Busso M., Portesani A., Regis P., Buonficio P.** A machine learning approach in the design of friction materials for automotive applications: Correlation among composition, process parameters and functional characteristics. Proceedings of the 24th annual brake colloquium and exhibition. SAE international, 2006-01-3201. 2006
43. **Ostermeyer G. P., Muller M., Abendroth H., Wernitz B.** Surface Topography and Wear dynamics of brake pads. Proceedings of the 24th annual brake colloquium and exhibition. SAE international, 2006-01-3202. 2006
44. **Ioannidis P.** Finite element analysis of low frequency drum brake squeal. Doctor of philosophy thesis. The University of Leeds. 2004.
45. **Shaw B. D.** Asymptotic analysis of the lumped heat capacitance approximation. International Journal of Heat and Mass Transfer. Volume 36, Issue 4, March 1993, Pages 999-1006 .

Appendix A

Ford Parking Brake test procedure

Instrumentation

All instruments must be calibrated and have laboratory calibration records. The instruments required are listed below:

- Accelerometer
- Parking brake lever effort gauge
- Parking brake lever travel gauge
- Two rubbing thermocouples on rear discs
- On-vehicle data logging system

Equipment and facilities

- Clean dry and level paved straightway
- Gradients of 30%, 16% and 12% with a smooth, dry or damp concrete or tarmac surface

Preparation

- Check that the correct brake components are installed and the vehicle tires are in good condition.
- Install the required instruments on the vehicle.
- Load the vehicle to the required test weight.
- Burnish brakes (following test CETP 06.00-R-501, Brake bedding – Cars and Derivatives)

Procedure

Static test

- Apply just sufficient effort to the parking brake lever to reach the first notch. Record the applied effort.
- Repeat the first step for all other remaining notches on the handbrake lever.

Gradient tests

- Drive the vehicle onto a 30% gradient facing up the slope. Stop and hold the vehicle by applying just sufficient service brake effort to prevent the vehicle from rolling.
- Shift transmission to neutral, apply a steady effort of 400 N to the parking brake, and release the service brake.
- If the vehicle rolls, repeat the previous two steps using increased effort until the maximum steady effort to prevent rolling is reached.
- If the vehicle does not roll at 400 N effort repeat the first two steps decreasing the effort until a minimum steady effort to prevent rolling is reached. Record the minimum steady effort to prevent rolling.
- Repeat the test with the vehicle facing down the hill
- Repeat the test on the 16% gradient
- Repeat the test on the 12% gradient
- If required repeat the test on the 12% and 16% gradients with a trailer attached to the vehicle.

General instructions

- Special attention must be given to the direction of the applied effort. For the handbrake, the pulling effort must be perpendicular to the longitudinal axis of the handbrake lever grip.

Appendix B

Federal Mogul Hot Hill Hold test procedure

Instrumentation

All instruments must be calibrated and have laboratory calibration records. The instruments required are listed below:

- Accelerometer
- Parking brake lever effort gauge
- Parking brake lever travel gauge
- Two rubbing thermocouples on the rear discs
- On-vehicle data logging system

Equipment and facilities

- Clean dry and level paved straightway
- Gradients of 25%, 16.6% and 12% with a smooth, dry or damp concrete or tarmac surface

Preparation

- Check that the correct brake components are installed and the vehicle tires are in good condition.
- Install the required instruments on the vehicle.
- Load the vehicle to the required test weight.
- Burnish brakes (conduct 200 brake stops decelerating the vehicle from 60km/h to 0km/h using a constant brake line pressure of 30bar).

Procedure

Static test

- Apply just sufficient effort to the parking brake lever to reach the first notch. Record the applied effort.
- Repeat the first step for all other remaining notches on the handbrake lever.

Gradient tests

- Drive the vehicle in an upwards direction on the 8% gradient.
- Determine the minimum line pressure for rear brakes only to hold the vehicle stationary on the gradient.
- Apply, simultaneously, the handbrake and determine the minimum effort required to just hold the vehicle on the slope.
- Apply the parking brake lever further until the next available notch on the ratchet mechanism is engaged. Record the parking brake lever effort and the number of notches on the ratchet mechanism required to park the vehicle.
- During the next 20 minutes notice parking time and brake temperature for each movement of the vehicle.
- If the vehicle starts to roll within 20 minutes, repeat the test with the handbrake applied for one notch more as established in the fourth point. Record the handbrake effort.
- Repeat the tests for rear disc temperatures of 100 C, 200 C and 300 C on gradients of 8%, 16.6% and 25%.

Appendix C

Rollaway On-Vehicle test procedure

Instrumentation

All instruments must be calibrated and have laboratory calibration records. The instruments required are listed below:

- Accelerometer
- Parking brake lever effort gauge
- Parking brake lever travel gauge
- Two rubbing thermocouple on the rear discs
- In-line hydraulic pressure sensor
- Shaft encoder mounted on rear wheel
- Microphone inside vehicle
- On-vehicle data logging system

Equipment and facilities

- Clean dry and level paved straightway
- Gradients of 25%, 16.6% and 12% with a smooth, dry or damp concrete or tarmac surface

Preparation

- Check that the correct brake components are installed and the vehicle tires are in good condition.
- Install the required instruments on the vehicle.
- Load the vehicle to the required test weight.

Procedure

Un-bedded gradient tests

- Use pads in an un-bedded condition
- Drive the vehicle in an upwards direction on the 8% gradient.
- Determine the minimum line pressure for rear brakes only to hold the vehicle stationary on the gradient.

- Apply, simultaneously, the handbrake and determine the minimum effort required to just hold the vehicle on the slope.
- Apply the parking brake lever further until the next available notch on the ratchet mechanism is engaged. Record the parking brake lever effort and the number of notches on the ratchet mechanism required to park the vehicle.
- Allow the rear discs to cool to a temperature of ambient plus 10C.
- During this time the temperature of the discs, movement of the rear axle and any noise are logged using the on-vehicle data logging system.
- If the vehicle rolls away the parking brake lever is applied to the next available notch. The effort required to achieve the next available notch is recorded.
- Repeat the test for temperatures of 50C and 100C with the vehicle facing up and down the slope on gradients of 8%, 16.6% and 25%

Bedded gradient tests

- Burnish brakes (for the required tests) by conducting 200 brake stops decelerating the vehicle from 60km/h to 0km/h using a constant brake line pressure of 30bar.
- Drive the vehicle in an upwards direction on the 8% gradient.
- Determine the minimum line pressure for rear brakes only to hold the vehicle stationary on the gradient.
- Apply, simultaneously, the handbrake and determine the minimum effort required to just hold the vehicle on the slope.
- Apply the parking brake lever further until the next available notch on the ratchet mechanism is engaged. Record the parking brake lever effort and the number of notches on the ratchet mechanism required to park the vehicle.
- Allow the rear discs to cool to a temperature of ambient plus 10C.
- During this time the temperature of the discs, movement of the rear axle and any noise are logged using the on-vehicle data logging system.

- If the vehicle rolls away the parking brake lever is applied to the next available notch. The effort required to achieve the next available notch is recorded.
- Repeat the test for temperatures of 50C, 100C, 200C and 300C with the vehicle facing up and down the slope on gradients of 8%, 16.6% and 25%

Appendix D

Dynamometer setup procedure

Instrumentation

- Torque wrench

Equipment and facilities

- Leeds parking brake dynamometer
- Parking brake dynamometer tool kit

Preparation

- Ensure that the correct brake components are installed.
- Check that the wheel nuts are tightened to a torque of 80Nm.
- Check that the calliper bolts are tightened to a torque of 55Nm.
- Lubricate the bearings on the drive rig.
- Check that the pulley wheels on the motor and drive rig are tightened to a torque of 80Nm.
- Make sure that the grub screws on the drive rig are tightened to a torque of 20Nm.
- Check that the shafts on the cable rig are in the correct position with grub screws tightened to a torque of 20Nm.
- Make sure that the correct hydraulic circuit is selected on the drive rig and that the appropriate taps/valves are open.
- Bleed the brake system

Appendix E

Normal load test procedure

Instrumentation

- Two 2kN Novatech load cells in-line with the rear parking brake cables
- Two K-type rubbing thermocouples on the rear discs
- Hohoner quadrature shaft encoder with 720 measurement locations per revolution.
- Sensotec hydraulic pressure sensor
- McLennon stepper motor to apply the parking brake cable

The full details and specifications of the instruments used are given in Chapter 5.

Equipment and facilities

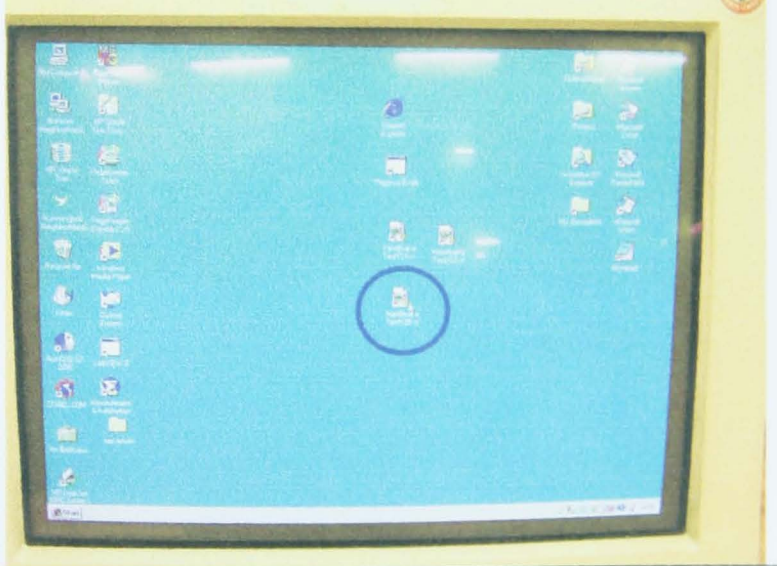
- Leeds parking brake dynamometer
- Leeds parking brake data logging and control equipment
- Desktop PC

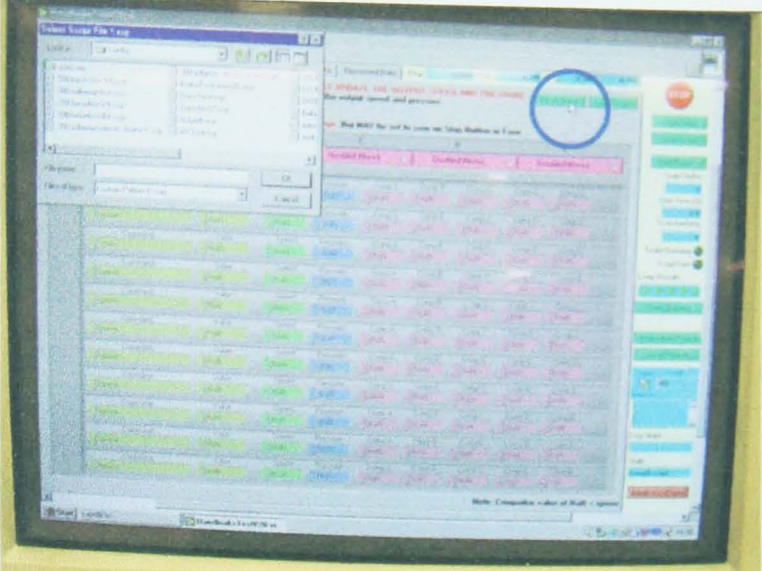
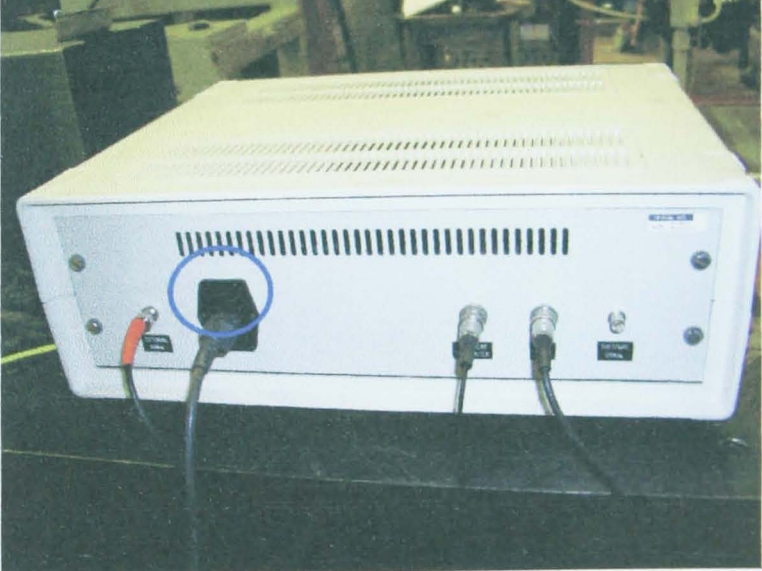
Preparation

- Follow the setup procedure described in Appendix D

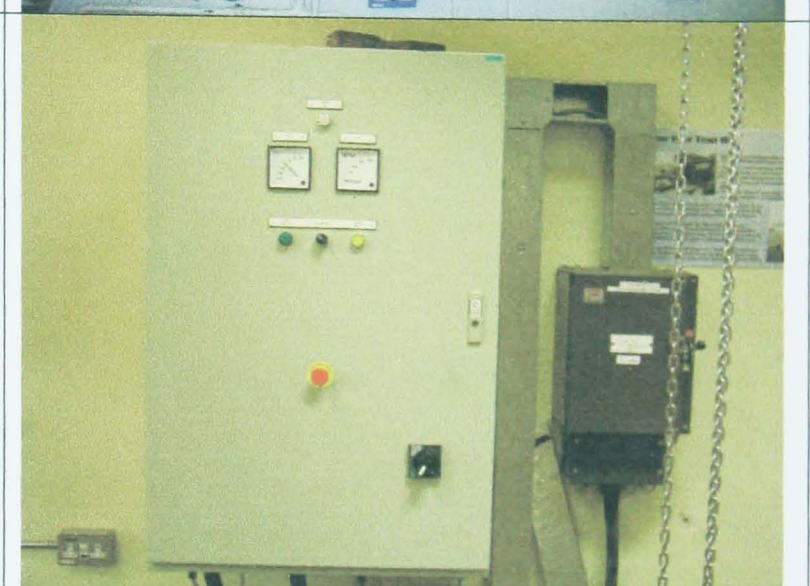
Procedure

Operation	Description	Photograph
1	Turn on PC	
2	Turn on solenoid power supply and turn both solenoids on	
3	Turn on stepper motor	

4	Turn on thermocouple amplifier	
5	Turn on load cell amplifier	
6	Load labview program	

<p>7</p>	<p>Load force test script</p>	
<p>8</p>	<p>Zero outputs</p>	
<p>9</p>	<p>Turn on hydraulic controller</p>	

10	Turn on hydraulic power pack	
11	Set hydraulic pressure to 20bar	
12	Check solenoids are working and the axle rotates	

<p>13</p>	<p>Turn on extraction</p>	
<p>14</p>	<p>Turn the power supply to the motor on, and reset the drive</p>	
<p>15</p>	<p>Close cage door</p>	

<p>16</p>	<p>Turn on the electric motor</p>	
<p>17</p>	<p>Start the labview test</p>	
<p>18</p>	<p>Turn the appropriate solenoid(s) off when prompted to do so by labview</p>	
<p>19</p>	<p>When the test has finished ensure that everything is turned off.</p>	

Appendix F

Static friction test procedure

Instrumentation

- Two 2kN Novatech load cells in-line with the rear parking brake cables
- Two K-type rubbing thermocouples on the rear discs
- Hohoner quadrature shaft encoder with 720 measurement locations per revolution
- Sensotec hydraulic pressure sensor
- McLennon stepper motor to apply the parking brake cable

The full details and specifications of the instruments used are given in Chapter 5.

Equipment and facilities

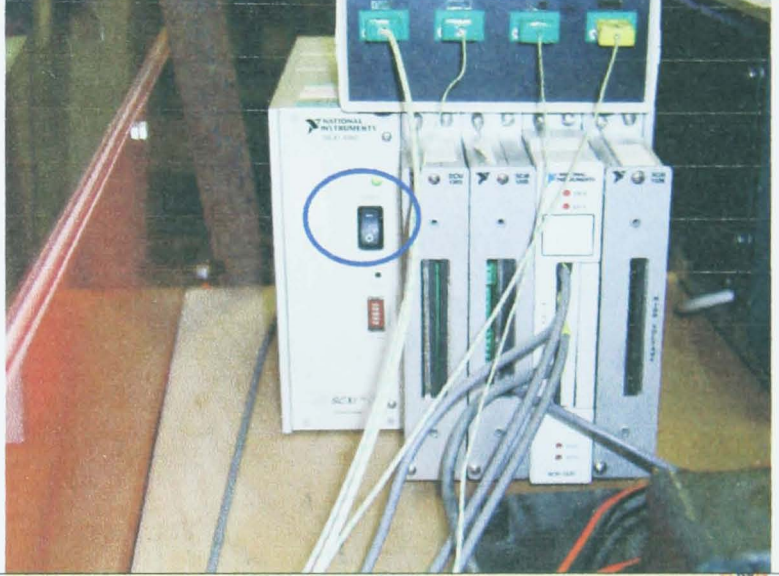
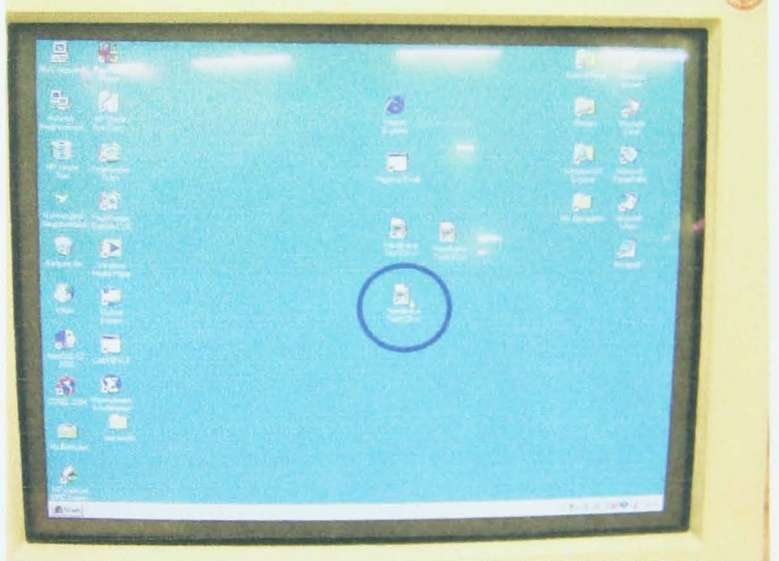
- Leeds parking brake dynamometer
- Leeds parking brake data logging and control equipment
- Desktop PC

Preparation

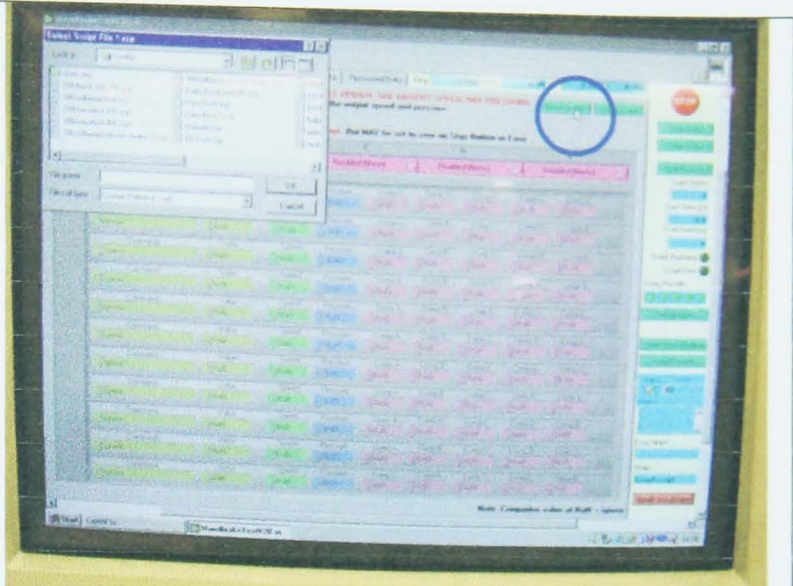
- Follow the setup procedure described in Appendix D

Procedure

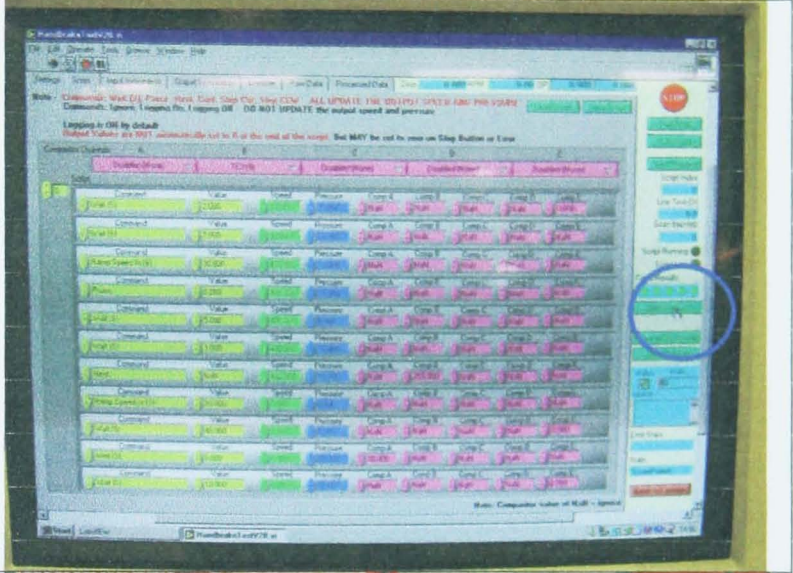
Operation	Description	Photograph
1	Turn on PC	
2	Turn on solenoid power supply and turn both solenoids on	
3	Turn on stepper motor	

4	Turn on thermocouple amplifier	
5	Turn on the load cell amplifier	
6	Load the labview program	

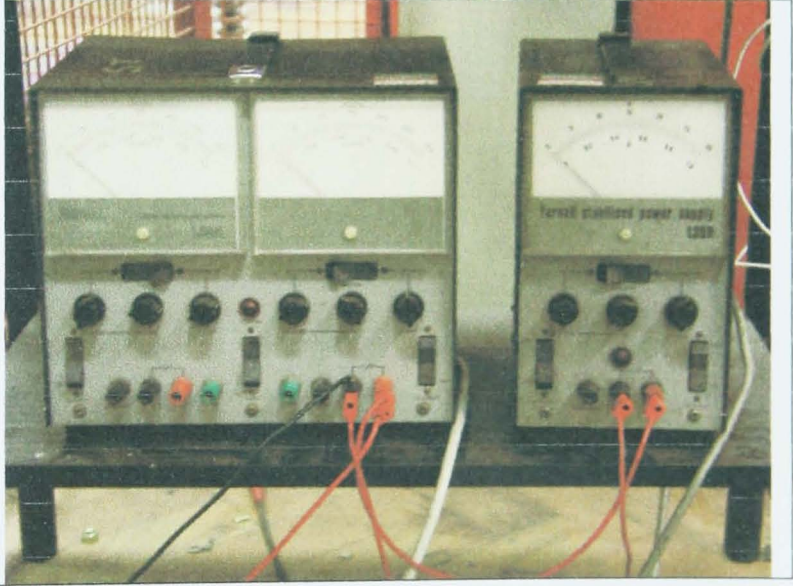
7
Load static
friction test
script



8
Zero outputs

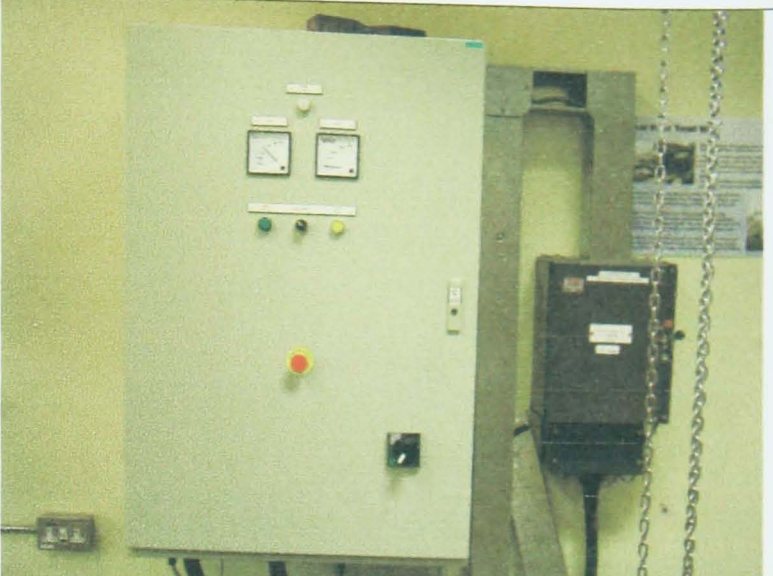


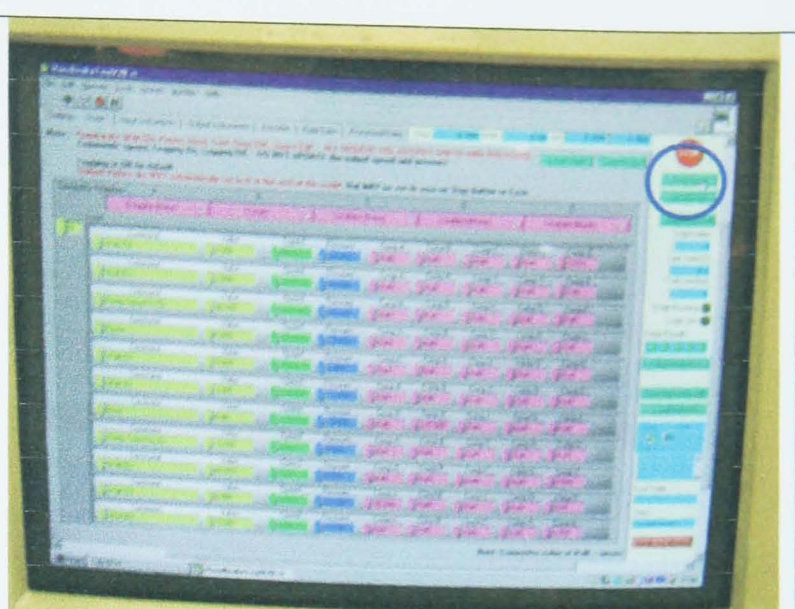
9
Turn on
hydraulic
actuator
solenoids

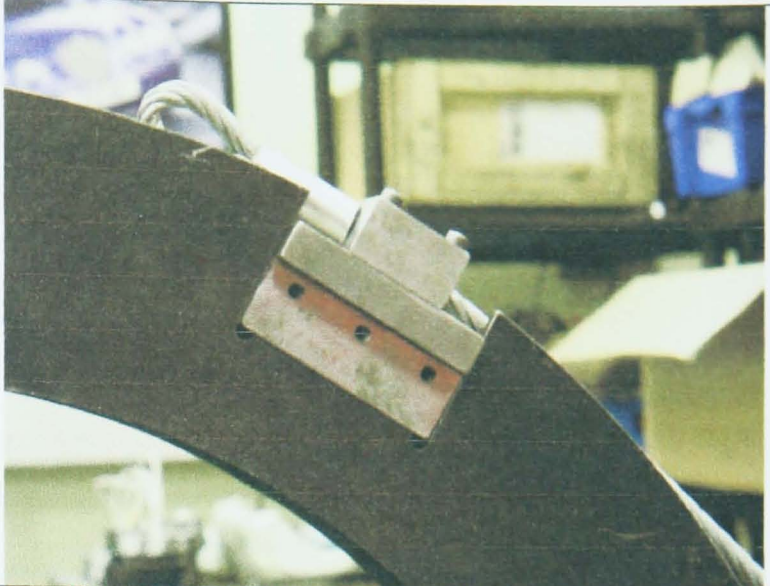


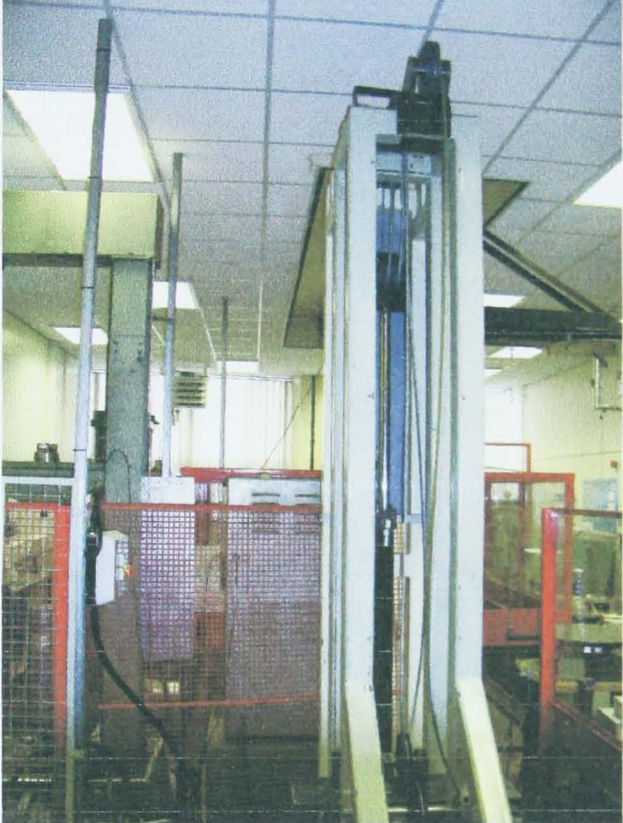
10	Make sure that the hydraulic actuator is out stroked and positioned at the top of the cable rig. If the actuator is not in this position, move it to this position.	
11	Turn on hydraulic controller	
12	Turn on hydraulic power pack	

13	Set hydraulic pressure to 20bar	
14	Check solenoids are working and the axle rotates	
15	Turn on extraction	

16	Turn the power supply to the motor on, and reset the drive	
17	Close cage door	
18	Turn on the electric motor	

<p>19</p>	<p>Start the labview test</p>	
<p>20</p>	<p>Turn the appropriate solenoid(s) off when prompted to do so by labview</p>	
<p>21</p>	<p>When the brakes are at the correct temperature and the motor has stopped, enter the cage and turn off the motor power supply</p>	

22	Attach the cable bracket to the large wheel on the drive rig	 A close-up photograph showing a metal cable bracket being secured to a large, dark-colored wheel. The bracket is a rectangular piece with a hole for the cable and is being fastened with a bolt and nut. The wheel is part of a larger mechanical assembly.
23	Rotate the large wheel wrapping the cable around it	 A photograph of a large industrial machine, likely a lathe or a similar rotating device. A large, dark wheel is being rotated, and a white cable is being wrapped around it. The machine is mounted on a white metal frame, and a green motor is visible on the right side.
24	The hydraulic pressure will then increase to 50bar	 A photograph of a white hydraulic pressure gauge. The gauge has a digital display showing the number '0022' in red. It also features a pressure gauge window on the left side and a control knob on the right. The gauge is sitting on a dark surface.

25	Turn on the hydraulic actuator power supply	
26	Lower the hydraulic actuator, raising the weights	
27	Once at the correct height switch the hydraulic controller to neutral	

28	The hydraulic pressure will now reduce	 A photograph of a white and grey electronic control unit. The unit has a digital display in the center showing the number '0022' in red. To the left of the display is a panel with several indicator lights and buttons. To the right is a single knob. The unit is sitting on a dark surface.
29	When the axle starts to rotate and the weights begin to fall, apply the handbrake lever to slow the acceleration of the weights. Slowly bring them down so that they locate into their original position.	 A photograph of a mechanical assembly. It features a black handbrake lever with a white grip, mounted on a metal frame. The assembly is positioned in front of a red metal safety cage. The background shows a workshop or laboratory setting.
30	Wait for the test to finish and the hydraulic brake pressure will return to 0 bar	 A photograph of a white and grey electronic control unit, identical to the one in the first image. The digital display shows '0022'. The unit is on a dark surface.

31	Raise the hydraulic actuator to its starting position (out stroked)	
32	When the test has finished turn off all of the equipment	

Appendix G

Compression tests with Jurid compression tester

Instrumentation

- Thermocouple embedded in back plate of pad
- Thermocouple embedded in hot plate
- Heidenhain digital displacement transducer.

Equipment and facilities

- Jurid compression tester

Preparation

- A hole is drilled into the backplate of the pad
- A thermocouple is placed inside the hole and bonded using adhesive

Procedure

- The pad is placed inside the jurid compression tester
- The data logging is started
- The hotplate is turned on and set to the correct temperature and left for 10 minutes to achieve a uniform temperature in the pad
- After 10 minutes the temperature of the pad back plate is checked to ensure that the pad is at the correct test temperature.
- If the pad has not achieved the correct temperature it is left for a further minute and re-checked.
- A load is applied on the piston equivalent to 5bar of hydraulic pressure in the brake line.
- The load is ramped to the required load for the test over a period of 2 seconds
- The load is reduced to an equivalent hydraulic pressure of 5 bar over a period of 2 seconds
- The test load is applied and released a further four times
- The maximum deflection of the pad is measured each time
- The data logging is stopped

- The results are displayed giving the deflection of the pad as a function of applied load and temperature.

Appendix H

Thermal expansion tests using DMA

Instrumentation

- Displacement transducer probe
- Thermocouple

Equipment and facilities

- DMA testing machine
- PC

Preparation

- Turn on the helium supply to the furnace
- Turn on the water cooling supply
- Turn PC on
- Load DMA software

Procedure

- Lower the furnace
- Place furnace cover over the hole on the furnace
- Move the measurement probe to the maximum position
- Remove protective rubber bung from sample platform
- Move the probe down to the platform base
- Tare the probe
- Move the probe to the maximum position
- Place silica disc on measurement platform
- Move the probe down
- Set the probe apply force to 2mN
- Read the zero value
- Move the probe up to the maximum position
- Place the test specimen on the silica disc
- Bring the probe down

- Read the height of the specimen
- Remove furnace cover
- Move furnace up to encase the sample platform
- Set the furnace temperature to 30C
- Start the DMA logging software
- Hold the temperature of the specimen at 30C for 1 minute
- Increase the specimen temperature from 30C to 300C at a rate of 10C per minute
- Wait for 1 minute with the temperature at 300C
- Stop the data logging
- Cool the sample to 30C
- Move the furnace down
- Place cover over the furnace hole
- Move the probe up to the maximum height
- Remove the specimen
- Remove the silica disc
- Place protective rubber bung in sample holder
- Bring the probe down
- Remove furnace cover
- Move furnace up to cover the sample
- Turn off the PC
- Turn off the water supply
- Turn off the helium supply.

Appendix I

Thermal expansion tests using the Jurid testing machine

Instrumentation

- Thermocouple embedded in back plate of pad
- Thermocouple embedded in hot plate
- Heidenhain digital displacement transducer.

Equipment and facilities

- Jurid compression tester

Preparation

- A hole is drilled into the back plate of the pad
- A thermocouple is placed inside the hole and bonded using adhesive

Procedure

- The pad is placed inside the Jurid testing machine
- The displacement transducer is placed in contact with the back plate of the pad
- The data logging is started
- The hotplate is turned on and set to the correct temperature and left for 10 minutes to achieve a uniform temperature in the pad
- After 10 minutes the temperature of the pad back plate is checked to ensure that the pad is at the correct test temperature.
- If the pad has not achieved the correct temperature it is left for a further minute and re-checked.
- Once at the correct temperature the data logging is stopped
- The hotplate is cooled back to ambient temperature
- The pad is removed